On the Melting and Crystallization of Linear Polyethylene, Poly(ethylene oxide) and Metallocene Linear Low-Density Polyethylene

By

Hadi Mohammadi

Dissertation submitted to the faculty of the Virginia Polytechnic Institute and State University in partial fulfillment of the requirements for the degree of

Doctor of Philosophy

in

Chemistry

Hervé L. Marand, Chair

Donald G. Baird

Alan R. Esker

Robert B. Moore

July 10, 2018

Blacksburg, Virginia

Keywords: Melting and Crystallization of Polymers, Polyethylene, Poly(ethylene oxide), Metallocene Linear Low-Density Polyethylene, Lauritzen-Hoffman Secondary Nucleation Theory, Spherulite Growth Rate, Lamellar Thickness, Friction Coefficient

On the Melting and Crystallization of Linear Polyethylene, Poly(ethylene oxide) and Metallocene Linear Low-Density Polyethylene

Hadi Mohammadi

ABSTRACT

The crystallization and melting behaviors of an ethylene/1-hexene copolymer and series of narrow molecular weight linear polyethylene and poly(ethylene oxide) fractions were studied using a combination of ultra-fast and conventional differential scanning calorimetry, optical microscopy, small angle X-ray scattering, and wide angle X-ray diffraction.

In the case of linear polyethylene and poly(ethylene oxide), the zero-entropy production melting temperatures of initial lamellae of isothermally crystallized fractions were analyzed in the context of the non-linear Hoffman-Weeks method. Using the Huggins equation, limiting equilibrium melting temperatures of 141.4 ± 0.8^{o}C and 81.4 ± 1.0^{o}C were estimated for linear polyethylene and poly(ethylene oxide), respectively. The former and the latter are about 4^{o}C lower and 12.5^{o}C higher than these predicted by Flory/Vrij and Buckley/Kovacs, respectively. Accuracy of the non-linear Hoffman-Weeks method was also examined using initial lamellar thickness literature data for a linear polyethylene fraction at different crystallization temperatures. The equilibrium melting temperature obtained by the Gibbs-Thomson approach and the C_2 value extracted from the initial lamellar thickness *vs.* reciprocal of undercooling plot were similar within the limits of experimental error to those obtained here through the non-linear Hoffman-Weeks method.

In the next step, the Lauritzen-Hoffman (LH) secondary nucleation theory was modified to account for the effect of stem length fluctuations, tilt angle of the crystallized stems, and

temperature dependence of the lateral surface free energy. Analysis of spherulite growth rate and wide angle X-ray diffraction data for 26 linear polyethylene and 5 poly(ethylene oxide) fractions revealed that the undercooling at the regime I/II transition, the equilibrium fold surface free energy, the strength of the stem length fluctuations and the substrate length at the regime I/II transition are independent of chain length. The value of the equilibrium fold surface free energy derived from crystal growth rate data using the modified Lauritzen-Hoffman theory matches that calculated from lamellar thickness and melting data through the Gibbs-Thomson equation for both linear polyethylene and poly(ethylene oxide). Larger spherulitic growth rates for linear polyethylene than for poly(ethylene oxide) at low undercooling is explained by the higher secondary nucleation constant of poly(ethylene oxide). While the apparent friction coefficient of a crystallizing linear polyethylene chain is 2 to 8 times higher than that of a chain undergoing reptation in the melt state, the apparent friction coefficient of a crystallizing poly(ethylene oxide) chain is about two orders of magnitude lower. This observation suggests that segmental mobility on the crystal phase plays a significant role in the crystal growth process.

In case of the statistical ethylene/1-hexene copolymer, the fold surface free energies of the copolymer lamellae at the time of crystallization and melting increase with increasing undercooling, approaching the same magnitude at high undercooling. As a result of this temperature dependence, the experimental melting *vs.* crystallization temperature plot is parallel to the $T_m = T_c$ line and the corresponding Gibbs-Thomson plot is non-linear. This behavior is attributed to the fact that longer ethylene sequences form a chain-folded structure with lower concentration of branch points on the lamellar surface at lower undercooling, while shorter ethylene sequences form lamellar structures at higher undercooling exhibiting a higher concentration of branch points on the lamellar surface. Branch points limit the ability of lamellar structures to relax their kinetic stem-length fluctuations during heating prior to melting.

On the Melting and Crystallization of Linear Polyethylene, Poly(ethylene oxide) and Metallocene Linear Low-Density Polyethylene

Hadi Mohammadi

GENERAL AUDIENCE ABSTRACT

Morphology of semi-crystalline polymers is strongly affected by their crystallization conditions. Thermodynamic and kinetic models allow us to understand the crystallization mechanism of a semi-crystalline polymer and relate its crystallization conditions to the final morphology. In this research, we studied the molar mass dependence of the crystallization and melting behaviors of narrow molecular weight distribution linear polyethylene (LPE) and poly(ethylene oxide) (PEO) fractions using a modified Lauritzen-Hoffman (LH) secondary nucleation theory. We have shown that the equilibrium melting temperature of LPE and PEO fractions found from the non-linear Hoffman-Weeks method are within the experimental uncertainty identical with these measured directly for extended chain crystals or derived from a Gibbs-Thomson analysis. The value of the equilibrium fold surface free energy derived from crystal growth rate data using the modified LH theory matches that calculated from lamellar thickness and melting data through the Gibbs-Thomson equation for both LPE and PEO. We reported that the higher segmental mobility of PEO in the crystalline phase leads to significantly lower apparent chain friction coefficients during crystal growth compared to LPE. We also studied the role of short-chain branching in the crystal growth kinetics of ethylene/1-hexene copolymers. We observed that the fold surface free energies during crystallization and during melting are both function of the undercooling while the ratio of the former to the latter decreases with increasing undercooling. We proposed that this behavior may be related to the

concentration of short-chain branches at the surface of the lamellae, where higher concentration leads to lower relaxation.

To my wife, Tina

Acknowledgements

I would like to first thank my advisor, Prof. Hervé L. Marand, for his patience, support, and encouragement for the development of this work. He guided me through the many challenges I came across during my research and was a tremendous help in writing and for the presentation of my paper and dissertation. I would also like to acknowledge Dr. Swapnil S. Sheth for his help and mentoring during my early years in the Marand Research Group. I am very thankful to Matthew Vincent for his friendship, his help with the ultra-fast DSC studies on LPE and m-LLDPE and for all the remarks and suggestions he provided throughout the stages of my research. I would like to thank the my colleagues in Marand Research Group, Clifton Murray, Jonathan Hoang, Marshall Chew, Shane Biesecker and Hoa Pham for their help and support over the years.

I would like to thank the Department of Chemistry for awarding me the graduate assistantship, and the head of the department, Prof. James M. Tanko for his help and support. I am very thankful to my committee members, Prof. Donald G. Baird, Prof. Alan R. Esker and Prof. Robert B. Moore, for kindly serving on my committee and for their useful guidance throughout my PhD studies. I feel truly appreciative of Dr. Gregory Fahs and Samantha Talley for their help with the wide angle X-ray diffraction measurements. I would like to thank Tony Williams and TA Instruments for the temporary loan of a Q2000 DSC. I want to specially thank Dr. Bruce Orler for his continuous encouragement. I would also like to thank ExxonMobil Company for providing the m-LLDPE samples. I truly appreciated the financial support provided by the National Science Foundation and American Chemical Society for my projects.

I would like to extend my sincere thanks to my parents, Dr. Naser Mohammadi and Mrs. Effat Shamohammadi for all their love and support and their sacrifice and blessings throughout

my life. At the end I would like to thank my wife Tina for her patience, support, encouragement and love, without which this would not have been possible.

Table of Contents

List of Figures

List of Tables

Chapter 1. Introduction

1.1. Scope of Dissertation

This work has three major objectives. The first objective is to estimate the equilibrium melting temperatures of linear flexible polymers using the non-linear Hoffman Weeks method. The second objective is to understand the effects of chain length and temperature on the crystal growth kinetics of polymers. A third objective is concerned with the effects of a non-crystallizable comonomer and temperature on the kinetics of crystal growth for semi-crystalline copolymers.

Apart from a review of the literature in Chapter 2, this dissertation consists of four manuscripts, which are published or are under review.[1] The main focus in Chapter 2 is on the morphology, thermodynamics and kinetics of crystallization of polymers and copolymers.

The equilibrium melting temperature of polymers has been routinely estimated in the literature using the linear Hoffman-Weeks method.[2] Recently, Marand et al.[3] introduced a non-linear treatment of melting temperature *vs.* crystallization temperature data to evaluate the equilibrium melting temperature of polymers, considering the effect of stem length fluctuations during crystal growth. It was shown that the neglect of the temperature dependence of the fold surface free energy in the linear Hoffman-Weeks methods leads to significant underestimation of the equilibrium melting temperature, which can have important consequences for the analysis of the chain length dependence of crystal growth rates.[3] Our first objective is to use the non-linear Hoffman-Weeks method to determine the equilibrium melting temperatures of linear polyethylene in Chapter 3 and poly(ethylene oxide) in Chapter 6. Comparison of the equilibrium melting temperatures so obtained with values calculated using the Gibbs-Thomson analysis and with melting temperatures measured for extended-chain crystals allows us to assess the accuracy of the non-linear Hoffman-Weeks method. Huggins fits relating the equilibrium melting

temperature of linear polyethylene and poly(ethylene oxide) to the chain length is also provided in Chapter 3 and 6, respectively. Analysis of the undercooling dependence of the lamellar thickness for a linear polyethylene fraction is carried out with both the modified Lauritzen-Hoffman theory and Strobl's multi-stage model.[4]

In Chapter 4, we modify the Lauritzen-Hoffman (LH) secondary nucleation theory to account for the effect of stem length fluctuations, tilt angle of the crystallized stems, and temperature dependence of the lateral surface free energy.[2, 5] Using the modified Lauritzen-Hoffman theory with equilibrium melting temperatures determined from the non-linear Hoffman-Weeks method, we analyze the spherulite growth rate data of 26 fractions of linear polyethylene (Chapter 4) and 5 fractions of poly(ethylene oxide) (Chapter 6) with different molecular weights. Substrate length measurements carried out for 3 linear polyethylene and 4 poly(ethylene oxide) fractions using wide angle X-ray diffraction allow us to investigate the chain length dependence of spherulite growth rates of these polymers, probe the role of segmental mobility on the crystal growth kinetics and determine whether chain transport during crystal growth can be explained solely on the basis of chain reptation, as was postulated by Hoffman and Miller.[5]

In Chapter 5 we study the melting and crystallization behaviors of a statistical ethylene/1-hexene copolymer using ultra-fast differential scanning calorimetry, small angle X-ray scattering and optical microscopy. The short-chain branches along the backbone of this copolymer do not enter the polyethylene crystal structure, interrupting the crystallization process.[6] The high heating rates achieved by the ultra-fast DSC technique enable us to minimize the effects of melting-recrystallization-remelting, annealing and thermal lag on the melting of this copolymer.[7] Comparison of the magnitudes of the fold surface free energy during crystallization (from spherulite growth rate and lamellar thickness data) and during melting (from melting endotherms and lamellar thickness data) allows us to gain valuable information regarding the role played by short-chain branches at different crystallization temperatures.

Finally, Chapter 7 offers concluding remarks and suggestions for future work.

1.2. References

1. Mohammadi, H.; Vincent, M.; Marand, H., Investigating the equilibrium melting temperature of linear polyethylene using the non-linear Hoffman-Weeks approach. *Polymer* **2018,** *146*, 344-360.
2. Hoffman, J. D.; Davis, G. T.; Lauritzen, J. I., The rate of crystallization of linear polymers with chain folding. In *Treatise on solid state chemistry*, Springer: 1976; pp 497-614.
3. Marand, H.; Xu, J.; Srinivas, S., Determination of the equilibrium melting temperature of polymer crystals: linear and nonlinear Hoffman− Weeks extrapolations. *Macromolecules* **1998,** *31* (23), 8219-8229.
4. Strobl, G., Crystallization and melting of bulk polymers: new observations, conclusions and a thermodynamic scheme. *Progress in polymer science* **2006,** *31* (4), 398-442.
5. Hoffman, J. D.; Miller, R. L., Kinetic of crystallization from the melt and chain folding in polyethylene fractions revisited: theory and experiment. *Polymer* **1997,** *38* (13), 3151-3212.
6. Perez, E.; VanderHart, D.; Crist Jr, B.; Howard, P., Morphological partitioning of ethyl branches in polyethylene by carbon-13 NMR. *Macromolecules* **1987,** *20* (1), 78-87.
7. Toda, A.; Taguchi, K.; Nozaki, K.; Konishi, M., Melting behaviors of polyethylene crystals: an application of fast-scan DSC. *Polymer* **2014,** *55* (14), 3186-3194.

Chapter 2. Literature Review

The physical properties of semi-crystalline polymers are governed by various factors such as the chemical structure and molecular weight of the polymer, molecular orientation, morphology, etc.[1] Morphology of semi-crystalline polymers is strongly affected by their crystallization conditions.[2] Crystallization temperature, time, and pressure are some of the variables controlling the morphology of a semi-crystalline polymer.[2] Thermodynamic and kinetic models allow us to relate those variables to the final morphology of a semi-crystalline polymer. Kinetic models also enable us to study the crystallization mechanism of a semi-crystalline polymer. We can comprehend the effects of molecular weight of the polymer and the chain topology on the crystallization of polymers by understanding their crystallization mechanism. In the first part of this chapter I will briefly review the main morphological characteristics of semi-crystalline polymers. I will also review the thermodynamic models describing crystallization and melting of homopolymers and copolymers. Finally, I will introduce two of the most commonly used crystallization kinetic models, the Lauritzen-Hoffman secondary nucleation model[3] and Strobl's multi-stage crystallization model[4].

2.1. Morphology of Semi-crystalline Polymers

Experimental evidence such as broad and diffuse X-ray diffraction patterns, bulk densities intermediate between the densities of the crystal and liquid state, and low values for the heat of fusion indicate that polymers crystallize partially.[5] In other words, the bulk of a semi-crystalline polymer consists of crystalline and amorphous phases. Early diffraction studies on the crystalline phase of polymers revealed that the unit cell of the crystals contains only few monomers and the bond distance in the cells are consistent with covalent bond distances.[6]

The first model describing semi-crystalline polymers based on X-ray diffraction, densitometry and mechanical property studies was the fringed micelle model, Figure 2.1.[7]

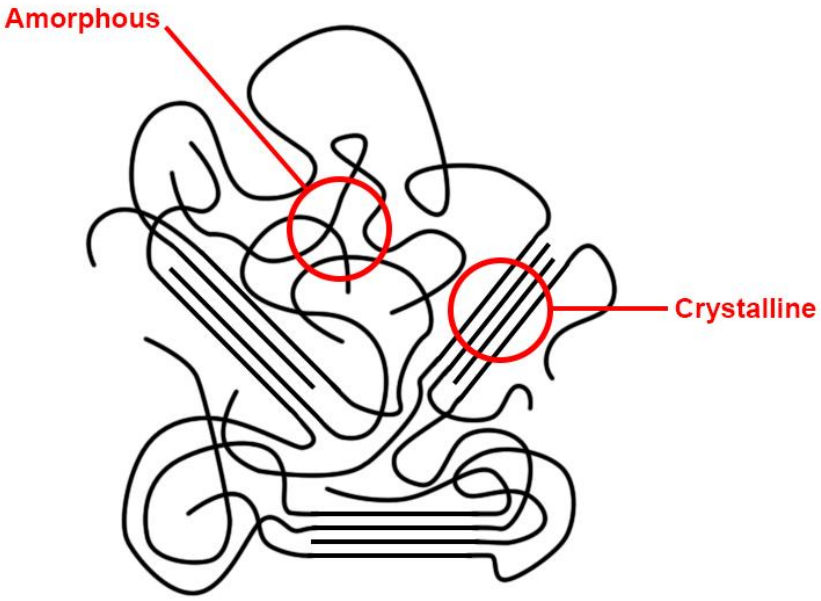

Figure 2.1. Schematic representation of the fringed-micelle model for a semi-crystalline polymer.[5]

In this model crystals are about 100 Å thick with chains long enough to wander through multiple amorphous and crystalline regions.[7] This model was able to explain the wide angle X-ray diffraction patterns and mechanical properties of semi-crystalline polymers. However, it could neither justify the spherulitic structures observed in many semi-crystalline polymers by optical microscopy nor rationalize their small angle X-ray scattering patterns.[5]

Keller's studies on polyethylene single crystals precipitated from a hot xylene solution revolutionized the concept of polymer crystallinity.[8] Keller's electron microscopy and electron diffraction studies suggested that the thickness of polyethylene single crystals was much smaller than the length of the chains and led him to propose the chain-folded lamellar crystal model, Figure 2.2.[8] In this model, polymer chains fold back and forth in the single crystal lamella, approximately perpendicular to the crystal basal plane. In polyethylene, however, the

crystallized stems exhibit a tilted conformation with respect to the lamella fold surface to lower the amount of steric hindrance between adjacent folds.[9-14] Each lamella could contain one or several chains.

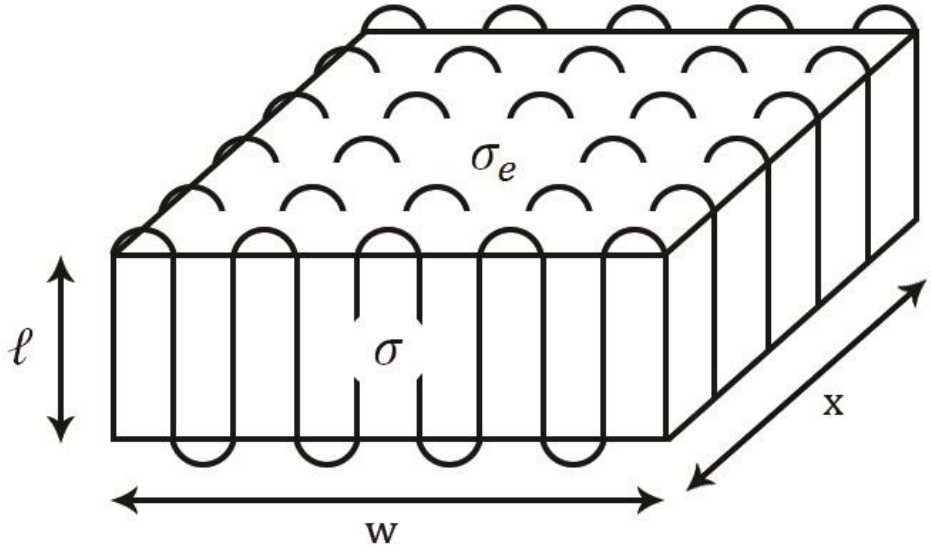

Figure 2.2. Schematic representation of a chain-folded lamellar structure. w, x, and ℓ are the length, width, and thickness of the lamella, respectively. σ and σ_e are the lateral and fold surface free energies of the lamella, respectively.

Lauritzen and Passaglia[15] showed that the length of polymer stems crystallizing on a lamella can fluctuate around the average lamellar thickness by few Angstroms. Their calculations showed that the entropic contribution caused by fold surface roughness can overcome the enthalpic penalty associated with new lateral surfaces resulting from the differences in adjacent stem lengths.[15] Figure 2.3 illustrates a schematic representation of stem length fluctuations in a polymeric crystal. Crystal stem length fluctuations are a function of the crystallization temperature, which results in a temperature dependent fold surface free energy.[15] Hoffman et al.[16] suggested that the crystal stem length fluctuations equilibrate by chain movements right before melting, lowering the fold surface free energy of the lamella.

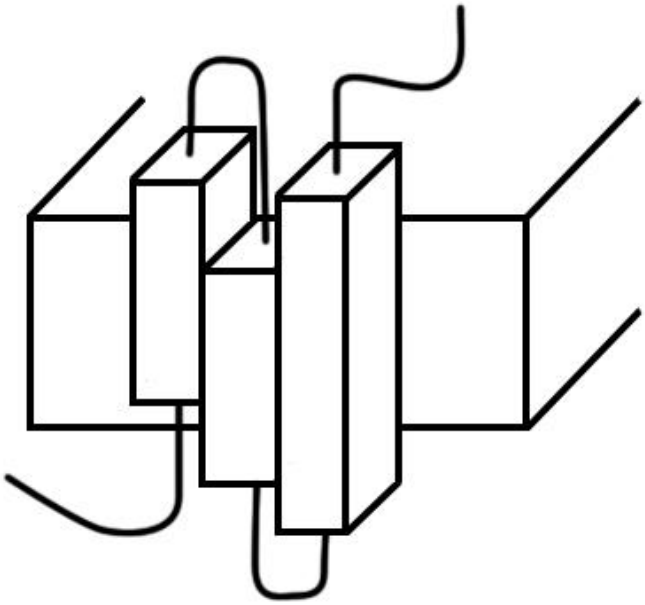

Figure 2.3. Schematic representation of a polymer chain crystallizing on a preexisting substrate. The length of the crystallized stems fluctuates around the average lamellar thickness by few Angstroms (grossly exaggerated in the schematic).

Upon cooling the polymer from the melt, crystallization initiates by formation of the primary nuclei through a homogenous (local order in the melt) or a heterogeneous (surface of impurities in the melt) process. Primary nucleation in polymers is generally heterogeneous.[2] Attachment of the chains to the primary nuclei accompanied with the chain folding process leads to the lamellar structures in the melt. Lamellae stack and branch and form multi-layered axialitic and hedritic morphologies. During this process, the tie-chains, cilia, loose and tight folds are rejected between the adjacent radial arrays and will form the amorphous regions between the lamellae. The dense and non-crystallographic branching results in a sheaf-like structure, which grows into the spherulite.[2] Spherulites are the most common structure observed during crystallization of polymers under quiescent conditions.[5] Figure 2.4 shows a schematic representation of formation of a spherulite in the super-cooled melt.

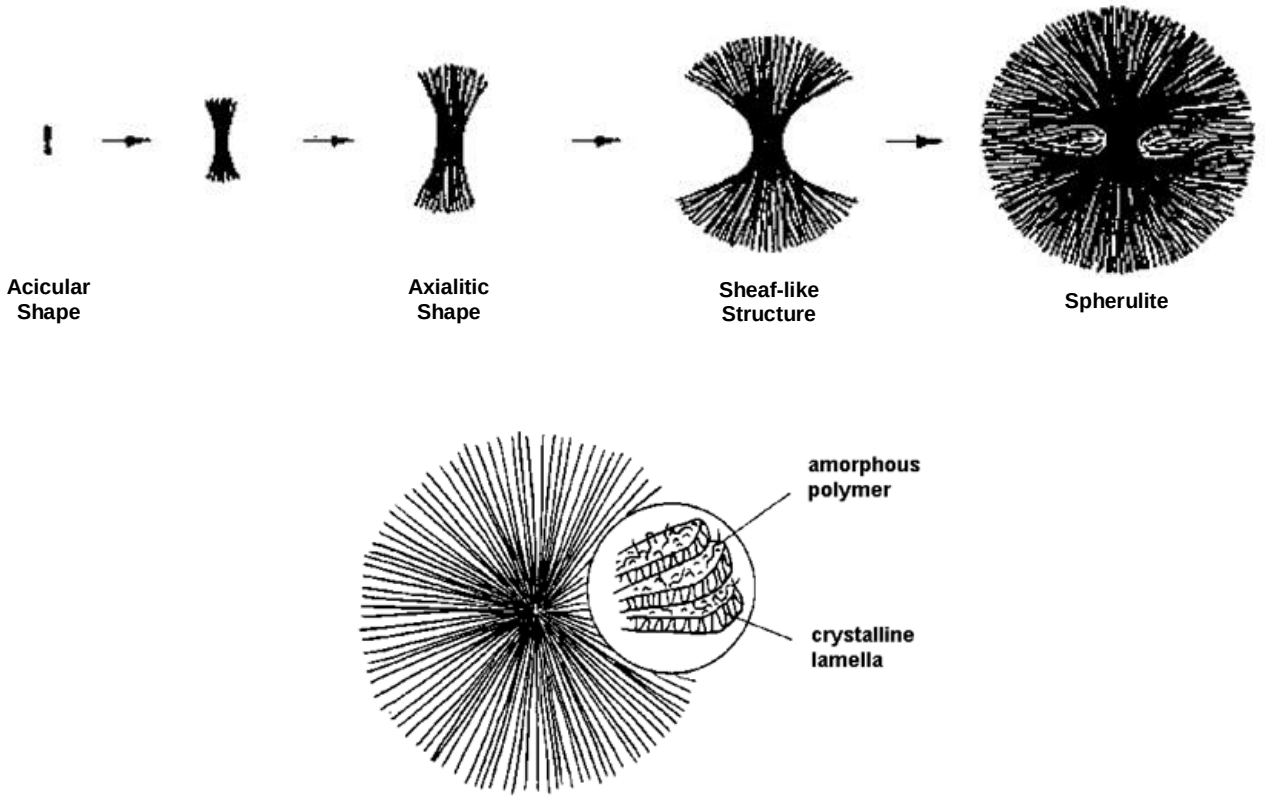

Figure 2.4. Schematic representation of the formation of a spherulite in the supercooled melt.[5]

In most cases, when polymers crystallize isothermally, the spherulite radius increases linearly with time until the spherulites impinge on each other. For a variety of polymers, the chains are normal to the radial direction of the spherulites.[2]

In random copolymers, the resulting morphology can be more complicated. Based on the relative size of the comonomers and the crystallization kinetics, one comonomer may enter the lamellae formed by the other comonomers or get rejected into the amorphous phase between the lamellae, disturbing the chain folding process.[17-19] The non-crystallizable comonomer reduces the thickness and lateral dimensions of the lamellae and the size of the spherulites.[2] The non-crystallizable comonomer can also disturb the growth of the spherulites.[20] If the amount of non-crystallizable comonomers passes a certain threshold, spherulites will not form under

isothermal crystallization conditions.[20] This threshold also depends on the size of the comonomer and the crystallization kinetics.[20]

2.2. Thermodynamics of Polymer Crystallization

2.2.1. Homopolymers

Considering the lamella shown in Figure 2.2, the Gibbs free energy of fusion of the lamella, ΔG, at its melting temperature, T_m, is

$$\Delta G(T_m) = -2(w + x)\ell\sigma - 2wx\sigma_{em} + wx\ell\Delta G^{\infty} = 0 \tag{2.1}$$

where ΔG^{∞} and σ_{em} are the Gibbs free energy of fusion per unit volume for an infinitely large crystal and the fold surface free energy of the crystal at the melting temperature, respectively.[5] When a crystal of infinite size is at equilibrium with its melt ΔG^{∞} is equal to zero and therefore,

$$\frac{M_R}{\rho(T_m^{eq})}\Delta G^{\infty} = \overline{\Delta H} - T_m^{eq}\overline{\Delta S} = 0 \tag{2.2}$$

or

$$\Delta G^{\infty} = \Delta H - T_m^{eq}\Delta S = 0 \rightarrow \Delta S = \frac{\Delta H}{T_m^{eq}} \tag{2.3}$$

Here $\rho(T_m^{eq})$ and M_R are the density of the crystalline phase at T_m^{eq} and molar mass of the repeat unit in the polymer chain, respectively. T_m^{eq} or the equilibrium melting temperature of the crystal is the temperature where an infinitely large extended chain crystal is in equilibrium with its melt. $\overline{\Delta H}$ and $\overline{\Delta S}$ are the enthalpy and the entropy of fusion per mole of repeat unit, respectively. ΔH and ΔS are the volumetric enthalpy of fusion and volumetric entropy of fusion of an infinitely large extended chain crystal, respectively. In Equation 2.3 it is assumed that the density of the crystalline and amorphous phase are nearly identical so $\frac{\rho(T_m^{eq})}{M_R}\overline{\Delta H} = \Delta H$ and

$\frac{\rho(T_m^{eq})}{M_R}\overline{\Delta S} = \Delta S$. Assuming that ΔH and ΔS are independent of temperature, we can express ΔG^{∞} at T_m as

$$\Delta G^{\infty} = \Delta H - T_m \frac{\Delta H}{T_m^{eq}} = \frac{\Delta H\left(T_m^{eq} - T_m\right)}{T_m^{eq}} \tag{2.4}$$

Accuracy of this approximation, constant ΔH and ΔS, can be examined using experimental values of ΔH and ΔS. Polyethylene is probably one of the most studied macromolecules in this regard. Wunderlich et al.[21-22] calculated the values of $\overline{\Delta H}$ and $\overline{\Delta S}$ for polyethylene at different temperatures using Equations 2.5 and 2.6:

$$\overline{\Delta H}(T) = \int_0^T C_{p,a}(T)dT - \int_0^T C_{p,c}(T)dT \tag{2.5}$$

$$\overline{\Delta S}(T) = \int_0^T \frac{C_{p,a}(T)}{T}dT - \int_0^T \frac{C_{p,c}(T)}{T}dT \tag{2.6}$$

Here, $C_{p,c}$ and $C_{p,a}$ are the molar heat capacity of crystalline and amorphous polyethylene at constant pressure, respectively. For temperatures between -273 and -23^{o}C, they found values of $C_{p,c}$ and $C_{p,a}$ after measuring the constant pressure heat capacities of semi-crystalline polyethylene samples and extrapolating them to 100 and 0 percent crystallinities.[22] The same procedure was applied for $C_{p,c}$ at temperatures beyond -23^{o}C. $C_{p,a}$ in the range of -23 to 187^{o}C was found by extrapolation from measurements performed on polyethylene melts as the aforementioned method loses its accuracy with the variable degree of crystallinity in this range.[22] Utilizing the density of polyethylene crystals,[23] values of $\overline{\Delta H}$ and $\overline{\Delta S}$ have been converted to ΔH and ΔS and plotted in Figure 2.5. From the data plotted in Figure 2.5 we can see that considering a constant value for ΔH and ΔS is a poor approximation. ΔH of polyethylene increases with temperature, reaches a maximum around 125^{o}C, ΔH_{max} = 283 J/cm^3, and

decreases thereafter.[22-23] On the other hand, $T\Delta S$ versus T starts to deviate from a straight line around 80°C, Figure 2.5.

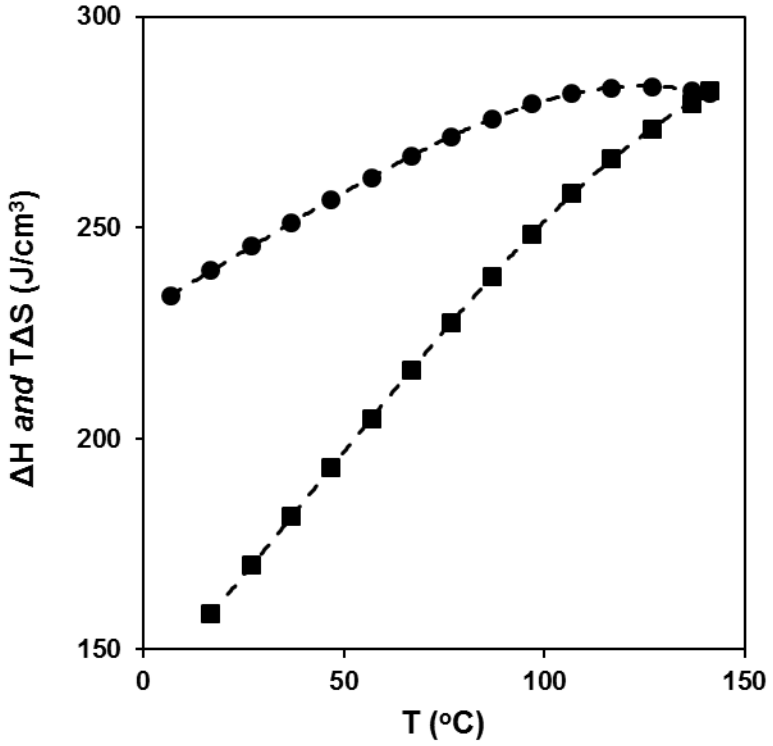

Figure 2.5. Experimental values of ΔH (●) and $T\Delta S$ (■) versus temperature. Dashed lines are drawn as a guide to the eye.[22]

However, comparing values of ΔG^{∞} calculated by Equation 2.4 with the experimental values found from $\Delta G^{\infty} = \Delta H - T\Delta S$ demonstrates little to no difference at temperatures above 80°C, Figure 2.6. ΔH of 283 J/cm^3 was used in Equation 2.4 as the constant value for ΔH. For temperatures above 80°C the maximum deviation of the calculated ΔG^{∞} from its experimental values is about 1%. At temperatures below 80°C the experimental values of ΔG^{∞} are smaller than those predicted by Equation 2.4. As was demonstrated in this example, using Equation 2.4 is only acceptable at temperatures close to T_m^{eq}.

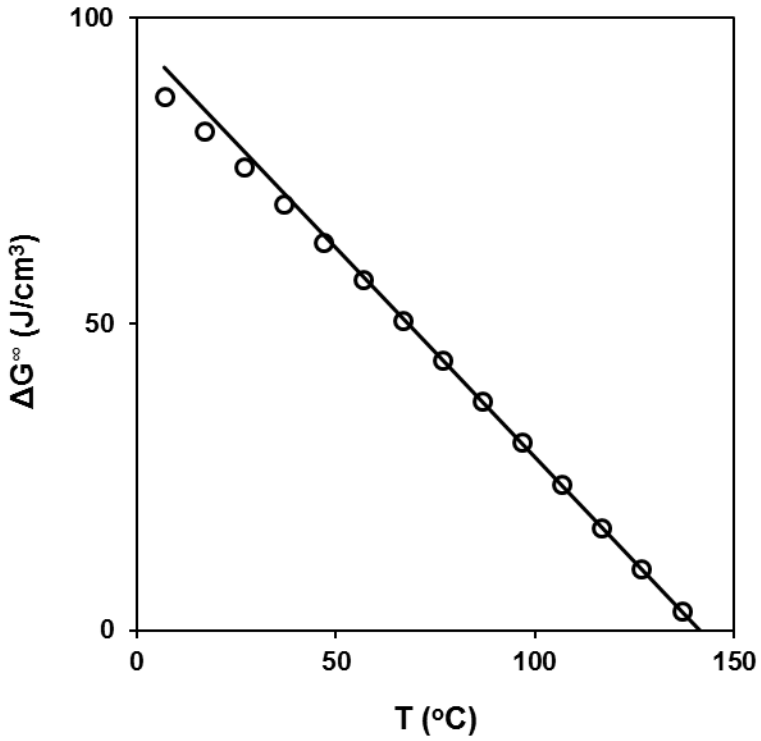

Figure 2.6. ΔG^{∞} versus T found from Equation 2.4 (—) and the experimental values (○).

Taking the temperature limits into account, Equations 2.1 and 2.4 can be combined to relate the melting temperature to the lamellar thickness. For $x, w \gg \ell$ and $\sigma_{em} > \sigma$ we find the melting temperature of the lamella as

$$T_m = T_m^{eq}\left[1 - \frac{2\sigma_{em}}{\ell \Delta H}\right] \tag{2.7}$$

Equation 2.7 is known as the Gibbs-Thomson equation, which defines the melting line in the T versus $1/\ell$ plot.[5] In addition, the Gibbs-Thomson equation provides access to the minimum thickness, ℓ_{min}, of lamellae that can form at the crystallization temperature, T_c5

$$\ell_{min} = \frac{2\sigma_{ec}}{\Delta G^{\infty}} = \frac{2\sigma_{ec} T_m^{eq}}{\left[\Delta H (T_m^{eq} - T_c)\right]} = \frac{2\sigma_{ec} T_m^{eq}}{\Delta H \Delta T} \tag{2.8}$$

where σ_{ec} and ΔT are the fold surface free energy at the crystallization temperature and the undercooling, respectively. Although Equation 2.8, a thermodynamic equation, gives us insight into the minimum lamellar thickness at T_c, the actual average lamellar thickness and the lamellar thickness distribution are controlled by the crystallization kinetics.

2.2.2. Copolymers with a Non-crystallizable Monomer

When units of comonomer B are added to a polymer chain made of A units, the B units can either be rejected into the amorphous phase or enter A crystals. The former behavior was modeled by Flory[24] (exclusion model) while the later (inclusion model) was studied by Sanchez and Eby.[25] In the exclusion model, Flory assumed that the B units of a A/B copolymer do not crystallize under experimental conditions.[24] Figure 2.7 shows a schematic representation of exclusion of the B units from the crystalline phase.

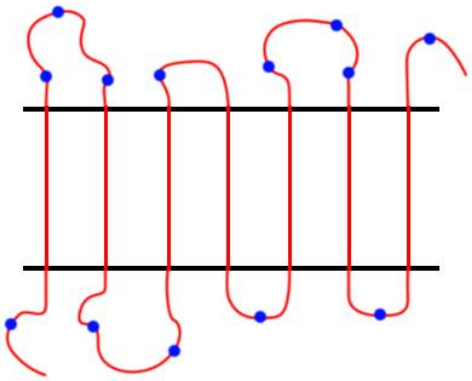

Figure 2.7. Schematic representation of a lamella of a A/B copolymer where the B units (●) are excluded from the crystalline phase of A units.

Flory stated that when the A/B copolymer is crystallized to the maximum amount possible, crystallized sequences of A are in equilibrium with same size A sequences in the amorphous phase. He expressed the probability to find a sequence made of ε units of A in the amorphous phase at a given crystallization temperature, P_{ε}^{eq}, as

$$P_{\varepsilon}^{eq} = \exp\left(-\frac{\Delta G_{\varepsilon}}{RT_c}\right) \tag{2.9}$$

where ΔG_{ε} and R are the free energy of fusion of a crystallized sequence of A made of ε units and the gas constant, respectively.[24] By considering $\theta = \frac{\Delta G_{\varepsilon}}{RT_c} = \left(\frac{\Delta H_u}{R}\right)\left(\frac{1}{T_c} - \frac{1}{T_m^{eq}}\right)$ and $D = \exp\left(-\frac{2\sigma_e^*}{RT_c}\right)$ he showed that the weight fraction of A sequences made of ε units in the amorphous phase under equilibrium conditions, w_{ε}^{am}, is

$$w_{\varepsilon}^{am} = \varepsilon D^{-1}[1 - \exp(-\theta)]^2 \exp(-\varepsilon\theta) \tag{2.10}$$

where ΔH_u and σ_e^* are heat of fusion and fold surface free energy per A unit, respectively.[24] T_m^{eq} is the equilibrium melting temperature of a pure A polymer. If w_{ε}^0 is the weight fraction of A sequences made of ε units in the polymer chains, thus, ε_{min} or the minimum number of units in a crystallized A sequence is obtained assuming $w_{\varepsilon}^o = w_{\varepsilon}^{am}$.[24] Taking p as the probability to find a A unit next to another A unit (in random copolymers p is equal to the mole fraction of A units, X_A), w_{ε}^o is

$$w_{\varepsilon}^o = \varepsilon\left(\frac{X_A}{p}\right)(1-p)^2 p^{\varepsilon} \tag{2.11}$$

Therefore, the minimum lamellar thickness at equilibrium is given as

$$\ell_{min} = -\ell_{u,A}\left\{\ln\left(\frac{DX_A}{p}\right) + 2\ln\left[\frac{(1-p)}{(1-\exp-\theta)}\right]\right\}/(\theta + \ln p) \tag{2.12}$$

where $\ell_{u,A}$ is the length of a A unit projected along the c-axis of the crystal.[24] Flory also defined the necessary condition for crystallization to occur as $P_{\varepsilon}^o > P_{\varepsilon}^{eq}$, where P_{ε}^o is the probability to find a sequence made of ε units of A in the copolymer chain. This relationship simplifies to $\theta > -\ln p$ for random copolymers. Therefore, the equilibrium melting temperature of the copolymer, $T_{m,c}^{eq}$, can be found at $\theta = -\ln p$, Equation 2.13.[24]

$$\frac{1}{T_{m,c}^{eq}} - \frac{1}{T_m^{eq}} = -\left(\frac{R}{\overline{\Delta H}}\right) \ln p \tag{2.13}$$

The exclusion model considers the preferential partitioning of A units into the crystal phase, an entropic effect, as the origin of the depression of the equilibrium melting temperature.[24] In a random copolymer this depression is directly related to the mole fraction of the B units, X_B. Finally, the weight fraction crystallinity under equilibrium conditions, w^c, is[24]

$$\begin{aligned} w^c &= \sum_{\varepsilon_{min}}^{\infty} w_\varepsilon^c = \sum_{\varepsilon_{min}}^{\infty} w_\varepsilon^0 - w_\varepsilon^{am} \\ &= \left(\frac{X_A}{p}\right)(1-p)^2 p^{\varepsilon_{min}} \begin{bmatrix} p(1-p)^{-2} - \exp -\theta\,(1-\exp -\theta)^{-2} \\ +\varepsilon_{min}\{(1-p)^{-1} - (1-\exp -\theta)^{-1}\} \end{bmatrix} \end{aligned} \tag{2.14}$$

The model predicts that for a random copolymer of A and B units an increase in X_B leads to a decrease in the overall crystallinity along with an increase of ℓ_{min}.[24]

2.3. Kinetics of Polymer Crystallization

2.3.1. Lauritzen-Hoffman Secondary Nucleation Theory

The faceted single crystals formed from polymer solutions along with the exponential dependence of the spherulitic growth rate, G, on the undercooling suggest that polymer crystallization is nucleation-controlled, which is the basis of the Lauritzen-Hoffman secondary nucleation theory (LH theory).[3, 26-27] The LH theory was first applied to interpret crystallization behavior of linear polyethylene and then developed for other polymers.[27] This model has also been used to analyze the crystallization kinetics of copolymers with a non-crystallizable unit.[28-29] The LH theory does not address the primary nucleation step in crystallization of polymers and only focuses on the growth kinetics of lamellar crystals. This model assumes that the initial

growth front exists in the melt and tries to rationalize the steady state growth (constant G) of crystals under isothermal conditions.[3, 27]

The basic LH model is shown schematically in Figure 2.8, depicting the crystal growth front. In the LH model, crystal growth is assumed to take place on a smooth substrate. The growth rates of spherulites and lamellae are assumed to be identical in this model. Also, the crystallized stems are perpendicular to the fold surface of the lamellae, Figure 2.8. Stem length fluctuations in the crystals were not considered in the initial model.[27]

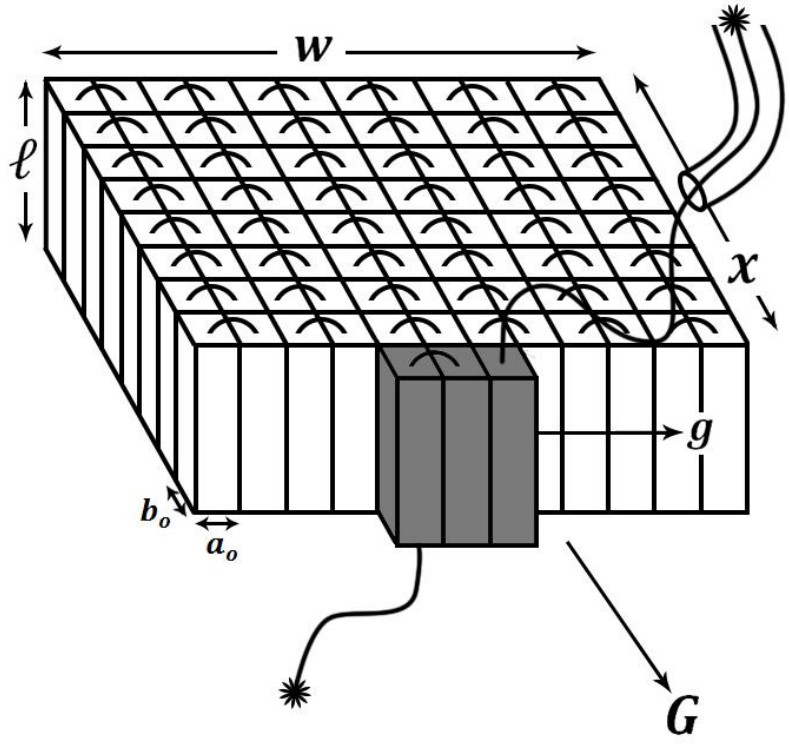

Figure 2.8. Schematic representation of a lamella. a_o and b_o are the width and thickness of the crystallized stems, respectively. A chain is moving in the reptation tube from the melt and crystallizing on the lamella, completing a new layer with the rate of g, leading to an overall crystal growth rate of G (the new layer is colored in gray).[27]

After cooling the melt to T_c the crystal growth process begins with primary nucleation, heterogeneous or homogenous. After the primary nuclei are formed, the first stem attaches to

the growth front with a rate constant of A_o, Figure 2.9. During this process the segment is adsorbed to the growth front without any crystallographic attachment. The free energy barrier for this process was initially defined as the work required to create two new lateral surfaces during this process, $2b_o\sigma\ell$.[30] In more recent treatments, this free energy barrier is viewed as an entropy penalty associated with the segmentalization of the chain as it approaches the crystal growth front.[30] After overcoming the free energy barrier, the stem will undergo a rapid crystallographic attachment on the substrate forming the first crystallized full stem.[27, 31] Since the crystallized stem is assumed to be in local equilibrium with the melt, it can go back to the melt in two steps: a slow step to the attached state with a rate constant of B_1followed by a rapid step to the melt. The slow step in melting has an energy barrier of $a_o b_o \Delta G^{\infty}\ell$. In the LH theory, the thermodynamics of fusion follows the Gibbs-Thomson approach, therefore, values of ΔG^{∞} at low to intermediate undercoolings can be found using Equation 2.4.[31]

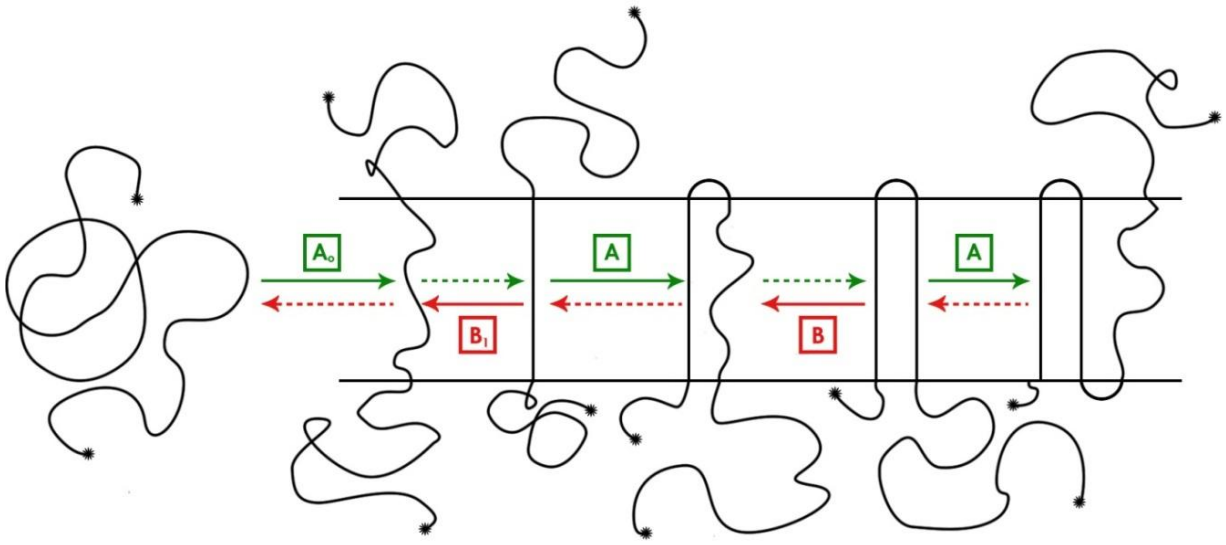

Figure 2.9. Schematic representation of the crystallization steps and their rate constants. The fast steps are shown with arrows with dashed lines.

After deposition of the first stem, the polymer chain can continue to attach another stem on the substrate by folding back on itself with a rate constant of A, Figure 2.9. The free energy

barrier for this step is related to the work of chain folding, $2a_o b_o \sigma_{ec}$. The second stem will then crystallize rapidly forming the second crystallographic attached full stem, which can melt with a rate constant of B. The reverse process has the same free energy barrier as the slow step of melting the first stem.[27, 31] By repeating this process, the crystallized stems will cover the whole substrate and form a new crystallized layer.[27, 31]

The theory provided above considers the $\psi = 0$ approach. In the early versions of the theory it was assumed that a fraction of the chain, ψ, crystallizes during deposition of the stems from the melt on the growth front, lowering the energy barrier of deposition and removal of the stems by $\psi a_o b_o \Delta G^{\infty} \ell$.[3] However, a high ψ would result in the divergence of δ at some finite undercooling (the δ catastrophe).[27] For example, a ψ > 0.25 leads to a δ catastrophe in linear polyethylene at temperatures above the glass transition temperature, T_g.[27] To avoid the physically unrealistic δ catastrophe I will use the ψ = 0 approach throughout my thesis. Lauritzen and Hoffman defined the rate constants for each step as[27]

$$A_o = \beta' \exp\left(-\frac{2b_o \sigma \ell}{kT_c}\right) \tag{2.15}$$

$$B_1 = \beta' \exp\left(-\frac{a_o b_o \Delta G^{\infty} \ell}{kT_c}\right) \tag{2.16}$$

$$A = \beta \exp\left(-\frac{2a_o b_o \sigma_{ec}}{kT_c}\right) \tag{2.17}$$

$$B = \beta \exp\left(-\frac{a_o b_o \Delta G^{\infty} \ell}{kT_c}\right) \tag{2.18}$$

where k, β', and β are the Boltzmann constant and factors representing retardation due to transfer of the polymer segments across the melt-crystal interface for the first stem and the subsequent stems, respectively.[27] The first segment attaching to the growth front is located in close proximity, therefore, local movements of the chain may be sufficient for transferring the stem across the melt-crystal interface. However, other segments have to move through the

entangled melt to pass that interface. As a result, β', and β may have different values. Hoffman and Miller[27] defined the β terms in Equations 2.15 to 2.18 by employing the reptation theory as

$$\beta = \frac{\kappa}{n}\left(\frac{kT_c}{h}\right)\exp\left(-\frac{Q_d^*}{RT_c}\right) \tag{2.19}$$

where n, h, and Q_d^* are the number of the covalent bonds in the polymer chain backbone, Planck's constant, and the activation energy for reptation, respectively. The Arrhenius form of the segmental transport equation provided in Equation 2.19 can be used when the crystallization temperatures are much higher than T_g.[27] At temperatures below T_g + 100, using an equation in the form of the Vogel-Fulcher-Tamman-Hesse equation is more appropriate.[27] In this thesis, I will use the β expression given by Equation 2.19 as the crystallization temperatures used in my studies are well above T_g + 100. κ is given in Equation 2.20.[27]

$$\kappa = \frac{h\exp\left(\frac{Q_d^*}{RT_o}\right)\exp\left(\frac{2a_o b_o \sigma_{ec}}{kT_c}\right)}{\xi_o {\ell_g^*}^2} \tag{2.20}$$

Where T_o, ξ_o, and ℓ_g^* are the reference temperature where the diffusion coefficient of the polymer is measured, Rouse regime monomeric friction coefficient at the reference temperature, and the average initial lamellar thickness, respectively.[27] The net free energy of formation of a new crystalline layer containing ν stems, ΔG_ν, can also be written as

$$\Delta G_\nu = 2b_o\sigma\ell - a_o b_o \Delta G^\infty\, \ell - (\nu - 1)a_o b_o[\ell \Delta G^\infty - 2\sigma_{ec}] \tag{2.21}$$

Figure 2.10 shows changes of ΔG_ν with number of deposited stems on the substrate, ν.

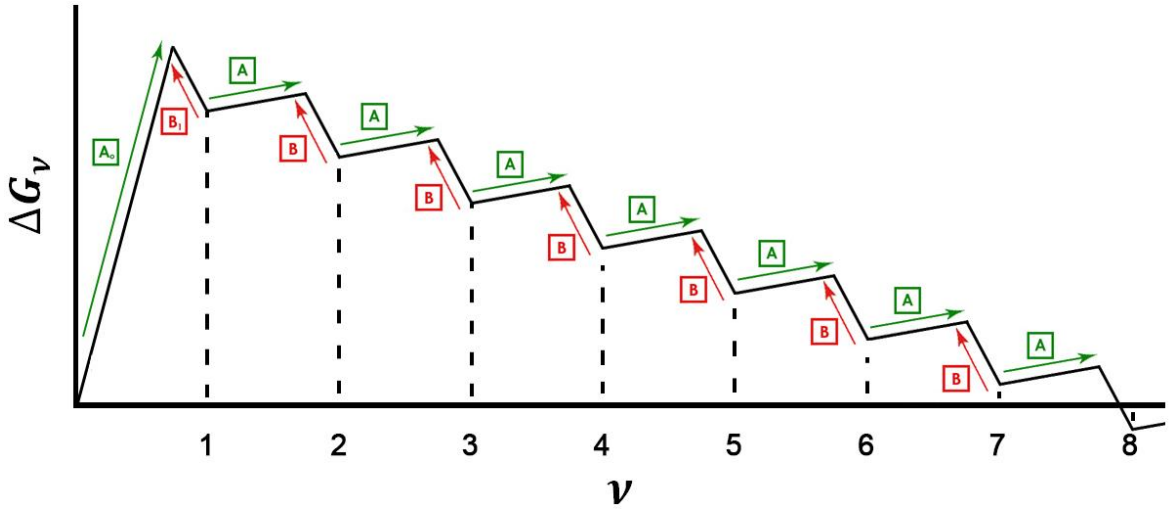

Figure 2.10. ΔG_ν versus υ. Rate constants of each step are shown on the diagram.

For a given lamellar thickness, the nucleus becomes "stable" when ΔG_ν becomes negative by crystallizing ν_s stems. In the figure above, ν_s = 8. Using Equation 2.21, ν_s for a given lamellar thickness is

$$\nu_s = \frac{2b_o\sigma\ell - a_o b_o \Delta G^\infty \ell}{a_o b_o[\ell \Delta G^\infty - 2\sigma_{ec}]} + 1 \tag{2.22}$$

which is rounded up to the nearest integer. The flux equations were written for the forward and backward steps shown in Figure 2.10 (except ν = 0 → ν = 1) as[3]

$$\frac{dN_2}{dt} = AN_1 - BN_2 - AN_2 + BN_3$$

$$\frac{dN_3}{dt} = AN_2 - BN_3 - AN_3 + BN_4$$

. . . . .

. . . . .

. . . . .

$$\frac{dN_{\upsilon-1}}{dt} = AN_{\upsilon-2} - BN_{\upsilon-1} - AN_{\upsilon-1} + BN_{\upsilon}$$

$$\frac{dN_{\upsilon}}{dt} = AN_{\upsilon-1} - BN_{\upsilon} - AN_{\upsilon} + BN_{\upsilon+1} \tag{2.23}$$

where N_ν is the occupation number for each ν. For $\nu = 0 \rightarrow \nu = 1$

$$\frac{dN_1}{dt} = A_o N_o - B_1 N_1 - AN_1 + BN_2 \tag{2.24}$$

Here N_o is the occupation number for $\nu = 0$, which was expressed as[27]

$$N_o = C_o n_L \tag{2.25}$$

where C_o is the configurational path degeneracy and n_L is the number of stems of width a_o comprising the substrate length L.[27] As another assumption in the LH theory, the crystal growth front shown in Figure 2.8, is divided into several substrates of length L, separated by defects in the crystal structure, Figure 2.11.[27] The existence of a finite substrate length is required for the theory to account for a constant crystal growth rate at high temperatures, in regime I.

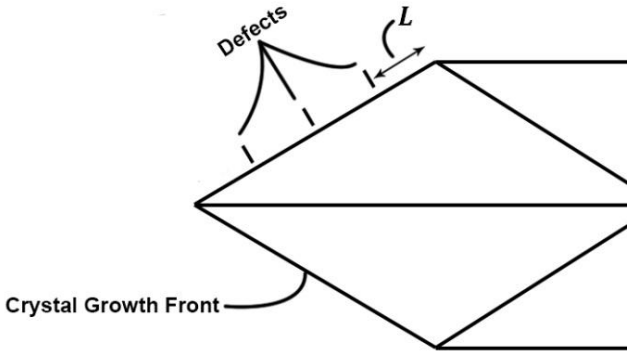

Figure 2.11. Schematic representation of the crystal growth front. The crystal growth front is divided into substrates with average length of L by defects in the crystal structure.

Applying the steady state approximation, $\frac{dN_\upsilon}{dt} = 0$, the flux over each barrier would be

$$S = AN_1 - BN_2 = AN_2 - BN_3 = \cdots = AN_{v-1} - BN_v = AN_v - BN_{v+1} \tag{2.26}$$

Therefore

$$N_{v+1} = \left(\frac{A}{B}\right) N_v - \frac{S}{B} \tag{2.27}$$

$$N_v = \left(\frac{A}{B}\right) N_{v-1} - \frac{S}{B} \tag{2.28}$$

Leading to

$$N_{v+1} = \left(\frac{A}{B}\right)^2 N_{v-1} - \frac{S}{B}\left(1 + \frac{A}{B}\right) = \left(\frac{A}{B}\right)^2 N_{v-1} - \frac{S}{B}\left(\frac{(A/B)^2 - 1}{A/B - 1}\right) \tag{2.29}$$

Generalized into the form of

$$N_{v+1} = \left(\frac{A}{B}\right)^{q+1} N_{v-q} - \frac{S}{B}\left[\frac{(A/B)^{q+1} - 1}{A/B - 1}\right] \tag{2.30}$$

For the case $q = v - 1$ [3]

$$N_{v+1} = \left(\frac{A}{B}\right)^{v} \left[N_1 - \frac{S}{A - B}\right] + \frac{S}{A - B} \tag{2.31}$$

Crystal growth with a constant growth rate requires that $A > B$ under steady-state conditions and that, N_{v+1} remain finite as v potentially becomes very large. Hence, S must be equal to $N_1(A - B)$. Combining this result with $S = A_o N_o - B_1 N_1$ from Equation 2.23, Lauritzen and Hoffman found the flux as[3]

$$S = \frac{N_o A_o (A - B)}{A - B + B_1} \tag{2.32}$$

To find the average initial lamellar thickness and the crystal growth rate, the flux should be integrated over all possible lamellar thicknesses. However, integral of the flux found by Equation 2.32 is non-elementary. To solve this problem, Lauritzen and Hoffman assumed that ψ and β

are the same for the first and subsequent stems (the first condition is already satisfied as I assumed $\psi = 0$) so B would be equal to B_1, and[3]

$$S = N_o A_o \left(1 - \frac{B}{A}\right) \tag{2.33}$$

The flux S was then expressed as a function of the lamellar thickness utilizing the stated rate constants as

$$S(\ell) = N_o \beta \left[\exp\left(-\frac{2b_o \sigma \ell}{kT_c}\right) - \exp\left(\frac{2a_o b_o \sigma_{ec}}{kT_c}\right) \exp\left(-\frac{(2b_o \sigma + a_o b_o \Delta G^{\infty})\ell}{kT_c}\right)\right] \tag{2.34}$$

The net flux over the barrier at T_c is the sum of the fluxes for all possible lamellar thicknesses at T_c, which is given by

$$S_{T_c} = \frac{1}{\ell_u} \int_{\ell_{min}=2\sigma_{ec}/\Delta G^{\infty}}^{\infty} S(\ell) d\ell = \frac{C_o n_L \beta}{\ell_u} \left[\frac{a_o \Delta G^{\infty} kT_c}{2b_o \sigma (2\sigma + a_o \Delta G)}\right] \exp\left(-\frac{4b_o \sigma \sigma_{ec}}{kT_c \Delta G^{\infty}}\right) \tag{2.35}$$

where ℓ_u is the length of the monomer projected along the c-axis of the crystal. The surface nucleation rate, i (in stems per second per meter), was defined as[27]

$$i = S_{T_c}/L = S_{T_c}/a_o n_L \tag{2.36}$$

Therefore

$$i = \frac{C_o \beta}{a_o \ell_u} \left[\frac{a_o \Delta G^{\infty} kT_c}{2b_o \sigma (2\sigma + a_o \Delta G^{\infty})}\right] \exp\left(-\frac{4b_o \sigma \sigma_{ec}}{kT_c \Delta G^{\infty}}\right) \tag{2.37}$$

The average initial lamellar thickness, ℓ_g^*, is the flux weighted average thickness of the lamellae and was calculated as[27]

$$\ell_g^* = \int_{\ell_{min}=2\sigma_{ec}/\Delta G^{\infty}}^{\infty} \ell S(\ell) d\ell \Big/ \int_{\ell_{min}=2\sigma_{ec}/\Delta G^{\infty}}^{\infty} S(\ell) d\ell \tag{2.38}$$

Resulting in

$$\ell_g^* = \frac{2\sigma_{ec}}{\Delta G^\infty} + \frac{kT_c}{2b_o\sigma}\left[\frac{a_o\Delta G^\infty + 4\sigma}{a_o\Delta G^\infty + 2\sigma}\right] = \frac{2\sigma_{ec}T_m^{eq}}{\Delta T\Delta H} + \frac{kT_c}{2b_o\sigma}\left[\frac{a_o\Delta G^\infty + 4\sigma}{a_o\Delta G^\infty + 2\sigma}\right] \quad (2.39)$$

which was rewritten employing Equation 2.8 as

$$\ell_g^* = \ell_{min} + \frac{kT_c}{2b_o\sigma}\left[\frac{a_o\Delta G^\infty + 4\sigma}{a_o\Delta G^\infty + 2\sigma}\right] = \ell_{min} + \delta \quad (2.40)$$

δ for polyethylene is about 10 Å, and is a weak function of temperature.[3, 27] As mentioned before, crystals with thicknesses lower than ℓ_{min} would be thermodynamically unstable. Therefore, the kinetic contribution to the average initial lamellar thickness, δ, makes the lamella stable. The substrate completion rate, g (in meter per second), is obtained by Equation 2.41.[27]

$$g \equiv a_0(A - B) = a_0\beta \exp(-2\, a_0 b_0 \sigma_e / kT)\left[1 - \exp(\frac{-a_0 b_0 \delta \Delta G^\infty}{kT})\right] \quad (2.41)$$

The ratio of g/i determines the mean distance between surface nuclei on the crystal growth front, L_k, Equation 2.42.[27]

$$L_k = \left(\frac{2g}{i}\right)^{1/2} \quad (2.42)$$

The mean distance between surface nuclei governs the crystal growth regime in the LH theory, Figure 2.12.[27] At low undercoolings, regime I, the surface nucleation rate is slow compared to the surface completion rate, therefore, $L_k \gg L$. Under these circumstances, attachment of one stem is sufficient for rapid completion of the substrate, Figure 2.12. The growth rate in regime I is controlled by i and is written as $G_I = b_0 iL$. Note that if the growth front was not divided into a set of substrates lengths L, the growth rate would increase with crystal size in this regime.

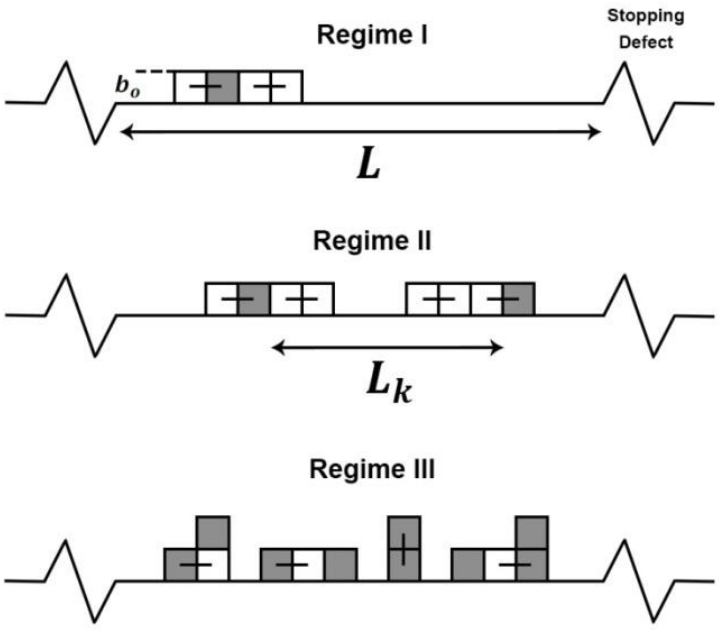

Figure 2.12. Schematic representation of the crystal growth in regime I, II, and III.[27] The surface nuclei are shown in gray.

In the regime II, at intermediate undercoolings, L_k is smaller than L but larger than ca. 2 to 2.5a_o.[27] In this regime, multiple stems are attaching on the surface and completing a crystallized layer together, Figure 2.12. Hence, both i and g determine the growth rate as $G_{II} = b_0(2ig)^{1/2}$.[27] In regime III, at high undercoolings, $L_k \ll L$. Rapid attachment of stems is observed in regime III as surface nucleation is much faster than substrate completion, Figure 2.12. Here, the growth rate is only dependent on i as $G_{III} = b_0 iL'$ where L' is the inter-stem distance in this regime.[27] Regime I to regime II and regime II to regime III transitions occur when $L_k = L$ and $L_k \sim 2a_o$, respectively.[27]

Lauritzen and Hoffman defined the unified growth rate equation, Equation 2.43, by applying Equations 2.37 and 2.42 to the crystal growth rate equations in regime I, II, and III.[26]

$$G = G_o \exp\left(-\frac{Q_d^*}{RT_c}\right)\exp\left(-\frac{K_{gj}}{T_c\Delta T}\right) \tag{2.43}$$

Here the nucleation constant is

$$K_{gj} = \frac{2jb_0\sigma\sigma_{ec}T_m^{eq}}{k\Delta H} \tag{2.44}$$

The constant term in the nucleation constant, j, is equal to 2 in regime I and III and 1 in regime II. Therefore, $K_{gI} = K_{gIII} = 2K_{gII}$.[27] The regime I to regime II and regime II to regime III transition temperatures can be obtained by plotting $\ln G + Q_d^*/RT_c$ versus $1/T_c\,\Delta T$, Figure 2.13. The slope of this plot represents the nucleation constant, K_{gj}, in Equation 2.43.[26] All three regimes of crystal growth are only observed in a few polymers, like polyethylene fractions.[32] The regime I to II transition is reported for poly (ethylene oxide) while the regime II to III transition is seen in polymers like isotactic polypropylene.[33-34]

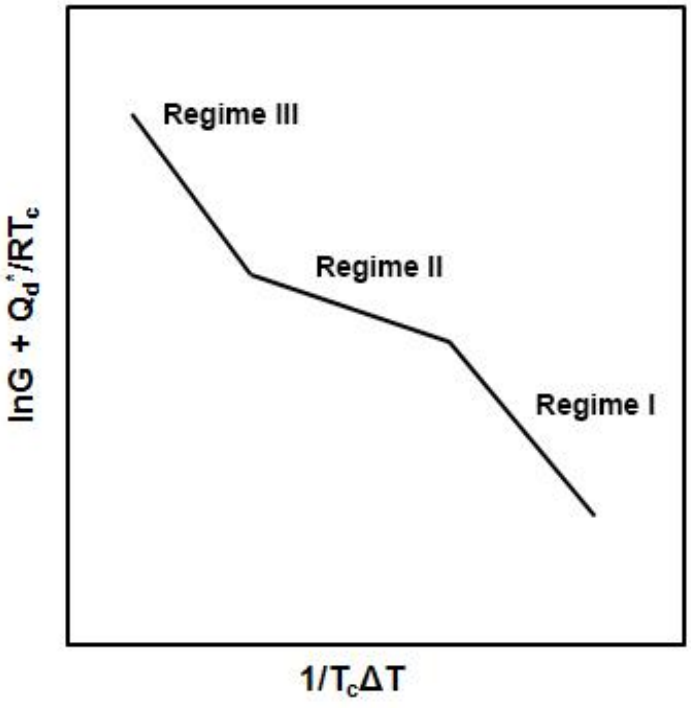

Figure 2.13. Schematic representation of the $\ln G + Q_d^*/RT_c$ versus $1/T_c\,\Delta T$ plot.

Morphological transitions are also seen during regime transitions of a few polymers. Hoffman et al.[35] reported that coarse-grained non-banded spherulites and axialites are formed

during crystallization of polyethylene fractions in regime I and regime II, respectively. Bassett et al.[14] also studied crystallization of polyethylene and stated that rigid sheets are the dominant species in regime I while the S-shape lamellae appear more frequently in regime II. A change in the number of the branches per lamella was observed in different crystallization regimes of cis-polyisoprene.[36]

2.3.2. Strobl's Multi-stage Model

Keller, Hikosaka, Rastogi, Toda, Barham and Goldbeck-Wood introduced the idea of multi-stage crystallization in their work on crystallization of polyethylene at elevated pressures.[37-39] Keller et al. observed that at high enough pressures, P > 3.6 × 10^8 Pa, and temperatures, polyethylene crystals are stable in the highly mobile hexagonal form, which can thicken easily and form lamellae with thicknesses as large as couple microns.[37, 39] By reducing the pressure, polyethylene crystals undergo a transition from hexagonal to orthorhombic. The Ostwald's rule of stages states that a phase transformation will always proceed through stages of metastable states whenever such metastable states exist.[40] Referring to this rule, they concluded that the crystallization of polyethylene at atmospheric pressure under specific conditions might be a multi-stage phenomenon: chains first crystallize in the hexagonal form and then transit to an orthorhombic structure as the lamellae get thicker. To satisfy these conditions, hexagonal crystals should be more stable at smaller thicknesses and grow faster.[38] Using this idea, Strobl further developed the multi-stage crystallization model.[4, 41-44]

In Strobl's multi-stage model, four phases exist: the amorphous melt phase labeled by "am", the crystalline mesomorphic phase labeled by "mes", the initial native crystals labeled by "cn", and the stable crystals labeled by "cs".[41] In the case of polyethylene, the mesomorphic phase is the hexagonal crystal phase, which during isothermal crystallization transforms to the orthorhombic phase at a specific lamellar thickness and forms the initial native crystals.[41] During heating, the initial native crystals melt and recrystallize in the form of stable crystals.[41] To

simplify the phase diagram, we will not talk about the stable crystal phase. Figure 2.14 shows a schematic representation of the phase diagram proposed by Strobl. The mesomorphic to initial native crystal, melt to mesomorphic, and melt to initial native crystal lines intersect at the triple point temperature, T_n.[41]

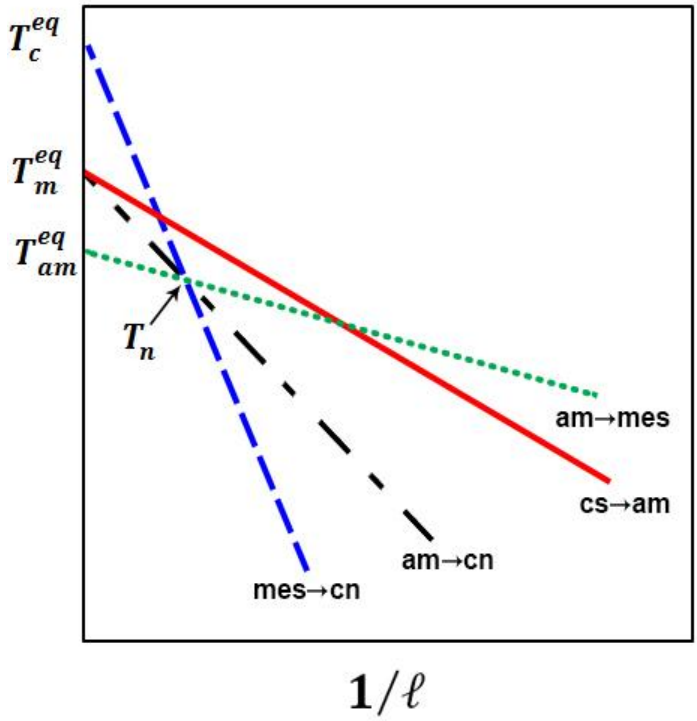

Figure 2.14. Schematic representation of Strobl's phase diagram. Melting (**—**), mesomorphic to initial native crystal (**- -**), melt to mesomorphic (**·····**), and melt to initial native crystal (**- · -**) lines are shown in the picture. T_c^{eq} and T_{am}^{eq} are the equilibrium mesomorphic to native crystals and melt to mesomorphic temperatures, respectively.[41]

Isothermal crystallization in Strobl's model can proceed through two different paths. In path one, at temperatures below the triple point temperature, T_n, the chains first form a mesomorphic phase as this is the stable phase at smaller thicknesses. These crystals will thicken with time and eventually get to the mesomorphic to native crystal line, a thickness were the native crystals are more stable than the mesomorphic phase. At this thickness a

mesomorphic to native crystal transition will occur.[41] Figure 2.15 shows a schematic representation of the crystallization process in path one.

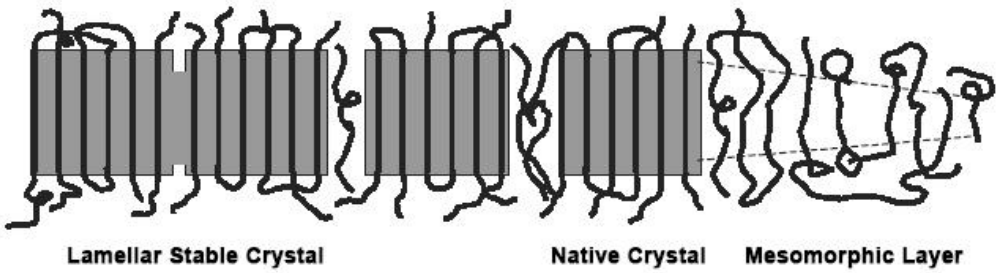

Figure 2.15. Schematic representation of the crystallization process of the polymer chains in path one of Strobl's multi-stage model.[43]

By crystallizing at temperatures above T_n, path two, a single step process from the melt to native crystals will occur as the mesomorphic phase is unstable compared to the native crystals. Under typical crystallization conditions, however, polymers cannot form crystals by this path. Only through the use of special crystallization techniques to lower the crystallization energy barrier, such as self-seeding, crystals can be obtained with the second path.[41]

Initial native crystals are the crystals that can be observed by experimental measurements. Therefore, the mesomorphic to native crystal line from path one and the melt to native crystal line from path two will form the crystallization lines and govern the measurable initial lamellar thicknesses, Equations 2.45 and 2.46.[41]

$$T_c = T_c^{eq}\left[1 - \frac{2\sigma_{ec}^{mc}}{\ell \Delta H^{mc}}\right] \tag{2.45}$$

$$T_c = T_m^{eq}\left[1 - \frac{2\sigma_{ec}^{ac}}{\ell \Delta H^{ac}}\right] \tag{2.46}$$

σ_{ec}^{mc} is the surface free energy of the crystals formed through the mesomorphic to native crystal transition. σ_{ec}^{ac} in Equation 2.46 is the surface free energy of the crystals formed through the melt to native crystal transition.[41] ΔH^{mc} and ΔH^{ac} are the volumetric enthalpy of transition from

the native crystal to the mesomorphic phase and the native crystal to the melt phase, respectively

In Strobl's model chain attachment to the mesomorphic layer is the rate determining step of path one. The thermodynamic minimum thickness of the mesomorphic layer, $\ell_{m,min}$, is calculated by

$$\ell_{m,min} = \frac{2T_{am}^{eq}\sigma_{ec}^{am}}{\Delta H_m\left(T_{am}^{eq} - T_c\right)} \tag{2.47}$$

where σ_{ec}^{am} and ΔH_m are the mesomorphic phase surface free energy and the volumetric enthalpy of fusion of the mesomorphic phase, respectively. As the entropic activation barrier in the chain attachment to the lamella is directly proportional to $\ell_{m,min}$ and the second term in Lauritzen-Hoffman secondary nucleation theory is related to the entropic activation barrier, the growth rate in path one of Strobl's multi-stage model is given by[42, 44]

$$G = G_o \exp\left(-\frac{Q_d^*}{RT_c}\right)\exp\left(-\frac{K_S}{T_{am}^{eq} - T_c}\right) \tag{2.48}$$

where K_S is the nucleation constant in Strobl's model. Differentiating Equation 2.48 respect to the crystallization temperature leads to Equation 2.49.[44]

$$\left(-\frac{d\ln(G/G_o)}{d\,T_c} + \frac{Q_d^*}{RT_c{}^2}\right)^{-1/2} = K_S{}^{-1/2}\left(T_{am}^{eq} - T_c\right) \tag{2.49}$$

By plotting the $\left(-\frac{d\ln(G/G_o)}{d\,T_c} + \frac{Q_d^*}{RT_c{}^2}\right)^{-1/2}$ versus T_c plot values of K_S and T_{am}^{eq} can be found from the slope and the intercept, respectively.[44] T_{am}^{eq} is also known as the zero growth rate temperature, T_{zg}^{S}, in Strobl's multi-stage model.[44] At this temperature, an infinitely large extended chain mesomorphic layer is in equilibrium with the melt. Direct crystallization from the melt cannot happen at temperatures below T_{am}^{eq}.[44]

2.4. References

1. Tervoort, T. A.; Visjager, J.; Smith, P., On abrasive wear of polyethylene. *Macromolecules* **2002,** *35* (22), 8467-8471.
2. Bassett, D. C., *Principles of polymer morphology*. CUP Archive: 1981.
3. Lauritzen Jr, J. I.; Hoffman, J. D., Extension of theory of growth of chain-folded polymer crystals to large undercoolings. *Journal of applied Physics* **1973,** *44* (10), 4340-4352.
4. Strobl, G., Crystallization and melting of bulk polymers: new observations, conclusions and a thermodynamic scheme. *Progress in polymer science* **2006,** *31* (4), 398-442.
5. Sperling, L. H., *Introduction to physical polymer science*. John Wiley & Sons: 2005.
6. Mark, H.; Meyer, K. H., Über den Bau des kristallisierten Anteils der Cellulose II. *Zeitschrift für Physikalische Chemie* **1929,** *2* (1), 115-145.
7. Herrmann, K.; Gerngross, O.; Abitz, W., Zur röntgenographischen Strukturerforschung des Gelatinemicells. *Zeitschrift für Physikalische Chemie* **1930,** *10* (1), 371-394.
8. Keller, A., A note on single crystals in polymers: evidence for a folded chain configuration. *Philosophical Magazine* **1957,** *2* (21), 1171-1175.
9. Bassett, D.; Hodge, A. In *On lamellar organization in certain polyethylene spherulites*, Proceedings of the Royal Society of London A: Mathematical, Physical and Engineering Sciences, The Royal Society: 1978; pp 121-132.
10. Gautam, S.; Balijepalli, S.; Rutledge, G., Molecular simulations of the interlamellar phase in polymers: effect of chain tilt. *Macromolecules* **2000,** *33* (24), 9136-9145.
11. Ungar, G.; Zeng, X.-b., Learning polymer crystallization with the aid of linear, branched and cyclic model compounds. *Chemical reviews* **2001,** *101* (12), 4157-4188.
12. Voigt-Martin, I.; Fischer, E.; Mandelkern, L., Morphology of melt-crystallized linear polyethylene fractions and its dependence on molecular weight and crystallization

temperature. *Journal of Polymer Science Part B: Polymer Physics* **1980,** *18* (12), 2347-2367.

13. Martinez-Salazar, J.; Barham, P.; Keller, A., Studies on polyethylene crystallized at unusually high supercoolings: Fold length, habit, growth rate, epitaxy. *Journal of Polymer Science Part B: Polymer Physics* **1984,** *22* (6), 1085-1096.
14. Bassett, D.; Hodge, A. In *On the morphology of melt-crystallized polyethylene I. Lamellar profiles*, Proceedings of the Royal Society of London A: Mathematical, Physical and Engineering Sciences, The Royal Society: 1981; pp 25-37.
15. Lauritzen, J.; Passaglia, E., Kinetics of crystallization in multicomponent systems: II chain-folded polymer crystals. *J Res Natl Bur Stand. A* **1967,** *71*, 261-75.
16. Hoffman, J.; Lauritzen, J.; Passaglia, E.; Ross, G.; Frolen, L.; Weeks, J., Kinetics of polymer crystallization from solution and the melt. *Colloid & Polymer Science* **1969,** *231* (1), 564-592.
17. Pfefferkorn, D.; Kyerematen, S. O.; Busse, K.; Kammer, H.-W.; Thurn-Albrecht, T.; Kressler, J. r., Crystallization and Melting of Poly (ethylene oxide) in Blends and Diblock Copolymers with Poly (methyl acrylate). *Macromolecules* **2011,** *44* (8), 2953-2963.
18. Sanchez, I.; Eby, R., Thermodynamics and crystallization of random copolymers. *Macromolecules* **1975,** *8* (5), 638-641.
19. Crist, B., Thermodynamics of statistical copolymer melting. *Polymer* **2003,** *44* (16), 4563-4572.
20. Abo el Maaty, M.; Bassett, D.; Olley, R.; Jääskeläinen, P., On cellulation in polyethylene spherulites. *Macromolecules* **1998,** *31* (22), 7800-7805.
21. Gaur, U.; Shu, H. C.; Mehta, A.; Wunderlich, B., Heat capacity and other thermodynamic properties of linear macromolecules. I. Selenium. *Journal of Physical and Chemical Reference Data* **1981,** *10* (1), 89-118.

22. Gaur, U.; Wunderlich, B., Heat capacity and other thermodynamic properties of linear macromolecules. II. Polyethylene. *Journal of Physical and Chemical Reference Data* **1981,** *10* (1), 119-152.
23. Kavesh, S.; Schultz, J., Lamellar and interlamellar structure in melt-crystallized polyethylene. I. Degree of crystallinity, atomic positions, particle size, and lattice disorder of the first and second kinds. *Journal of Polymer Science Part B: Polymer Physics* **1970,** *8* (2), 243-276.
24. Flory, P. J., Theory of crystallization in copolymers. *Transactions of the Faraday Society* **1955,** *51*, 848-857.
25. Sanchez, I. C.; Eby, R., Crystallization of random copolymers. *J Res Natl Bur Stand Sect A* **1973,** *77* (3), 353-358.
26. Hoffman, J. D.; Davis, G. T.; Lauritzen Jr, J. I., The rate of crystallization of linear polymers with chain folding. In *Treatise on solid state chemistry*, Springer: 1976; pp 497-614.
27. Hoffman, J. D.; Miller, R. L., Kinetic of crystallization from the melt and chain folding in polyethylene fractions revisited: theory and experiment. *Polymer* **1997,** *38* (13), 3151-3212.
28. Lambert, W. S.; Phillips, P. J., Crystallization kinetics of low molecular weight fractions of branched polyethylenes. *Macromolecules* **1994,** *27* (13), 3537-3542.
29. Khariwala, D.; Taha, A.; Chum, S.; Hiltner, A.; Baer, E., Crystallization kinetics of some new olefinic block copolymers. *Polymer* **2008,** *49* (5), 1365-1375.
30. Hoffman, J. D.; Miller, R. L.; Marand, H.; Roitman, D. B., Relationship between the lateral surface free energy. sigma. and the chain structure of melt-crystallized polymers. *Macromolecules* **1992,** *25* (8), 2221-2229.
31. Lauritzen, J. I.; Hoffman, J. D., Theory of formation of polymer crystals with folded chains in dilute solution. *J. Res. Natl. Bur. Stand. A* **1960,** *64* (1), 73102.
32. Armistead, J.; Hoffman, J. D., Direct evidence of regimes I, II, and III in linear polyethylene fractions as revealed by spherulite growth rates. *Macromolecules* **2002,** *35* (10), 3895-3913.

33. Ding, N.; Amis, E. J., Kinetics of poly (ethylene oxide) crystallization from solution: Temperature and molecular weight dependence. *Macromolecules* **1991,** *24* (13), 3906-3914.
34. Xu, J.; Srinivas, S.; Marand, H.; Agarwal, P., Equilibrium melting temperature and undercooling dependence of the spherulitic growth rate of isotactic polypropylene. *Macromolecules* **1998,** *31* (23), 8230-8242.
35. Hoffman, J. D.; Frolen, L. J.; Ross, G. S.; Lauritzen, J. I., Growth-rate of spherulites and axialites from melt in polyethylene fractions-regime-1 and regime-2 crystallization. *Journal of Research of the National Bureau of Standards Section a-Physics and Chemistry* **1975,** *79* (6), 671-699.
36. Phillips, P.; Vatansever, N., Regime transitions in fractions of cis-polyisoprene. *Macromolecules* **1987,** *20* (9), 2138-2146.
37. Hikosaka, M.; Tsukijima, K.; Rastogi, S.; Keller, A., Equilibrium triple point pressure and pressure-temperature phase diagram of polyethylene. *Polymer* **1992,** *33* (12), 2502-2507.
38. Keller, A.; Hikosaka, M.; Rastogi, S.; Toda, A.; Barham, P.; Goldbeck-Wood, G., An approach to the formation and growth of new phases with application to polymer crystallization: effect of finite size, metastability, and Ostwald's rule of stages. *Journal of Materials Science* **1994,** *29* (10), 2579-2604.
39. Rastogi, S.; Hikosaka, M.; Kawabata, H.; Keller, A., Role of mobile phases in the crystallization of polyethylene. Part 1. Metastability and lateral growth. *Macromolecules* **1991,** *24* (24), 6384-6391.
40. Ostwald, W., Studien über die Bildung und Umwandlung fester Körper. *Zeitschrift für Physikalische Chemie* **1897,** *22* (1), 289-330.
41. Strobl, G., A thermodynamic multiphase scheme treating polymer crystallization and melting. *The European Physical Journal E: Soft Matter and Biological Physics* **2005,** *18* (3), 295-309.

42. Strobl, G., Colloquium: Laws controlling crystallization and melting in bulk polymers. *Reviews of modern physics* **2009,** *81* (3), 1287.
43. Strobl, G., A multiphase model describing polymer crystallization and melting. *LECTURE NOTES IN PHYSICS-NEW YORK THEN BERLIN-* **2007,** *714*, 481.
44. Cho, T.; Stille, W.; Strobl, G., Zero growth temperature of crystallizing polyethylene. *Macromolecules* **2007,** *40* (7), 2596-2599.

Chapter 3. Investigating the Equilibrium Melting Temperature of Linear Polyethylene Using the Non-Linear Hoffman-Weeks Approach

Hadi Mohammadi, Matthew Vincent and Hervé Marand

3.1. Attribution

Matthew Vincent contributed to this work by conducting the ultra-fast DSC experiments and providing insight on the analysis of the ultra-fast DSC data. Design of the experiments, conventional DSC experiments, and processing and analysis of the data were all performed by Hadi Mohammadi. The paper was prepared by Hadi Mohammadi and Hervé Marand. Matthew Vincent also provided useful comments throughout the review of the paper.

3.2. Abstract

The melting behavior of three linear polyethylene fractions with number average molecular weights of 11, 29, and 100.5 kg/mol was studied as a function of crystallization time with conventional and ultrafast calorimetry. The initial melting temperatures of non-thickened lamellae formed under isothermal conditions over a range of crystallization temperatures were analyzed with the non-linear Hoffman-Weeks method to determine the equilibrium melting temperature. T_m^{eq} values of 138.4 ± 0.9°C, 139.7 ± 0.9°C, and 140.9 ± 0.8°C were estimated for PE 11K, PE 29K, and PE 100K, respectively, in close agreement with those reported in the literature for the melting of extended-chain crystals or with the Gibbs-Thomson analysis. The Lauritzen-Hoffman theory and the non-linear Hoffman-Weeks treatment were modified to account for the effect of the tilt angle, θ, of the crystallized stems of linear polyethylene on the

initial average lamellar thickness. Accuracy of the non-linear Hoffman-Weeks method was examined using initial lamellar thickness, ℓ_g^* , data reported for PE 29K in the literature at different crystallization temperatures. The equilibrium melting temperature obtained by the Gibbs-Thomson approach and the C_2 value extracted from the ℓ_g^* *vs.* $1/\Delta T$ plot were similar within the limits of experimental error to those obtained here through the non-linear Hoffman-Weeks method. Using the Huggins equation, the equilibrium melting temperature of an infinitely long linear polyethylene chain is found to be equal to 141.4 ± 0.8°C, the same value proposed by Wunderlich.

3.3. Introduction

Many research groups have studied the crystallization and melting of linear polyethylene (LPE) under quiescent conditions.[1-5] The first step in the analysis of crystallization kinetics data for any polymer consists of determining the equilibrium melting temperature, T_m^{eq}, for the relevant crystal phase, as this is the reference temperature from which the undercooling, that is, the crystallization driving force, is determined.[6] The equilibrium melting temperature is the temperature at which an infinitely large and perfect extended-chain crystal is in equilibrium with the melt. Determination of an accurate T_m^{eq} value for LPEs has been a point of intense controversy for more than five decades.[6-14] To understand why this is so, one must recall that the morphology of semi-crystalline polymers is controlled by kinetic factors.[6, 15] In the case of linear polyethylene, its quiescent isothermal crystallization will only take place on a reasonable time scale using conventional techniques, if it is carried out in the 120-130°C temperature range, depending on molecular weight.[16-17] Under these conditions, crystallization yields thin, metastable, chain-folded, lamellar crystals, not the equilibrium, infinitely large, extended-chain crystals.[1, 15, 18-19] As a result, T_m^{eq} is typically estimated by one of two common extrapolative methods:[6] 1) the Gibbs-Thomson thermodynamic approach,[6, 14, 20-22] which makes use of a

correlation between the thickness and the melting temperature of lamellar crystals and 2) the Hoffman-Weeks method,[23-24] which describes the correlation between crystallization and melting temperatures. Linear polyethylene is somewhat unique in the sense that the T_m^{eq} value for its orthorhombic crystal phase can also be estimated by two other techniques. First, theoretical approaches have been used by Broadhurst[7] and Flory-Vrij[8-9] to estimate the equilibrium melting temperature of crystals of high molecular weight linear polyethylene by extrapolation of the melting data of normal paraffin crystals. Second, Bassett et al.[15, 25-26] have shown that one can make use of the exceptionally high segmental mobility in the hexagonal crystal phase of LPE formed under high pressure to prepare micrometer-size, extended-chain, orthorhombic crystals. Wunderlich et al.[10, 13] showed that the melting temperature of such crystals provides an excellent estimate of the equilibrium melting temperature for the orthorhombic phase. From the standpoint of theory, linear polyethylene is, therefore, an unique material that should allow its equilibrium melting temperature to be determined unequivocally by a number of methods. The mere fact that the determination of LPE's equilibrium melting has been controversial is an indication that some of the experimental methods used in its determination need to be scrutinized further.

In this publication, we first justify the use of the non-linear Hoffman-Weeks treatment,[27] reminding the reader of the many reasons why its linear counterpart[23-24] is not supported by theory and observations. Then, we discuss melting data obtained, using both conventional and ultra-fast chip calorimeters, for three LPE fractions crystallized isothermally at different temperatures over a range of crystallization times. We considered the sample mass, crystallization time and heating rate dependences of the calorimetric data to minimize annealing and melting-recrystallization-remelting phenomena and account for superheating and thermal lag effects.[13] We extrapolated experimental melting data to zero heating rate, zero crystallinity conditions, and use these extrapolated melting temperatures in the context of the non-linear

Hoffman-Weeks method[27] to determine the equilibrium melting temperature for three LPE fractions. Results of the present studies show that there is perfect agreement between the equilibrium melting temperature estimates obtained using extended-chain crystals prepared under high pressure,[10, 13, 28] the Gibbs-Thomson approach,[14, 21-22] the Huggins extrapolation procedure,[7, 29] and the non-linear Hoffman-Weeks method. Finally, the T_m^{eq} values obtained in this work will also be used to rationalize the initial lamellar thickness data obtained by Barham et al.[30] for a linear polyethylene fraction in the context of the Lauritzen-Hoffman (LH) theory and Strobl's multi-stage model.[3, 5-6]

3.3.1. Justification of the Non-linear Hoffman-Weeks Treatment

Pertinent theoretical aspects of the extrapolative method devised by Hoffman and Weeks[23] for the estimation of T_m^{eq} are discussed in Appendix A. In this method, the melting temperature of a polymer is correlated with its crystallization temperature for samples that are usually crystallized for long times. A linear regression of the observed melting temperature versus crystallization temperature plot is linearly extrapolated to the equilibrium line, $T_m = T_c$, to yield the equilibrium melting temperature.[23]

Observation of linearity in any data set over a narrow range of variables does not enable one to claim that the same linearity should be observed outside this narrow range of variables, unless, of course, such claim is guided by sound theory. The linearity in the Hoffman-Weeks treatment can only be justified if two assumptions are met (see Appendix A): first, given that the slope of a linear Hoffman-Weeks plot is associated with the reciprocal of the lamellar thickening coefficient, every data point in such a plot must be characterized by the same lamellar thickening coefficient,[27, 31] and second, the intercept, C_2, of a plot of ℓ_g^* versus $1/\Delta T$ for the polymer of interest must have a magnitude much smaller than that of the lamellar thickness.[27] Neither of these assumptions is met in practice, as we outline below.

In regard to the constancy of the thickening coefficient, Alamo et al.[31] have demonstrated that both the slope of the T_m *vs.* T_c regression line and the extrapolated equilibrium melting temperature vary systematically with the chosen range of crystallization temperatures and crystallization times. In recent reports, Toda et al.[24, 32] suggested that the linear Hoffman-Weeks treatment can be successfully applied to linear polyethylene. In this study, the crystallization times appeared to be chosen in such a way that primary crystallization was complete. From the approximate linearity of their T_m *vs.* T_c data, and the observation of a slope equal to ½, they conclude that the lamellar thickness doubled before the end of the primary crystallization stage and did so at all temperatures. The constancy of the slope also suggested that further thickening subsequent to the lamellar doubling was either slow or non-existent. This is not the first time a doubling of the lamellar thickness has been suggested to take place during the isothermal melt crystallization of linear polyethylene. Barham et al.[33] proposed that doubling, tripling and even quadrupling of the long spacing took place subsequent to lamellar formation. Studies aimed at reproducing that work were not successful.[34-36] Other evidence provided in support of the doubling in lamellar thickness is based on slow heating studies of solution crystallized ultra-high molar mass linear polyethylene single crystal mats.[37] The lamellar thickness doubling mechanism invoked by Rastogi et al.[37] for single crystal mats requires highly regular fold surfaces and adjacent reentry folding, an unlikely situation for crystallization from the melt, especially at moderate to high undercooling. Finally, the lamellar doubling mechanism was only observed during slow heating, never under isothermal conditions. Hence, the claim of an instantaneous doubling in lamellar thickness during isothermal melt crystallization without subsequent isothermal thickening does not appear to be supported by previous work in the case of linear polyethylene. The doubling in lamellar thickness at an early stage of primary crystallization followed by an invariance of the lamellar thickness at later times is also inconsistent with a number of Raman, transmission electron microscopy and small angle X-ray scattering (SAXS) studies that have unequivocally proven the existence of a continuous lamellar

thickening process occurring at higher rate at higher temperature.[34-36, 38-43] Hence, to ensure that all samples in a Hoffman-Weeks plot are characterized by the same thickening coefficient, γ, the crystallization times at successive crystallization temperatures must be very carefully adjusted.

In regard to the magnitude of C_2, experimental values for linear polyethylene are found to be several times larger than δ', the value predicted by the LH theory and thus contribute significantly to the lamellar thickness.[30, 44-48] Similar conclusions have been reported by Jones et al. [49] for isotactic poly(styrene), by Korenaga et al.[50] for poly(oxymethylene), and by Cheng et al.[51] for poly(ethylene oxide).

A number of authors have also shown the linear Hoffman-Weeks approach to be untenable on other grounds. For instance, some have shown that the linear Hoffman-Weeks approach leads to T_m^{eq} values that are much lower than these obtained by other methods.[14, 45, 52] Others, have noticed upon cursory examination of the underlying theory that the linear Hoffman-Weeks equation loses its functionality for initial or non-thickened lamellae (when $\gamma(t_c, T_c)$ = 1), where it simplifies to $T_m = T_c$.[31] In other words, the linear Hoffman-Weeks equation incorrectly suggests that non-thickened lamellae are always in equilibrium with the melt. Finally, we shall see that the intrinsic non-linearity between crystallization and melting temperatures sheds light on the discrepancy[3, 14, 46, 53-54] between the fold surface free energy obtained from a Gibbs-Thomson analysis (σ_{em}) and that determined from spherulite growth rate data (σ_{ec})[12, 17, 21, 27].

Large C_2 values can be rationalized in the context of the Lauritzen and Passaglia (LP) model,[55] which introduced the concept of stem-length fluctuation in the framework of the LH theory. Fluctuations in the stem length lead to the formation of a fold surface exhibiting a temperature-dependent roughness and, hence, a temperature dependent fold-surface energy, σ_{ec}. In the LP model, the quantity C_2 is expressed as the sum of δ, the thickness increment above the minimum thermodynamically stable lamellar thickness (kinetic stabilization) and a

term accounting for the dependence of fold surface energy.[27, 45, 48, 53, 55] We show in the Appendix A that large values of C_2 lead to a non-linear relationship between T_m and T_c even in the absence of thickening effects. A similar conclusion was reached by Huseby and Bair[45] for crystallization of LPE from solution.

The non-linear Hoffman-Weeks method[27] is expected to yield a better estimate of the equilibrium melting temperature because it accounts more accurately for the dependence of the lamellar thickness on undercooling. However, its application to linear polyethylene crystals requires first a slight adjustment to account for the existence of chain tilt.[15, 18-19, 56] Revision of the LH theory to account for the effect of chain tilt on the initial average lamellar thickness expression, followed by brief derivations of the linear and non-linear Hoffman-Weeks equations are given in the Appendix A.

3.4. Experimental

3.4.1. Experimental Strategy

To obtain the melting temperature of initial non-thickened lamellae, we first recorded the melting of samples crystallized at different temperatures for various crystallization times using a TA Instruments Q2000 conventional DSC and a Mettler-Toledo Flash™ DSC 1 operated over a range of heating rates. The initial melting temperature was defined as the melting temperature of samples exhibiting the lowest observable crystallinity since under these conditions the melting temperature is approximately independent of crystallization time. The initial melting temperature needed to be corrected for the effects of instrument thermal lag and melting kinetics, which become more prevalent at higher heating rates. Other thermal lag effects, such as those associated with the mass/thickness of the chosen samples, were minimized with the use of sufficiently thin films.[57-59] To eliminate the former non-equilibrium effects, the melting

temperature of initial lamellae was measured at various heating rates and extrapolated to zero heating rate using a fitting equation suggested by Toda et al.[59] Heating rates in excess of 70°C/min in conventional DSC experiments were chosen (conservatively) to ensure that annealing and melting-recrystallization-remelting phenomena would not occur during heating of linear polyethylene.[24, 54, 60-61] Since the shape of a melting peak is affected by the ratio of the relaxation time to the response time of a sample during heating in the calorimeter, melting experiments were performed with metal standards in each instrument to study the heating rate dependence of response and relaxation times.[57] From these studies we concluded that for heating rates between 70 and 110°C/min for the conventional DSC and between 1000 and 10000°C/s for the Flash™ DSC 1, the shape of the DSC trace, as characterized by the ratio of relaxation to response times, was independent of the heating rate. The Flash™ DSC 1 results obtained in this work were used to confirm the reliability of the more precise conventional DSC results.

3.4.2. Sample Preparation

Three narrow molecular weight linear polyethylene samples with M_n = 11.4, 28.9, and 100.5 kg/mol and corresponding M_w/M_n of 1.19, 1.11, and 1.11 (SRM 1482, 1483, and 1484, respectively) were obtained from NIST and used as received. The samples are coded as PE 11K, PE 29K and PE 100K, respectively. The films used in these experiments were prepared using a Carver laboratory press operated at 150°C under a nitrogen atmosphere.

Thermal lag studies for the conventional DSC were carried out following the melting of a small piece of Indium (mass less than 0.1 mg) sandwiched between two PE 100K films.[57] Our results indicate that Indium and Indium sandwiched between two 50 μm thick PE films had the same melting temperature in the range of heating rates between 70 and 110°C/min.[57] Similar experiments carried out with significantly thicker (e.g. 1 mm thick PE films) showed systematic

deviations between the Indium sandwich and the Indium standard.[57] All conventional DSC studies discussed here used 50 μm thick PE films with average mass of about 1.5 mg.

Linear polyethylene films used in the Flash™ DSC were first prepared with a thickness of 1 mm and cut into 1×1×1 mm^3 specimens. 1 μm thick samples were cut from such specimens using a Leica RMC Cryo-Ultramicrotome operated at -110°C. Previous experiments by Toda et al.[24] indicated that temperature gradients in such samples were minimized even for heating rates as high as 10000°C/s. Cryomicrotomed films were subsequently immersed in 60/40 wt/wt % DMSO/Water mixture at -60°C. After washing with deionized water, these samples were left to dry in a vacuum oven at room temperature for a week. Samples were then cut to smaller pieces (ca. 10 ng estimated from their volume and density[59]) and placed carefully on the Flash™ DSC 1 UFS1 microchip using an eyelash.

3.4.3. DSC Calibration

The conventional DSC experiments were carried out in sealed Tzero pans in the TA Instruments Q2000 DSC under a dry nitrogen flow of 50 mL/min. Thermal calibration during heating was performed with indium, tin, and zinc standards using TA Instruments' calibration wizard.

All Flash™ DSC 1 experiments were carried out under a dry nitrogen flow of 15 mL/min with the sample support temperature at -100°C. Temperature calibration was performed on each chip as chips differ slightly from one another. Since the indium and linear polyethylene melting peaks interfere at high heating rates, tin was chosen as the calibration standard for the Flash™ DSC 1 chips. During calibration, a small piece of tin was positioned on top of the polyethylene sample. Our experiments revealed that the chip calibration was stable over repeated heating and cooling cycles. Therefore, the calibration procedure was completed after collecting all polymer crystallization and melting data in order to avoid measurement errors due to possible confinement effects caused by the calibration standard. The mass (ca. 10 ng) of the Tin

standard was estimated from the heat of fusion measurement at a heating rate of 3000°C/s. These experiments were repeated three times for each standard. The onset melting temperature of the Tin standard was measured at different heating rates varying from 1000 to 10000°C/s and extrapolated to zero heating rate using Equation 3.1 proposed by Toda et al.[24, 59]

$$T_m = T_m(\mathrm{K} = 0) + \omega_1 \mathrm{K}^z + \omega_2 \mathrm{K} \tag{3.1}$$

where K, ω_1, and ω_2 are the heating rate, and constant prefactors, respectively. The terms $\omega_1 \mathrm{K}^z$ and $\omega_2 \mathrm{K}$ represent the effect of the melting kinetics and the instrumental thermal lag on the melting temperature of the standard, respectively. For polymer samples, the value of z is typically less than or equal to 0.5 depending on the activation barrier for melting.[24] For metal standards, which melt without kinetic effects, z is considered to be the contribution of the latent heat of fusion during melting, and is expected to be near 0.5 for samples with small masses.[24, 58] $T_m(\mathrm{K} = 0)$ is the zero-entropy production melting temperature of the tin standard in the absence of any non-equilibrium effects. Values of $T_m(\mathrm{K} = 0)$ were used for the single-point calibration of the melting temperatures of the linear polyethylene samples for the Flash™ DSC 1 measurements.

3.4.4. DSC Experiments

All calorimetric experiments were initiated by heating the sample to 160°C and holding it at this temperature for 2 minutes to erase prior thermal history. In the conventional DSC, samples were then cooled to specific crystallization temperatures at a rate of 10°C/min and crystallized for various times, t_c. Samples were subsequently melted with a heating rate ranging between 70 and 110°C/min (in increments of 5°C/min) and their peak melting temperature and heat of fusion were recorded. For every crystallization temperature, a baseline heating trace was also recorded for a sufficiently short crystallization time that no crystallinity had time to develop. This baseline was subtracted from the heating trace of partially crystallized samples to minimize the error (less than 1%) in the measured heat of fusion. The lower the degree of crystallinity, the

narrower the breadth of the melting endotherm, the smaller the expected error. For each crystallization temperature, the initial melting temperature, T_m, of non-thickened lamellae is defined as the melting temperature of samples exhibiting the lowest crystallinity, where T_m does not change with time. The zero-entropy production melting temperature of these non-thickened lamellae was obtained for each crystallization temperature by extrapolation to zero heating rate using Equation 3.1.[24, 59]

Similar crystallization and melting procedures were applied to samples studied in the Flash™ DSC 1 with a cooling rate of 1000°C/s and heating rates varying from 1000 to 10000°C/s in increments of 1000°C/s. In contrast with Toda et al.[24] who used non-isothermal melt crystallization, all data reported here was collected for crystallization temperatures where the development of crystallinity could be measured in its entirety under isothermal conditions.

Crystallization temperatures, T_c, were chosen on the low temperature side to ensure that crystallization did not take place during cooling or during subsequent heating prior to melting. On the high temperature side, as is further discussed in the next section, crystallization was limited to temperatures where crystal growth occurs much faster than isothermal lamellar thickening. Under such conditions, the melting temperature is approximately constant at the earliest stages of crystallization. With these limitations in mind, conventional DSC experiments could only span a 3 to 4°C range of crystallization temperature (ca. 121.5°C to 125.5°C), while the fast calorimetry experiments could probe a significantly broader temperature range, ca. 8 to 10°C.

3.5. Results and Discussion

3.5.1. Calorimetric Data

Since the present melting studies were carried out with isothermally melt crystallized LPE samples at rates in excess of 70°C/min, annealing or melting-recrystallization-remelting were easily avoided during heating.[13, 24, 54, 60-61] Figure 3.1 shows the evolution of the melting endotherm recorded with a heating rate of 70°C/min in the conventional calorimeter for PE 29K crystallized for different times at 122.5°C.

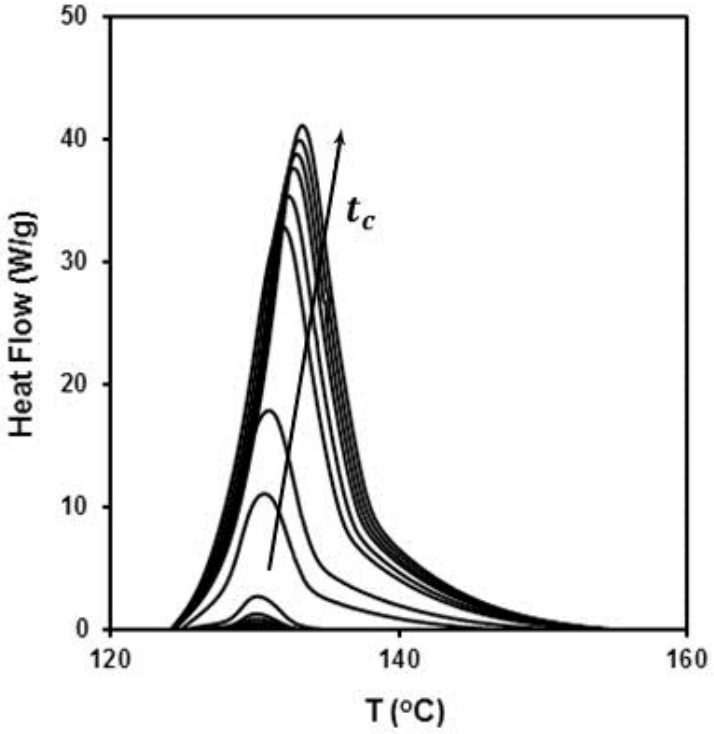

Figure 3.1. Evolution of the melting endotherm for PE 29K crystallized for different times at 122.5°C. Heating traces were recorded in the conventional DSC at a rate of 70°C/min.

As expected, the degree of crystallinity, as inferred from the endotherm area increases with the crystallization time and is accounted for by the nucleation and growth of new lamellae at short crystallization time, along with thickening of old lamellae at later times.[16, 34-36, 39-40]

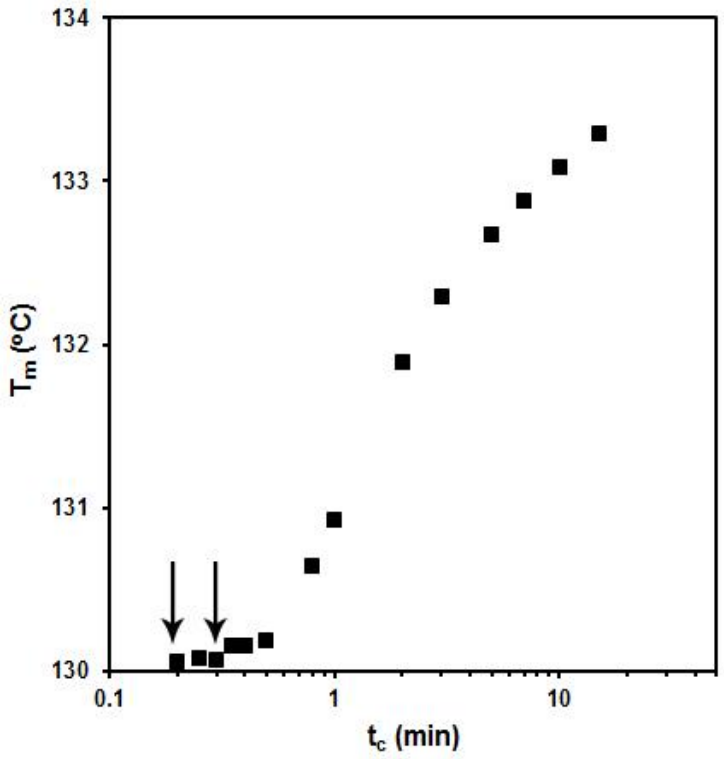

Figure 3.2. Melting temperature *vs.* crystallization time for PE 29K crystallized at 122.5°C. These peak melting temperatures were recorded in the conventional DSC at a rate of 70°C/min. The range of crystallization times used to define the melting temperature of initial non-thickened lamellae is marked by arrows.

The melting temperature (Figure 3.2) and the degree of crystallinity (Figure 3.3) exhibit a sigmoidal increase with logarithm of crystallization time as was previously reported.[16-17] At the earliest stage, lamellae have formed without any restriction and have not had sufficient time to thicken. These lamellae start to thicken after their formation, leading to an increase in the observed melting temperature. The parallel evolution of the degree of crystallinity and melting temperature with time indicates that the increase in lamellar stability is directly correlated with the "age" of the lamella, hence, with the time of its formation.[17]

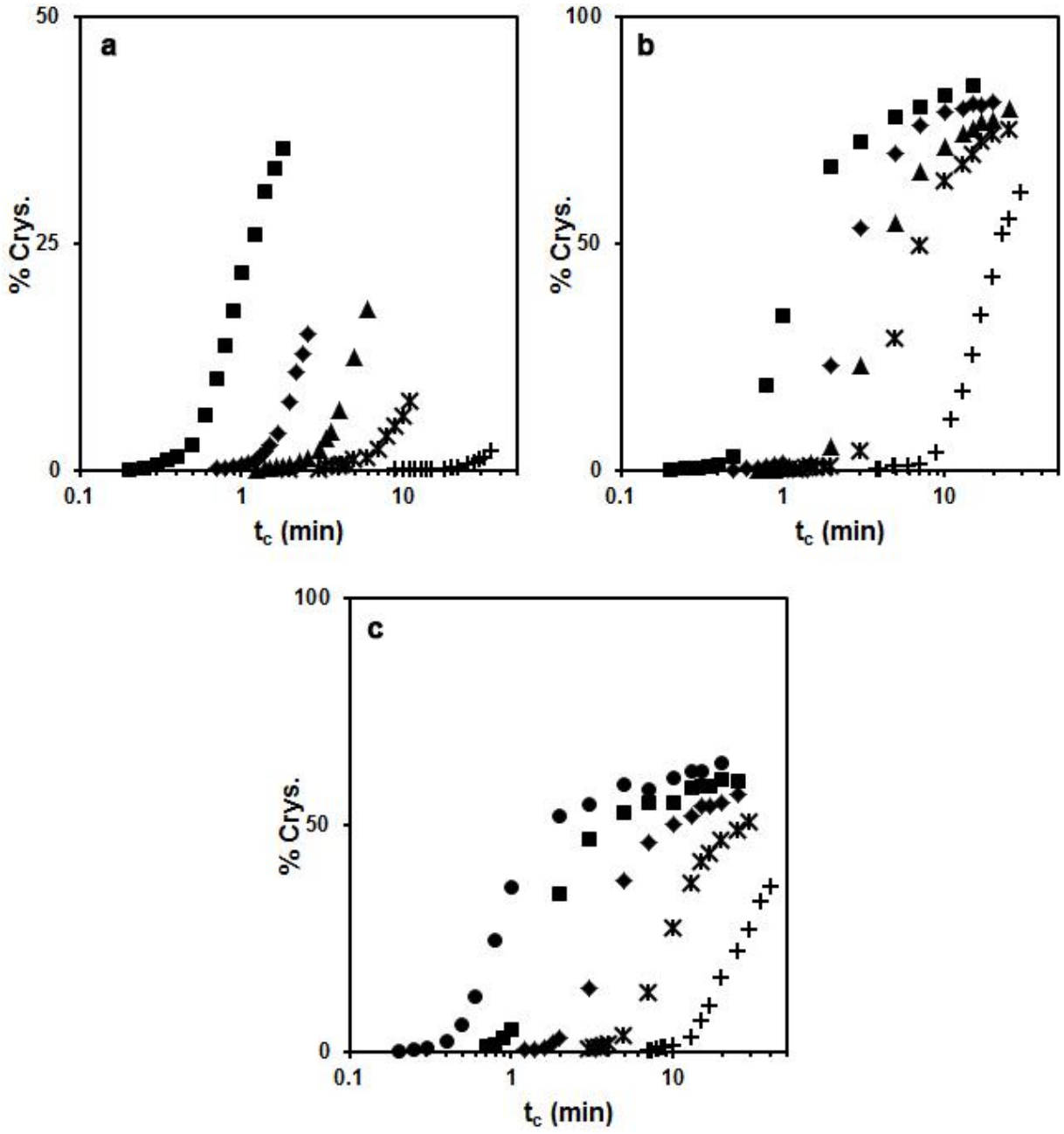

Figure 3.3. Percentage crystallinity *vs.* crystallization time for (a) PE 11K crystallized at 122.5(■), 123.5(♦), 124.0(▲), 124.5 (*) and 125.5°C (+), (b) PE 29K crystallized at 122.5(■), 123.5(♦), 124.0(▲), 124.5 (*) and 125.5°C (+) and (c) PE100K crystallized at 121.5(●), 122.5(■), 123.5(♦), 124.5 (*) and 125.5°C (+).The percentage of crystallinity was calculated using the value[3] of 293 J/g for the heat of fusion from conventional DSC traces recorded at a rate of 70°C/min.

A similar observation of parallel increase in melting temperature and degree of crystallinity with time is made for LPE fractions crystallized in the Flash™ DSC 1 and heated at a rate of 1000°C/s, Figures 3.4 and 3.5. Absolute values of the enthalpy of fusion and their corresponding degree of crystallinity were not obtained for samples melted in the Flash™ DSC 1 calorimeter since the heat flow rate was not calibrated. To provide a qualitative description of the evolution of the crystallization process, we plotted the ratio of the enthalpy of fusion after crystallization for time t_c over the maximum enthalpy of fusion observed after very long times *vs.* the crystallization time. The time scale over which changes are observed in the Flash™ DSC 1 was much shorter than that characteristic of the conventional DSC, possibly a consequence of enhanced nucleation effects.

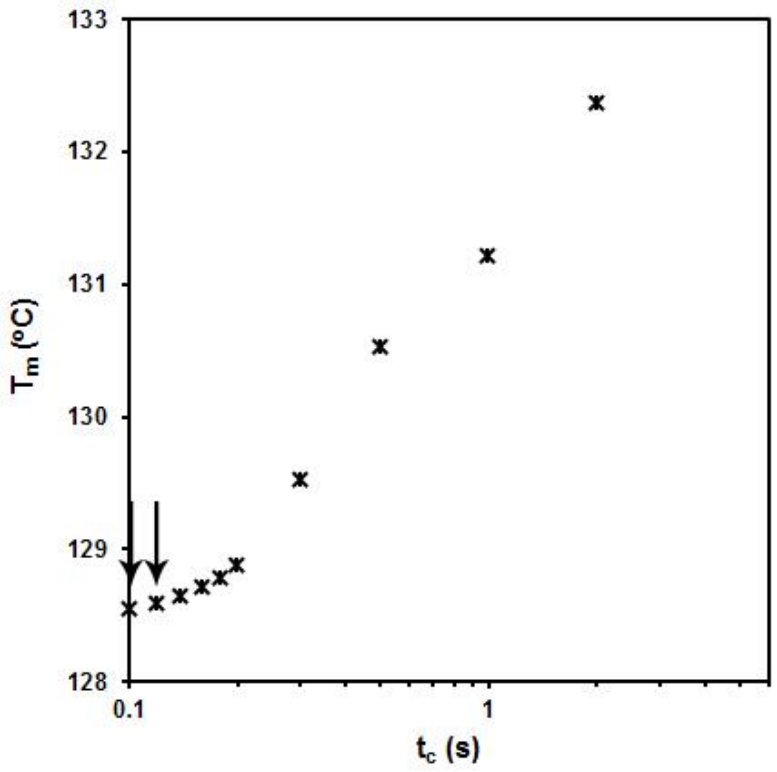

Figure 3.4. Melting temperature *vs.* crystallization time for PE 29K crystallized at 114.3°C. These peak melting temperatures were recorded in the Flash™ DSC 1 at a rate of 1000°C/s. The range of crystallization times used to define the melting temperature of initial non-thickened lamellae is marked by arrows.

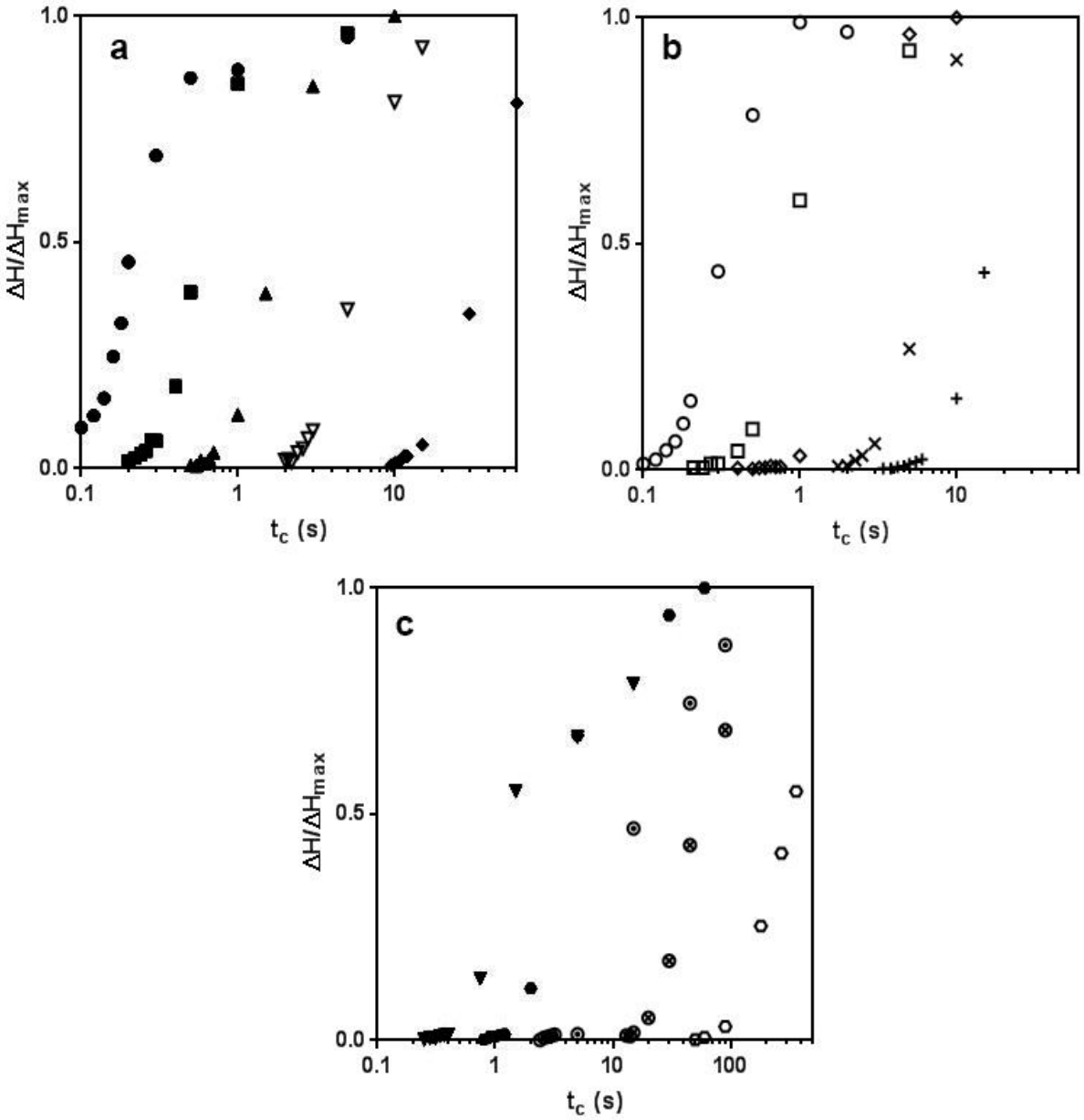

Figure 3.5. $\Delta H/\Delta H_{max}$ *vs.* crystallization time for (a) PE 11K crystallized at 116.1 (●), 118.1 (■), 120.1 (▲),122.1 (▽) and 124.1°C (♦) , (b) PE 29K crystallized at 114.3 (○), 116.3 (□), 118.3 (◊), 120.3 (×) and 122.3°C (+) and (c) PE 100K crystallized at 114.5 (▼), 116.5 (⬣), 118.5 (⊛), 120.5 (⊗) and 122.5°C (⭘) . Flash™ DSC 1 melting data were recorded at a rate of 1000°C/s.

Examination of Figures 3.2 and 3.4 show that the melting temperature increases steadily with time at long crystallization time with no apparent plateau. A similar observation was reported earlier by Marand et al.[17] for linear polyethylene and by Huang et al.[62] for low styrene

content ethylene-styrene copolymers, which is consistent with the continuous isothermal lamellar thickening mechanism[63] evidenced using Raman scattering by Stack et al.,[40] transmission electron microscopy imaging by Voigt-Martin et al.[41] and x-ray scattering by Fischer et al.[64] None of the above studies on melt crystallized LPE support the lamellar doubling mechanism proposed for stacked single crystals.[37]

The melting temperature of initial or non-thickened lamellae was defined at each crystallization temperature for a specific heating rate as the peak melting temperature for crystallization times associated with the very low crystallinity region where no significant thickening is observed (marked by arrows in Figures 3.2 and 3.4). Under these conditions the melting temperature, while dependent on heating rate, was approximately independent of time. Since high heating rates were used in these measurements, a proper account of the associated superheating was necessary. Figure 3.6 shows the increase in melting temperature with increase in heating rate (from 70^{o}C/min to 110^{o}C/min in increments of 5^{o}C/min) for PE 100K crystallized at 121.5^{o}C for 30 s in the conventional DSC.

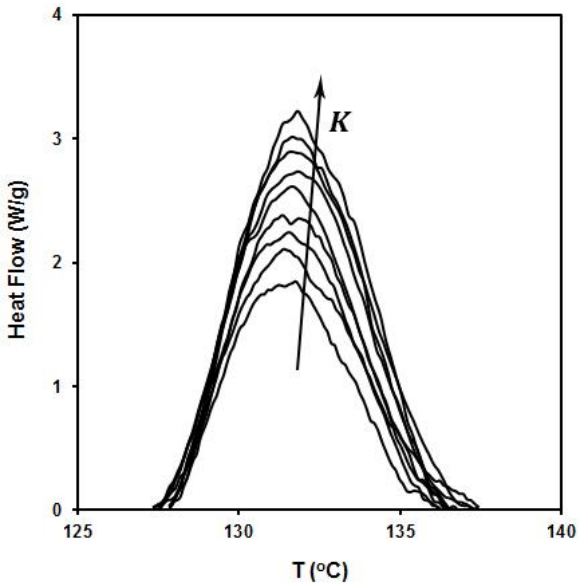

Figure 3.6. Evolution of the melting endotherm for PE 100K crystallized in the conventional DSC at 121.5^{o}C for 30 s. Heating traces were recorded at rates varying from 70^{o}C/min to 110^{o}C/min in increments of 5^{o}C/min.

Initial melting temperatures were corrected for the effect of instrumental thermal lag using the thermal lag constant ($\omega_2 \times 10^3$ = 5.1 ± 0.1 min) determined from the slope of a plot of Indium melting temperature *vs.* heating rate. Figure 3.7 shows the changes in the thermal lag corrected initial melting temperature *vs.* square root of heating rate for the three fractions crystallized isothermally at different temperatures in the conventional DSC.

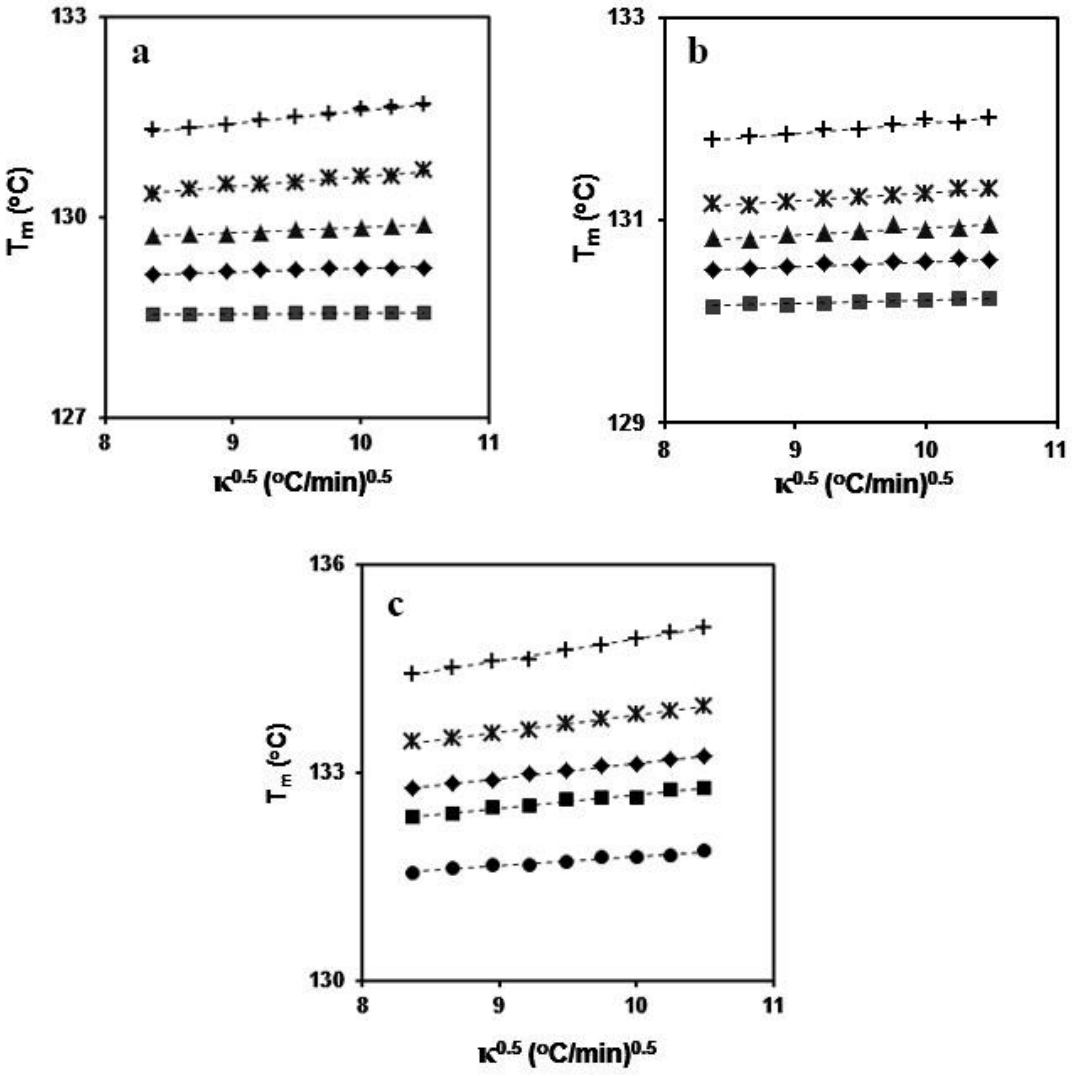

Figure 3.7. Melting temperature in the conventional DSC versus $K^{0.5}$ for non-thickened lamellae of: (a) PE 11K crystallized at 122.5(■), 123.5(♦), 124.0(▲), 124.5 (*) and 125.5°C (+), (b) PE 29K crystallized at 122.5(■), 123.5(♦), 124.0(▲), 124.5 (*) and 125.5°C (+), and (c) PE 100K crystallized at 121.5(●), 122.5(■), 123.5(♦), 124.5 (*) and 125.5°C (+). The dashed lines represent the best fit of the melting temperature data to Equation 3.1.

As expected from Equation 3.1, the melting temperature, after subtraction of thermal lag effects (term $\omega_2 \mathrm{K}$ in Equation 3.1), increases linearly with the square root of heating rate. Hence, extrapolation of the heating rate dependent initial melting temperature to zero-heating rate was carried out using Toda's equation (Equation 3.1) with z = 0.5, yielding $T_m(\mathrm{K}=0)$ the zero-entropy production melting temperature of initial or non-thickened lamellae at each crystallization temperature (Table 3.1). Our choice of z = 0.5 for the non-thickened lamellae of linear polyethylene was motivated by the discovery of Toda et al.[24] that crystals of low thermal stability undergo melting without an activation barrier. Errors in the $T_m(\mathrm{K}=0)$ and ω_1 values shown in Table 1 were determined through the non-linear least square regression to Equation 3.1. In the model proposed by Toda and Konishi,[59] the value of ω_1 is proportional to $1/z$, thus, should be independent of the crystallization temperature. In contrast, our results show that ω_1 increases with crystallization temperature.

Table 3.1. $T_m(\mathrm{K}=0)$ and ω_1 for non-thickened lamellae at different crystallization temperatures (conventional DSC data, $\omega_2 \times 10^3$ = 5.1 ± 0.1 min)

PE 11K					
T_c (^{o}C)	122.5 ± 0.1	123.5 ± 0.1	124.0 ± 0.1	124.5 ± 0.1	125.5 ± 0.1
$T_m(\mathrm{K}=0)$ (^{o}C)	128.4 ± 0.1	128.7 ± 0.1	129.0 ± 0.1	129.1 ± 0.1	129.7 ± 0.1
$\omega_1 \times 10$ ($[\mathrm{min.K}]^{1/2}$)	0.2 ± 0.1	0.5 ± 0.1	0.8 ± 0.1	1.5 ± 0.1	2.0 ± 0.1
PE 29K					
T_c (^{o}C)	122.5 ± 0.1	123.5 ± 0.1	124.0 ± 0.1	124.5 ± 0.1	125.5 ± 0.1
$T_m(\mathrm{K}=0)$ (^{o}C)	129.9 ± 0.1	130.1 ± 0.1	130.3 ± 0.1	130.5 ± 0.1	130.9 ± 0.1
$\omega_1 \times 10$ ($[\mathrm{min.K}]^{1/2}$)	0.4 ± 0.1	0.5 ± 0.1	0.7 ± 0.1	0.8 ± 0.1	1.0 ± 0.1
PE 100K					
T_c (^{o}C)	121.5 ± 0.1	122.5 ± 0.1	123.5 ± 0.1	124.5 ± 0.1	125.5 ± 0.1
$T_m(\mathrm{K}=0)$ (^{o}C)	130.5 ± 0.1	130.8 ± 0.1	131.0 ± 0.1	131.3 ± 0.1	130.8 ± 0.1
$\omega_1 \times 10$ ($[\mathrm{min.K}]^{1/2}$)	1.3 ± 0.1	1.9 ± 0.1	2.2 ± 0.1	3.5 ± 0.2	3.1 ± 0.1

Toda et al.[24, 58-59] suggest that small and thin samples (thickness less than a couple μm) should be used to minimize the influence of thermal lag on the melting temperature observed in the Flash™ DSC-1. Plots of initial melting temperature vs. $K^{0.5}$ in Figure 3.8 are non-linear with a positive curvature, suggesting the importance of thermal lag effects.

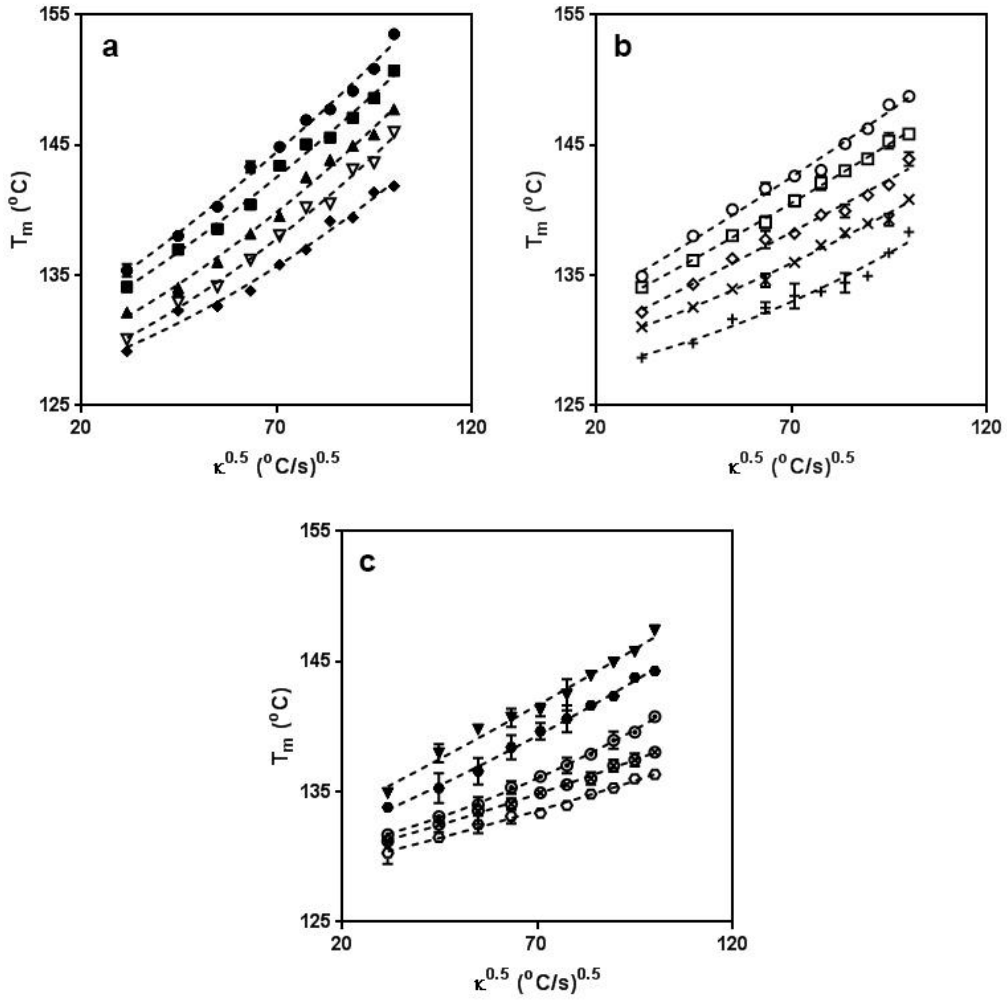

Figure 3.8. Initial melting temperature *vs.* $K^{0.5}$ for: (a) PE 11K crystallized at 116.1 (●), 118.1 (■), 120.1 (▲), 122.1 (▽) and 124.1°C (♦) , (b) PE 29K crystallized at 114.3 (○), 116.3 (□), 118.3 (◊), 120.3 (×) and 122.3°C (+) and (c) PE100K crystallized at 114.5 (▼), 116.5 (⬣), 118.5 (⊙), 120.5 (⊗) and 122.5°C (⊙) (Flash™ DSC 1 data). The dashed lines represent the best fit of the melting temperature data to Equation 3.1.

The existence of thermal lag may be related to the small amount of crystallinity or rather the predominant amorphous character of our samples at short crystallization times. The thermal

conductivity of the amorphous phase in linear polyethylene is about 10 times smaller than that of the crystalline phase.[65-66] As thermal conductivity is inversely proportional to the thermal lag, we expect the low crystallinity samples studied here to be more strongly influenced by thermal lag than the high crystallinity samples studied by Toda et al.[24, 59] In contrast to the conventional DSC data where instrumental thermal lag and melting kinetics effects were accounted for sequentially, the heating rate dependence of initial melting temperatures in the Flash™ DSC 1 was analyzed in a single step through non-linear regression with Equation 3.1 (Figure 3.8). Melting kinetics and thermal lag contributions (coefficients ω_1 and ω_2) as well as zero-entropy production initial melting temperatures, $T_m(\mathrm{K}=0)$, are given in Table 3.2.

Table 3.2. $T_m(\mathrm{K}=0)$, ω_1 and ω_2 for the non-thickened lamellae crystallized isothermally at different crystallization temperatures. These results were obtained using the Flash™ DSC-1.

PE 11K					
T_c (^{o}C)	116.1 ± 0.3	118.1 ± 0.3	120.1 ± 0.3	122.1 ± 0.3	124.1 ± 0.3
$T_m(\mathrm{K}=0)$ (^{o}C)	126.1 ± 1.9	126.0 ± 1.6	127.1 ± 1.7	128.4 ± 1.7	129.0 ± 1.7
$\omega_1 \times 10$ ($[\mathrm{s.K}]^{1/2}$)	0.8 ± 0.6	1.0 ± 0.5	1.3 ± 0.5	1.6 ± 0.05	1.8 ± 0.5
$\omega_2 \times 10^4$ (s)	8.0 ± 4.3	9.2 ± 3.7	8.3 ± 3.9	5.8 ± 3.9	5.8 ± 4.0
PE 29K					
T_c (^{o}C)	114.3 ± 0.2	116.3 ± 0.2	118.3 ± 0.2	120.3 ± 0.2	122.3 ± 0.2
$T_m(\mathrm{K}=0)$ (^{o}C)	126.9 ± 1.8	127.9 ± 0.9	127.7 ± 1.5	129.1 ± 0.6	129.8 ± 1.7
$\omega_1 \times 10$ ($[\mathrm{s.K}]^{1/2}$)	0.4 ± 0.6	0.9 ± 0.3	1.4 ± 0.5	1.5 ± 0.2	1.7 ± 0.5
$\omega_2 \times 10^4$ (s)	6.6 ± 4.3	4.1 ± 2.2	1.0 ± 3.6	1.8 ± 1.5	2.1 ± 4.0
PE 100K					
T_c (^{o}C)	114.5 ± 0.1	116.5 ± 0.1	118.5 ± 0.1	120.5 ± 0.1	122.5 ± 0.1
$T_m(\mathrm{K}=0)$ (^{o}C)	128.2 ± 0.6	128.8 ± 0.4	129.5 ± 0.4	129.7 ± 0.8	130.6 ± 1.6
$\omega_1 \times 10$ ($[\mathrm{s.K}]^{1/2}$)	0.7 ± 0.2	0.7 ± 0.1	0.5 ± 0.1	1.1 ± 0.2	1.5 ± 0.5
$\omega_2 \times 10^4$ (s)	1.6 ± 1.4	2.0 ± 1.0	6.0 ± 1.0	3.3 ± 1.8	1.6 ± 3.8

While ω_1 increases with increasing crystallization temperature, no relation between ω_2 and crystallization temperature is observed. The uncertainties associated with the $T_m(\mathrm{K}=0)$ values measured by the Flash™ DSC 1 are much larger than these estimated from conventional DSC, partly as a result of the very long extrapolation of T_m values to $\mathrm{K}=0$.

3.5.2. Non-Linear Hoffman-Weeks Analysis

Once the initial melting temperatures $T_m(\mathrm{K}=0)$ for non-thickened lamellae formed at different crystallization temperatures are known (Tables 3.1 and 3.2), normalized melting, M, and crystallization, X, temperatures can be calculated for different choices of the equilibrium melting temperature. According to the non-linear Hoffman-Weeks theory, M and X should exhibit a linear relationship with a slope of one when the correct equilibrium melting temperature is used in the calculation of M and X. Figure 3.9 shows the dependence of m, the slope of the $M-X$ plot, on the choice of equilibrium melting temperature for the data collected with the conventional DSC for each of the LPE fractions. Equilibrium melting temperatures of 138.4 ± 0.9°C, 139.7 ± 0.9°C, and 140.9 ± 0.8°C are determined from the condition m = 1 for PE 11K, PE 29K, and PE 100K, respectively. While the error bars on the equilibrium melting temperatures for the three LPE fractions overlap somewhat, the data obtained in this work is consistent with the increase in equilibrium melting temperature with increasing molecular weight, expected on the basis of chain-end effects.[7-9, 29]

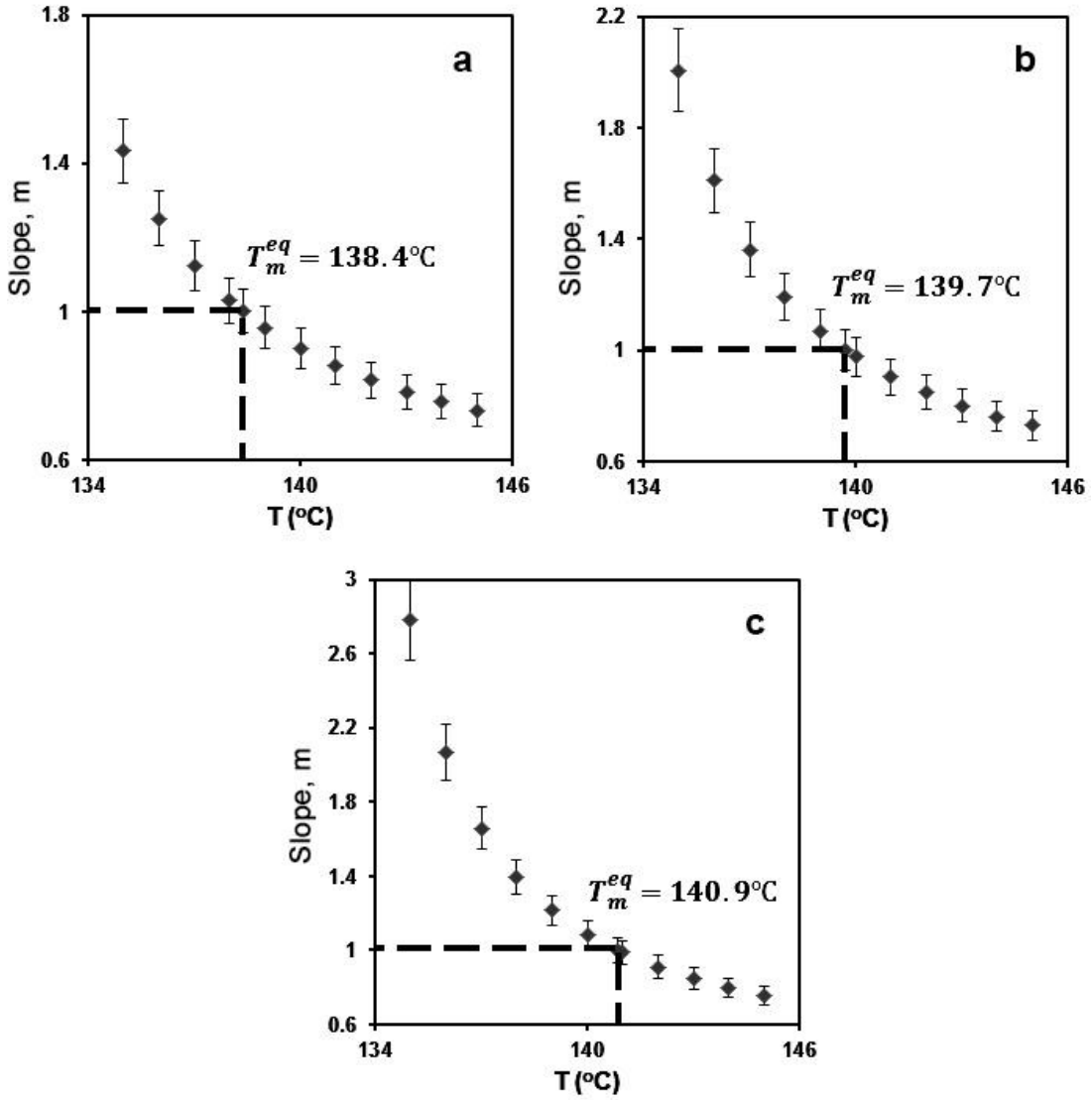

Figure 3.9. Slope m of the $M - X$ plot *vs.* choice for the equilibrium melting temperature for the T_m- T_c data obtained with the conventional DSC: (a) PE 11K, (b) PE 29K, and (c) PE 100K. The true equilibrium melting temperature is obtained when the slope m of the $M - X$ plot is equal to one. Error bars correspond to the 95% confidence interval associated with the linear regression of M *vs.* X.

The $M - X$ plots drawn with the appropriate equilibrium melting temperatures are shown in Figure 3.10, where data obtained from the Flash™ DSC 1 experiments have been added (filled square symbols). Data from the Flash™ DSC 1 experiments superpose quite well on the $M - X$ plot established with data from the conventional DSC data, which is reassuring considering the

very narrow crystallization temperature range probed by conventional DSC. As a consequence of larger error bars, the Flash™ DSC 1 data was not used in the determination of the equilibrium melting temperature for each fraction. The compatibility of Flash™ DSC 1 and conventional DSC data support our assertion that annealing and melting-recrystallization-remelting phenomena were properly avoided in the conventional DSC experiments and heating rate corrections were reliably taken care of in the Flash™ DSC 1 data.

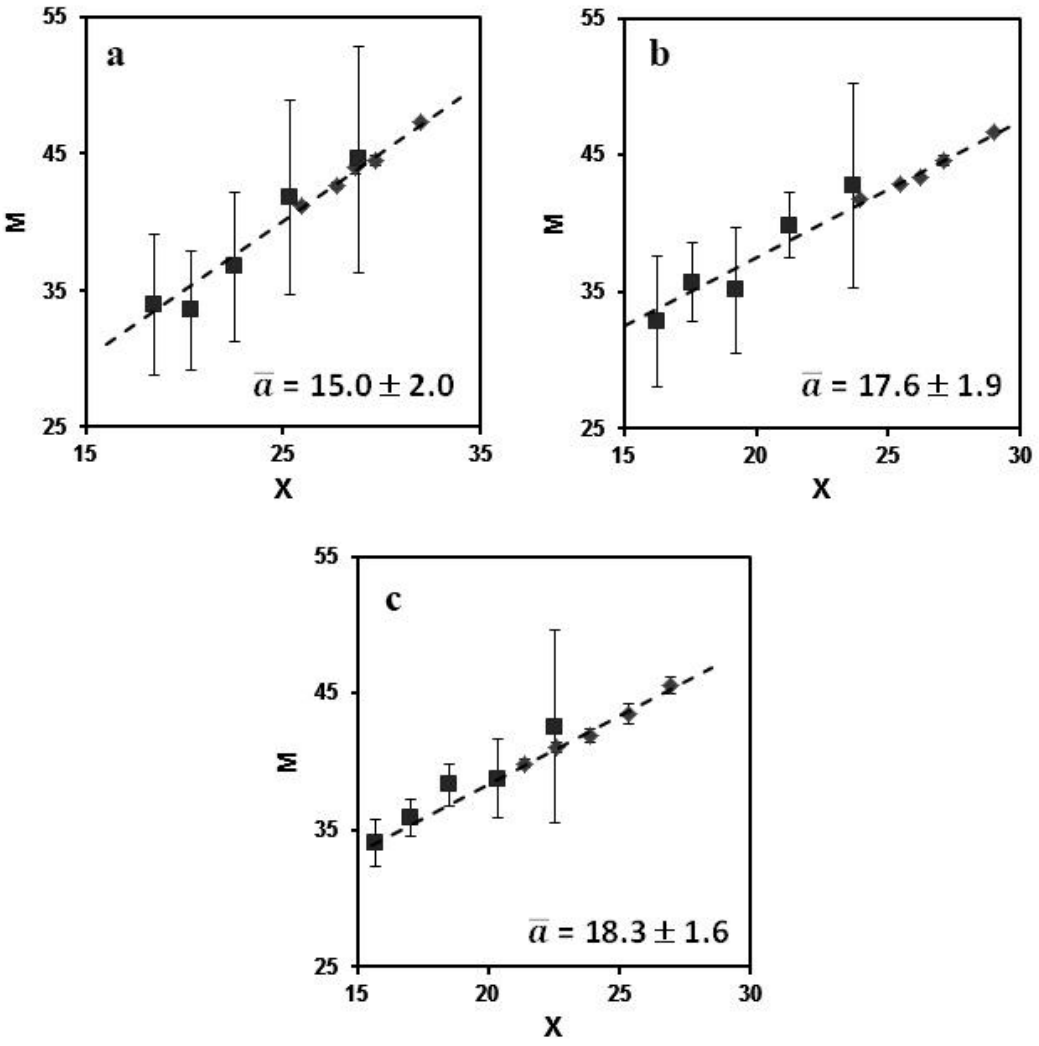

Figure 3.10. *M vs. X* for (a) PE 11K, (b) PE 29K and (c) PE 100K using the data obtained from conventional DSC (♦) and Flash™ DSC 1 (■). The plots were drawn using the equilibrium melting temperature leading to a slope of unity for each $M - X$ plot. Error bars associated with M values arises from the uncertainty in the observed melting temperature.

Our results also suggest that the magnitude of $\bar{a}$, the intercept of the $M - X$ plot (given in Figure 3.10), may be increasing with increasing molecular weight of the LPE fraction. In the Appendix A (Equation A.18), we show that $\bar{a}$ is defined in terms of C_2 and σ_{ec}^o. Analysis of the temperature dependence of spherulite growth rates for LPE fractions[57] suggests that the equilibrium fold surface free energy σ_{ec}^o is independent of molecular weight for molecular weights in the range from 10 to 130 kg/mol. As a result, an increase in $\bar{a}$ would be attributed to the increase of C_2 and therefore, the increase of y (the parameter characterizing the strength of stem length fluctuations) with molecular weight.

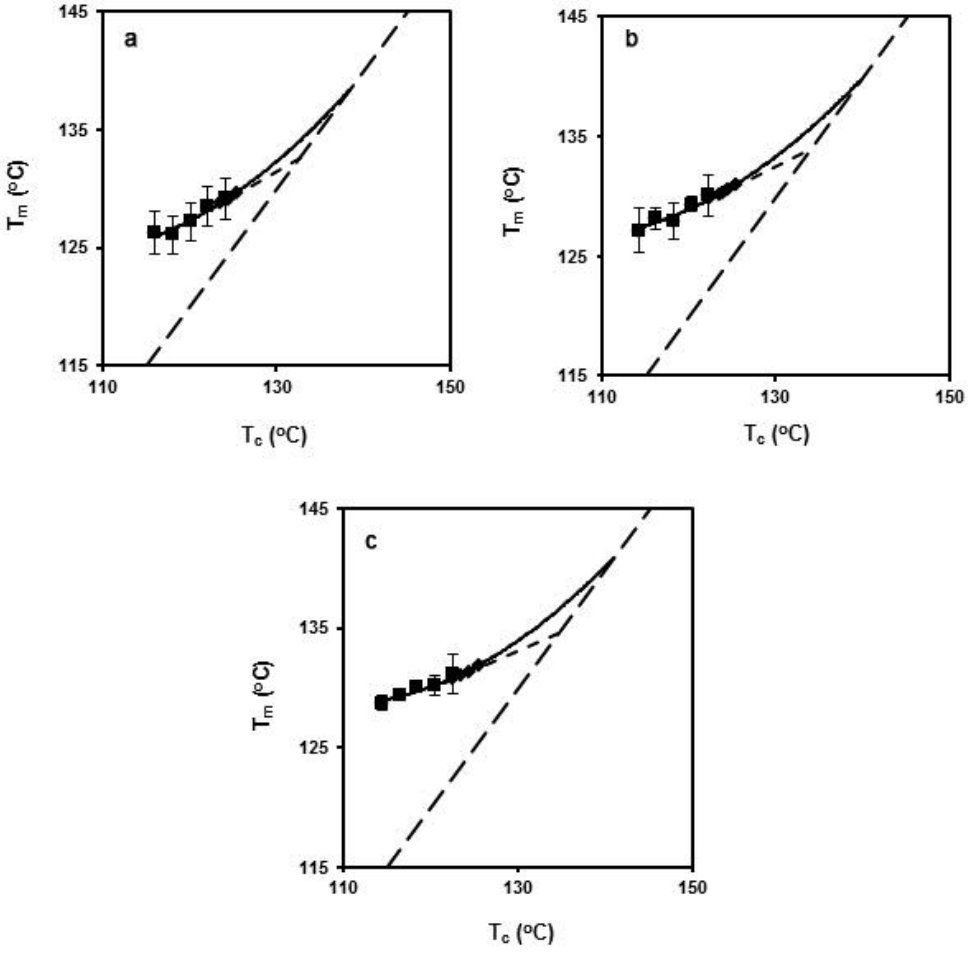

Figure 3.11. T_m *vs.* T_c for (a) PE 11K, (b) PE 29K and (c) PE 100K using the data obtained from conventional DSC (♦) and Flash™ DSC 1 (■). The short dash line and the solid line are the Hoffman-Weeks and the non-linear Hoffman-Weeks extrapolations, respectively. The long dash line is the $T_m = T_c$ line.

On Figure 3.11, we have plotted observed melting vs. crystallization temperatures from conventional and Flash™ DSC 1 experiments for the three narrow molar mass LPE fractions. In each case, the intercept of the regression line with the $T_m = T_c$ line (linear Hoffman-Weeks extrapolation) yields an apparent equilibrium melting temperature that is about 6°C lower than its non-linear counterpart. The apparent equilibrium melting temperatures obtained by the linear Hoffman-Weeks analysis are actually lower than observed melting temperatures reported for LPE in the literature[24] for samples of similar molecular weights.

3.5.3. Comparison of Predictions of T_m^{eq} for LPE by Different Approaches

The T_m^{eq} estimates obtained using the non-linear Hoffman-Weeks method are about 4°C lower than those obtained with the Flory-Vrij equation for linear polyethylene (Figure 3.12).[3] On the other hand, our estimates are very similar to those reported by Wunderlich et al.[10] and Okada et al.[28] for the melting of extended-chain crystals. To obtain the equilibrium melting temperature of an infinitely long polyethylene chain, $T_m^{eq,\infty}$, we used a Huggins equation to fit the equilibrium melting temperature data for short linear alkanes reported by Dirand et al.,[67] the LPE data reported by Wunderlich et al.,[10] Okada et al.,[28] as well as the data obtained here using the non-linear Hoffman-Weeks approach. Figure 3.12 also includes the SAXS data of Cho et al.[22] as analyzed by Crist.[14] This composite dataset spans a very large range of chain lengths ($4 \leq n_n < 41000$, where n_n is the number of backbone carbon atoms per chain). Equation 3.2 shows the parameters associated with the best fit of the experimental data by the Huggins[29] equation:

$$T_m^{eq} = 414.6\ K \left(\frac{n_n - 1.2}{n_n + 5.3}\right) \tag{3.2}$$

Upon examination of Figure 3.12, we can conclude that while both the Flory-Vrij and the Huggins equations provide excellent fits for linear alkanes in the range of n_n = 10 - 100, systematic deviations from the Flory-Vrij[8] equation are observed for very short (n_n < 10) and for

very long (n_n > 200) alkanes. Stack and Mandelkern[11] indicated that a linear polyethylene sample, no matter how well fractionated, cannot satisfy the assumptions made in the Flory-Vrij theory, as its chains do not all have the exact same lengths.

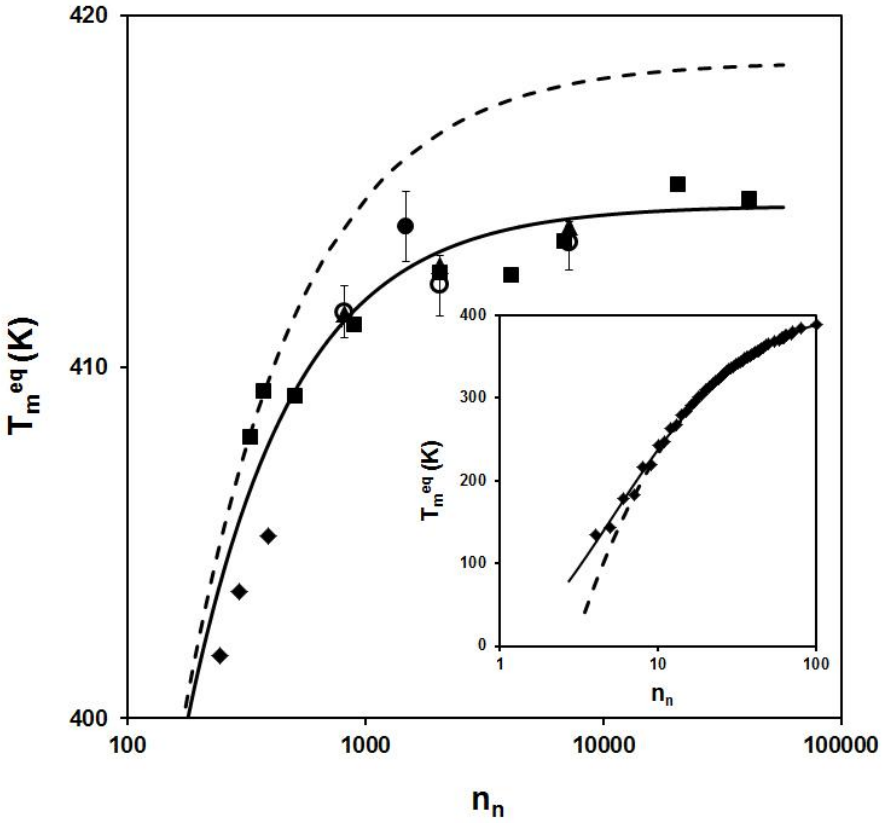

Figure 3.12. Equilibrium melting temperature *vs.* n_n, the number average number of backbone carbon atoms per chain. Data from: Dirand et al.[67] for short alkanes (♦),Wunderlich et al. (■),[10, 13] and Okada et al. (▲),[28] for extended-chain crystals, Cho et al.[22] analyzed by Crist[14] using the Gibbs-Thomson method (●) and the present work using the non-linear Hoffman-Weeks approach (○). The solid line shows the best fit to the experimental results with a Huggins equation while the dash line represents the prediction from the Flory-Vrij equation. The inner plot shows the data and associated fits for short alkanes.

They concluded that since pairing of chain ends could not be expected in non-monodisperse linear polyethylenes, the Flory-Vrij equation should not be used for estimation of their equilibrium melting temperature. Mandelkern et al.[12] later realized that premelting takes place in

crystals of short linear alkanes (n > 50) some 30 to 40°C below their equilibrium melting temperature. They concluded that since layers containing chain ends disorganize during the premelting process, the Flory-Vrij equation may only be appropriate for short linear alkanes (n > 50) where the effect of premelting is negligible. Our results suggest that the Huggins equation can fit data from alkanes to high molecular weight polyethylenes.

Equation 3.2 also indicates that $T_m^{eq,\infty}$, the equilibrium melting temperature of an infinitely long linear polyethylene chain is equal to 141.4 ± 0.8°C, the same value proposed by Wunderlich and Czornyj.[10] The $T_m^{eq,\infty}$ reported by Flory and Vrij[8] is 4.1°C higher than the value obtained in this work. Many analyses of the temperature dependence of the lamellar thickness or of the spherulite growth rate rely on the Flory-Vrij predictions when equilibrium melting temperatures are not available for the material studied.[3, 68] While a 4.1°C difference may seem trivial, it has a significant effect on the analysis of the crystal growth kinetics of linear polyethylene. As the polyethylene crystallization is studied at low undercooling, a change in the equilibrium melting temperature by few degrees leads to a significant change in the magnitude of the undercooling where crystal growth rates are measured. This difference will also affect the analysis of the molecular weight dependence of crystal growth rates.[57]

3.5.4. Analysis of Lamellar Thickness Data and Phase Diagram

Using longitudinal acoustic mode (LAM) Raman scattering measurements, Barham et al.[30] determined the initial stem length, $\mathcal{L}_g^*$, of PE 29K crystallized from the melt under isothermal conditions with or without self-seeding before quenching in water prior to the measurements. We reanalyzed Barham's data using the crystal modulus of 295 GPa recommended for LPE by Strobl et al.[69] and Hocquet et al.[44, 70] The crystalline stem length, $\mathcal{L}$, in melt crystallized linear polyethylene crystals is related to the lamellar thickness, ℓ, in polyethylene lamellae by the tilt angle θ = 35°,[1, 19, 71-74] (see Appendix A). The plot of initial crystalline lamella thickness, ℓ_g^* *vs*. $1/\Delta T$, where each undercooling is calculated using T_m^{eq} = 139.7°C determined here for PE 29K

is shown on Figure 3.13. A linear relationship between ℓ_g^* and $1/\Delta T$ is observed for this data over a wide range of crystallization temperatures (85°C to 128°C) covering all three regimes of crystal growth in PE 29K, and confirms that for melt crystallized LPE the tilt angle, θ, is approximately independent of crystallization temperature. Using Equations A.14 in the Appendix A, we calculated σ_{ec}^o = 45.5 ± 2.0 erg/cm^2 and C_2 = 4.4 ± 0.4 nm from the slope and intercept of the ℓ_g^* versus $1/\Delta T$ plot for PE 29K. Upon reanalysis of the Gibbs-Thomson plot reported by Cho et al.,[15] Crist[6] reported σ_{em} = 44 ± 5 erg/cm^2, for a melt crystallized linear polyethylene sample (M_n = 21 kg/mol, M_w/M_n = 2.9).

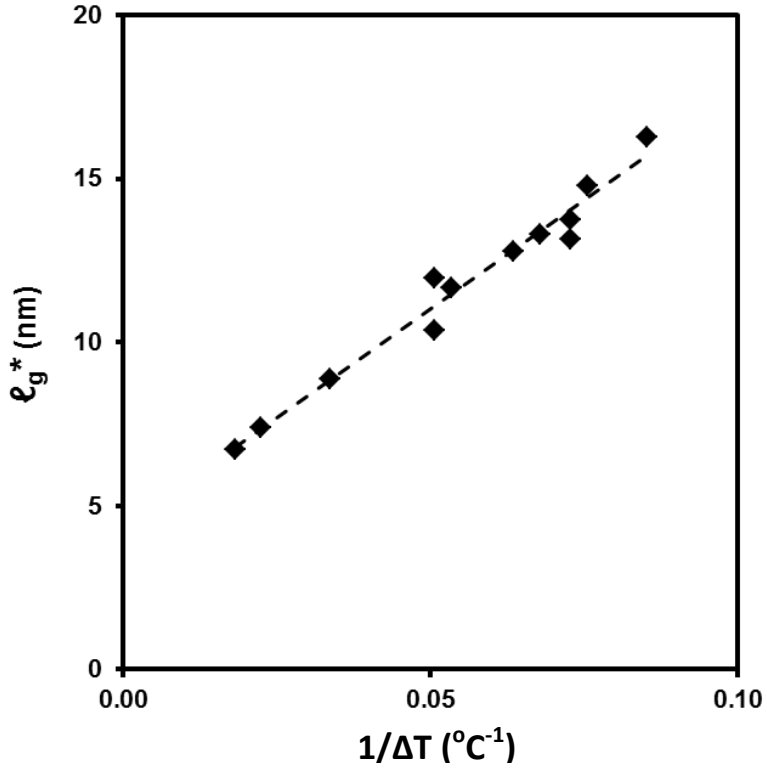

Figure 3.13. ℓ_g^* *vs.* $1/\Delta T$ for PE 29K using the data from Barham et al.[30]

Using the σ_{ec}^o value obtained from the ℓ_g^* *vs.* $1/\Delta T$ plot in combination with the constant $\bar{a}$ obtained from the non-linear Hoffman-Weeks analysis and Equation A.18 (Appendix A), we can derive a new value of C_2 = 5.7 ± 0.6 nm. The values of C_2 obtained from the ℓ_g^* vs. $1/\Delta T$ plot

and the non-linear Hoffman-Weeks treatment differ only by about 20% providing support for the applicability of the non-linear Hoffman-Weeks approach. It is worth mentioning that as σ_{ec}^{o} and C_2 are inversely related to $\cos\theta$, choosing any other tilt angle would not affect the agreement between the lamellar thickness and the melting temperature data. Assuming a δ' value of 1 nm and using Equation A.15 leads to a magnitude of 0.029 ± 0.003 $^{o}C^{-1}$ for the fluctuation strength parameter, y. This value compares favorably with estimates by Hoffman et al.[53] ($y = 0.014\ ^{o}C^{-1}$) and by Miller[48] ($y = 0.026\ ^{o}C^{-1}$) for the solution crystallized linear polyethylene.[75]

Using the best fit parameters obtained from the ℓ_g^* versus $1/\Delta T$ plot, we calculate the initial lamellar thickness for the crystallization temperatures used in our melting studies for PE 29K. Combining the initial lamellar thicknesses at these crystallization temperatures with the melting temperatures obtained from the DSC measurements, we can plot the melting line, (a.k.a.) the Gibbs-Thomson line, in a T_m *vs.* $1/\ell$ plot, Figure 3.14.

The equilibrium melting temperature determined from the intercept of the Gibbs-Thomson plot, 139.0 ± 0.5^{o}C, is within experimental error identical with the value found with the non-linear Hoffman-Weeks method. The slope of the Gibbs-Thomson line yields σ_{em} = 41.5 ± 2.0 erg/cm^2, within experimental uncertainty equal to the value of σ_{ec}^{o}. This finding supports the assumption of $\frac{\sigma_{ec}^{o}}{\sigma_{em}} = 1$, used in the non-linear Hoffman-Weeks approach. This observation suggests that upon heating linear polyethylene the stem length fluctuations may be able to equilibrate before melting, possibly as a result of local chain segmental diffusion, as was noted by Hoffman et al.[53]

To examine the thermodynamic predictions offered by Strobl,[5] we added Barham's crystallization temperature *vs.* initial lamellar thickness data to the melting data in Figure 3.14 to construct the phase diagram for PE 29K. On Figure 3.14, we also plotted the crystallization line for the LH theory, obtained by rearrangement of Equation A.14 (Appendix A):

$$T_c = T_m^{eq}\left[1 - \frac{2\sigma_{ec}^o}{\left(\ell_g^* - C_2\right)\Delta H}\right] \tag{3.3}$$

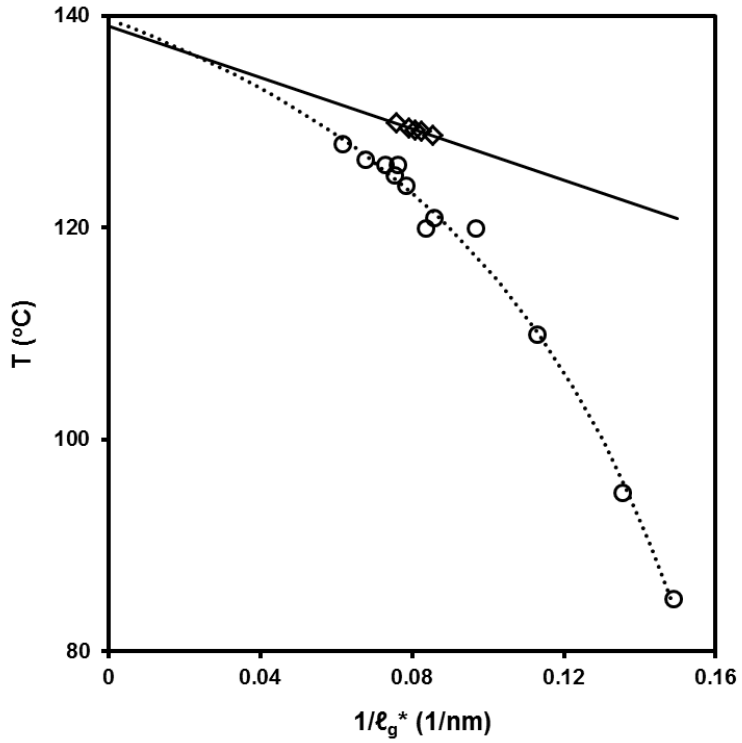

Figure 3.14. T *vs.* $1/\ell_g^*$ for PE 29K: T_m *vs.* $1/\ell_g^*$ (◇) and T_c vs. $1/\ell_g^*$ (○). The Gibbs-Thomson melting line (—) and the crystallization line predicted by the LH theory (…) are also plotted.

The crystallization line derived from the LH theory (Equation 3.3) describes perfectly all data points, self-seeded at low undercooling where $\ell_g^* \gg C_2$ and regular crystals at high undercooling where C_2 is close to ℓ_g^*, Figure 3.14. These observations indicate that crystallization of linear polyethylene can be well described by a single-stage mechanism involving only two phases without the need to invoke the multi-stage, three-phase approach of Strobl.[5] While the transitions predicted by the Ostwald rule of stages[2, 76] may occur, they may not constitute rate-determining steps during the crystallization of linear polyethylene. Further discussion of this question will be offered when we examine the spherulite growth rate data of linear polyethylene in a subsequent manuscript.

3.6. Conclusion

The melting behavior of three linear polyethylene fractions with number average molecular weight of 11, 29, and 100.5 kg/mol was studied as a function of crystallization time with conventional and ultrafast calorimetry. The initial melting temperatures of non-thickened lamellae formed under isothermal conditions over a range of crystallization temperatures were used in the non-linear Hoffman-Weeks method to determine the equilibrium melting temperature. T_m^{eq} values of 138.4 ± 0.9°C, 139.7 ± 0.9°C, and 140.9 ± 0.8°C were estimated for PE 11K, PE 29K, and PE 100K, respectively, in close agreement with those reported by Wunderlich et al.[10] and Okada et al.[28] for the melting of extended-chain crystals and by Crist[14] with the Gibbs-Thomson analysis. The Lauritzen-Hoffman theory and the non-linear Hoffman-Weeks treatment were modified to account for the effect of the tilt angle, θ, of the crystallized stems of linear polyethylene on the initial average lamellar thickness. Tilt angle of the crystallized stems contributes an additional $\cos\theta$ in the expression for the δ parameter. Accuracy of the non-linear Hoffman-Weeks method was examined using Barham's initial lamellar thickness data for PE 29K measured at different crystallization temperatures. The equilibrium melting temperature obtained by the Gibbs-Thomson approach and the C_2 value extracted from the ℓ_g^* *vs.* $1/\Delta T$ plot of Barham's data were similar within the limits of experimental error to those obtained here through the non-linear Hoffman-Weeks method. The ratio of $\frac{\sigma_{ec}^o}{\sigma_{em}}$ was also found to be approximately equal to one, satisfying an important assumption in the non-linear Hoffman-Weeks treatment.

3.7. Acknowledgments

This research did not receive any specific grant from funding agencies in the public, commercial or not-for-profit sectors. However, the authors would like to thank TA Instruments for the temporary loan of a Q2000 differential scanning calorimeter.

3.8. Appendix A: Modification of the LH Theory for Tilted Stems, Linear and Non-linear Hoffman-Weeks Treatments

We first propose a trivial modification of the Lauritzen-Hoffman secondary nucleation theory[3, 6] to account for the presence of chain-tilt in lamellar LPE crystals.

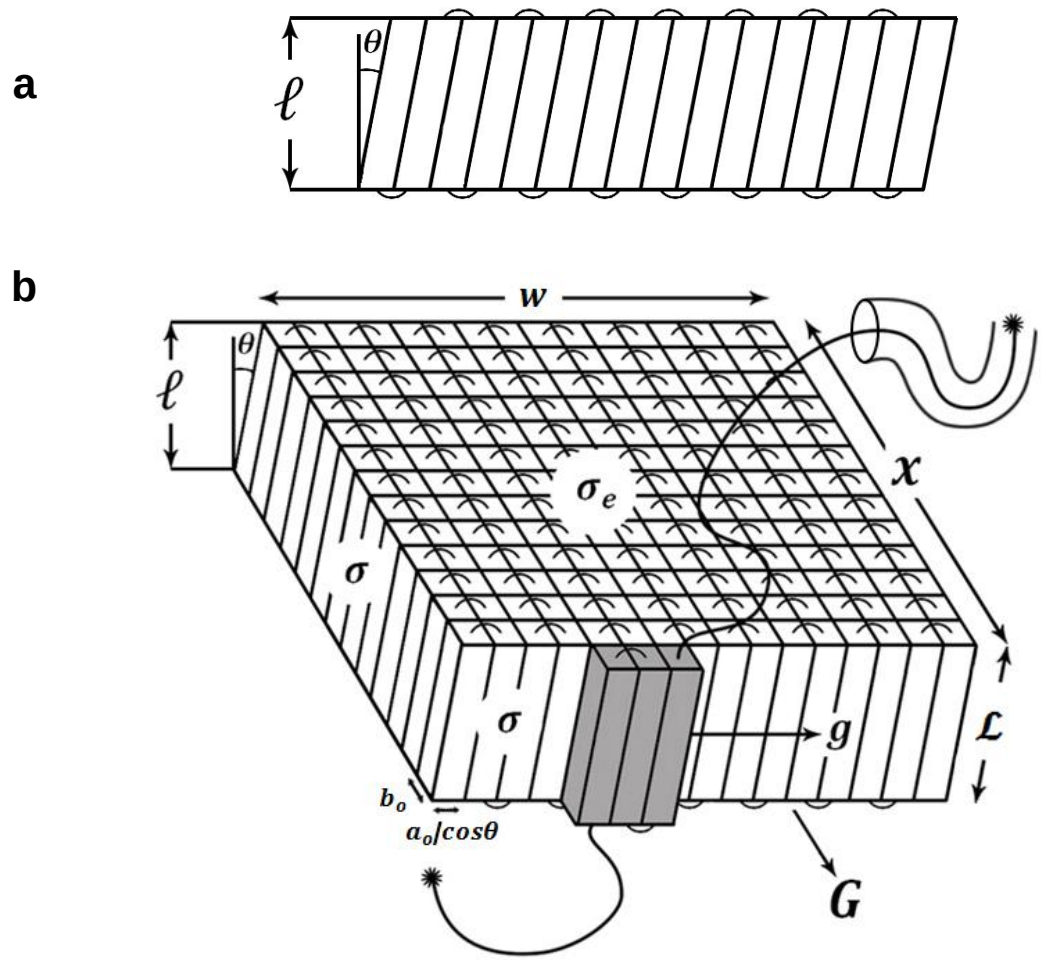

Figure A.1 (a) Projection in the a-c plane of a linear polyethylene lamella with tilted crystallized stems and (b) its 3D schematic representation. w, x, and ℓ are the width, length, and thickness of the lamella, respectively. $\mathcal{L}$ and θ are the length and tilt angle of the crystallized stems, respectively. a_o and b_o are the width and thickness of the crystallized stems, respectively. A chain has crystallized from the melt on the lamella by moving in the tube, completing a new layer with the rate of g, leading to an overall crystal growth rate of G (the new layer is colored in gray).

Crystallized stems of linear polyethylene exhibit a tilted conformation relative to the normal of the lamellar fold surface to reduce the amount of steric hindrance between adjacent folds. Figure A-1.a shows the projection in the a-c plane of a linear polyethylene lamella with tilted stems. Tilting leads to a change in the stem lateral and fold surface areas, introducing a $\cos\theta$ term in the rate constants for stem attachment to and removal from the substrate in the LH theory. Using the same nomenclature as Hoffman et al.[3] the modified rate constants for each step are expressed as:

$$A_o = \beta \exp\left(-\frac{2b_o\sigma\ell}{kT_c\cos\theta}\right) \tag{A.1}$$

$$A = \beta \exp\left(-\frac{2a_o b_o\sigma_{ec}}{kT_c\cos\theta}\right) \tag{A.2}$$

$$B = B_1 = \beta \exp\left(-\frac{a_o b_o\Delta G^\infty\ell}{kT_c\cos\theta}\right) \tag{A.3}$$

and the flux $S(\ell)$ over the secondary nucleation barrier for a lamellar crystal of thickness ℓ is

$$S(\ell) = N_o\beta\left[\exp\left(-\frac{2b_o\sigma\ell}{kT_c\cos\theta}\right) - \exp\left(\frac{2a_o b_o\sigma_{ec}}{kT_c\cos\theta}\right)\exp\left(-\frac{(2b_o\sigma + a_o b_o\Delta G^\infty)\ell}{kT_c\cos\theta}\right)\right] \tag{A.4}$$

The net flux over the barrier at T_c is expressed as

$$S_{T_c} = \frac{1}{\ell_u}\int_{\ell_{min}=2\sigma_{ec}/\Delta G^\infty}^{\infty} S(\ell)d\ell$$

$$S_{T_c} = \frac{C_o n_L\beta}{\ell_u}\left[\frac{a_o\Delta G^\infty kT_c\cos\theta}{2b_o\sigma(2\sigma + a_o\Delta G^\infty)}\right]\exp\left(-\frac{4b_o\sigma\sigma_{ec}}{kT_c\Delta G^\infty\cos\theta}\right) \tag{A.5}$$

The initial average lamellar thickness, ℓ_g^*, can be calculated as

$$\ell_g^* = \int_{\ell_{min}=2\sigma_{ec}/\Delta G^\infty}^{\infty}\ell S(\ell)d\ell \Big/ \int_{\ell_{min}=2\sigma_{ec}/\Delta G^\infty}^{\infty} S(\ell)d\ell \tag{A.6}$$

$$\ell_g^* = \frac{2\sigma_{ec}}{\Delta G^\infty} + \frac{kT_c \cos\theta}{2b_o\sigma}\left[\frac{a_o\Delta G^\infty + 4\sigma}{a_o\Delta G^\infty + 2\sigma}\right] = \frac{2\sigma_{ec}T_m^{eq}}{\Delta T\Delta H} + \frac{kT_c \cos\theta}{2b_o\sigma}\left[\frac{a_o\Delta G^\infty + 4\sigma}{a_o\Delta G^\infty + 2\sigma}\right] \quad \text{(A.7)}$$

The first term on the R.H.S. of Equation A.7 is the minimum lamellar thickness that is thermodynamically stable at an undercooling ΔT or temperature T_c. The second term, labeled δ in the LH theory, is understood as the thickness increment that brings the secondary nucleus into the region of stability and allows the crystal to grow near its maximum rate. Accounting for the tilt angle of the stems adds a $\cos\theta$ term to the definition of δ found in the LH theory. Hence, we write the average initial lamellar thickness as:

$$\ell_g^* = \ell_{min} + \frac{kT_c \cos\theta}{2b_o\sigma}\left[\frac{a_o\Delta G^\infty + 4\sigma}{a_o\Delta G^\infty + 2\sigma}\right] = \ell_{min} + \delta' \quad \text{(A.8)}$$

Since the terms δ or δ' have a negligible temperature dependence in the temperature range where LPEs crystallize isothermally, a plot of ℓ_g^* versus $1/\Delta T$ is expected to be linear with slope and intercept yielding σ_{ec} and δ'.

In the Hoffman-Weeks method, the lamellar thickness, ℓ, at any stage of crystallization is related to the initial lamellar thickness, ℓ_g^*, using a thickening coefficient, $\gamma(t_c, T_c)$, as

$$\ell = \gamma(t_c, T_c)\ell_g^* \quad \text{(A.9)}$$

where t_c is the crystallization time. Finally, to relate the melting temperature of a lamella to its thickness, Hoffman and Weeks invoke the Gibbs-Thomson equation,[6, 20] (Equation A.10), which is derived in a straightforward manner through consideration of the equilibrium between a lamella of thickness ℓ and the melt at T_m.

$$T_m = T_m^{eq}\left(1 - \frac{2\sigma_{em}}{\ell\Delta H}\right) \quad \text{(A.10)}$$

Combination of Equations A.8 through A.10 leads to the following non-linear relationship between the melting and crystallization temperatures

$$T_m = T_m^{eq}\left(1 - \frac{1}{\gamma(t_c, T_c)}\left[\frac{T_m^{eq} - T_c}{T_m^{eq}}\right]\left[\frac{2\sigma_{em}}{2\sigma_{ec} + \frac{\delta' \Delta H\left(T_m^{eq} - T_c\right)}{T_m^{eq}}}\right]\right) \tag{A.11}$$

Hoffman and Weeks assumed that at low undercooling, the influence of δ' on ℓ_g^* can be neglected since δ' is typically less than 1 nm and almost independent of temperature. They also assumed that σ_{ec} can be well approximated by σ_{em}. Use of these two approximations reduces the term in the second square bracket to 1 and leads to the linear form of the Hoffman-Weeks equation (Equation A.12)

$$T_m = T_m^{eq}\left(1 - \frac{1}{\gamma(t_c, T_c)}\right) + \frac{T_c}{\gamma(t_c, T_c)} \tag{A.12}$$

A linear regression of the experimental T_m versus T_c data is then extrapolated to the equilibrium line, $T_m = T_c$, to yield the equilibrium melting temperature, T_m^{eq}. The slope of the regression line is equal to the reciprocal of the thickening coefficient, assumed in this treatment to be independent of time and temperature.

A few years after the seminal work of Hoffman and Weeks was published,[23] Lauritzen and Passaglia[55] suggested that if the stem length was allowed to fluctuate during crystal growth, the fold surface free energy constant in the LH theory would need to be replaced by a temperature dependent effective, or kinetic, fold surface free energy. At low to moderate undercooling, the undercooling dependence of the apparent fold surface free energy, σ_{ec}, is approximated by a simple first-order correction (Equation A.13).

$$\sigma_{ec} = \sigma_{ec}^{o}(1 + y\Delta T) \tag{A.13}$$

where σ_{ec}^{o} the magnitude of the fold surface free energy for lamellae with equilibrium roughness and y is a constant characterizing the mean strength of the kinetic stem length fluctuations. Under these conditions, the initial lamellar thickness, ℓ_g^*, is rewritten as

$$\ell_g^* = \frac{2\sigma_{ec}^{o} T_m^{eq}}{\Delta H \Delta T} + C_2 \tag{A.14}$$

with

$$C_2 = \frac{2\sigma_{ec}^{o} y T_m^{eq}}{\Delta H} + \delta' \tag{A.15}$$

Observation[28] that the quantity C_2 was several times larger than δ' led Marand et al.[27] to question the validity of the linear Hoffman-Weeks treatment. Indeed, combining Equations A.14 and A.15 with the Gibbs-Thomson equation leads to the general non-linear relationship between melting and crystallization temperatures:

$$T_m = T_m^{eq}\left(1 - \frac{1}{\gamma(t_c, T_c)}\left[\frac{T_m^{eq} - T_c}{T_m^{eq}}\right]\left[\frac{2\sigma_{em}}{2\sigma_{ec}^{o} + \frac{C_2 \Delta H\left(T_m^{eq} - T_c\right)}{T_m^{eq}}}\right]\right) \tag{A.16}$$

which differs from Hoffman-Weeks equation (Equation A-12) in two ways; first, δ' has been replaced by C_2 and, second, σ_{ec} was substituted by σ_{ec}^{o}. The main consequence of the first substitution is that the C_2 term in the second square bracket on the R.H.S. of Equation A.16 is no longer negligible in comparison to $2\sigma_{ec}^{o}$. Equation A.16 can then be rearranged as:

$$\frac{T_m^{eq}}{T_m^{eq} - T_m} = \gamma(t_c, T_c)\frac{\sigma_{ec}^{o}}{\sigma_{em}}\left(\frac{T_m^{eq}}{T_m^{eq} - T_c} + \frac{C_2 \Delta H}{2\sigma_{ec}^{o}}\right) \tag{A.17}$$

Where we define the constant $\bar{a}$ by:

$$\bar{a} = \frac{C_2 \Delta H}{2\sigma_{ec}^{o}} \tag{A.18}$$

Introducing the normalized melting temperature $M = \frac{T_m^{eq}}{T_m^{eq} - T_m}$ and the normalized crystallization temperature $X = \frac{T_m^{eq}}{T_m^{eq} - T_c}$, where T_c, T_m and T_m^{eq} are absolute temperatures, the general non-linear Hoffman-Weeks equation is written as:

$$M = \gamma(t_c, T_c)\frac{\sigma_{ec}^o}{\sigma_{em}}(X + \bar{a}) \tag{A.19}$$

Following the arguments advanced by Hoffman et al.,[53] the ratio $\frac{\sigma_{ec}^o}{\sigma_{em}}$ is set to 1, to reflect the assumption that the stem length fluctuations equilibrate as a result of segmental transport at the crystallization temperature after lamellar formation and during heating prior to melting. Hence, for samples crystallized for sufficiently short times such that its lamellae have not thickened ($\gamma = 1$), the M *vs.* X plot should be linear with a slope of one and intercept $\bar{a}$, if T_m^{eq} is selected correctly. Note that the non-linear Hoffman-Weeks treatment, assumes that the quantity C_2 has negligible temperature dependence. This approximation is justified in the context of the LH theory since the δ' parameter can be taken as a constant at low undercooling.[3, 6, 53] Similarly, use of the LP model, has been restricted to low undercooling conditions, where a linear dependence of σ_{ec} on undercooling is generally assumed.[45, 48, 53] Should crystallization at large undercoolings be of interest, modification of the non-linear Hoffman-Weeks treatment may be necessary to account more rigorously for the undercooling dependence of the fold surface free energy, possibly through a series expansion of the undercooling.

3.9. References

1. Bassett, D.; Hodge, A. In *On lamellar organization in certain polyethylene spherulites*, Proceedings of the Royal Society of London A: Mathematical, Physical and Engineering Sciences, The Royal Society: 1978; pp 121-132.
2. Keller, A.; Hikosaka, M.; Rastogi, S.; Toda, A.; Barham, P.; Goldbeck-Wood, G., An approach to the formation and growth of new phases with application to polymer crystallization: effect of finite size, metastability, and Ostwald's rule of stages. *Journal of materials science* **1994,** *29* (10), 2579-2604.
3. Hoffman, J. D.; Miller, R. L., Kinetic of crystallization from the melt and chain folding in polyethylene fractions revisited: theory and experiment. *Polymer* **1997,** *38* (13), 3151-3212.
4. Hikosaka, M.; Watanabe, K.; Okada, K.; Yamazaki, S., Topological mechanism of polymer nucleation and growth–the role of chain sliding diffusion and entanglement. *Interphases and Mesophases in Polymer Crystallization III* **2005**, 137-186.
5. Strobl, G., Colloquium: Laws controlling crystallization and melting in bulk polymers. *Reviews of modern physics* **2009,** *81* (3), 1287.
6. Hoffman, J. D.; Davis, G. T.; Lauritzen, J. I., The rate of crystallization of linear polymers with chain folding. In *Treatise on solid state chemistry*, Springer: 1976; pp 497-614.
7. Broadhurst, M. G., An analysis of the solid phase behavior of the normal paraffins. *J. Res. Natl. Bur. Stand. A* **1962,** *66*, 241-249.
8. Flory, P.; Vrij, A., Melting points of linear-chain homologs. The normal paraffin hydrocarbons. *Journal of the American Chemical Society* **1963,** *85* (22), 3548-3553.
9. Broadhurst, M. G., The melting temperatures of the n-paraffins and the convergence temperature for polyethylene. *J. Res. Natl. Bur. Stand., A: Phys. Chem. A* **1966,** *70*, 481-486.

10. Wunderlich, B.; Czornyj, G., A study of equilibrium melting of polyethylene. *Macromolecules* **1977,** *10* (5), 906-913.
11. Mandelkern, L.; Stack, G. M., Equilibrium melting temperature of long-chain molecules. *Macromolecules* **1984,** *17* (4), 871-878.
12. Mandelkern, L.; Prasad, A.; Alamo, R.; Stack, G., Melting temperature of the n-alkanes and the linear polyethylenes. *Macromolecules* **1990,** *23* (15), 3696-3700.
13. Wunderlich, B., Macromolecular Physics 1980. *Vol: 3* **2003,** *69*.
14. Crist, B., Yet another visit to the melting of polyethylene crystals. *Journal of Polymer Science Part B: Polymer Physics* **2007,** *45* (24), 3231-3236.
15. Bassett, D. C., *Principles of polymer morphology*. CUP Archive: 1981.
16. Ergoz, E.; Fatou, J.; Mandelkern, L., Molecular weight dependence of the crystallization kinetics of linear polyethylene. I. Experimental results. *Macromolecules* **1972,** *5* (2), 147-157.
17. Marand, H.; Huang, Z., Isothermal lamellar thickening in linear polyethylene: Correlation between the evolution of the degree of crystallinity and the melting temperature. *Macromolecules* **2004,** *37* (17), 6492-6497.
18. Khoury, F.; Passaglia, E., The morphology of crystalline synthetic polymers. In *Treatise on solid state chemistry*, Springer: 1976; pp 335-496.
19. Bassett, D.; Hodge, A. In *On the morphology of melt-crystallized polyethylene I. Lamellar profiles*, Proceedings of the Royal Society of London A: Mathematical, Physical and Engineering Sciences, The Royal Society: 1981; pp 25-37.
20. Thomson, W., W. Thomson, Philos. Mag. 42, 448 (1871). *Philos. Mag.* **1871,** *42*, 448.
21. Illers, V. K. H.; Hendus, H., Schmelzpunkt und kristallitgröße von aus schmelze und lösung kristallisiertem polyäthylen. *Macromolecular Chemistry and Physics* **1968,** *113* (1), 1-22.

22. Cho, T.; Heck, B.; Strobl, G., Equations describing lamellar structure parameters and melting points of polyethylene-co-(butene/octene) s. *Colloid and Polymer Science* **2004,** *282* (8), 825-832.
23. Hoffman, J. D.; Weeks, J. J., Melting process and the equilibrium melting temperature of polychlorotrifluoroethylene. *J Res Natl Bur Stand A* **1962,** *66* (1), 13-28.
24. Toda, A.; Taguchi, K.; Nozaki, K.; Konishi, M., Melting behaviors of polyethylene crystals: an application of fast-scan DSC. *Polymer* **2014,** *55* (14), 3186-3194.
25. Bassett, D., Chain-extended polyethylene in context: a review. *Polymer* **1976,** *17* (6), 460-470.
26. Bassett, D.; Turner, B., Chain extended crystallization of polyethylene: Evidence of a new high-pressure phase. *Nature (London), Phys. Sci* **1972,** *240*, 146.
27. Marand, H.; Xu, J.; Srinivas, S., Determination of the equilibrium melting temperature of polymer crystals: linear and nonlinear Hoffman− Weeks extrapolations. *Macromolecules* **1998,** *31* (23), 8219-8229.
28. Okada, M.; Nishi, M.; Takahashi, M.; Matsuda, H.; Toda, A.; Hikosaka, M., Molecular weight dependence of the lateral growth rate of polyethylene 2. Folded-chain crystals. *Polymer* **1998,** *39* (19), 4535-4539.
29. Huggins, M. L., Certain Properties of Long-chain Compounds as Functions of Chain Length. *Journal of Physical Chemistry* **1939,** *43* (8), 1083-1098.
30. Barham, P.; Chivers, R.; Keller, A.; Martinez-Salazar, J.; Organ, S., The supercooling dependence of the initial fold length of polyethylene crystallized from the melt: unification of melt and solution crystallization. *Journal of materials science* **1985,** *20* (5), 1625-1630.
31. Alamo, R. G.; Viers, B. D.; Mandelkern, L., A re-examination of the relation between the melting temperature and the crystallization temperature: linear polyethylene. *Macromolecules* **1995,** *28* (9), 3205-3213.

32. Toda, A.; Androsch, R.; Schick, C., Insights into polymer crystallization and melting from fast scanning chip calorimetry. *Polymer* **2016,** *91*, 239-263.
33. Barham, P.; Keller, A., The initial stages of crystallization of polyethylene from the melt. *Journal of Polymer Science Part B: Polymer Physics* **1989,** *27* (5), 1029-1042.
34. Akpalu, Y. A.; Amis, E. J., Evolution of density fluctuations to lamellar crystals in linear polyethylene. *The Journal of chemical physics* **1999,** *111* (18), 8686-8695.
35. Akpalu, Y. A.; Amis, E. J., Effect of polydispersity on the evolution of density fluctuations to lamellar crystals in linear polyethylene. *The Journal of Chemical Physics* **2000,** *113* (1), 392-403.
36. Bark, M.; Zachmann, H. G.; Alamo, R.; Mandelkern, L., Investigations of the crystallization of polyethylene by means of simultaneous small-angle and wide-angle X-ray scattering. *Macromolecular Chemistry and Physics* **1992,** *193* (9), 2363-2377.
37. Rastogi, S.; Spoelstra, A.; Goossens, J.; Lemstra, P., Chain mobility in polymer systems: on the borderline between solid and melt. 1. Lamellar doubling during annealing of polyethylene. *Macromolecules* **1997,** *30* (25), 7880-7889.
38. Fischer, E., Effect of annealing and temperature on the morphological structure of polymers. *Pure and applied chemistry* **1972,** *31* (1-2), 113-132.
39. McCready, M.; Schultz, J.; Lin, J.; Hendricks, R., Effect of crystallization time on the properties of melt-crystallized linear polyethylene. *Journal of Polymer Science Part B: Polymer Physics* **1979,** *17* (5), 725-740.
40. Stack, G.; Mandelkern, L.; Voigt-Martin, I., Changes in crystallite size distribution during the isothermal crystallization of linear polyethylene. *Polymer Bulletin* **1982,** *8* (9-10), 421-428.
41. Voigt-Martin, I.; Stack, G.; Peacock, A.; Mandelkern, L., A comparison of the Raman LAM and electron microscopy in determining crystallite thickness distributions: polyethylenes with narrow size distributions. *Journal of Polymer Science Part B: Polymer Physics* **1989,** *27* (5), 957-965.

42. Voigt-Martin, I.; Fischer, E.; Mandelkern, L., Morphology of melt-crystallized linear polyethylene fractions and its dependence on molecular weight and crystallization temperature. *Journal of Polymer Science: Polymer Physics Edition* **1980,** *18* (12), 2347-2367.
43. el Maaty, M. A.; Bassett, D., Evidence for isothermal lamellar thickening at and behind the growth front as polyethylene crystallizes from the melt. *Polymer* **2005,** *46* (20), 8682-8688.
44. Hocquet, S.; Dosière, M.; Thierry, A.; Lotz, B.; Koch, M.; Dubreuil, N.; Ivanov, D., Morphology and melting of truncated single crystals of linear polyethylene. *Macromolecules* **2003,** *36* (22), 8376-8384.
45. Huseby, T.; Bair, H., Dissolution of polyethylene single crystals in xylene and octadecane. *Journal of Applied Physics* **1968,** *39* (11), 4969-4973.
46. Leung, W.; Manley, S.; Panaras, A., Isothermal growth of low molecular weight polyethylene single crystals from solution. I: Variation of equilibrium dissolution temperature with molecular weight and lamellar thickness with crystallization temperature. *Macromolecules* **1985,** *18* (4), 746-752.
47. Nakagawa, Y.; Hayashi, H.; Takahagi, T.; Soeda, F.; Ishitani, A.; Toda, A.; Miyaji, H., Atomic force microscopy of solution grown polyethylene single crystals. *Japanese journal of applied physics* **1994,** *33* (6S), 3771.
48. Miller, R. L., Polymer crystal formation: On an analysis of the dilute solution lamellar thickness-crystallization temperature data for poly (ethylene). *Kolloid-Zeitschrift und Zeitschrift für Polymere* **1968,** *225* (1), 62-69.
49. Jones, D.; Latham, A.; Keller, A.; Girolamo, M., Fold length of single crystals of polystyrene: A conflict with crystallization theories at high supercoolings. *Journal of Polymer Science Part B: Polymer Physics* **1973,** *11* (9), 1759-1767.
50. Korenaga, T.; Hamada, F.; Nakajima, A., Surface free energy of poly (oxymethylene) single crystals grown in various solvents. *Polymer Journal* **1972,** *3* (1), 21.

51. Cheng, S. Z.; Chen, J.; Barley, J. S.; Zhang, A.; Habenschuss, A.; Zschack, P. R., Isothermal thickening and thinning processes in low molecular-weight poly (ethylene oxide) fractions crystallized from the melt. 3. Molecular weight dependence. *Macromolecules* **1992,** *25* (5), 1453-1460.
52. Organ, S.; Keller, A., Solution crystallization of polyethylene at high temperatures. *Journal of materials science* **1985,** *20* (5), 1602-1615.
53. Hoffman, J.; Lauritzen, J.; Passaglia, E.; Ross, G.; Frolen, L.; Weeks, J., Kinetics of polymer crystallization from solution and the melt. *Colloid & Polymer Science* **1969,** *231* (1), 564-592.
54. Leung, W.; St. John Manley, R.; Panaras, A., Isothermal growth of low molecular weight polyethylene single crystals from solution. 2. Melting and dissolution behavior. *Macromolecules* **1985,** *18* (4), 753-759.
55. Lauritzen, J.; Passaglia, E., Kinetics of crystallization in multicomponent systems: II. Chain-folded polymer crystals. *J Res Natl Bur Stand. A* **1967,** *71*, 261-75.
56. Keith, H.; Padden Jr, F.; Lotz, B.; Wittmann, J., Asymmetries of habit in polyethylene crystals grown from the melt. *Macromolecules* **1989,** *22* (5), 2230-2238.
57. Mohammadi, H. On Melting and Crystallization of Linear Polyethylene, Poly(ethylene oxide) and Metallocene Linear Low Density Polyethylene. Virginia Polytechnic Institute and State University, 2018.
58. Toda, A., Heating rate dependence of melting peak temperature examined by DSC of heat flux type. *Journal of Thermal Analysis and Calorimetry* **2016,** *123* (3), 1795-1808.
59. Toda, A.; Konishi, M., An evaluation of thermal lags of fast-scan microchip DSC with polymer film samples. *Thermochimica Acta* **2014,** *589*, 262-269.
60. Hellmuth, E.; Wunderlich, B., Superheating of Linear High-Polymer Polyethylene Crystals. *Journal of Applied Physics* **1965,** *36* (10), 3039-3044.
61. Illers, K.-H., Die ermittlung des schmelzpunktes von kristallinen polymeren mittels wärmeflusskalorimetrie (DSC). *European Polymer Journal* **1974,** *10* (10), 911-916.

62. Huang, Z.; Marand, H.; Cheung, W. Y.; Guest, M., Study of Crystallization Processes in Ethylene− Styrene Copolymers by Conventional DSC and Temperature-Modulated Calorimetry: Linear Polyethylene and Low Styrene Content Copolymers. *Macromolecules* **2004,** *37* (26), 9922-9932.
63. Peterlin, A., Thickening of polymer single crystals during annealing. *Journal of Polymer Science Part C: Polymer Letters* **1963,** *1* (6), 279-284.
64. Fischer, E.; Schmidt, G., Long periods in drawn polyethylene. *Angewandte Chemie International Edition* **1962,** *1* (9), 488-499.
65. Hansen, D.; Bernier, G., Thermal conductivity of polyethylene: the effects of crystal size, density and orientation on the thermal conductivity. *Polymer Engineering & Science* **1972,** *12* (3), 204-208.
66. Sheldon, R.; Lane, S. K., Thermal conductivities of polymers II—Polyethylene. *Polymer* **1965,** *6* (4), 205-212.
67. Dirand, M.; Bouroukba, M.; Chevallier, V.; Petitjean, D.; Behar, E.; Ruffier-Meray, V., Normal alkanes, multialkane synthetic model mixtures, and real petroleum waxes: crystallographic structures, thermodynamic properties, and crystallization. *Journal of Chemical & Engineering Data* **2002,** *47* (2), 115-143.
68. Armistead, J.; Hoffman, J. D., Direct evidence of regimes I, II, and III in linear polyethylene fractions as revealed by spherulite growth rates. *Macromolecules* **2002,** *35* (10), 3895-3913.
69. Strobl, G.; Eckel, R., A raman spectroscopic determination of the interlamellar forces in crystalline n-alkanes and of the limiting elastic modulus Ec of polyethylene. *Journal of Polymer Science Part B: Polymer Physics* **1976,** *14* (5), 913-920.
70. Hocquet, S.; Dosiere, M.; Tanzawa, Y.; Koch, M., Lamellar and crystalline layer thickness of single crystals of narrow molecular weight fractions of linear polyethylene. *Macromolecules* **2002,** *35* (13), 5025-5033.

71. Gautam, S.; Balijepalli, S.; Rutledge, G., Molecular simulations of the interlamellar phase in polymers: effect of chain tilt. *Macromolecules* **2000,** *33* (24), 9136-9145.
72. Ungar, G.; Zeng, X.-b., Learning polymer crystallization with the aid of linear, branched and cyclic model compounds. *Chemical reviews* **2001,** *101* (12), 4157-4188.
73. Note that different chain tilt angles have been reported for solution crystallized linear polyethylene (see for instance references 33, 51 and 64).
74. Khoury, F., Organization of macromolecules in the condensed phase: General discussion. *Faraday Discuss. Chem. Soc* **1979,** *68*, 404-405.
75. It should be noted that the y-value reported in reference 3 is incorrectly given as 0.0025 (1/K), that is an order of magnitude too low.
76. Ostwald, W., The formation and changes of solids. *Z. Phys. Chem* **1897,** *22*, 289-330.

Chapter 4. Analysis of the Temperature and Chain Length Dependences of the Spherulite Growth Rate for Linear Polyethylene Fractions

Hadi Mohammadi, Gregory Fahs and Hervé Marand

4.1. Attribution

Gregory Fahs contributed to this work by conducting the wide angle X-ray diffraction experiments. Design of the experiments and processing and analysis of the data were performed by Hadi Mohammadi. The Lauritzen-Hoffman secondary nucleation theory was modified by Hadi Mohammadi. The paper was prepared by Hadi Mohammadi and Hervé Marand.

4.2. Abstract

The Lauritzen-Hoffman (LH) secondary nucleation theory is modified to account for the effect of stem length fluctuations, tilt angle of the crystallized stems, θ, and temperature dependence of the lateral surface free energy. Spherulite growth rate data of 26 linear narrow molecular weight distribution polyethylene fractions (M_n from 9K to 120K) are analyzed at low to moderate undercoolings using the modified LH theory. Equilibrium melting temperatures of the fractions are estimated using the Huggins equation proposed in a previous publication. A regime I to II transition is observed at an undercooling $\Delta T_{I \to II}$ = 12.7 ± 0.5°C, independent of chain length. In both regimes, G scales as $n^{-1.6 \pm 0.2}$. This chain length dependence differs from that predicted by the classical LH theory but is similar to that reported by Hikosaka et al. The

magnitude of $\sigma_{ec}^{o}/\cos\theta$ is equal to 45.5 ± 5.2 erg/cm^2, independent of chain length and within experimental error identical to that derived from the undercooling dependence of the initial lamellar thickness and to $\sigma_{em}/\cos\theta$ derived from the Gibbs-Thomson equation. The ratio K_{gI}^{o}/K_{gII}^{o} is equal to 2.1 ± 0.3, in accord with prediction from the LH model. If the analysis of the growth rate data is carried out with a chain length dependent $\bar{a}$, the growth rate front factors G_{oI} and G_{oII} exhibit slightly different dependencies on chain length, $G_{oI} \propto n^{-0.9\pm0.3}$ and $G_{oII} \propto n^{-1.6\pm0.2}$, and the strength of the stem length fluctuations, y, increases with chain length. If on the other hand, the quantity $\bar{a}$ is assumed to be independent of chain length, (i.e. the strength of the stem length fluctuations, y, is a constant equal to 0.032 ^{o}C^{-1} at $\Delta T_{I\rightarrow II}$), then the exponents of the power law dependencies of G_{oI}, G_{oII} and G on chain length are identical. The (110) and (200) crystal substrate lengths of three linear polyethylene fractions, approximated by their respective lattice coherence lengths, were measured for at their respective I/II regime transition temperatures using wide angle X-ray diffraction. These substrate lengths exhibit a magnitude of 30 to 40 nm, independent of chain length. The average apparent friction coefficient of a crystallizing linear polyethylene chain, $\xi_c^o \sim n^{2.1\pm0.2}$, exhibits a stronger chain length dependence than that of a chain undergoing reptation in the melt state, $\xi^o \sim n^{1.3}$, when accounting for contributions from constraint release and contour length fluctuations. Shorter chains exhibit $\xi_c^o \sim \xi^o$ while for longer chains $\xi_c^o \gg \xi^o$. This observation indicates that reptation is not the only mechanism at play in the transport of segments through the melt-crystal interface during crystal growth.

4.3. Introduction

The temperature and chain length dependence of spherulite or crystal growth rates for linear polyethylene (LPE) have been extensively studied in the context of nucleation theories.[1-8]

These and similar studies[9] established the existence of a discontinuity in the temperature dependence of the growth rate at low undercooling, commonly referred as to a transition between regime I and regime II growth. Investigation of bulk crystallization kinetics led to similar observations.[10] While the transition temperature has been shown to be independent of the experimental technique employed for its evaluation, the molecular origin of its existence is still debated.[1, 9-11] Toda[9] argues that it is a consequence of morphological changes at the crystal growth front while Hoffman et al.[1, 5] associate it with the existence of a coherent crystal growth substrate of finite length. Analysis of the temperature dependence of spherulite or crystal growth rates leads to an estimation of the secondary nucleation constant, hence, to a value for the fold surface free energy, σ_e. The value of ca. 90 mJ/m^2 typically reported for this quantity from growth rate measurements is about twice as large as that reported in investigations of the temperature dependence of the initial lamellar thickness or in studies of the melting behavior using the Gibbs-Thomson approach.[12-17] Other discrepancies in the literature are concerned with the chain length (i.e. molecular weight) dependence of spherulite growth rates at fixed undercooling. Examination of ten relatively narrow molecular weight LPE fractions with number average molecular weights (M_n's) ranging from 13 to 71 kg/mol led Hoffman et al.[6] to suggest the existence of two distinct crystal growth laws. In the range denoted B-B' (M_{nw} from 15.3 to 38.6 kg/mol where M_{nw} is $(M_n \times M_w)^{1/2}$ and M_w is the weight average molecular weight of LPE)[18] crystal growth occurs under conditions of near ideal reptation with $G \sim 1/M_{nw}$, while in the range denoted C-C' (M_{nw} from 53.6 to 90.6 kg/mol) the pure reptational motion of the longest polymer chains is perturbed by an increasing frequency of multiple attachments/nucleation events per chain leading to with $G \sim 1/M_z$. The absence of theoretical justification for the use of the z-average molecular weight, the lack of statistical significance of these results (use of a small set of fractions and significant scatter in the log-log plot of G *vs.* n data) and, more importantly, the fact that studies of chain dynamics in the melt state have

shown the need for corrections to the classical reptation theory (cf. constraint release and contour length fluctuation contributions) suggest that the chain length dependence of spherulite growth rates needs to be revisited. This specific claim is further substantiated by results from Hikosaka et al.[3] suggesting a different power law relationship ($G \sim n^{-1.7}$). A reexamination of LPE spherulite growth rate analysis is also justified by the fact that all versions of the Lauritzen-Hoffman (LH) theory have ignored the effect of chain tilt with respect to the lamella basal plane as well as the effect of chain length fluctuations.[6, 11, 19-21] Both effects were shown to play a significant role in analyses of the correlations between lamellar thickness and crystallization or melting temperatures.[15] A thorough examination of the self-consistency of the LH theory also requires proper equilibrium melting temperatures to be used for each of the LPE fractions of varying molecular weights. All analyses carried out by Hoffman and coworkers relied on the Flory-Vrij[22] melting temperature estimations. In a recent paper, we advocated strongly against the use of such reference temperatures and suggested that a Huggins equation with a limiting (infinite molecular weight) equilibrium melting temperature of 141.4^{o}C was more appropriate.[15]

In this manuscript, we derive a set of equations allowing a more rigorous analysis of temperature and chain length dependence of spherulite growth rates for linear polyethylene (see Appendix B). This formalism preserves the basic tenets of the classical LH theory but accounts for the temperature dependence of both the lateral and surface free energies and the existence of crystallized stem tilt. Furthermore, this formalism does not equate the ratio of the force of crystallization to the reeling-in rate to the curvilinear friction coefficient of a chain in the melt. It assumes that other retardation processes during crystal growth may lead to a deviation from the $\xi_c \sim n^{1.3}$ law expected for pure melts when considering reptation in the context of contour length fluctuations and constraint release mechanisms (see Appendix C). To maximize the statistical reliability of our results, we will analyze spherulite growth rate data reported in the literature for 26 fractions with number average molecular weights ranging from 9 to 120 kg/mol.[1-

[2, 4, 6-8] Quantized chain folding is not present in linear polyethylene fractions with molecular weights higher than 9 kg/mol, while fractions with molecular weights higher than 120 kg/mol do not show a distinct regime I to II transition.[2, 4, 6-7] In contrast with previous studies,[1-2, 6-7] the equilibrium melting temperature for each of these fractions will be determined using the Huggins equation reported in our previous work.[15] These equilibrium melting temperatures are ca. 4°C lower than the Flory-Vrij[22] estimates, which is very significant when considering the low undercooling characteristic of LPE isothermal crystallization conditions $\Delta T \sim$ 10 – 20°C. To broaden the scope of previous studies we will also estimate the substrate length for three narrow molecular weight distribution linear polyethylene samples at their regime I/II transition undercooling, $\Delta T_{I \to II}$, from lattice coherence length measurements using wide angle X-ray diffraction. Obtaining an accurate value for the substrate length is a crucial step in the determination of the apparent chain friction coefficient during crystallization. The result of such analyses will be examined in the context of previous investigations of the temperature dependence of the initial lamellar thickness, and of correlations between melting and crystallization temperatures through non-linear Hoffman-Weeks treatment to evaluate the self-consistency of our analytical approach.

4.4. Experimental

4.4.1. Lattice Coherence Length Measurements

Three narrow molecular weight LPE samples with M_n= 11.4, 28.9, and 100.5 kg/mol with corresponding M_w/M_n of 1.19, 1.11, and 1.11 (SRM 1482, 1483, and 1484 respectively) were purchased from NIST and used as received. Frank[23] suggested that the substrate length of a growing crystal is similar to its lattice coherence length. The widths of the (110) and (200) reflections of semicrystalline LPE were measured at the regime I to regime II transition

temperature using a Rigaku S-Max 3000 SAXS/WAXD instrument at Virginia Tech. This diffraction set-up was equipped with a Micromax-007HF high intensity microfocus rotating anode copper source (CuK_α, λ = 0.154 nm, operated at 40 kV and 30 mA) and a gas filled 2-D multiwire, proportional counting detector. The X-ray beam was collimated using three pinholes.

Samples were pressed into 1 mm thick films using a Carver Laboratory Press (Model C) at 160^{o}C under a nitrogen atmosphere. The films were then cut into 1×1×1 mm^3 specimens and sandwiched between two Kapton™ films. Each sandwich was then affixed to the sample platform of a Linkam THMS 600 heating/cooling stage using an O-ring and then placed in the diffractometer. The Linkam stage had a 1 mm diameter hole to allow the passage of the X-rays. The sample temperature was regulated within ±0.1^{o}C using a Linkam T-95-PE temperature controller. Temperature calibration of the heating stage was performed in the range of 50 to 150^{o}C using 6 melting standards: Benzophenone (T_m = 48.5^{o}C), 2,6-di-tert-butyl-4-methylphenol (T_m = 70^{o}C), imidazole (T_m = 90^{o}C), m-toluic acid (T_m = 111^{o}C), methylhydroquinone (T_m =128^{o}C), and l-xylose (T_m = 150^{o}C). Before each WAXD measurement, the LPE samples were heated to 160^{o}C at a heating rate of 30^{o}C/min under vacuum and kept at this temperature for 2 minutes to erase their previous thermal history. The specimens were then cooled to $T_{I\rightarrow II}$ at a rate of 30^{o}C/min and crystallized isothermally for 12 hr. Goderis et al.[24] showed that the lattice coherence length of LPE crystals does not change significantly with time for crystallization at $T_{I\rightarrow II}$. WAXD patterns of the crystallized samples were recorded in a 0.05 - 0.28 nm^{-1} q range (i.e. 2θ between 7 and 40^o) for 20 min under vacuum at their respective crystallization temperatures using a Fujifilm™ HR-V image plate (with an aperture of 0.375" diameter and a sample-to-image plate distance of 92.0 mm). The image plate was scanned using a RAXIA-Di™ image plate reader. Angular calibration was performed using the third-order diffraction ring of a silver behenate standard. Using the SAXSGUI™ software package, the WAXD scattering intensity was corrected for Kapton™ scattering as well as absorption. Similar measurements

were performed using a lanthanum hexaboride standard to evaluate the instrumental peak broadening.

After subtraction of the amorphous halo, the (110), θ_p = 10.5°, and (200), θ_p = 11.5°, diffraction peaks of LPE crystals were fitted with Gaussian functions, Equation 4.1.

$$I(\theta) = a_1 \exp\left(-\frac{\left(\theta - \theta_p\right)^2}{2a_2^2}\right) \tag{4.1}$$

where θ_p, $I(\theta)$, a_1 and a_2 are the Bragg angle at maximum intensity, the angular dependent diffraction intensity, the diffraction peak height and the standard deviation of the Gaussian intensity distribution, respectively. The integral breath of each diffraction peak, Λ, was then obtained using:

$$\Lambda = a_2\sqrt{2\pi} \tag{4.2}$$

The integral breadth ($\Lambda_{stnd} = 0.206$) for the diffraction of lanthanum hexaboride at θ_p = 10.5° was obtained following the same method. The instrumental broadening contribution to the observed peak broadening of LPE crystals was then accounted for using the integral breadth of the standard, Λ_{stnd}, Equation 4.3.

$$\Lambda_{corr}^2 = \Lambda^2 - \Lambda_{stnd}^2 \tag{4.3}$$

Λ_{corr} is the corrected integral breadth for each diffraction peak. The lattice coherence length associated with each growth front, $D_{(hjk)}$, was then calculated using the Scherrer equation,[25] Equation 4.4.

$$D_{(hjk)} = \frac{\lambda}{2\Lambda_{corr}\cos\theta_p} \tag{4.4}$$

Measurements were performed in triplicate for each LPE sample.

4.5. Results and Discussion

4.5.1. Modified Lauritzen-Hoffman Secondary Nucleation Theory

Following Hoffman and Miller,[6] the average number of CH_2 units per chain, n, was calculated for each fraction used in the isothermal spherulite growth rate analysis, Equation 4.5.

$$n = \sqrt{n_n \times n_w} \tag{4.5}$$

Here n_n and n_w are the number- and weight-average numbers of CH_2 units per chain, respectively. Table 4.1 lists n and the polydispersity index (PDI) for each fraction. References for the temperature-dependent spherulite growth rate data of these LPE fractions are also included in Table 4.1 along with the respective equilibrium melting temperatures estimated using the Huggins equation.[15]

$$T_m^{eq} = 414.6\ K \left(\frac{n_n - 1.2}{n_n + 5.3}\right) \tag{4.6}$$

Table 4.1. Average number of CH_2 units per chain, polydispersity index, and equilibrium melting temperature for the LPE fractions used here (reported in the literature).

n	**PDI**	T_m^{eq} (°C)	**Ref.**	***N***	**PDI**	T_m^{eq} (°C)	**Ref.**
690	1.13	137.4	[2]	2000	1.19	140.0	[4]
780	1.09	137.9	[4]	2030	1.12	140.1	[4]
790	1.13	137.9	[7]	2360	1.12	140.3	[7]
800	1.09	138.0	[4]	2560	1.10	130.4	[4]
810	1.07	138.1	[4]	2750	1.22	130.4	[4]
1080	1.10	138.1	[7]	3480	1.09	130.7	[7]
1170	1.08	138.3	[4]	3830	1.37	130.7	[4]
1100	1.39	138.6	[4]	4140	1.30	130.8	[8]
1390	1.14	139.4	[2]	4530	1.17	130.9	[4]
1410	1.02	139.6	[4]	5020	1.12	130.9	[1, 4]
1600	1.10	139.7	[7]	6620	1.10	141.1	[7]
1640	1.07	139.8	[4]	7590	1.26	141.1	[4]
1700	1.07	139.9	[4]	8990	1.12	141.2	[7]

Figure 4.1a-d illustrates the isothermal spherulite growth rate *vs.* crystallization temperature data found in the literature for 26 narrow molar mass distribution LPE fractions (PDI < 1.4). In all instances, the isothermal spherulite growth rates were measured by optical microscopy.[1-2, 4, 7-8] All thermodynamic, crystallographic and other constants necessary for the analysis of spherulite growth rate data are given in Table 4.2. The value of $\bar{a}$ for each fraction was estimated by interpolation from a data set obtained using the non-linear Hoffman-Weeks analysis of similar materials, Figure 4.2.[15] The significant scatter observed in Figure 4.2 led us to carry out two different analyses in this manuscript. First, we assumed that $\bar{a}$ is independent of chain length (dashed line in Figure 4.2) and used the average value of $\bar{a}$ measured for three narrow molar mass distribution NIST fractions ($\bar{a}$ = 17.7 ± 1.7). In the second approach, we used a Huggins type equation ($\bar{a} = 18.57\left[\frac{n_n-420}{n_n-330}\right]$) (solid line in Figure 4.2) to estimate the value of $\bar{a}$ for each fraction. We recall that $\bar{a}$ is given by $\frac{C_2\Delta H}{2\sigma_{ec}^o}$ and C_2, the limiting lamellar thickness at infinite undercooling, varies with chain length similarly to y, the strength of stem length fluctuations.[15, 26] Speculating that the strength of stem length fluctuations correlates with the thickness of the melt-crystal interphase in the case of linear polyethylene could explain the increase of $\bar{a}$ with chain length (solid line in Figure 4.2).[27-30]

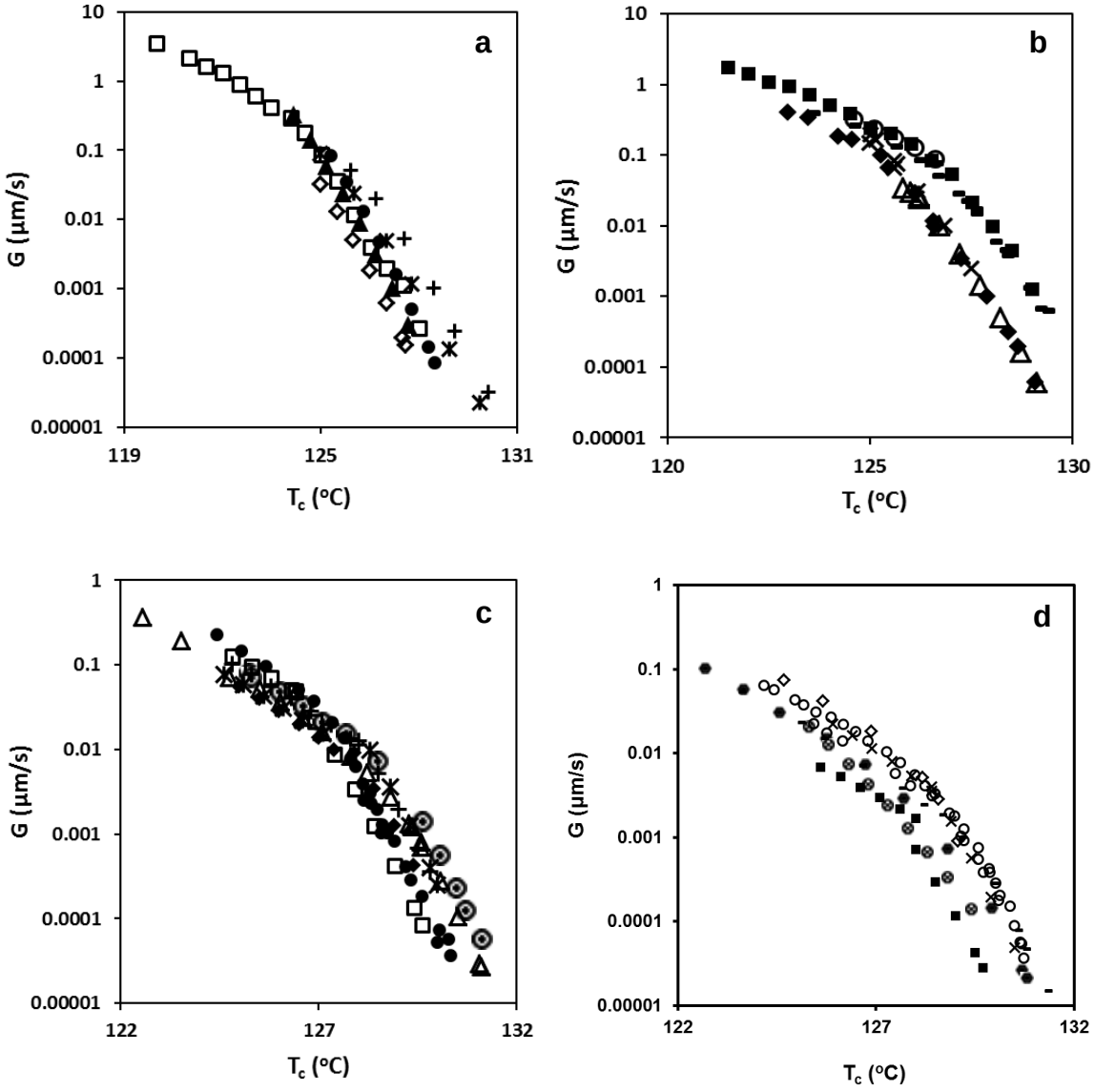

Figure 4.1. Spherulite growth rate *vs.* crystallization temperature for LPE fractions characterized by n of: a) 690 (□), 780 (▲), 790 (*), 800 (◊) and 810 (●) b) 1080 (+), 1100 (♦), 1170 (×), 1390 (■), 1410 (Δ), 1600 (-) and 1640 (○) c) 1700 (□), 2000 (●), 2030 (♦), 2360 (◎), 2560 (*), 2750 (+) and 3480 (Δ) d) 3830 (×), 4140 (◊), 4530 (■), 5020 (○), 6620 (●), 7590 (⊗) and 8990 (-).

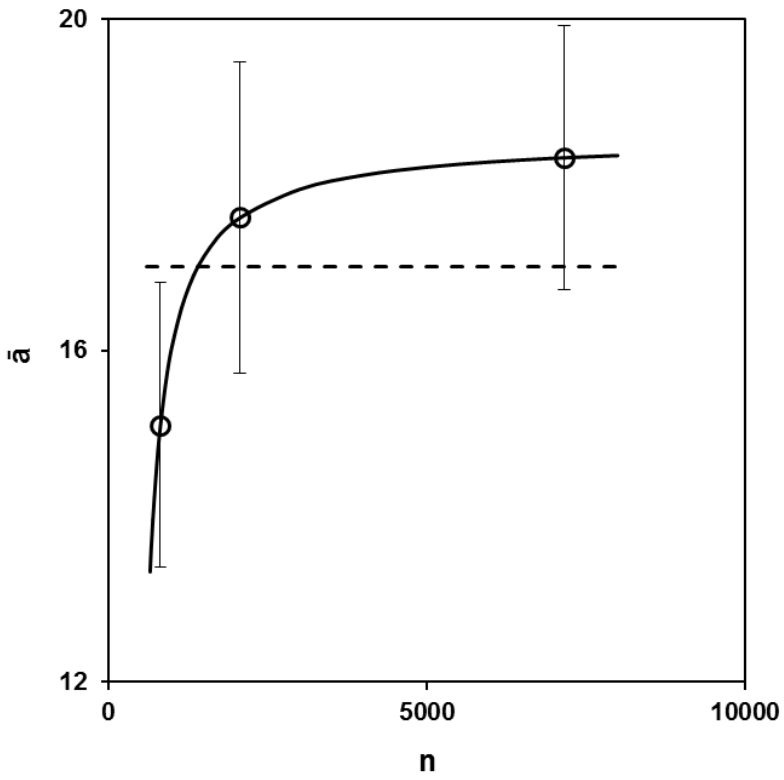

Figure 4.2. $\bar{a}$ *vs.* n for three LPE fractions. The dashed line shows the average value for $\bar{a} = 17 \pm 1.7$ while the solid line represents the best fit to the data, using a Huggins like equation. Error bars correspond to one standard deviation associated with the linear fit of M vs. X data.[15]

Table 4.2. Constants used for the analysis of spherulite growth rate data of LPE.

a_o	4.55×10^{-8} cm [31]	ζ	-1.2×10^{-3} °C [32]
b_o	4.15×10^{-8} cm [31]	θ	35° [33-36]
ℓ_b	1.54×10^{-8} cm	α	109.5°
ℓ_u	1.273×10^{-8} cm	m_o	14.03 g/mol
ΔH	283 J/cm^3 [37]	n_t	21.3 [38]
Q_d^*	24 kJ/mol [39]	N_{av}	6.022×10^{23}
R	8.3145 J/mol	ρ^*	1.1 g/cm^3 [40]
k	1.3806×10^{-23} J/K	ϵ	8.11×10^{-4} K^{-1} [40]
C_∞	7.38 at 140°C [32]	D_1^o	4.3×10^{-2} cm^2/sec [41]

As discussed in Appendix B, the crystal growth regimes can be determined by plotting $\ln G + \frac{Q_d^*}{RT_c} - \ln \psi(T_c) - \Sigma(T_c)[1-\chi(T_c)]$ and $\ln G + \frac{Q_d^*}{RT_c} - \ln \varphi(T_c) - \frac{\Sigma(T_c)}{2}[1-\chi(T_c)]$ *vs.* $\exp(\zeta \Delta T)\left[\frac{1}{\Delta T} + \frac{\bar{a}}{T_m^{eq}}\right][1-\chi(T_c)]$, Equations B.29 and B.30. The regime I/II transition temperature is related to the change of slope in such plots. The location of the regime transition temperature is not affected by our choice of $\bar{a}$. Given the undercooling limits associated with regimes I and II, we can evaluate the dependence of spherulite growth rate on chain length for each regime, Figures 4.3 and 4.4.

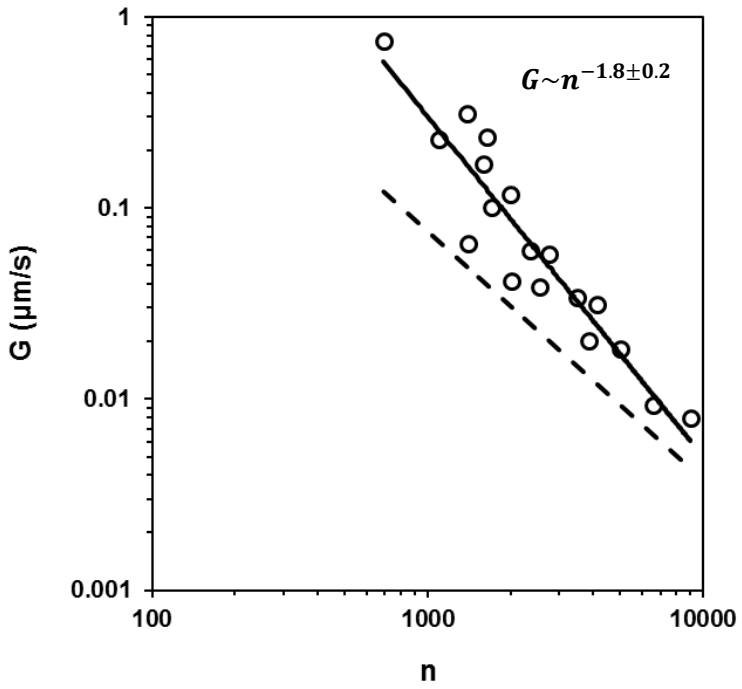

Figure 4.3. G *vs.* n at ΔT = 14.6°C, in regime II. The solid line represents the best fit to the data. The dashed line is a power law behavior with exponent of -1.3.

Figure 4.3 shows a plot of G *vs.* n at ΔT = 14.6°C in regime II. The chain length dependence of the spherulite growth rate exhibits a power law behavior with an exponent of -1.8 ± 0.2. A similar analysis carried out at ΔT = 11.4°C in regime I leads to an exponent of -1.5 ± 0.2. The average power law exponent found here (-1.6 ± 0.2) is much larger than that reported

by Hoffman and Miller,[6] ($G \propto n^{-1}$) but is similar to that reported (-1.7) by Hikosaka et al.[3] for folded chain single crystals and spherulites of LPE fractions. The data presented here does not support the existence of distinct spherulite growth regimes with different chain length dependences.[1, 6] The calculated power law exponents and associated conclusions are obviously independent of the interpolation method for $\bar{a}$. Figure 4.4 illustrates changes in $-s$ the power law exponent in $G \propto n^{-s}$ with undercooling. The chain length dependence of G is the same in both regimes I and II within experimental uncertainty.

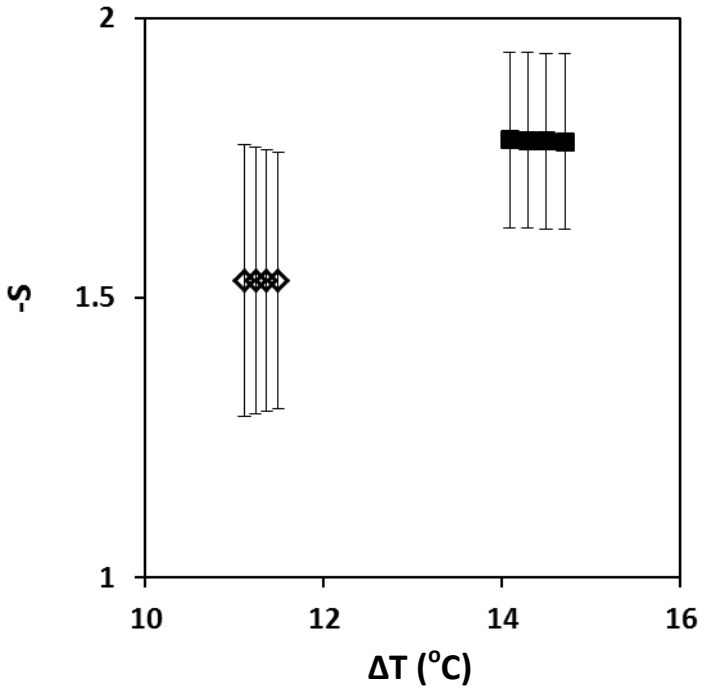

Figure 4.4. Power law exponent for the dependence of G on n in regime I (◊) and regime II (■). Error bars correspond to one standard deviation.

We then determined the values of K_g^o and $\sigma_{ec}^o/\cos\theta$ for each fraction in regimes I and II using Equations B.24, B.28, B.29 and B.30, Figure 4.5. Within each regime the data displays a constant slope.

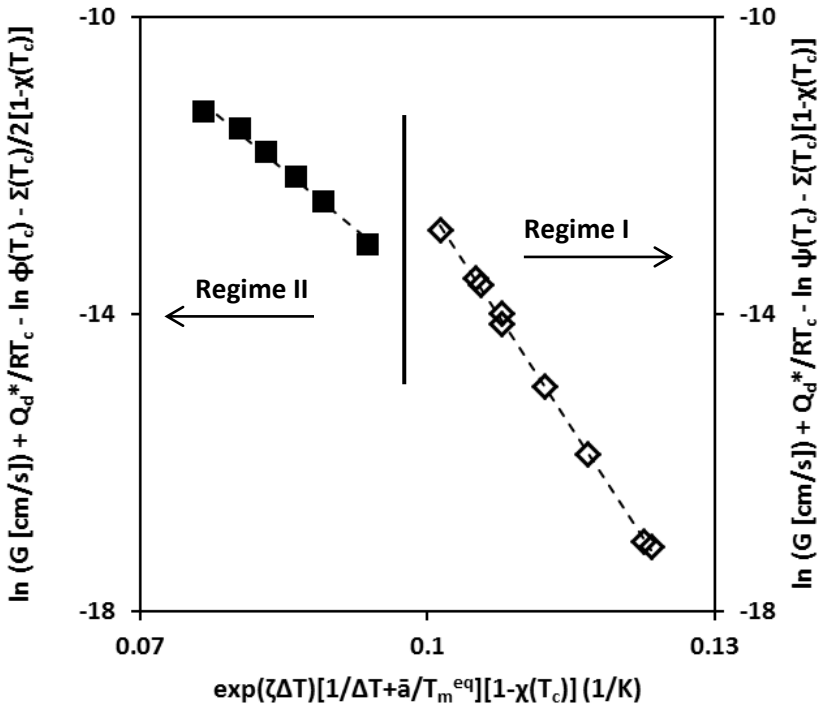

Figure 4.5. $\ln G + \frac{Q_d^*}{RT_c} - \ln\psi(T_c) - \Sigma(T_c)[1-\chi(T_c)]$ and $\ln G + \frac{Q_d^*}{RT_c} - \ln\varphi(T_c) - \frac{\Sigma(T_c)}{2}[1-\chi(T_c)]$ *vs.* $\exp(\zeta\Delta T)\left[\frac{1}{\Delta T} + \frac{\bar{a}}{T_m^{eq}}\right][1-\chi(T_c)]$ for the n = 3480 fraction. The dashed lines represent the best fit to the data in regime I (◊) and regime II (■). The solid line shows the transition between regimes I and II.

The ratio K_{gI}^o/K_{gII}^o is equal to 2.1 ± 0.3, in accordance with theoretical predictions.[6] Figure 4.6 shows the changes of $\sigma_{ec}^o/\cos\theta$ with n assuming $\bar{a}$ is independent of chain length. Values of $\sigma_{ec}^o/\cos\theta$ in regimes I and II are randomly scattered about their average $\sigma_{ec,I}^o/\cos\theta$ = 46.1 ± 5.7 erg/cm^2 and $\sigma_{ec,II}^o/\cos\theta$ = 44.5 ± 4.3 erg/cm^2. The average value of $\sigma_{ec}^o/\cos\theta$ in regimes I and II for polyethylene fractions with M_n values ranging from 9 to 120 kg/mol is 45.5 ± 5.2 erg/cm^2, independent of chain length. The same magnitude and uncertainty are obtained for $\sigma_{ec}^o/\cos\theta$ when the calculations are repeated with a chain length dependent $\bar{a}$. Considering the often quoted tilt angles of 19^o and 35^o for melt crystallized LPE (associated with (101) and (201) fold surfaces), respective values of 42.9 ± 4.9 and 37.2 ± 4.3 erg/cm^2 are found for the equilibrium

fold surface free energy, σ_{ec}^{o}.[33-36] Analysis of the initial lamellar thickness data of Barham et al.[42] for a melt-crystallized 29K LPE fraction led to σ_{ec}^{o} = 45.5 ± 2.0 erg/cm^2.[15] Hoffman et al.[43] suggested that the fold surface of melt-crystallized LPE lamellae equilibrate during heating to the melting point, therefore, $\sigma_{ec}^{o} = \sigma_{em}$. A Gibbs-Thomson analysis of Barham's 29K LPE data led us to σ_{em} = 41.5 ± 2.0 erg/cm^2.[15] A similar analysis of Cho et al.'s data[12] led Crist[13] to σ_{em} = 44 ± 5 erg/cm^2. Within the limits of experimental error, all values reported here for σ_{ec}^{o} and σ_{em} for melt crystallized polyethylene fractions are identical. These values are about half that reported by Hoffman et al.[4-6, 11, 43-45]

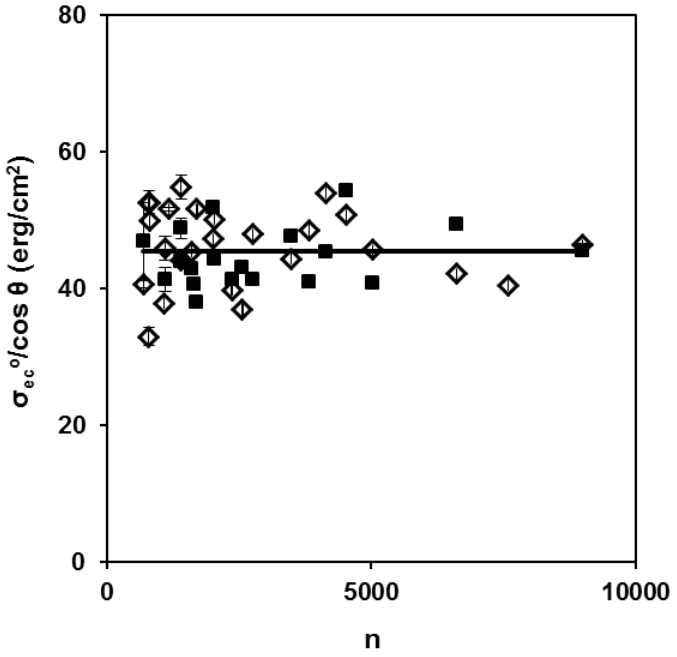

Figure 4.6. $\sigma_{ec}^{o}/\cos\theta$ *vs.* n for crystal growth of LPE fractions in regime I (◊) and in regime II (■). Fold surface free energies reported here were obtained assuming $\bar{a}$ is independent of chain length. The solid line shows the average value $\sigma_{ec}^{o}/\cos\theta$ = 45.5 ± 5.2 erg/cm^2 . The same average value is obtained when assuming that $\bar{a}$ increases with chain length (see Figure 4.2).

To determine more reliably the location of the regime transition temperature and the magnitude of G_o in each regime for each fraction, we took advantage of the observation (Figure

4.6) that K_{gI}^{o} and K_{gII}^{o} are independent of chain length and carried out the linear regression (Equations B.29 and B.30) by constraining the fits with the assumption of a constant K_{gI}^{o} or K_{gII}^{o} value. The transition temperature between regimes I and II is located at the point of intersection of the linear regression fits for each regime. For all fractions studied here, the transition between regimes I and II is sharp. The values of $T_{I\to II}$ found by this method are very close to these estimated by Hoffman et al.[4] from spherulite growth rate measurements and by Allen et al.[10] from calorimetric data, independent of the method used to interpolate $\bar{a}$.

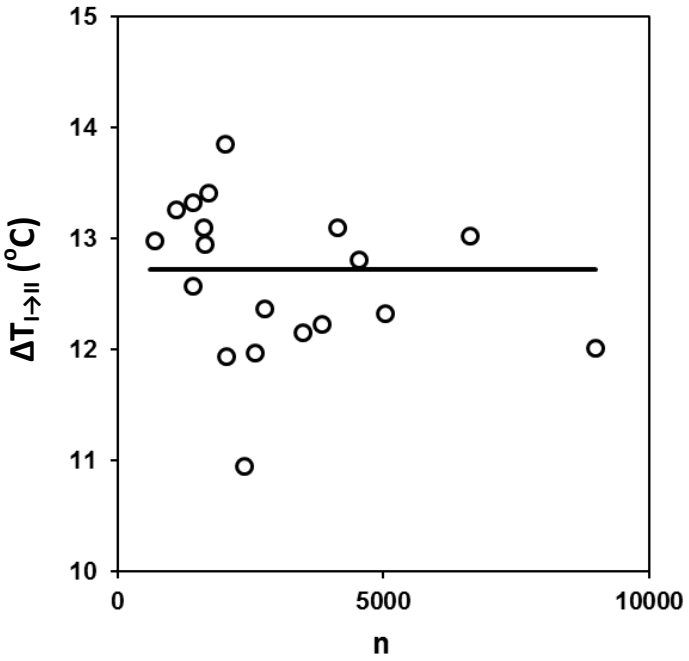

Figure 4.7. $\Delta T_{I\to II}$ *vs.* n. The solid line represents the average $\Delta T_{I\to II}$ = 12.7 ± 0.5°C.

Figure 4.7 depicts the dependence of $\Delta T_{I\to II}$, the undercooling at the I/II regime transition on chain length, n. The undercooling at the I/II regime transition shows no dependence on chain length and has an average value $\Delta T_{I\to II}^{avg}$ = 12.7 ± 0.5°C, about 4°C lower than the value reported by Hoffman and Miller.[6] This difference in the $\Delta T_{I\to II}^{avg}$ value is a reflection of the different methods used to determine the equilibrium melting temperatures (Flory-Vrij vs. Higgins-Broadhurst).[15]

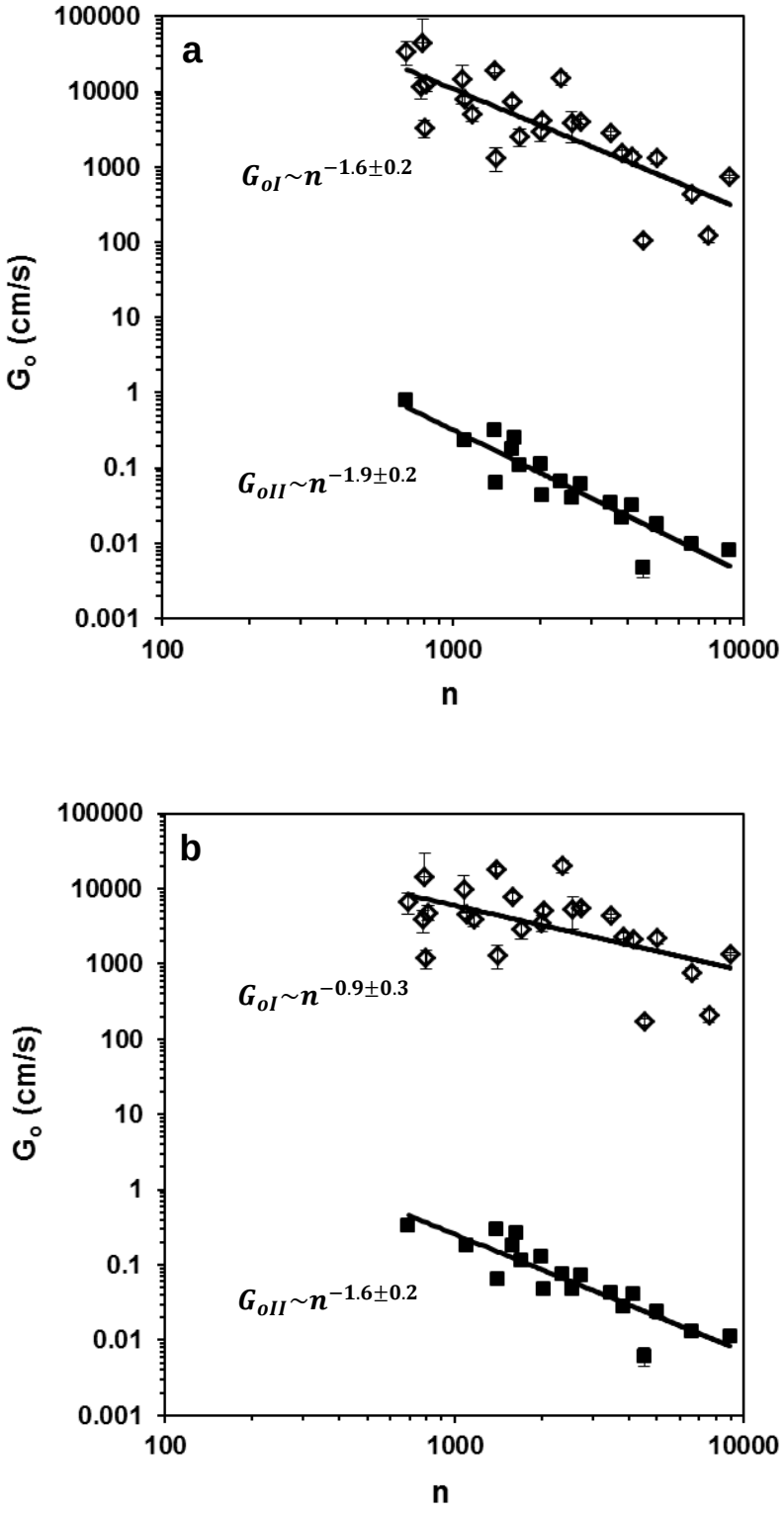

Figure 4.8. G_o *vs.* n for regime I (◊) and regime II (■) calculated: (a) assuming $\bar{a}$ to be constant and (b) assuming $\bar{a}$ to be chain length dependent (see Figure 4.2).
The solid lines represent the best fit to the data.

Figures 4.8.a and 4.8.b illustrate the power law dependence of G_o on chain length ($G_o \sim n^{-t}$) in regimes I and II for LPE. We note that the chain length dependences of G_{oI} and G_{oII} depend on the method used to assign the value of $\bar{a}$ for each fraction (Figure 4.8). When $\bar{a}$ is assumed independent of chain length, the power law exponents for G_{oI} and G_{oII}, in regimes I and II, are similar, within experimental error, to the power law exponent for G (t and s ~ 1.75). These results are expected from an inspection of Equations B.29 and B.30 where K_{gI}^{o} and K_{gII}^{o} are independent of chain length. In the range of chain lengths considered here, we find y = 0.032 $^{o}C^{-1}$, approximately independent of chain length (Figure 4.9.a). When $\bar{a}$ is assumed to increase with chain length, the power law exponents for G_{oI} and G_{oII}, in regimes I and II, are different (Figure 4.8). Under these conditions, y is observed to increase with chain length (Figure 4.9.b) following the behavior of $\bar{a}$ (Equation B.17). The difference in behaviors shown by the stem length fluctuation parameter, y, in Figures 4.9.a. and 4.9.b is easily understood by consulting Equation B.17. The $\bar{a}$-containing term on the left hand-side of Equation B.17 is about five times larger than the δ' term, that is, the largest contribution to the limiting initial lamellar thickness at infinite undercooling, C_2, is from stem length fluctuations.

Figure 4.10 shows the WAXD pattern for the LPE fraction with M_n = 28.9 kg/mol crystallized isothermally at 127.4^{o}C (regime I/II transition temperature) for 12 hr. Integral breadth, Bragg spacing and coherence length for the (110) and (200) reflections of the three LPE fractions are shown in Table 4.3 at their regime I/II transition temperature. The (110) and (200) coherence lengths corrected for the tilt angle of the crystallized stems are 42 ± 1 nm and 29 ± 2 nm, within experimental uncertainty independent of chain length, Table 4.3. The average (110) substrate of linear polyethylene crystals at the regime I to II transition temperature is made of 75 ± 2 crystallized stems. Using the isohypse technique, Point et al.[46-47] showed that the substrate of linear polyethylene crystals must be made of less than 1800 stems (L < 1 μm).

Toda,[9] studying single crystal growth from the melt, pushed the upper bound further down to 100 nm for linear polyethylene.

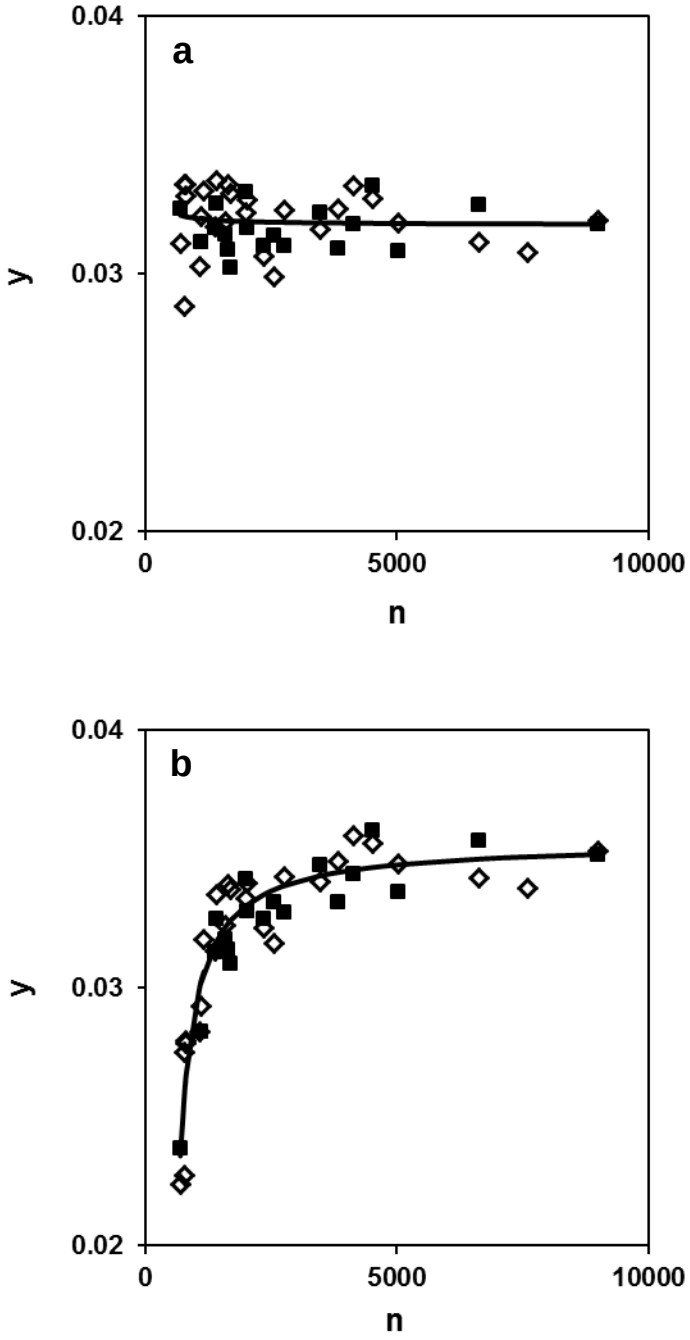

Figure 4.9. y *vs.* n in regime I (◊) and in regime II (■) calculated at the regime I/II transition temperature: (a) assuming $\bar{a}$ to be constant and (b) assuming $\bar{a}$ to be chain length dependent (see Figure 4.2). The solid lines represent the best fit to the data.

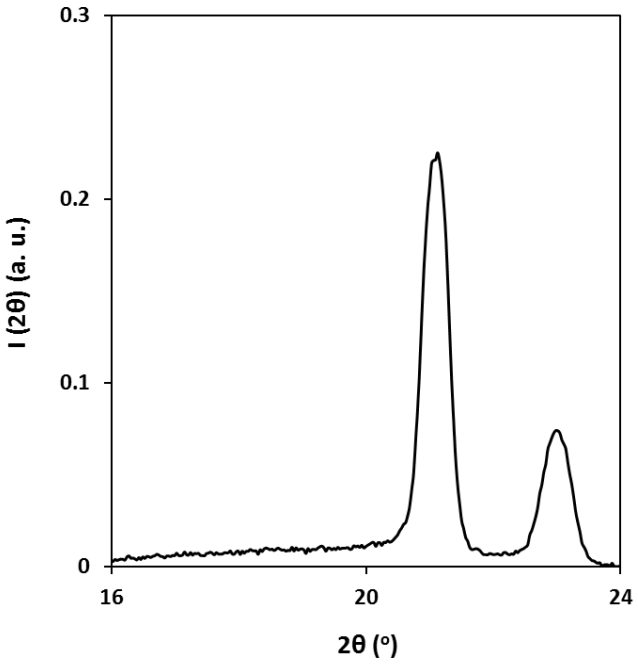

Figure 4.10. Diffracted intensity *vs.* 2θ for the sample with M_n = 28.9 kg/mol crystallized isothermally at 127.4°C for 12 hr.

Table 4.3. Integral breadth, Bragg spacing and substrate length for the (110) and (200) growth fronts of three LPE fractions at their respective I/II regime transition temperatures.

M_n (kg/mol)	$\Lambda_{(110)}$	$\theta_{p(110)}$	$L_{(110)}$ (nm)	$\Lambda_{(200)}$	$\theta_{p(200)}$	$L_{(200)}$ (nm)
11.4	0.24 ± 0.02	10.6 ± 0.1	43 ± 6	0.27 ± 0.01	11.5 ± 0.1	31 ± 2
28.9	0.24 ± 0.01	10.5 ± 0.1	42 ± 1	0.28 ± 0.01	11.5 ± 0.1	28 ± 1
100.5	0.25 ± 0.02	10.6 ± 0.1	41 ± 4	0.29 ± 0.01	11.5 ± 0.1	26 ± 2

Alcazar et al.[48] measured the substrate length of isotactic poly(vinylcyclohexane) at different temperatures. This polymer displays twinned growth sectors, which makes the direct measurement of the substrate length feasible via dark field electron microscopy imaging. They found that in regime II the substrate of poly(vinylcyclohexane) crystals is made of 35 to 60

stems and becomes larger at higher temperatures.[48] The number of stems comprising the substrate length for poly(vinylcyclohexane) is comparable with that for linear polyethylene.

The width of the critical nucleus, defined by $L_s = \nu_s a_o / \cos\theta$, is the minimum size necessary for a nucleus to reach the zone of thermodynamic stability (Appendix B). L_s and $L_{(110)}$, the (110) substrate length measured at the regime I to II transition temperature, are plotted as a function of chain length in Figure 4.11. The measured (110) substrate length is larger than the width of the critical nucleus, satisfying an important criterion for any physical model of crystal growth.

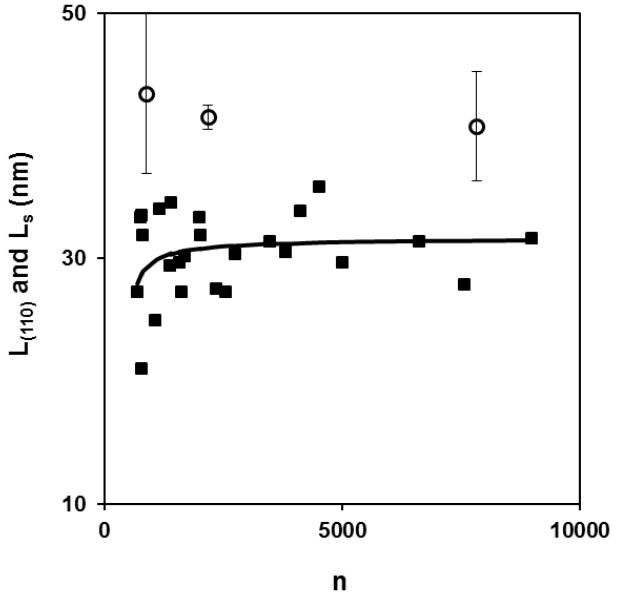

Figure 4.11. $L_{(110)}$ (○) and L_s (■) *vs.* n at the regime I/II transition temperature. The solid line is the best fit to the L_s *vs.* n data assuming K_g^o is independent of chain length. Error bars correspond to the standard deviation on triplicate measurements.

Knowledge of the quantities $L_{(110)}$, $\sigma_{ec}^o/\cos\theta$, G_{oI}, and G_{oII} at the regime I to II transition temperature, allows determination of C_o, the path degeneracy, and ξ_c^o, the apparent chain friction coefficient during crystallization normalized to a reference temperature of T_o = 448.15 K. Examination of Equation B.31 indicates that, when $\bar{a}$ is constant, the path degeneracy, C_o,

should be independent of chain length (see Figure 4.12.a). On the other hand, when $\bar{a}$ is assumed to increase with chain length, the power law exponents in regimes I and II differ from each other, leading to a chain-length dependent configurational path degeneracy (see Figure 4.12.b).

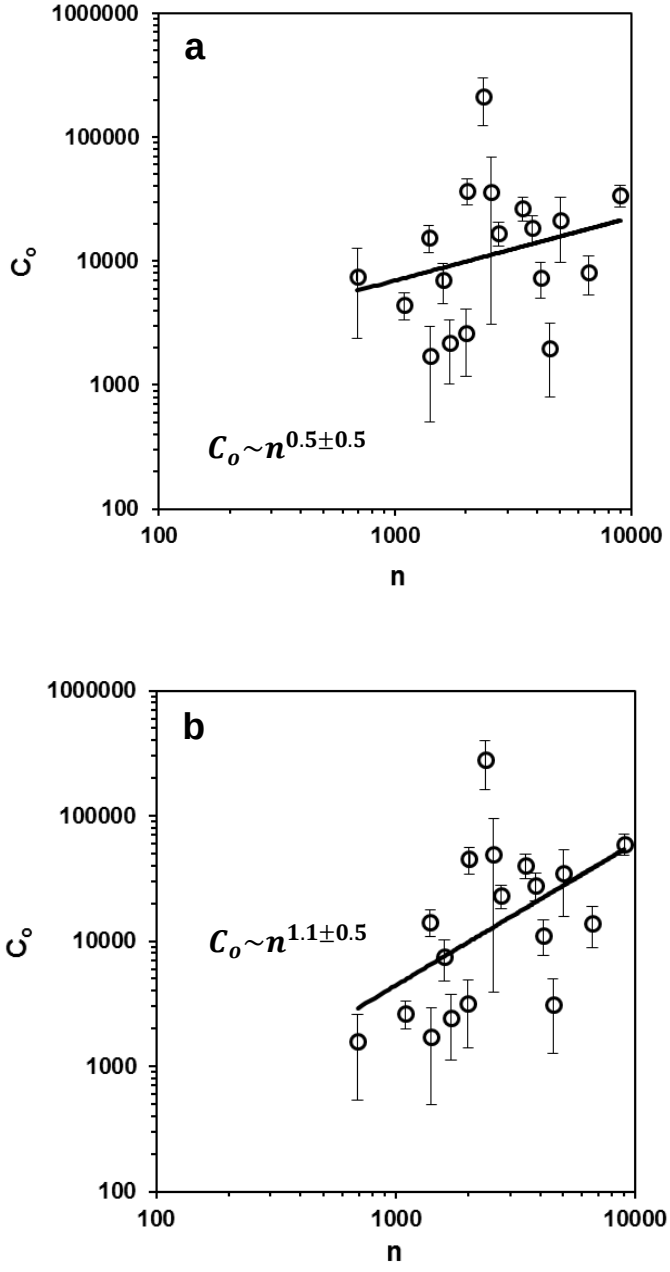

Figure 4.12. C_o *vs.* n at the regime I/II transition temperature estimated: (a) assuming $\bar{a}$ to be constant and (b) assuming $\bar{a}$ to be chain length dependent (see Figure 4.2).
The solid lines represent the best fit to the data.

The apparent friction coefficient during crystallization normalized to a reference temperature of T_o = 175°C (Figure 4.13) exhibits a power law dependence on chain length, $\xi_c^o \sim n^{2.1\pm0.2}$, that is independent of the interpolation method for $\bar{a}$ (see Equation B.32). This power dependence is stronger than the dependence of the friction coefficient associated with the curvilinear reptation process of the chain in a pure melt accounting for constraint release and contour length fluctuations at the reference temperature of T_o = 175°C, $\xi^o \sim n^{1.3}$, Figure 4.13.

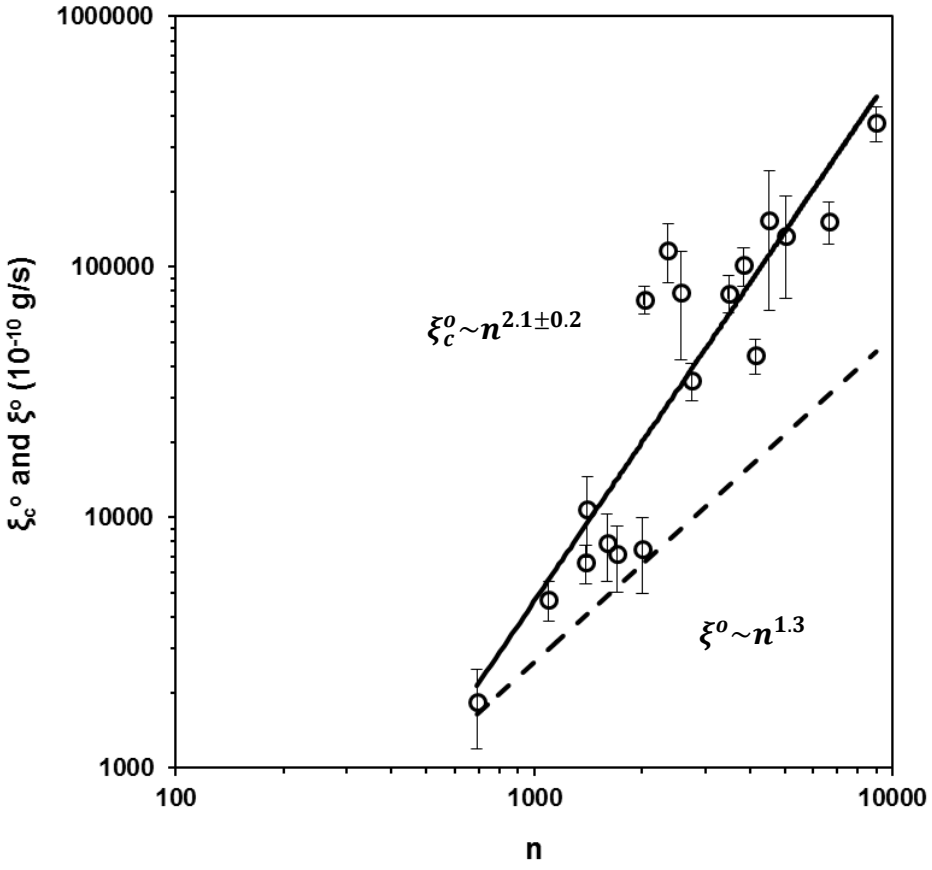

Figure 4.13. Apparent chain friction coefficient for LPE during crystallization (○) and curvilinear chain friction coefficient in the melt (- - -) at the reference temperature of 175°C. The solid line is the best fit to the apparent chain friction coefficient of LPE during crystallization.

For short chains the magnitude of ξ_c^o is very close to ξ^o, Figure 4. 13. The difference between ξ_c^o and ξ^oincreases with increasing chain length. Therefore, other processes must be involved in the transport of chain segments through the melt-crystal interface. Self-poisoning[49-51] is an example of such processes. During crystallization of longer LPE chains, wrongly attached stems on the crystal growth front detach slower, increasing the retardation time of crystallization and hence, the apparent friction coefficient.

Studying the chain length dependence of the crystal growth rate of folded chain crystals (FCCs) and extended chain crystals (ECCs), Hikosaka et al.[3] claimed that during crystallization of LPE, the sliding diffusion of the chains on the crystal growth front is much slower than the forced reptation process, hence, it is the main process controlling the chain length dependence of the crystal growth rate. Our results in the shorter chain region ($\xi_c^o \sim \xi^o$ at n = 700 - 2000) contradicts the proposed mechanism by Hikosaka et al.[3] On the other hand, appointing the sliding diffusion of the chains on the crystal growth front as the main source of friction implies that crystallizing segments from other chains should be much more feasible than adjacent re-entry of a crystallizing chain, a behavior only observed at high undercoolings (regime III). For further evaluation of the apparent friction coefficient data of the chains crystallizing into FCCs and ECCs, the chain length dependence of $\bar{a}$ and the configurational path degeneracy of the FCCs and ECCs needs to be considered carefully.

4.6. Conclusions

The Lauritzen-Hoffman secondary nucleation theory is modified to account for the effect of stem length fluctuations on crystallization kinetics of polymers. The tilt angle of the crystallized stems and the temperature dependence of the lateral surface free energy are also considered in the model. Spherulite growth rate data of 26 linear narrow molecular weight polyethylene samples are analyzed at low to moderate undercoolings using the modified LH theory. Equilibrium melting temperature of the fractions are estimated by a Huggins equation. The regime I to II transition occurs at an undercooling $\Delta T_{I\to II}$ = 12.7 ± 0.5°C independent of chain length. In both regimes, G is proportional to $n^{-1.6\pm0.2}$. This power law dependence was much stronger than that reported by Hoffman and Miller.[6] The value of $\sigma_{ec}^{o}/\cos\theta$ is equal to 45.5 ± 5.2 erg/cm^2 and independent of chain length. The ratio of K_{gI}^{o}/K_{gII}^{o} is equal to 2.1 ± 0.3, matching the LH model's prediction. On one hand, if we assume a chain length dependent $\bar{a}$, then, G_{oI} and G_{oII} exhibit different dependencies on chain length (i.e. $G_{oI} \propto n^{-0.9\pm0.3}$ and $G_{oII} \propto n^{-1.6\pm0.2}$). At $\Delta T_{I\to II}$, the strength of the stem length fluctuations, y, increases with molecular weight and reaches a plateau at high molecular weights. If on the other hand, we assume a constant value of 17 for $\bar{a}$, we obtain a constant value y of 0.032 $^{o}C^{-1}$ at $\Delta T_{I\to II}$. Under these circumstances, G_{oI} and G_{oII} exhibit similar dependencies on chain length as G. The substrate lengths of three linear polyethylene fractions were measured at their $\Delta T_{I\to II}$ using WAXD. The substrate lengths of the (110) and (200) growth fronts were independent of molecular weight. The apparent friction coefficient of a crystallizing linear polyethylene chain was proportional to $n^{2.1\pm0.2}$. Higher apparent friction coefficients indicate that additional mechanisms are involved in the transport of chain segments through the melt-crystal interface during crystal growth.

4.7. Appendix B: Modification of the LH Theory

Figure B.1 shows the schematic three dimensional representation of a linear polyethylene lamella with tilted crystallized stems.

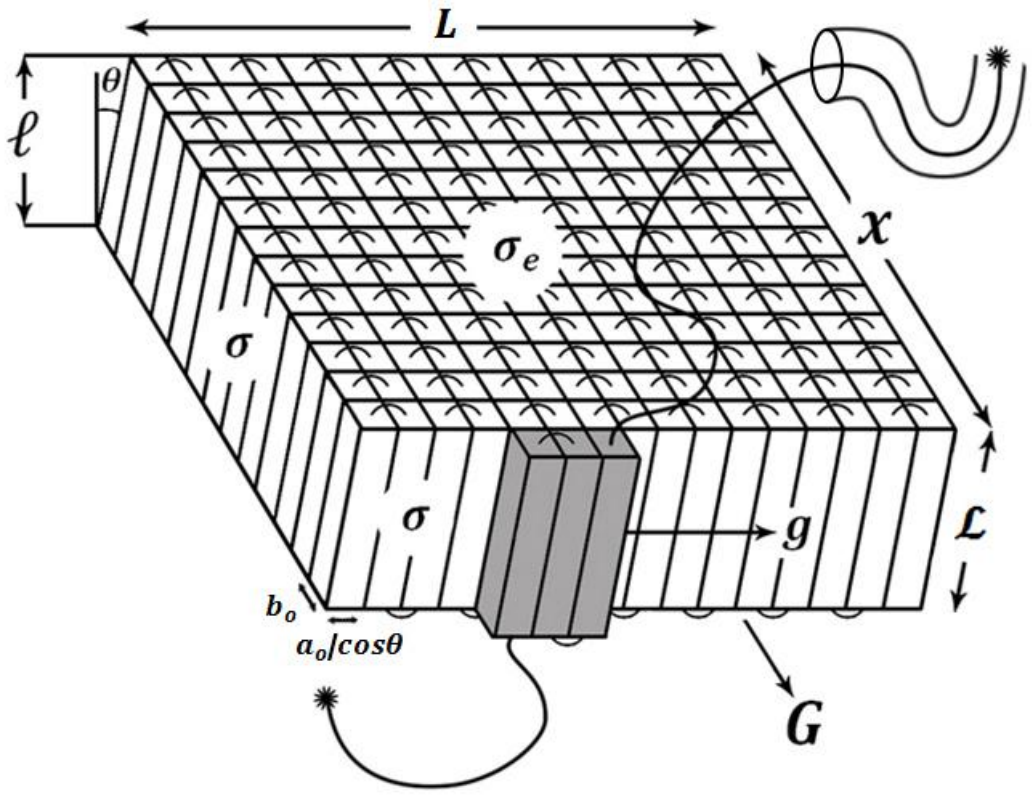

Figure B.1. Schematic three-dimensional representation of a linear polyethylene lamella with tilted crystallized stems. a_o, b_o, $\mathcal{L}$ and θ are the width, thickness, length and tilt angle of crystallized stems, respectively. x, and ℓ are the length and thickness of the lamella, respectively. L is the substrate length. A chain, moving in the reptation tube, has crystallized from the melt on the lamella, completing a new layer at the rate of g, leading to an overall crystal growth rate of G (the new layer is colored in gray).

Accounting for the tilt angle, the average substrate completion rate, $\bar{g}$, in the LH theory is expressed as:[11]

$$\bar{g} \equiv \frac{a_o}{\cos\theta}(A - \bar{B}) \tag{B.1}$$

Given the expression for the rate of stem attachments (A) and detachments (B) at low undercoolings in regimes I and II,[15] the substrate completion rate at the crystallization temperature, T_c, is given by:

$$\bar{g} = \frac{a_o \beta}{\cos\theta}\left(\frac{a_o \Delta G^{\infty}}{2\sigma}\left[\frac{a_o \Delta G^{\infty} + 4\sigma}{a_o \Delta G^{\infty} + 2\sigma}\right]\right)\exp\left(-\frac{2 a_o b_o \sigma_{ec}}{k T_c \cos\theta}\right) \tag{B.2}$$

β is a retardation factor associated with the transfer of polymer segments across the melt-crystal interface. ΔG^{∞} and k are the Gibbs free energy of fusion per unit volume for an infinitely large crystal and the Boltzmann constant, respectively. The average substrate completion rate is related to the average reeling-in rate of a polymer chain onto the crystal growth front, $\bar{r}$, by:[6, 44]

$$\bar{g} = \bar{r}\left(\frac{a_o}{\mathcal{L}_g^* \cos\theta}\right) \tag{B.3}$$

where $\mathcal{L}_g^*$ is the initial crystallized stem-length. The average reeling-in rate associated with displacement of polymer chains during crystallization in a viscous polymer melt is[6, 44]

$$\bar{r} = \frac{\bar{f}}{\xi_c} \tag{B.4}$$

where $\bar{f}$ and ξ_c are the average force felt by the chain during crystallization and the apparent friction coefficient of the chain in the subcooled melt at T_c, respectively. The average force of crystallization is related to the gradient in free energy of crystallization, which accounting for chain tilt leads to:[6, 15, 44, 52]

$$\bar{f} = \frac{1}{\mathcal{L}_g^*} a_o b_o \Delta G^{\infty}\left[\mathcal{L}_g^* - \frac{2\sigma_{ec}}{\Delta G^{\infty}\cos\theta}\right]$$

$$\bar{f} = \frac{1}{\mathcal{L}_g^*} a_o \Delta G^{\infty} \frac{k T_c}{2\sigma}\left[\frac{a_o \Delta G^{\infty} + 4\sigma}{a_o \Delta G^{\infty} + 2\sigma}\right] \tag{B.5}$$

where σ_{ec} is the fold surface free energy during crystal growth. Combining Equations B.3, B.4 and B.5 leads to:

$$\bar{g} = \left(\frac{1}{\xi_c \mathcal{L}_g^*} a_o \Delta G^\infty \frac{kT_c}{2\sigma}\left[\frac{a_o \Delta G^\infty + 4\sigma}{a_o \Delta G^\infty + 2\sigma}\right]\right)\left(\frac{a_o}{\mathcal{L}_g^* \cos\theta}\right) \tag{B.6}$$

Comparison of Equations B.2 and B.6 leads to the expression for β given in Equation B.7.

$$\beta = \left(\frac{kT_c}{\xi_c \mathcal{L}_g^{*2}}\right) \exp\left(\frac{2a_o b_o \sigma_{ec}}{kT_c \cos\theta}\right) \tag{B.7}$$

In the LH theory, the crystal growth rates in regime I, G_I, and regime II, G_{II}, are expressed as[6, 11]

$$G_I \equiv b_o i L = b_o \left(\frac{S_{T_c}}{L}\right) L = b_o S_{T_c} \tag{B.8}$$

$$G_{II} \equiv b_o \sqrt{2i\bar{g}} = b_o \sqrt{\frac{2\cos\theta \, S_{T_c} \bar{g}}{n_L a_o}} \tag{B.9}$$

where n_L is the number of stems of width a_o comprising the substrate of length L. Using the expression of the net flux over the barrier at the crystallization temperature, S_{T_c}, derived for lamellae with tilted chains,[15] we obtain:

$$G_I = \frac{kC_o n_L}{\xi_c \ell_u \mathcal{L}_g^{*2}}\left[\frac{a_o \Delta G^\infty {kT_c}^2 \cos\theta}{2\sigma(2\sigma + a_o \Delta G^\infty)}\right] \exp\left(\frac{2a_o b_o \sigma_{ec}}{kT_c \cos\theta}\right) \exp\left(-\frac{4b_o \sigma \sigma_{ec}}{kT_c \Delta G^\infty \cos\theta}\right) \tag{B.10}$$

and

$$G_{II} = \left(\sqrt{\frac{2k^3 b_o C_o \cos\theta}{\ell_u}} \frac{1}{\xi_c \mathcal{L}_g^{*2}}\right) \sqrt{T_c(a_o \Delta G^\infty + 4\sigma)}\left[\frac{a_o \Delta G^\infty T_c}{2\sigma(a_o \Delta G^\infty + 2\sigma)}\right] \times$$
$$\exp\left(\frac{a_o b_o \sigma_{ec}}{kT_c \cos\theta}\right) \exp\left(-\frac{2b_o \sigma \sigma_{ec}}{kT_c \Delta G^\infty \cos\theta}\right) \tag{B.11}$$

where C_o and ℓ_u are the configurational path degeneracy and the C-C bond length projected along the crystal c-axis, respectively. In the most recent version of the LH theory, the lateral surface free energy is understood as the entropic penalty associated the localization of chain segments on the growth front during stem deposition.[45] For a crystallizing chain, the magnitude

of this entropic penalty is controlled by the chain stiffness, and therefore is related to the characteristic ratio, C_n.[45] Given the range of molecular weights studied here, we can use the limiting characteristic ratio, C_∞, and express the lateral surface free energy as:[45]

$$\sigma = \frac{T_c}{T_m^{eq}}\left(\frac{\Delta H a_o}{2}\right)\left(\frac{\ell_u}{\ell_b}\right)\frac{1}{C_\infty} \tag{B.12}$$

where T_m^{eq}, ΔH and ℓ_b are the equilibrium melting temperature, the volumetric heat of fusion and the C-C bond length, respectively. The temperature dependence of the limiting characteristic ratio is given by:[32, 38]

$$\frac{d \ln C_\infty}{dT} = \zeta \tag{B.13}$$

where ζ is a constant.[32, 38] Using Equation B.13, we can express the quantity C_∞ as a function of the undercooling and the limiting characteristic ratio at the equilibrium melting temperature, $C_{\infty,T_m^{eq}}$, showing explicitly the temperature dependence of the lateral surface free energy, Equation B.14.

$$\sigma = \frac{T_c \exp(\zeta \Delta T)}{T_m^{eq}}\left(\frac{\Delta H a_o}{2}\right)\left(\frac{\ell_b}{\ell_u}\right)\frac{1}{C_{\infty,T_m^{eq}}} \tag{B.14}$$

Introducing the lateral surface free energy at the equilibrium melting temperature, $\sigma^o = \left(\frac{\Delta H a_o}{2}\right)\left(\frac{\ell_b}{\ell_u}\right)\frac{1}{C_{\infty,T_m^{eq}}}$, we can simplify Equation B.14 to:

$$\sigma = \frac{T_c \exp(\zeta \Delta T)}{T_m^{eq}}\sigma^o \tag{B.15}$$

Consideration of stem length fluctuations during crystal growth leads to the following temperature dependence of σ_{ec} at low to intermediate undercoolings:[19, 43]

$$\sigma_{ec} = \sigma_{ec}^o(1 + y\Delta T) \tag{B.16}$$

The term y in Equation B.16 accounts for the strength of stem length fluctuations.[43] Recalling the expressions for C_2 and δ',[15]

$$C_2 = \delta' + \frac{2y\sigma_{ec}^o T_m^{eq}}{\Delta H}$$

$$\delta' = \frac{kT_c \cos\theta}{2b_o\sigma}\left[\frac{a_o\Delta G^\infty + 4\sigma}{a_o\Delta G^\infty + 2\sigma}\right]$$

we obtain the following expression for y:

$$y = \frac{\bar{a}}{T_m^{eq}} - \frac{k\Delta H \cos\theta \exp(-\zeta\Delta T)}{4b_o\sigma^o\sigma_{ec}^o}\left[\frac{a_o\Delta H\Delta T + 4\sigma^o T_c \exp(\zeta\Delta T)}{a_o\Delta H\Delta T + 2\sigma^o T_c \exp(\zeta\Delta T)}\right] \quad \text{(B.17)}$$

where $\bar{a}$ is the constant in the non-linear Hoffman-Weeks equation defined as $\frac{C_2\Delta H}{2\sigma_{ec}^o}$.[26] Hoffman and Miller[6] assumed that the chain friction coefficient during crystal growth is the same as that associated with the reptation process in the melt and use an Arrhenius expression to account for changes in ξ_c with temperature.[39, 53-54] One should note that other mechanisms, such as sliding diffusion[3] and poisoning,[51] may be involved in the transport of crystallizing segments across the melt-crystal interface and may or may not exhibit the same temperature dependence as reptation. In the absence of a detailed knowledge of the mechanisms involved, we will also make the assumption that the temperature dependence of ξ_c is calculated using Q_d^*, the activation energy for center of mass diffusion. Therefore,

$$\xi_c = \xi_c^o \exp\left(\frac{Q_d^*}{RT_c}\right)\exp\left(-\frac{Q_d^*}{RT_o}\right) \quad \text{(B.18)}$$

where ξ_c^o and R are the apparent chain friction coefficient at the reference temperature T_o = 175°C and the gas constant, respectively. Given the range of molecular weights studied here, Q_d^* is independent of molecular weight.[39] Using the appropriate temperature dependences for y, σ_{ec}, σ and ξ_c we obtain:

$$G_I = G_{oI} \exp\left(-\frac{Q_d^*}{RT_c}\right)\psi(T_c) \times$$

$$\exp(\Sigma(T_c)[1-\chi(T_c)]) \exp\left(-K_{gI}^o \exp(\zeta\Delta T)\left[\frac{1}{\Delta T}+\frac{\bar{a}}{T_m^{eq}}\right](1-\chi(T_c))\right) \tag{B.19}$$

where

$$G_{oI} = \frac{k^2 a_o C_o n_L \Delta H^3 \cos\theta}{8\xi_c^o \ell_u \sigma^o \left(\frac{\sigma_{ec}^o}{\cos\theta}\right)^2 T_m^{eq}} \exp\left(\frac{Q_d^*}{RT_o}\right) \tag{B.20}$$

$$\psi(T_c) = \left[\frac{T_c \Delta T \exp(-\zeta\Delta T)}{2\sigma^o T_c \exp(\zeta\Delta T) + a_o \Delta H \Delta T}\right]\left[\frac{1}{\Delta T}+\frac{\bar{a}}{T_m^{eq}}\right]^{-2} \tag{B.21}$$

$$\Sigma(T_c) = \left[\frac{a_o \Delta H \Delta T + 4\sigma^o T_c \exp(\zeta\Delta T)}{a_o \Delta H \Delta T + 2\sigma^o T_c \exp(\zeta\Delta T)}\right] \tag{B.22}$$

$$\chi(T_c) = \frac{a_o \Delta H \Delta T}{2\sigma^o T_c \exp(\zeta\Delta T)} \tag{B.23}$$

$$K_{gI}^o = \frac{4 b_o \sigma^o \sigma_{ec}^o}{k\Delta H \cos\theta} \tag{B.24}$$

For regime II we obtain

$$G_{II} = G_{oII} \exp\left(-\frac{Q_d^*}{RT_c}\right)\varphi(T_c) \times$$

$$\exp\left(\frac{\Sigma(T_c)}{2}[1-\chi(T_c)]\right) \exp\left(-K_{gII}^o \exp(\zeta\Delta T)\left[\frac{1}{\Delta T}+\frac{\bar{a}}{T_m^{eq}}\right][1-\chi(T_c)]\right) \tag{B.25}$$

where

$$G_{oII} = \frac{a_o \Delta H^3 \exp\left(\frac{Q_d^*}{RT_o}\right)}{\xi_c^o \sigma^o \left(\frac{\sigma_{ec}^o}{\cos\theta}\right)^2} \sqrt{\frac{k^3 b_o C_o \cos\theta}{32 \ell_u T_m^{eq\,3}}} \tag{B.26}$$

$$\varphi(T_c) = \psi(T_c)\sqrt{\frac{4\sigma^o T_c \exp(\zeta\Delta T) + a_o \Delta H \Delta T}{T_c}} \tag{B.27}$$

$$K_{gII}^o = \frac{2b_o\sigma^o\sigma_{ec}^o}{k\Delta H\cos\theta} \tag{B.28}$$

Taking the natural logarithm on both sides of Equations B.19 and B.25, we obtain

$$\ln G_I + \frac{Q_d^*}{RT_c} - \ln\psi(T_c) - \Sigma(T_c)[1-\chi(T_c)] = \ln G_{oI} - K_{gI}^o \exp(\zeta\Delta T)\left[\frac{1}{\Delta T} + \frac{\bar{a}}{T_m^{eq}}\right][1-\chi(T_c)] \tag{B.29}$$

$$\ln G_{II} + \frac{Q_d^*}{RT_c} - \ln\varphi(T_c) - \frac{\Sigma(T_c)}{2}[1-\chi(T_c)] = \ln G_{oII} - K_{gII}^o \exp(\zeta\Delta T)\left[\frac{1}{\Delta T} + \frac{\bar{a}}{T_m^{eq}}\right][1-\chi(T_c)] \tag{B.30}$$

We will show that plots of the right-hand sides of Equations B.29 and B.30 *vs.* $\exp(\zeta\Delta T)\left[\frac{1}{\Delta T} + \frac{\bar{a}}{T_m^{eq}}\right][1-\chi(T_c)]$ are linear within experimental error. Hence, the quantities K_{gI}^o , G_{oI}, K_{gII}^o and G_{oII} obtained from the slope and intercept of each plot, must be approximately independent of temperature. Values of K_{gI}^o and K_{gII}^o lead to the determination of $\sigma_{ec}^o/\cos\theta$ in regimes I and II using Equations B.24 and B.28. Since there are good reasons to expect that the substrate length varies with crystallization temperature,[31, 48] we can only calculate the configurational path degeneracy and the apparent friction coefficient for the crystallizing chain at the regimes I/II transition temperature through a combination of Equations B.20 and B.26.

$$C_o = \frac{2\ell_u b_o}{k\cos\theta\, {n_L}^2 T_m^{eq}}\left(\frac{G_{oI}}{G_{oII}}\right)^2 \tag{B.31}$$

$$\xi_c^o = \frac{ka_o b_o \Delta H^3}{4n_L\sigma^o\left(\frac{\sigma_{ec}^o}{\cos\theta}\right)^2 T_m^{eq2}}\left(\frac{G_{oI}}{{G_{oII}}^2}\right)\exp\left(\frac{Q_d^*}{RT_o}\right) \tag{B.32}$$

Two separate criteria are set to determine the reliability of the proposed approach. First, the values of σ_{ec}^o calculated for regimes I and II should be identical. Second, n_L, the number of stems per substrate length, should be larger than ν_s, the minimum number of stems necessary

for a secondary surface embryo to become a stable nucleus.[6] We can calculate ν_s by setting the Gibbs free energy of formation of ν crystalline stems to zero or $\Delta G_\nu = 0$, which leads to:

$$\nu_s = \frac{2\left(\sigma \ell_g^* - a_o \sigma_{ec}\right)}{a_o\left(\ell_g^* \Delta G^\infty - 2\sigma_{ec}\right)}$$

$$\nu_s = \frac{4\sigma\sigma_{ec} {T_m^{eq}}^2}{a_o \delta \Delta H^2 \Delta T^2} - \frac{2T_m^{eq}}{\Delta H \Delta T}\left[\frac{\sigma_{ec}}{\delta} - \frac{\sigma}{a_o}\right] \tag{B.33}$$

4.8. Appendix C: the Curvilinear Friction Coefficient

Hoffman and Miller[6] calculated the curvilinear friction coefficient of linear polyethylene chains under steady-state forced reptation using the approach provided by DiMarzio et al.[52] However, their simplifications led to a monomeric friction coefficient larger than expected.[6] Hoffman and Miller[6] assumed that during crystal growth in regimes I and II, the polymer segments transfer to the crystal growth front with a Rouse regime movement of the chain in the reptation tube.[6] The curvilinear diffusion coefficient at the reference temperature, D_c^o, can be related to the center of mass diffusion coefficient as[52, 55]

$$D_c^o = \frac{kT_o}{\xi^o} = \frac{3D^o {\Omega_{tube}^o}^2}{\langle {r_o}^2 \rangle} \tag{C.1}$$

where ξ^o, D^o, Ω_{tube}^o and $\langle {r_o}^2 \rangle$ are the curvilinear friction coefficient, the center of mass diffusion coefficient, the length of the reptation tube and the average square end-to-end distance of the chain in the melt at the reference temperature, respectively.[6] Following Klein and Ball[55] and DiMarzio et al.[52] we get

$$\frac{kT_o}{\xi^o} = \frac{3D^o {\Omega_{tube}^o}^2}{\langle {r_o}^2 \rangle} = \frac{3D^o(\langle {r_o}^2 \rangle / {d_o})^2}{\langle {r_o}^2 \rangle} = \frac{3D^o \langle {r_o}^2 \rangle}{{d_o}^2} = \frac{3D^o C_{\infty,T_o} n \ell_b^2}{{d_o}^2} \tag{C.2}$$

d_o is the reptation tube diameter at the reference temperature, which can be found by approximating the polyethylene chain with a freely-jointed chain made of N Kuhn segments of length, $\bar{b}$, and mass, M_o.

$$d_o = \bar{b}\sqrt{N_e} \tag{C.3}$$

Here, N_e is the average number of Kuhn segments between entanglements.[32] The freely-jointed chain is related to the real chain by:

$$\bar{b} = \frac{C_{\infty,T_o}\ell_b}{\cos\alpha/2} \tag{C.4}$$

$$N = \frac{n(\cos\alpha/2)^2}{C_{\infty,T_o}} \tag{C.5}$$

$$M_o = \frac{M}{N} = \frac{m_o n}{\frac{n(\cos\alpha/2)^2}{C_{\infty,T_o}}} = \frac{m_o C_{\infty,T_o}}{(\cos\alpha/2)^2} \tag{C.6}$$

where C_{∞,T_o}, α and m_o are the limiting characteristic ratio at the reference temperature, the C-C-C bond angle and the molecular weight of a CH_2 unit, respectively. For flexible linear Gaussian chains the average molecular weight between entanglements, M_e, is:[38]

$$M_e = \left(\frac{n_t}{N_{av}\rho_o}\right)^2 \left(\frac{m_o}{C_{\infty,T_o}\ell_b^2}\right)^3 \tag{C.7}$$

n_t is a dimensionless constant, which is insensitive to temperature and denotes the number of entanglement strands present per cube of the reptation tube diameter. N_{av} and ρ_o are the Avogadro number and the density of the polyethylene melt at the reference temperature, respectively. Considering the melt density of linear polyethylene at the reference temperature as $\rho_o = \rho^* \exp(-\epsilon T_o)$ where ρ^* and ϵ are constants,[40] we obtain:

$$N_e = \frac{M_e}{M_o} = \left(\frac{n_t}{N_{av}\rho_o}\right)^2 \left(\frac{m_o}{C_{\infty,T_o}\ell_b^2}\right)^3 \times \frac{(\cos\alpha/2)^2}{m_o C_{\infty,T_o}} = \left(\frac{n_t\, m_o \cos\alpha/2}{N_{av}\rho^* \exp(-\epsilon T_o) C_{\infty,T_o}^2 \ell_b^3}\right)^2 \quad \text{(C.8)}$$

$$d_o = \frac{C_{\infty,T_o}\ell_b}{\cos\alpha/2} \times \frac{n_t\, m_o \cos\alpha/2}{N_{av}\rho^* \exp(-\epsilon T_o) C_{\infty,T_o}^2 \ell_b^3} = \frac{n_t m_o}{N_{av}\rho^* \exp(-\epsilon T_o) C_{\infty,T_o} \ell_b^2} \quad \text{(C.9)}$$

Equation B.9 leads to d_o = 3.86 nm at a temperature of 175°C for polyethylene, 30% higher than the 3 nm value quoted by Hoffman and Miller.[6] Note that the value calculated here for the tube diameter is consistent with that (3.6 nm) given by Fetters et al. at 175°C.[32] Furthermore, Lodge[41] has shown that the center-of-mass diffusion coefficient of linear polyethylene is proportional to $n^{-2.3}$ rather than n^{-2}. Under these conditions, Equation C.2 leads to:

$$\xi^o = \frac{kT_o n^{1.3}}{3D_1^o} \left(\frac{n_t m_o}{N_{av}\rho^* \exp(-\alpha T_o)\, C_{\infty,T_o}^{3/2} \ell_b^3}\right)^2 \quad \text{(C.10)}$$

where D_1^o is a constant.[41] The non-linear relation between the chain friction coefficient and the number of repeat units is understood as arising from a combination of the effects of constant release and contour length fluctuations, which lead to a faster escape of the chain from its reptation tube.[41]

4.9. References

1. Armistead, J.; Hoffman, J. D., Direct evidence of regimes I, II, and III in linear polyethylene fractions as revealed by spherulite growth rates. *Macromolecules* **2002,** *35* (10), 3895-3913.
2. Chiu, F.-C.; Fu, Q.; Hsieh, E. T., Molecular weight dependence of melt crystallization behavior and crystal morphology of low molecular weight linear polyethylene fractions. *Journal of Polymer Research* **1999,** *6* (4), 219-229.
3. Hikosaka, M.; Watanabe, K.; Okada, K.; Yamazaki, S., Topological mechanism of polymer nucleation and growth–the role of chain sliding diffusion and entanglement. In *Interphases and Mesophases in Polymer Crystallization III*, Springer: 2005; pp 137-186.
4. Hoffman, J.; Frolen, L.; Ross, G.; Lauritzen, J., Growth-rate of spherulites and axialites from melt in polyethylene fractions-regime-1 and regime-2 crystallization. *Journal of Research of the National Bureau of Standards Section a-Physics and Chemistry* **1975,** *79* (6), 671-699.
5. Hoffman, J. D.; Miller, R. L., Test of the reptation concept: crystal growth rate as a function of molecular weight in polyethylene crystallized from the melt. *Macromolecules* **1988,** *21* (10), 3038-3051.
6. Hoffman, J. D.; Miller, R. L., Kinetic of crystallization from the melt and chain folding in polyethylene fractions revisited: theory and experiment. *Polymer* **1997,** *38* (13), 3151-3212.
7. Labaig, J. J. Variation in the Morphology and Structure of Polyethylene Crystals and their Rate of Growth as a Function of Temperature and Chain Length. University of Strasbourg, 1978.
8. Lopez, J. R.; Braña, M. C.; Terselius, B.; Gedde, U., Crystallization of binary linear polyethylene blends. *Polymer* **1988,** *29* (6), 1045-1051.
9. Toda, A., Growth of polyethylene single crystals from the melt: change in lateral habit and regime I–II transition. *Colloid and Polymer Science* **1992,** *270* (7), 667-681.

10. Allen, R. C.; Mandelkern, L., On regimes I and II during polymer crystallization. *Polymer Bulletin* **1987,** *17* (5), 473-480.
11. Lauritzen Jr, J. I.; Hoffman, J. D., Extension of theory of growth of chain-folded polymer crystals to large undercoolings. *Journal of applied Physics* **1973,** *44* (10), 4340-4352.
12. Cho, T.; Heck, B.; Strobl, G., Equations describing lamellar structure parameters and melting points of polyethylene-co-(butene/octene) s. *Colloid and Polymer Science* **2004,** *282* (8), 825-832.
13. Crist, B., Yet another visit to the melting of polyethylene crystals. *Journal of Polymer Science Part B: Polymer Physics* **2007,** *45* (24), 3231-3236.
14. Hocquet, S.; Dosière, M.; Thierry, A.; Lotz, B.; Koch, M.; Dubreuil, N.; Ivanov, D., Morphology and melting of truncated single crystals of linear polyethylene. *Macromolecules* **2003,** *36* (22), 8376-8384.
15. Mohammadi, H.; Vincent, M.; Marand, H., Investigating the Equilibrium Melting Temperature of Linear Polyethylene Using the Non-Linear Hoffman-Weeks Approach. *Polymer* **2018**.
16. Harrison, I. R., Polyethylene single crystals: Melting and morphology. *Journal of Polymer Science Part B: Polymer Physics* **1973,** *11* (5), 991-1003.
17. Nakagawa, Y.; Hayashi, H.; Takahagi, T.; Soeda, F.; Ishitani, A.; Toda, A.; Miyaji, H., Atomic force microscopy of solution grown polyethylene single crystals. *Japanese journal of applied physics* **1994,** *33* (6S), 3771.
18. Hoffman and Miller (reference 6) define Mnw as the geometrical average of Mn and Mw.
19. Lauritzen, J.; Passaglia, E., Kinetics of crystallization in multicomponent systems: II. Chain-folded polymer crystals. *J Res Natl Bur Stand. A* **1967,** *71*, 261-75.
20. Miller, R. L., Polymer crystal formation: On an analysis of the dilute solution lamellar thickness-crystallization temperature data for poly (ethylene). *Kolloid-Zeitschrift und Zeitschrift für Polymere* **1968,** *225* (1), 62-69.

21. Huseby, T.; Bair, H., Dissolution of polyethylene single crystals in xylene and octadecane. *Journal of Applied Physics* **1968,** *39* (11), 4969-4973.
22. Flory, P.; Vrij, A., Melting points of linear-chain homologs. The normal paraffin hydrocarbons. *Journal of the American Chemical Society* **1963,** *85* (22), 3548-3553.
23. Frank, F., Nucleation-controlled growth on a one-dimensional growth of finite length. *Journal of Crystal Growth* **1974,** *22* (3), 233-236.
24. Goderis, B.; Reynaers, H.; Scherrenberg, R.; Mathot, V. B.; Koch, M. H., Temperature reversible transitions in linear polyethylene studied by TMDSC and time-resolved, temperature-modulated WAXD/SAXS. *Macromolecules* **2001,** *34* (6), 1779-1787.
25. Scherrer, P., Estimation of the size and internal structure of colloidal particles by means of röntgen. *Nachr. Ges. Wiss. Göttingen* **1918,** *2*, 96-100.
26. Marand, H.; Xu, J.; Srinivas, S., Determination of the equilibrium melting temperature of polymer crystals: linear and nonlinear Hoffman− Weeks extrapolations. *Macromolecules* **1998,** *31* (23), 8219-8229.
27. He, G.; Lu, P., In situ confocal micro-Raman spectroscopic investigation of rearrangement kinetics and phase evolution of UHMWPE during annealing. *Journal of Raman Spectroscopy* **2015,** *46* (1), 155-160.
28. Kajiyama, T.; Ohki, I.; Takahara, A., Surface morphology and frictional property of polyethylene single crystals studied by scanning force microscopy. *Macromolecules* **1995,** *28* (13), 4768-4770.
29. Litvinov, V. M.; Ries, M. E.; Baughman, T. W.; Henke, A.; Matloka, P. P., Chain Entanglements in Polyethylene Melts. Why Is It Studied Again? *Macromolecules* **2013,** *46* (2), 541-547.
30. Mandelkern, L.; Alamo, R.; Kennedy, M., The interphase thickness of linear polyethylene. *Macromolecules* **1990,** *23* (21), 4721-4723.

31. Kavesh, S.; Schultz, J., Lamellar and interlamellar structure in melt-crystallized polyethylene. I. Degree of crystallinity, atomic positions, particle size, and lattice disorder of the first and second kinds. *Journal of Polymer Science Part B: Polymer Physics* **1970,** *8* (2), 243-276.
32. Fetters, L.; Lohse, D.; Colby, R., Chain dimensions and entanglement spacings. In *Physical properties of polymers handbook*, Springer: 2007; pp 447-454.
33. Khoury, F., Organization of macromolecules in the condensed phase: General discussion. *Faraday Discuss. Chem. Soc* **1979,** *68*, 404-405.
34. Gautam, S.; Balijepalli, S.; Rutledge, G., Molecular simulations of the interlamellar phase in polymers: effect of chain tilt. *Macromolecules* **2000,** *33* (24), 9136-9145.
35. Ungar, G.; Zeng, X.-b., Learning polymer crystallization with the aid of linear, branched and cyclic model compounds. *Chemical reviews* **2001,** *101* (12), 4157-4188.
36. Voigt-Martin, I.; Fischer, E.; Mandelkern, L., Morphology of melt-crystallized linear polyethylene fractions and its dependence on molecular weight and crystallization temperature. *Journal of Polymer Science Part B: Polymer Physics* **1980,** *18* (12), 2347-2367.
37. Gaur, U.; Wunderlich, B., Heat capacity and other thermodynamic properties of linear macromolecules. II. Polyethylene. *Journal of Physical and Chemical Reference Data* **1981,** *10* (1), 119-152.
38. Fetters, L. J.; Lohse, D. J.; Milner, S. T.; Graessley, W. W., Packing length influence in linear polymer melts on the entanglement, critical, and reptation molecular weights. *Macromolecules* **1999,** *32* (20), 6847-6851.
39. Pearson, D.; Ver Strate, G.; Von Meerwall, E.; Schilling, F., Viscosity and self-diffusion coefficient of linear polyethylene. *Macromolecules* **1987,** *20* (5), 1133-1141.
40. Han, S.; Lohse, D.; Condo, P.; Sperling, L., Pressure–volume–temperature properties of polyolefin liquids and their melt miscibility. *Journal of Polymer Science Part B: Polymer Physics* **1999,** *37* (20), 2835-2844.

41. Lodge, T. P., Reconciliation of the molecular weight dependence of diffusion and viscosity in entangled polymers. *Physical Review Letters* **1999,** *83* (16), 3218.
42. Barham, P.; Chivers, R.; Keller, A.; Martinez-Salazar, J.; Organ, S., The supercooling dependence of the initial fold length of polyethylene crystallized from the melt: unification of melt and solution crystallization. *Journal of materials science* **1985,** *20* (5), 1625-1630.
43. Hoffman, J.; Lauritzen, J.; Passaglia, E.; Ross, G.; Frolen, L.; Weeks, J., Kinetics of polymer crystallization from solution and the melt. *Kolloid-Zeitschrift und Zeitschrift für Polymere* **1969,** *231* (1-2), 564-592.
44. Hoffman, J. D., Role of reptation in the rate of crystallization of polyethylene fractions from the melt. *Polymer* **1982,** *23* (5), 656-670.
45. Hoffman, J. D.; Miller, R. L.; Marand, H.; Roitman, D. B., Relationship between the lateral surface free energy. sigma. and the chain structure of melt-crystallized polymers. *Macromolecules* **1992,** *25* (8), 2221-2229.
46. Point, J.; Colet, M. C.; Dosiere, M., Experimental criterion for the crystallization regime in polymer crystals grown from dilute solution: possible limitation due to fractionation. *Journal of Polymer Science Part B: Polymer Physics* **1986,** *24* (2), 357-388.
47. Point, J.-J.; Damman, P.; Janimak, J., Is the break in the curve giving the thermal dependence of crystal growth rate a signature of regime II→ III transition? *Polymer* **1993,** *34* (18), 3771-3773.
48. Alcazar, D.; Thierry, A.; Schultz, P.; Kawaguchi, A.; Cheng, S. Z.; Lotz, B., Determination of the extent of lateral spread and density of secondary nucleation in polymer single crystal growth. *Macromolecules* **2006,** *39* (26), 9120-9131.
49. Toda, A., Rounded lateral habits of polyethylene single crystals. *Polymer* **1991,** *32* (5), 771-780.
50. Ungar, G.; Keller, A., Inversion of the temperature dependence of crystallization rates due to onset of chain folding. *Polymer* **1987,** *28* (11), 1899-1907.

51. Higgs, P. G.; Ungar, G., The growth of polymer crystals at the transition from extended chains to folded chains. *The Journal of chemical physics* **1994,** *100* (1), 640-648.
52. DiMarzio, E. A.; Guttman, C. M.; Hoffman, J. D., Is crystallization from the melt controlled by melt viscosity and entanglement effects? *Faraday Discussions of the Chemical Society* **1979,** *68*, 210-217.
53. Bartels, C. R.; Crist, B.; Graessley, W. W., Self-diffusion coefficient in melts of linear polymers: chain length and temperature dependence for hydrogenated polybutadiene. *Macromolecules* **1984,** *17* (12), 2702-2708.
54. Von Seggern, J.; Klotz, S.; Cantow, H., Reptation and constraint release in linear polymer melts: an experimental study. *Macromolecules* **1991,** *24* (11), 3300-3303.
55. Klein, J.; Ball, R., Kinetic and topological limits on melt crystallisation in polyethylene. *Faraday Discussions of the Chemical Society* **1979,** *68*, 198-209.

Chapter 5. On the Crystallization and Melting Behaviors of Metallocene Linear Low-Density Polyethylene

Hadi Mohammadi, Matthew Vincent and Hervé Marand

5.1. Attribution

Matthew Vincent contributed to this work by conducting the ultra-fast DSC experiments and providing insight on the analysis of the ultra-fast DSC data. Design of the experiments, spherulite growth rate measurements, and processing and analysis of the data were performed by Hadi Mohammadi. The paper was prepared by Hadi Mohammadi and Hervé Marand.

5.2. Abstract

The crystallization and melting behaviors of a random ethylene/1-hexene copolymer were studied by a combination of optical microscopy, small angle X-ray scattering, and ultra-fast differential scanning calorimetry. Fold surface free energies of the copolymer lamellae at the time of crystallization and melting increase with increasing undercooling, approaching the same magnitude at high undercooling. As a result of this temperature dependence, the experimental melting *vs.* crystallization temperature plot is parallel to the $T_m = T_c$ line and the corresponding Gibbs-Thomson plot is non-linear. This behavior is attributed to the fact that longer ethylene sequences form a chain-folded structure with lower concentration of branch points on the lamellar surface at lower undercooling, while shorter ethylene sequences form lamellar structures at higher undercooling exhibiting a higher concentration of branch points on the lamellar surface. Branch

points limit the ability of lamellar structures to relax their kinetic stem-length fluctuations during heating prior to melting.

5.3. Introduction

Metallocene linear low density polyethylenes (m-LLDPEs) are copolymers synthesized from ethylene and α-olefins in the presence of a homogenous catalyst.[1] The α-olefin comonomers introduce short branches on an otherwise linear ethylene backbone. As a consequence of homogenous catalysis, m-LLDPEs exhibit narrow molecular weight and random branch distributions.[1] When the α-olefin is a 1-butene or larger comonomer, the short branches (ethyl or larger) are rejected from the polyethylene crystal structure.[2-4] Effect of short-chain branching on the crystallization and melting of m-LLDPEs is very complex.[3, 5] The spherulite growth rate, degree of crystallinity, and melting temperature of m-LLDPE are typically lower than these of a linear polyethylene (LPE) of similar chain length crystallized under similar conditions.[3, 5-6] We limit our discussion here to the case of low short-chain branch content copolymers, which undergo chain-folded lamellar crystallization at low to intermediate undercoolings.[7]

In general, the relationship between polymer morphology and crystallization conditions is ascribed to the crystal growth mechanism. The average crystal growth rate of a polymer lamella results from a balance between a nucleation barrier and the crystallization driving force.[8-9] The driving force for passage over the crystallization barrier is directly proportional to the difference between the actual lamellar thickness and the minimum lamellar thickness, ℓ_{min} that is thermodynamically stable.[8-9] The net flux of passage over the barrier also dictates the secondary nucleation rate, which controls the actual initial lamellar thickness distribution.[8-9] If we now focus on random copolymers made of crystallizable (ethylene) and non-crystallizable (α-olefin) units, the net flux over the nucleation barrier is also a function of the actual composition of the melt at the interface with the crystal growth front.[10-13] Indeed, as we learned from Flory's thermodynamic

theory of copolymer crystallization,[10-11] the "crystallizability" of such copolymers, that is their maximum degree of crystallinity, depends on the crystallization temperature. Specifically, only the longest crystallizable sequences can participate in crystal growth at high temperature, while shorter sequences crystallize at relatively lower temperatures.[11] Hence, the actual lamellar thickness resulting from crystallization is governed by the kinetic constraints associated with the transport and nucleation of the crystallizable ethylene sequences.[5] Therefore, for crystallization of an ethylene sequence to occur at a finite rate at a given temperature, it must result in a lamella, whose thickness is lower than Flory's estimate of the minimum lamellar thickness for that sequence.[10-11] In other words, Flory theory cannot be used to provide a reliable estimate of the lamellar thickness of m-LLDPE during crystallization. As an alternative, the minimum thermodynamically stable lamellar thickness during crystallization of m-LLDPE can be assessed by the Gibbs-Thomson method,[8, 14] which predicts that $\ell_{min} = 2\sigma_{ec,c}/\Delta G_c^{\infty}$, where $\sigma_{ec,c}$ and ΔG_c^{∞} are the fold surface free energy during crystallization and the Gibbs free energy of fusion per unit volume of an infinitely large crystal of the copolymer, respectively.[8, 14-15] Here, the effects of crystallizable and non-crystallizable sequence length distributions on the minimum thermodynamically stable lamellar thickness at a given crystallization temperature are incorporated in the fold surface free energy during crystallization. In this context, we apply the formalism of the Lauritzen-Hoffman secondary nucleation theory (originally developed for crystallization of linear homopolymers) to the crystal growth of m-LLDPE and determine the temperature dependence of $\sigma_{ec,c}$ from the lamellar thickness and spherulite growth rate data.[9, 15-16]

In the case of linear polyethylene, the temperature dependence of the fold surface free energy during crystallization, σ_{ec}, was approximated by a linear function of the undercooling at low to moderate undercoolings, $\sigma_{ec} = \sigma_{ec}^{o}(1 + y\Delta T)$, where σ_{ec}^{o} and y represent the equilibrium fold surface free energy and the strength of stem-length fluctuations, respectively, both independent of the crystallization temperature.[17-20] The quantity σ_{ec}^{o} was also shown to be equal to the fold surface

free energy of the lamellae during melting, σ_{em}, i.e. the stem length fluctuations of LPE equilibrate before the melting of lamellae.[19-20] While a similar correlation may be used to rationalize the temperature dependence of the fold surface free energy of m-LLDPE during crystallization, one should expect the magnitude of σ_{em} to vary with the crystallizable and non-crystallizable sequence length distributions and, therefore, with the crystallization temperature. A temperature dependent σ_{em} should lead to a non-linear Gibbs-Thomson plot (i.e. the plot of melting temperature *vs.* reciprocal of lamellar thickness should exhibit curvature) for m-LLDPE. However, such behavior has not yet been reported for m-LLDPE copolymers.[21]

To understand this discrepancy, we emphasize first that crystallization of m-LLDPE may result in the segregation between ethylene and short branch units, which would affect the resulting melting endotherm.[5, 22-23] The extent of segregation at the time of melting increases with crystallization time, and depends on temperature and bulk copolymer composition.[23] Melting of sufficiently crystalline copolymers into a heterogeneous amorphous "phase" generates an entropic effect, which leads to superheating of the crystalline lamellae. In the context of the Gibbs-Thomson equation, ignoring the existence of superheating would result in overestimating $\sigma_{em,c}$, the fold surface free energy of copolymer lamellae at the time of melting.[5, 22, 24] Crist et al.[5, 22, 24] suggested that the quantity $\sigma_{em,c}$ can only be reliably estimated when the melt composition is very close to the bulk composition, i.e. when the crystallinity is very small. They claimed that such conditions only occur at the upper end of the melting range.[5, 22, 24] Crist and Mirabella[24] also showed that the DSC peak melting temperature does not correspond to the melting of lamellae with the average thickness. Their model, following previous work by Alberola,[25] considers that the weight distribution function of lamellar thicknesses is proportional to the square of the temperature difference ($T_{m,c}^{eq} - T$) where $T_{m,c}^{eq}$ is the equilibrium melting temperature of the copolymer.[24] This model, however, can only be used in the limit of zero-superheating. The implications of these two important studies[23-24] can be only reconciled if one investigates the melting of initial lamellae since

the associated melting temperatures are not affected by segregation-induced superheating. Finally, it is worth noting that the melting endotherm of m-LLPDE copolymers recorded with the low heating rate characteristic of a conventional DSC can be affected by melting-recrystallization-remelting and/or annealing phenomena.[26-29] Hence, one should investigate the melting behavior of these materials under high heating rate conditions and extrapolate to zero-heating rate to account for superheating.

In this paper we study the spherulite growth and melting of a m-LLDPE sample containing 3 mol% butyl branches. Spherulite growth rates and lamellar thickness data collected at different temperatures are analyzed using a modified LH theory.[19-20] Crystallized stems of m-LLDPE exhibit a tilted conformation in the lamellae, reducing the steric hindrance between adjacent folds.[6, 30] The modified LH theory accounts for the effects of tilt angle of the crystallized stems, θ, and for the temperature dependence of both the fold ($\sigma_{ec,c}$) and lateral (σ) surface free energies on the spherulite growth rate and average lamellar thickness of m-LLDPE [19, 31] This analysis provides two estimates of the magnitude of the fold surface free energy during crystallization, one from the spherulite growth rate data and one from the lamellar thickness data. Comparison of these $\sigma_{ec,c}$ values allows us to determine the tilt angle necessary for self-consistency of the modified LH theory in the case of m-LLDPE copolymers.

We also investigate the melting behavior of isothermally crystallized m-LLDPE using a Mettler-Toledo Flash™ DSC 1. The high heating rates achieved in this calorimeter enable us to minimize the effects of melting-recrystallization-remelting and annealing on the melting behavior. We crystallize this copolymer at different temperatures for different times and first determine the characteristics of the melting endotherm associated with initial lamellae. Studying the melting behavior of initial lamellae enables us to ensure that 1) the melt composition is equal to the bulk composition and 2) melting results in a homogeneous amorphous phase. We then extrapolate the characteristics of the melting endotherm associated with initial lamellae to zero-heating rate to

account for the effects of superheating, melting kinetics and thermal lag. Using these extrapolated melting traces in the context of the method developed by Crist and Mirabella,[24] we obtain, for each crystallization temperature, the lamellar thickness distribution function and the fold surface free energy of the copolymer at the time of melting. Finally, we attempt to rationalize the temperature dependence of the fold surface free energy of m-LLDPE during crystallization using the melting data.

5.4. Experimental

5.4.1. Material

The m-LLDPE sample studied in this work (EH3) was kindly provided by ExxonMobil Co. EH3 is an ethylene/1-hexene copolymer containing 3 mol% 1-hexene comonomer and a weight-average molecular weight of 85 kg/mol and polydispersity index of 2. This material was used as is without further purification. The peak melting temperature recorded for this material at 10^{o}C/min subsequent to crystallization by cooling to –20^{o}C at a rate of 40^{o}C/min from the melt was found to be equal to 112.7^{o}C, consistent with data obtained under similar conditions for a variety of ethylene/α-olefin copolymers and hydrogenated poly(butadiene)s.[32-33]

5.4.2. Spherulite Growth Rate Measurements

Thin EH3 films (ca. 25 μm) were prepared using a Carver laboratory press operated at 150^{o}C under a nitrogen atmosphere. Small pieces of the films were sandwiched between clean glass cover slips and placed in a Linkam THM 600 heating-cooling stage under a dry nitrogen flow of 50 ml/min. The sample temperature was regulated within ±0.1^{o}C using a Linkam TMS 93 temperature controller. Temperature calibration for the stage and temperature controller was performed in the range of 60 to 150^{o}C using 5 melting standards: 1,3-diphenoxy-benzene (T_m = 60^{o}C), imidazole (T_m =90^{o}C) m-toluic acid (T_m = 111^{o}C) methylhydroquinone (T_m = 128^{o}C), and l-

xylose (T_m = 150^{o}C). Before each spherulite growth rate measurement, the EH3 films were heated to 160^{o}C and kept in the melt state for 1 minute to erase previous thermal history. The films were subsequently cooled at a rate of 50^{o}C/min to the desired crystallization temperature and the spherulite growth was monitored using an Olympus BX-50 polarized light optical microscope interfaced to a video camera. Using the ImageJ image analysis software, spherulite radii were measured as a function of time for five to ten spherulites at each crystallization temperature. Spherulite growth rates were calculated as the slope of the observed linear increase of the radius with time. For all isothermal spherulite growth experiments in the 107 to 118^{o}C temperature range, the relative standard deviation on the average spherulite growth rate was determined to be less than 5%.

5.4.3. Differential Scanning Calorimetry

Differential scanning calorimetry (DSC) experiments were performed using a Mettler Toledo Flash™ DSC 1 instrument operated under a dry nitrogen flow of 15 mL/min with the sample support temperature at -100^{o}C. Using a Carver laboratory press operated at 150^{o}C under a nitrogen atmosphere, an EH3 film with a thickness of 1 mm was prepared and then cut into a 1×1×1 mm^3 specimen. 1 μm thick samples were cut from the specimen using a Leica RMC Cryo-Ultramicrotome operated at -110^{o}C. Cryomicrotomed films were subsequently immersed in a 60/40 wt/wt % dimethylsulfoxide/water mixture at -60^{o}C. After washing with deionized water, these samples were left to dry in a vacuum oven at room temperature for a week. Samples were then cut to smaller pieces (ca. 20 ± 1 ng estimated from their specific heat capacity in the melt) and placed carefully on the Flash™ DSC 1 UFS1 microchip using an eyelash. Our experiments revealed that the chip calibration was stable over repeated heating and cooling cycles. Therefore, the calibration procedure was completed after collecting all crystallization and melting data in order to avoid measurement errors due to possible confinement effects caused by the calibration standard. To calibrate the Flash™ DSC 1 chip, a small piece of tin was positioned on top of the m-LLDPE

sample. The mass (ca. 11 ± 1 ng) of the tin standard was estimated from the heat of fusion measurement at a heating rate of 3000°C/s. The onset melting temperature of the tin standard was measured at different heating rates varying from 1000 to 10000°C/s and extrapolated to zero heating rate using Equation 5.1 proposed by Toda et al.[34-35]

$$T_m = T_m(\mathrm{K} = 0) + \omega_1 \mathrm{K}^z + \omega_2 \mathrm{K} \tag{5.1}$$

where K, ω_1, and ω_2 are the heating rate, and constant prefactors, respectively. The terms $\omega_1 \mathrm{K}^z$ and $\omega_2 \mathrm{K}$ account for the effect of melting kinetics and instrumental thermal lag on the melting temperature of the standard, respectively. For metal standards, which melt without kinetic effects, z reflects the contribution from the latent heat of fusion during melting, and is expected to be near 0.5 for samples with small masses.[34, 36] $T_m(\mathrm{K} = 0)$ is the zero-entropy production melting temperature of the tin standard in the absence of any non-equilibrium effects. Values of $T_m(\mathrm{K} = 0)$ were used for the single-point calibration of the melting temperatures of the EH3 sample in the Flash™ DSC 1.

All calorimetric experiments were initiated by heating the EH3 sample to 190°C and holding it at this temperature for 1 s to erase prior thermal history. The EH3 sample was then cooled to specific crystallization temperatures at a rate of 1000°C/s and crystallized for various times, t_c. Crystallization temperatures were chosen in such a way that crystallization occurred on a practical time scale under isothermal conditions and did not take place during cooling or during subsequent heating. The sample was then melted with a heating rate ranging between 1000 and 10000°C/s (in increments of 1000°C/s). For every crystallization temperature, a baseline heating trace was also recorded for a sufficiently short crystallization time that no crystallinity had time to develop. This baseline was subtracted from the heating trace of partially crystallized samples to minimize the error (less than 1%) in the measured heat of fusion. The lower the degree of crystallinity, the narrower the breadth of the melting endotherm, the smaller the expected error.[37] Melting endotherms of EH3 exhibited a Gaussian distribution (see Figures 5.5 and 5.6). Each melting trace

was fitted with a Gaussian function and the peak melting temperature, half-width at half-height of the melting endotherm and heat of fusion were recorded. The degree of crystallinity of each sample was estimated using the heat of fusion of LPE, 293 J/g.[38-39] For each crystallization temperature, the initial melting temperature, T_m, was defined as the peak temperature for the endotherm of samples exhibiting the lowest crystallinity, where T_m does not change with time (see Figure 5.5). The zero-entropy production melting temperature of these initial lamellae was obtained for each crystallization temperature by extrapolation to zero-heating rate using Equation 5.1.[34-35]

5.5. Results and Discussion

For each crystallization temperature, the spherulite radius increases linearly with crystallization time, i.e. spherulite growth rates are independent of crystallization time. Therefore, the diffusion-controlled spherulite growth process reported by Bassett et al.[40] for an ethylene/1-butene copolymer obtained by homogeneous catalysis and containing the same number of branches per 1000 carbon atoms, is not observed for the EH3 copolymer. Observations of linear spherulitic growth for homogeneous ethylene/α-olefins copolymers have been reported by others.[41-44] As a result, we can assume that the chemical composition of the melt in the vicinity of the growth front does not change during isothermal crystallization of EH3. Spherulite growth rates for the EH3 copolymer are shown as a function of crystallization temperature in Figure 5.1. The insert in Figure 5.1 demonstrates that spherulite radius increases linearly with time.

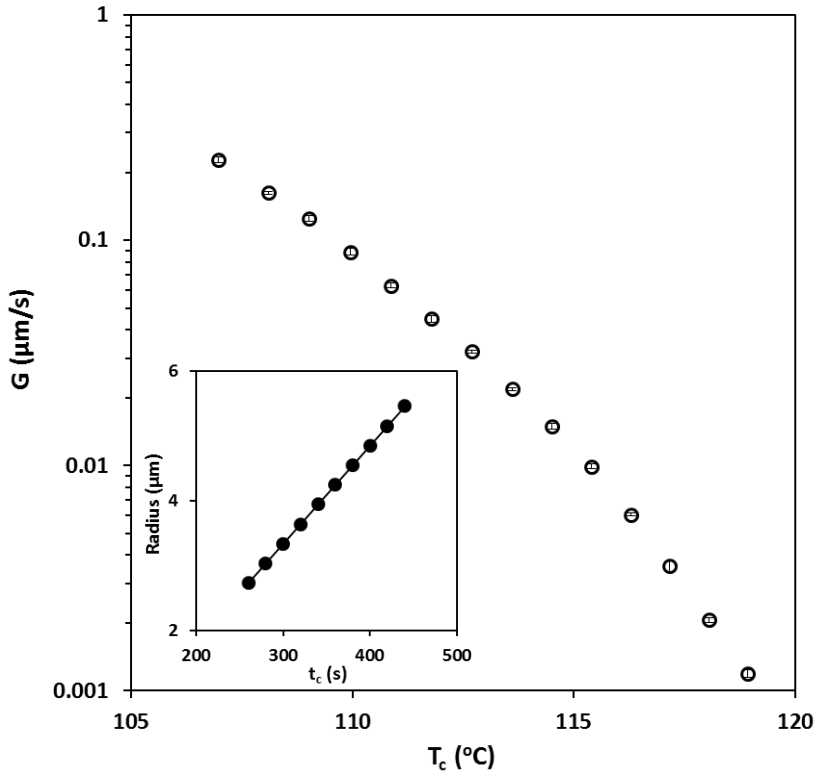

Figure 5.1. Spherulite growth rate *vs.* crystallization temperature for the EH3 copolymer. The insert shows spherulite radius *vs.* crystallization time for a sample crystallizing isothermally at 114.5^{o}C. The solid line is the best linear fit to the data. Error bars correspond to one standard deviation.

Using small angle X-ray scattering, Cho et al.[21, 45] studied the isothermal crystallization of various m-LLDPEs with different amounts of ethyl and hexyl branches at different temperatures, T_c. Figure 5.2 shows the average lamellar thickness, ℓ, at different undercoolings, $\Delta T = T_{m,c}^{eq} - T_c$, obtained by Cho et al.[21, 45] for a metallocene ethylene/1-octene copolymer with a weight-average molecular weight of 85 kg/mol and the same branch content as EH3.

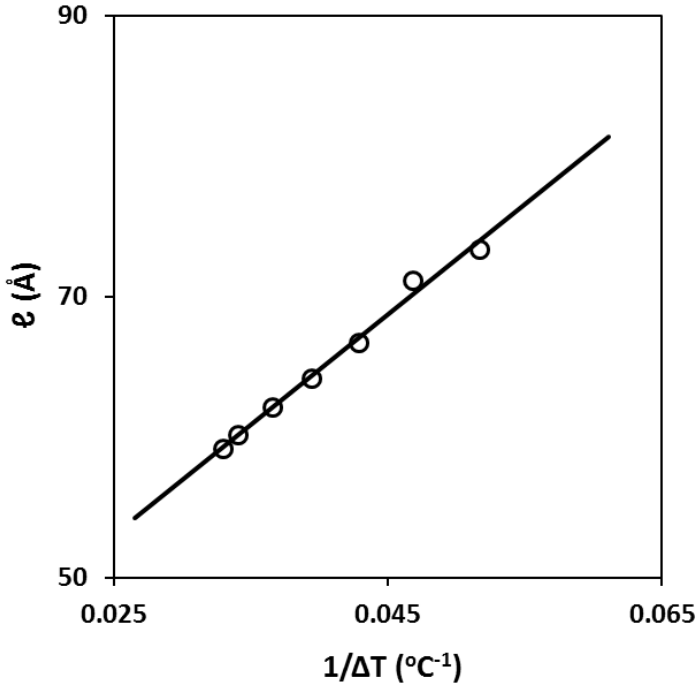

Figure 5.2. Number-average lamellar thickness *vs.* reciprocal of the undercooling from Cho et al.[21, 45] for a metallocene ethylene/1-octene copolymer with 3 mol% hexyl branches and molecular weight of 85 kg/mol. The solid line represents the best linear fit to the experimental data, using an equilibrium melting temperature of 135.4°C.

Since the scattering data was analyzed using the interface distribution function approach,[21, 45] ℓ, represents the number-average lamellar thickness.[46-47] The equilibrium melting temperature of this copolymer, $T_{m,c}^{eq}$ = 135.4°C is estimated using Flory's equation:[10-11]

$$\frac{1}{T_{m,c}^{eq}} - \frac{1}{T_m^{eq}} = -\left(\frac{R}{\overline{\Delta H}}\right)\ln(1 - X_B) \tag{5.2}$$

where T_m^{eq}, $\overline{\Delta H}$, and X_B are the equilibrium melting temperature of a similar chain length LPE sample, the molar enthalpy of fusion of LPE, and the mole fraction of non-crystallizable units in the copolymer, respectively. The value of T_m^{eq} = 140.6°C is estimated using the Huggins equation discussed in our previous publication.[20] The solid line in the ℓ *vs.* $1/\Delta T$ plot is the best linear fit to the experimental data ($\ell = C_1/\Delta T + C_2$). For m-LLDPE samples with more than 2 mol% branch

content, the average lamellar thickness measured by Cho et al.[21, 45] was independent of the branch size and the crystallization time. This observation can be related to the fact that the short-chain branches cannot enter the crystal structure of m-LLDPE, hence, m-LLDPE crystals do not exhibit α_c-relaxation and do not thicken during isothermal crystallization.[32] As the molecular weight and branch content of our sample are similar to these in the samples studied by Cho et al.,[21, 45] the fit to the ℓ *vs.* $1/\Delta T$ plot can be used to estimate the lamellar thickness of EH3 at different crystallization temperatures.

Applying the modified LH theory to the crystallization of m-LLDPE, we can relate the spherulite growth rate, G, and the lamellar thickness, ℓ, of isothermally crystallized m-LLDPE to the crystallization temperature and the fold surface free energy during crystallization, Equations 5.3 and 5.4.[19] Equation 5.3 is derived under the assumption that in this range of crystallization temperatures, crystal growth occurs in regime II.

$$\ln G + \frac{Q_d^*}{RT_c} + 2\ln \ell - \ln \varphi'(T_c) = \ln G_o - \frac{2b_o\sigma^o\sigma_{ec,c}}{k\Delta H \cos\theta}\left[\frac{1-\chi(T_c)}{\Delta T}\right] \tag{5.3}$$

$$\ell = \frac{2\sigma_{ec,c}T_{m,c}^{eq}}{\Delta H \Delta T} + \frac{kT_{m,c}^{eq}\cos\theta}{2b_o\sigma^o}\left[\frac{a_o\Delta H\Delta T + 4\sigma^o T_c}{a_o\Delta H\Delta T + 2\sigma^o T_c}\right] \tag{5.4}$$

Q_d^*, R, a_o, b_o, k and ΔH are the activation energy for center-of-mass diffusion, the universal gas constant, the width and thickness of a crystallized stem, Boltzmann's constant and the volumetric enthalpy of fusion of the copolymer, respectively.[19] Values of Q_d^* and ΔH for EH3 are similar to these reported for LPE as the melt dynamics and the crystal structure of low branch content m-LLDPEs and LPE are nearly identical.[48-50] Values of a_o and b_o are estimated for EH3 at its equilibrium melting temperature from analyses of the temperature dependence of the unit cell dimensions for a metallocene ethylene/1-hexene copolymer with 2.3 mol% butyl branches.[48] The lateral surface free energy at the equilibrium melting temperature, σ^o is calculated using:[20, 31]

$$\sigma^o = \left(\frac{\Delta H a_o}{2}\right)\left(\frac{\ell_b}{\ell_u}\right)\frac{1}{C_\infty} \tag{5.5}$$

where ℓ_b, ℓ_u, and C_∞ are the C-C bond length, the C-C bond length projected along the crystal c-axis, and the limiting characteristic ratio, respectively. The temperature dependence of C_∞ in Equations 5.3 and 5.4 is considered negligible in the given range of crystallization temperatures. $\chi(T_c)$ and $\varphi'(T_c)$ are functions of the crystallization temperature written as:[19]

$$\chi(T_c) = \frac{a_o \Delta H \Delta T}{2\sigma^o T_c} \tag{5.6}$$

$$\varphi'(T_c) = \left[\frac{\Delta T}{1+\chi(T_c)}\right]\sqrt{\frac{2+\chi(T_c)}{2\sigma^o}} \tag{5.7}$$

All thermodynamic, crystallographic and other constants necessary for the analysis of the lamellar thickness and spherulite growth rate data are given in Table 5.1.

The $\ln G + \frac{Q_d^*}{RT_c} + 2\ln\ell - \ln\varphi'(T_c)$ *vs.* $\left[\frac{1-\chi(T_c)}{\Delta T}\right]$ plot for isothermally crystallized EH3 is shown in Figure 5.3. The ordinates in Figure 5.3 were determined using experimental spherulite growth rates measured here (Figure 5.1) and interpolated values of the lamellar thickness at the same crystallization temperature (Figure 5.2). Values of $\sigma_{ec,c}$ calculated from the slope of the line tangent to this plot are shown as a function of the crystallization temperature for three different crystallized stem tilt angles in the insert in Figure 5.3.

Table 5.1. Constants used for the analysis of the lamellar thickness and spherulite growth rate data of m-LLDPE.

a_o	4.58×10^{-8} cm [48]
b_o	4.17×10^{-8} cm [48]
ℓ_b	1.54×10^{-8} cm
ℓ_u	1.273×10^{-8} cm
ΔH	283 J/cm^3 [39]
Q_d^*	24 kJ/mol [50]
R	8.3145 J/mol
k	1.3806×10^{-23} J/K
C_∞	7.38 at 140^{o}C [49]

Values of $\sigma_{ec,c}$ estimated from the lamellar thickness data, Equation 5.4, are also depicted on the same plot, Figure 5.3. The fold surface free energies of EH3 during crystallization determined from analyses of the spherulite growth rate and the lamellar thickness data superimpose when a value of 53.2^o is chosen for θ. Using θ values lower (19^o) or higher (70^o) than 53.2^o result in significant differences between the lamellar thickness and the spherulite growth rate estimates of the fold surface free energy, Figure 5.3. It is noteworthy that a tilt angle of θ = 50 ± 7^o was recently reported by Fritzsching et al.[30] for a hydrogenated polybutadiene sample with similar molar mass and 4.6 mol% ethyl branches using small angle X-ray scattering, transmission electron microscopy, and longitudinal acoustic-mode Raman scattering data of Alamo et al.[6]

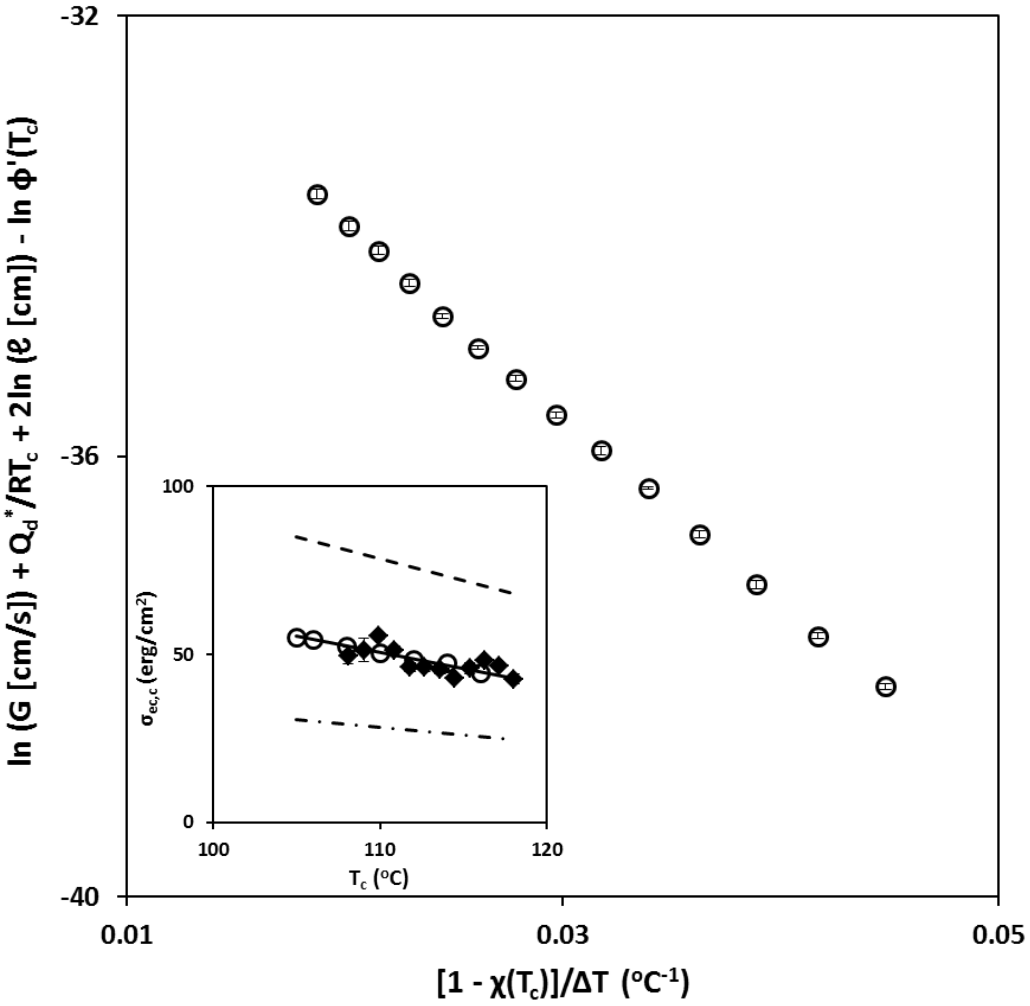

Figure 5.3. $\ln G + \frac{Q_d^*}{RT_c} + 2\ln \ell - \ln \varphi'(T_c)$ *vs.* $\left[\frac{1-\chi(T_c)}{\Delta T}\right]$ for the EH3 copolymer (○). The inner plot shows the fold surface free energy during crystallization obtained from the spherulite growth rate data (♦) and from the lamellar thickness data (○) using θ = 53.2°.The solid line is the best fit to this data. The best fit to the $\sigma_{ec,c}$ values found from the spherulite growth rate data using θ = 19° (**- - -**) and θ = 70° (**- · -**) are also shown in the insert. Error bars correspond to one standard deviation.

We then estimated the magnitude of the fold surface free energy per crystallized stem of linear polyethylene in the same range of undercooling using y = 0.032 $^{o}C^{-1}$ and $\sigma_{ec}^{o}/\cos\theta$ = 45.5 ± 5.2 erg/cm^2, Figure 5.4.[19] As in the case of linear polyethylene, the magnitude of the fold surface free energy per crystallized stem increases with increasing degree of undercooling for the EH3 copolymer, Figure 5.4. Within the limits of error, the fold surface free energies per crystallized stem

are identical for EH3 and LPE, suggesting that the growth rate of EH3 spherulites is controlled by the availability of the crystallizable sequences in the vicinity of the crystal growth front. It is interesting to note that m-LLDPE adopts the same fold surface free energy per crystallized stem as LPE, favoring a higher tilt angle to compensate for the increased steric hindrance associated with the short branches.

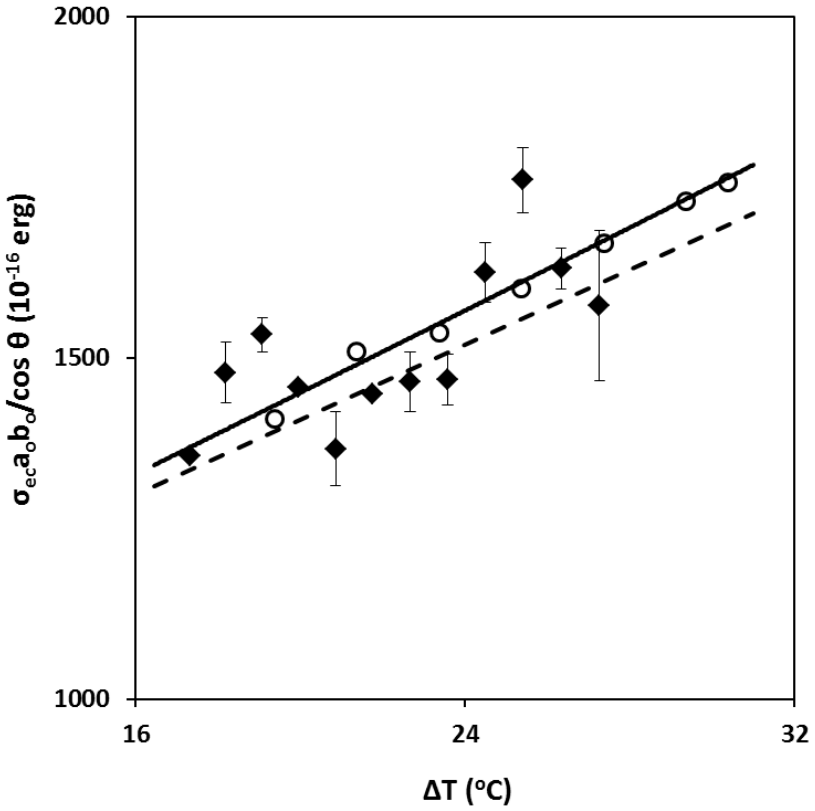

Figure 5.4. Fold surface free energy during crystallization per stem *vs.* undercooling for EH3 copolymer estimated from: spherulite growth rate and lamellar thickness data (♦) and only lamellar thickness data (○). The solid line is the best fit to the experimental data. The dashed line is the fold surface free energy during crystallization per stem for linear polyethylene. Error bars correspond to one standard deviation.

We now turn our attention to the melting behavior of the EH3 copolymer. The degree of crystallinity, melting temperature, and half-width at half-height of the Gaussian fit to the melting endotherm of the EH3 copolymer increase with logarithm of crystallization time, Figure 5.5.

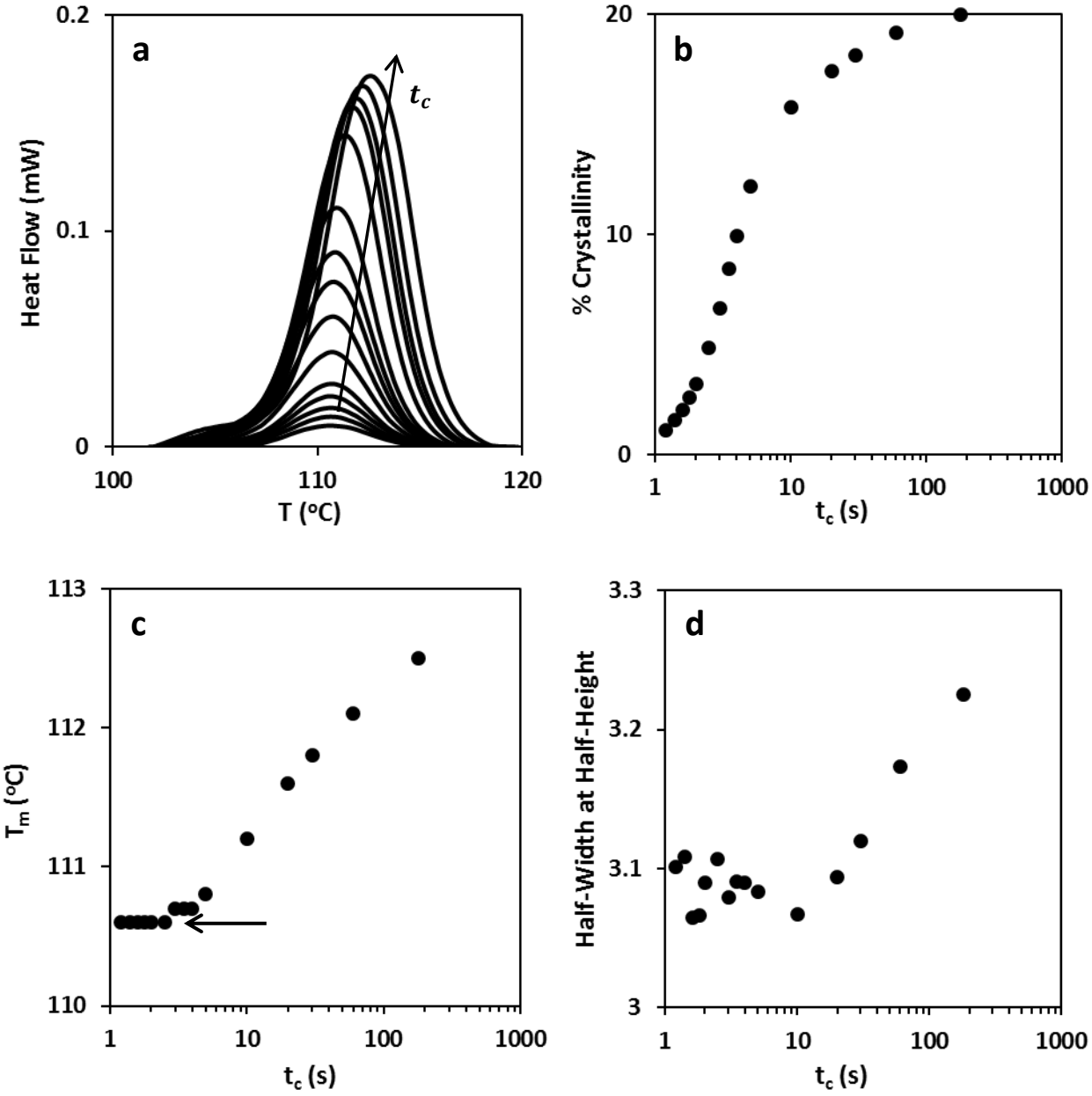

Figure 5.5. (a) Heat Flow *vs.* T for different crystallization times (endotherm up) for T_c = 101.6°C. (b) Percent crystallinity *vs.* t_c for T_c = 101.6°C. (c) Peak melting temperature *vs.* t_c for T_c = 101.6°C. (d) Half-width at half-height of the Gaussian fit to the melting endotherm *vs.* t_c for the EH3 copolymer crystallized isothermally at 101.6°C. The sample was melted using a heating rate of 1000°C/s. The arrow in Figure 5-c indicates the peak melting temperature of the initial lamellae.

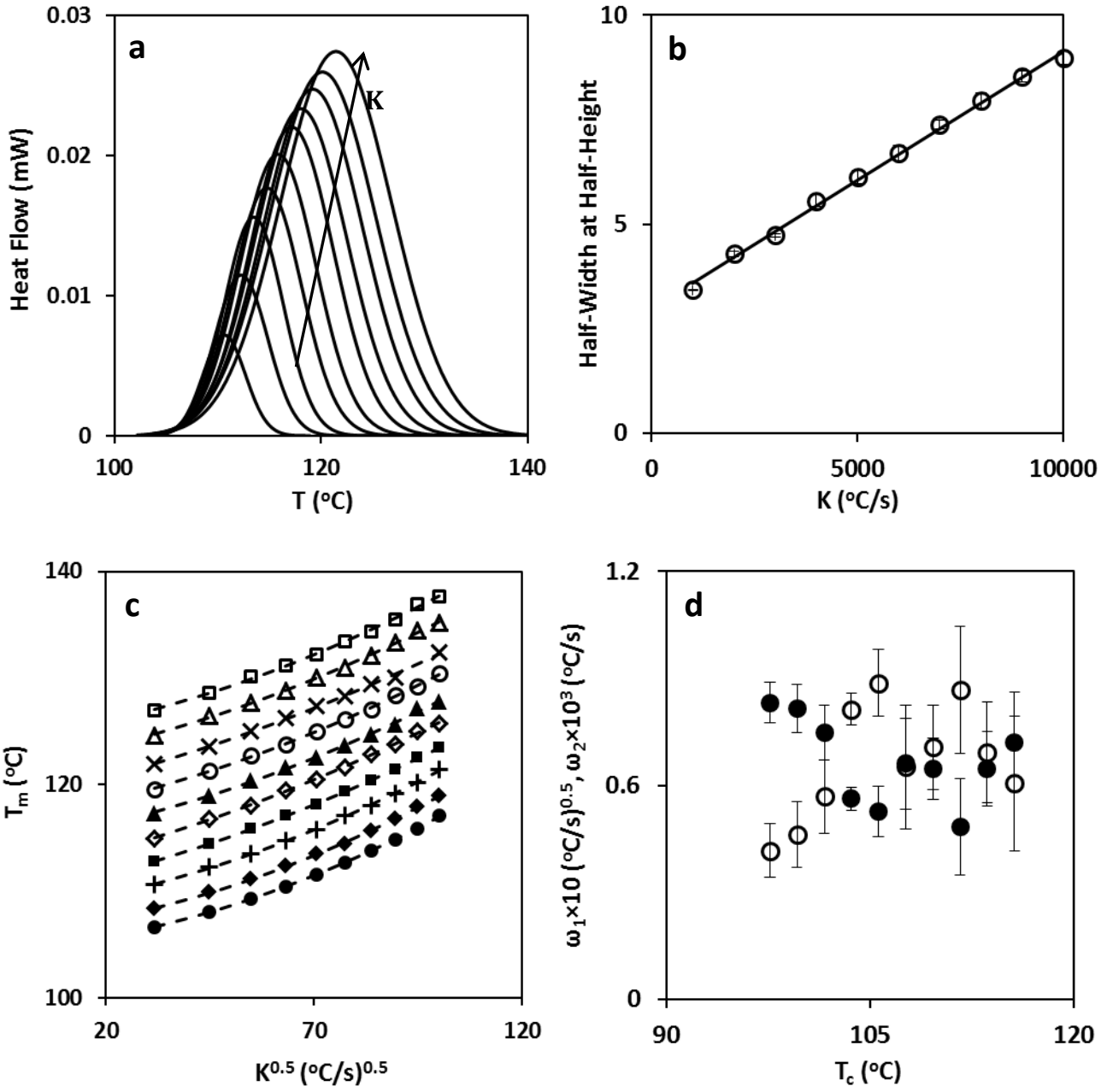

Figure 5.6. (a) Heat Flow (Gaussian fit) *vs.* temperature for heating rates between 1000 and 10000 °C/s, in increment of 1000°C/s for T_c = 101.6°C. (b) Half-width at half-height of the Gaussian fit to the melting endotherm *vs.* heating rate for the EH3 copolymer crystallized isothermally at 101.6°C. (c) Melting temperature of initial lamellae *vs.* $K^{0.5}$ for the EH3 copolymer crystallized isothermally at 97.6 (●), 99.6 (♦), 101.6 (+), 103.6 (■), 105.6 (◊), 107.6 (▲), 109.6 (○), 111.6 (×), 113.6 (Δ) and 115.6 °C (□). The dashed curves are the best fits to the experimental data by Equation 5.1. (d) ω_1 (○) and ω_2 (●) *vs.* T_c for the initial lamellae of EH3. Error bars correspond to one standard deviation.

The parallel evolution of the degree of crystallinity and melting temperature with time has been reported for LPE and m-LLDPE in previous studies.[6, 20] The increase in melting temperature and half-width at half-height of the melting endotherm with time, however, results from the increase in the concentration of short chain branches in the amorphous phase.[12, 21, 45] The melting temperature of initial lamellae is shown by the arrow on Figure 5.5 for crystallization at 101.6°C. The melting temperature and the half-width at half-height of the melting endotherm of isothermally crystallized lamellae of EH3 are strongly influenced by the heating rate, Figure 5.6. The half-width at half-height of the melting endotherm of EH3 increases linearly with increasing heating rate, Figure 5.6b. Figure 5.6c shows the changes in the peak melting temperature of initial lamellae *vs.* the square root of heating rate for the EH3 sample isothermally crystallized at different temperatures. Crystals of low thermal stability undergo melting without an activation barrier, therefore, a z of 0.5 was used to extrapolate the peak melting temperatures of initial lamellae to zero heating rate, Equation 5.1.[20, 35] Plots of initial melting temperature vs. $\mathrm{K}^{0.5}$ in Figure 5.6c are non-linear with a positive curvature, suggesting the importance of thermal lag effects during the melting of EH3. The existence of thermal lag is related to the low crystallinity level at short crystallization times.[19] Changes of ω_1, and ω_2 (the melting kinetics and instrumental thermal lag prefactors in Equation 5.1) with crystallization temperature are depicted in Figure 5.6d. As suggested by Toda et al.[34-36] ω_1 and ω_2 are independent of crystallization temperature, their product, $\omega_1\omega_2$, being constant and equal to $4.27 \pm 0.04 \times 10^{-5}$ $(^{o}C/s)^{1.5}$.

Using the heating rate dependence of the half-width at half-height of the melting endotherm and Equation 5.1 we can construct the zero-heating rate endotherm for the initial lamellae of EH3 at each crystallization temperature. Using Crist and Mirabella's framework[24] (Equation 5.8) we determined, for each crystallization temperature, the $\sigma_{em,c}$ value necessary to ensure that the lamellar thickness distribution derived from the melting endotherm through Equation 5.8 leads to the same number-average lamellar thickness as reported experimentally (Figure 5.2). To correlate

melting temperature and lamellar thickness, we used the Gibbs-Thomson equation[14] (Equation 5.9) and introduce $\sigma_{em,c}$, the fold surface free energy of initial lamellae during melting.

$$g(\ell) \propto P(T)\left(T_{m,c}^{eq} - T\right)^2 \tag{5.8}$$

$$\ell = \frac{2\sigma_{em,c}T_{m,c}^{eq}}{\Delta H\left(T_{m,c}^{eq} - T\right)} \tag{5.9}$$

Here, $g(\ell)$ and $P(T)$ are the normalized weight distribution function of the lamellar thickness and the power absorbed by the DSC at temperature T during melting, respectively.[15] As EH3 lamellae do not thicken with time,[21, 45] the lamellar thickness distribution obtained for the initial lamellae remains mostly unchanged until long crystallization times where secondary crystallization occurs.[32] The distribution polydispersity index (PDI) increases with increasing crystallization temperature, Figure 5.7, but the distribution remains sharp (PDI < 1.03). Crist and Mirabella[24] showed that a m-LLDPE copolymer containing more short-chain branches (more constraints) exhibits narrower lamellar thickness distribution. Therefore, we can attribute the increase in the breadth of the lamellar thickness distribution at higher crystallization temperatures to the crystallization of longer crystallizable sequences (less constraints on lamellar surfaces).[11]

Figure 5.8 depicts the fold surface free energy of EH3 during crystallization and melting as a function of undercooling. At low undercooling, the magnitude of the fold surface free energy during melting is significantly lower than the fold surface free energy during crystallization but approaches the value of σ_{em} = 27.0 ± 3.1 erg/cm^2 estimated for linear polyethylene with θ = 53.2^o, Figure 5.8 ($\sigma_{em,c} \ll \sigma_{ec,c}$).[19] On the other hand, at higher undercooling, similar fold surface free energies are observed for the copolymer during crystallization and melting ($\sigma_{em,c} \sim \sigma_{ec,c}$), Figure 5.8. Using the values of $\sigma_{em,c}$ as the equilibrium fold surface free energy for EH3, we can calculate the apparent strength of the stem length fluctuations, insert in Figure 5.8.

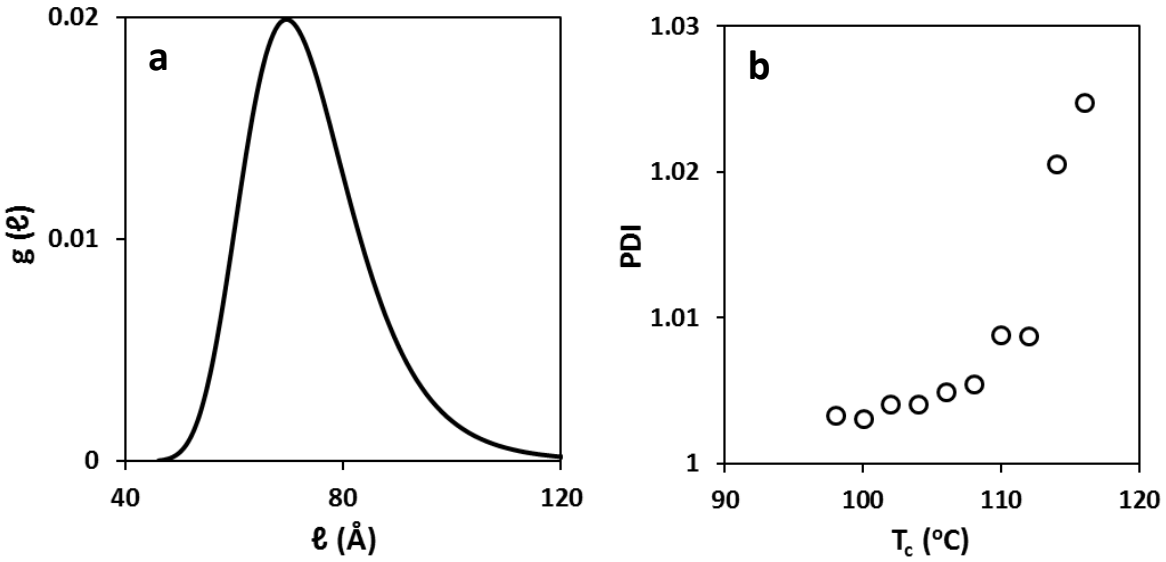

Figure 5.7. (a) Normalized weight distribution function of the lamellar thickness for the initial lamellae of EH3 crystallized isothermally at 113.6°C. (b) Polydispersity index of the initial lamella of EH3 *vs.* crystallization temperature.

Again, at low undercoolings the magnitude of y approaches that of linear polyethylene (y_{LPE} = 0.032 $^{o}C^{-1}$) while at higher undercoolings much lower values of y are observed.[19-20] Reorganization of the crystallized stems during crystallization and subsequent melting results in equilibration of the kinetic stem length fluctuations.[17] Short chain branches at the surface of the m-LLDPE lamellae limit such reorganization. Examination of the variation of $\sigma_{ec,c}$ and $\sigma_{ec,m}$ with undercooling (Figure 5.8) allows us to conclude that at low undercooling the long crystallizable sequences of m-LLDPE fold multiple times, leading to lamellar structures similar to these in linear polyethylene. A large fraction of the stem length fluctuations in these lamellae can equilibrate before melting as the concentration of short-chain branches on the lamellar surface is low. At high undercooling, short crystallizable sequences increase the concentration of short-chain branches on the lamellar surface, resulting in lamellae, whose stem length fluctuations cannot equilibrate before melting. As a result of a temperature-dependent fold surface free energy during melting, the zero-entropy production melting temperature for the number-average lamellar thickness, $T_{m,n}$(K =

0), estimated using Equation 5.9 is almost parallel to the $T_{m,n} = T_c$ line ($T_{m,n}(\mathrm{K} = 0) = T_c$ + 6.4°C) Figure 5.9a.

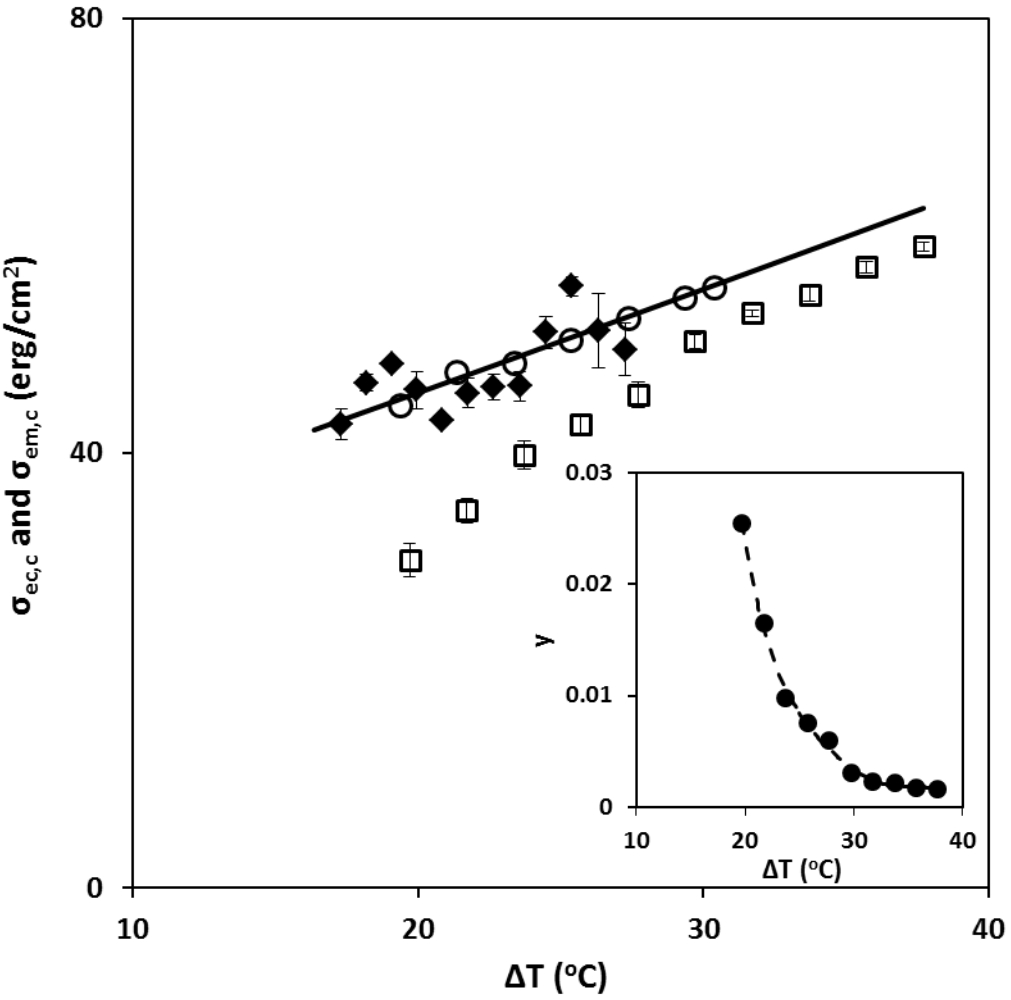

Figure 5.8. Fold surface free energy of initial crystals of EH3 during crystallization: using spherulite growth rate and lamellar thickness data (♦) and using only lamellar thickness data (○). The solid line is the best fit to the experimental data. Fold surface free energy of initial crystals of EH3 during melting from peak melting temperature *vs.* undercooling (□). The insert shows the apparent strength of stem length fluctuations *vs.* undercooling. The dashed line is the best fit to the experimental data. Error bars correspond to one standard deviation.

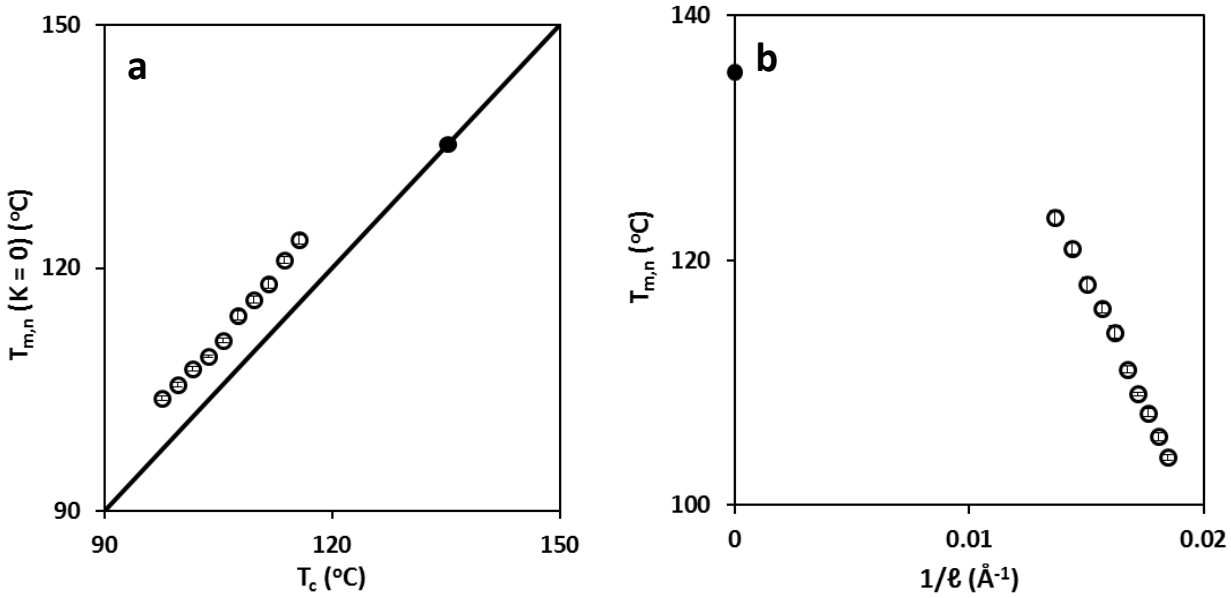

Figure 5.9. (a) $T_{m,n}\ (\mathrm{K} = 0)$ *vs.* T_c for EH3 lamellae. The solid line represents $T_{m,n} = T_c$. The filled circle is the equilibrium melting temperature of EH3 obtained using Flory theory (Equation 5.2). (b) Gibbs-Thomson plot for the EH3 copolymer. The filled circle is the equilibrium melting temperature found using Flory's equation. Error bars correspond to one standard deviation.

A similar behavior was observed by Alamo et al.[6] for the melting of low crystallinity (~5%) LLDPE samples. The effect of a temperature dependent fold surface free energy during melting is also obvious in the Gibbs-Thomson plot, Figure 5.9b. A linear fit to the experimental data leads to the physically meaningless $T_{m,c}^{eq}$ = 180.2 ± 1.2°C, about 40°C higher than the equilibrium melting temperature of linear polyethylene.[20] Therefore, the melting temperature *vs.* reciprocal of lamellar thickness plot for this copolymer sample must be non-linear.

5.6. Conclusions

Spherulite growth rate and lamellar thickness data of an m-LLDPE sample containing 3 mol% butyl branches were analyzed using the modified LH theory. Values of the fold surface free energy during crystallization determined from these different datasets superimpose if a crystallized stem tilt angle of 53.2^{o} is chosen. Independent support for this tilt angle value from a combination of transmission electron microscopy, X-ray and Raman scattering provide strong support for the use of the modified LH theory in such materials. The fold surface free energy during crystallization increases with increasing undercooling for the copolymer as it does for linear polyethylene. The fold surface free energy per stem during crystallization approaches that of linear polyethylene at low undercooling. The peak melting temperature and the half-width at half-height of melting endotherms of initial lamellae were measured for different heating rates using the Flash™ DSC 1 for samples isothermally crystallized at different temperatures. Extrapolation to zero-heating rate allowed to account for the effects of superheating, melting kinetics and thermal lag. The initial lamellar thickness distribution estimated from the melting endotherm for each crystallization temperature is narrow with a polydispersity index increasing slightly with increasing crystallization temperature. At low undercooling the magnitude of the fold surface free energy during melting is significantly lower than the fold surface free energy during crystallization, while at higher undercooling, similar fold surface free energies are observed for the copolymer during crystallization and melting. As a result of this temperature dependence, the experimental T_m *vs.* T_c plot is parallel to the $T_m = T_c$ line while the corresponding Gibbs-Thomson plot is non-linear. This behavior is attributed to the fact that longer crystallizable sequences form a chain-folded structure with lower concentration of branch points on the lamellar surface at lower undercooling, similar to the case of linear polyethylene. On the other hand, at higher undercooling the crystallization of shorter ethylene sequences results in the formation of lamellar structures exhibiting a higher concentration of branch points. An increase in the concentration of branch points on the lamellar

surface is expected to lead to a reduction in the ability of lamellar structures to relax their kinetic stem-length fluctuations during heating prior to melting.

5.7. References

1. Mark, H. F., Encyclopedia of polymer science and technology . Hoboken. NJ: Wiley-Interscience: 2003.
2. Perez, E.; VanderHart, D.; Crist Jr, B.; Howard, P., Morphological partitioning of ethyl branches in polyethylene by carbon-13 NMR. *Macromolecules* **1987,** *20* (1), 78-87.
3. Alamo, R.; Mandelkern, L., The crystallization behavior of random copolymers of ethylene. *Thermochimica Acta* **1994,** *238*, 155-201.
4. Perez, E.; Bello, A.; Perena, J.; Benavente, R.; Martinez, M.; Aguilar, C., Solid-state nuclear magnetic resonance study of linear low-density polyethylenes: 1. Ethylene-1-butene copolymers. *Polymer* **1989,** *30* (8), 1508-1512.
5. Crist, B.; Howard, P., Crystallization and melting of model ethylene− butene copolymers. *Macromolecules* **1999,** *32* (9), 3057-3067.
6. Alamo, R.; Chan, E.; Mandelkern, L.; Voigt-Martin, I., Influence of molecular weight on the melting and phase structure of random copolymers of ethylene. *Macromolecules* **1992,** *25* (24), 6381-6394.
7. Bensason, S.; Minick, J.; Moet, A.; Chum, S.; Hiltner, A.; Baer, E., Classification of homogeneous ethylene-octene copolymers based on comonomer content. *Journal of Polymer Science Part B: Polymer Physics* **1996,** *34* (7), 1301-1315.
8. Hoffman, J. D.; Davis, G. T.; Lauritzen, J. I., The rate of crystallization of linear polymers with chain folding. In *Treatise on solid state chemistry*, Springer: 1976; pp 497-614.
9. Hoffman, J. D.; Miller, R. L., Kinetic of crystallization from the melt and chain folding in polyethylene fractions revisited: theory and experiment. *Polymer* **1997,** *38* (13), 3151-3212.

10. Flory, P. J., Thermodynamics of Crystallization in High Polymers II. Simplified Derivation of Melting-Point Relationships. *The Journal of Chemical Physics* **1947,** *15* (9), 684-684.
11. Flory, P. J., Theory of crystallization in copolymers. *Transactions of the Faraday Society* **1955,** *51*, 848-857.
12. Goldbeck-Wood, G., On the melting-point depression of copolymer crystals. *Polymer* **1992,** *33* (4), 778-782.
13. Sanchez, I.; Eby, R., Thermodynamics and crystallization of random copolymers. *Macromolecules* **1975,** *8* (5), 638-641.
14. Thomson, W., W. Thomson, Philos. Mag. 42, 448 (1871). *Philos. Mag.* **1871,** *42*, 448.
15. Alamo, R.; Mandelkern, L., Crystallization kinetics of random ethylene copolymers. *Macromolecules* **1991,** *24* (24), 6480-6493.
16. Lauritzen Jr, J. I.; Hoffman, J. D., Extension of theory of growth of chain-folded polymer crystals to large undercoolings. *Journal of applied Physics* **1973,** *44* (10), 4340-4352.
17. Hoffman, J.; Lauritzen, J.; Passaglia, E.; Ross, G.; Frolen, s. L.; Weeks, J., Kinetics of polymer crystallization from solution and the melt. *Kolloid-Zeitschrift und Zeitschrift für Polymere* **1969,** *231* (1-2), 564-592.
18. Lauritzen, J.; Passaglia, E., Kinetics of crystallization in multicomponent systems: II. Chain-folded polymer crystals. *J Res Natl Bur Stand. A* **1967,** *71*, 261-75.
19. Mohammadi, H. On Melting and Crystallization of Linear Polyethylene, Poly(ethylene oxide), and Metallocene Linear Low Density Polyethylene. Virginia Polythecnic Institute and State University, 2018.
20. Mohammadi, H.; Vincent, M.; Marand, H., Investigating the Equilibrium Melting Temperature of Linear Polyethylene Using the Non-Linear Hoffman-Weeks Approach. *Polymer* **2018,** *146C*, 344-360.

21. Cho, T.; Heck, B.; Strobl, G., Equations describing lamellar structure parameters and melting points of polyethylene-co-(butene/octene) s. *Colloid and Polymer Science* **2004,** *282* (8), 825-832.
22. Crist, B., Thermodynamics of statistical copolymer melting. *Polymer* **2003,** *44* (16), 4563-4572.
23. Reid, B. O.; Vadlamudi, M.; Mamun, A.; Janani, H.; Gao, H.; Hu, W.; Alamo, R. G., Strong memory effect of crystallization above the equilibrium melting point of random copolymers. *Macromolecules* **2013,** *46* (16), 6485-6497.
24. Crist, B.; Mirabella, F. M., Crystal thickness distributions from melting homopolymers or random copolymers. *Journal of Polymer Science Part B: Polymer Physics* **1999,** *37* (21), 3131-3140.
25. Alberola, N.; Cavaille, J.; Perez, J., Mechanical spectrometry of alpha relaxations of high-density polyethylene. *Journal of Polymer Science Part B: Polymer Physics* **1990,** *28* (4), 569-586.
26. Crist, B.; Claudio, E. S., Isothermal Crystallization of Random Ethylene− Butene Copolymers: Bimodal Kinetics. *Macromolecules* **1999,** *32* (26), 8945-8951.
27. Alamo, R.; Mandelkern, L., Origins of endothermic peaks in differential scanning calorimetry. *Journal of Polymer Science Part B: Polymer Physics* **1986,** *24* (9), 2087-2105.
28. Kim, M. H.; Phillips, P. J., Nonisothermal melting and crystallization studies of homogeneous ethylene/α-olefin random copolymers. *Journal of applied polymer science* **1998,** *70* (10), 1893-1905.
29. Godovsky, Y. K.; Magonov, S. N., Atomic Force Microscopy Visualization of Morphology and Nanostructure of an Ultrathin Layer of Polyethylene during Melting and Crystallization. *Langmuir* **2000,** *16* (7), 3549-3552.
30. Fritzsching, K. J.; Mao, K.; Schmidt-Rohr, K., Avoidance of density anomalies as a structural principle for semicrystalline polymers: the importance of chain ends and chain tilt. *Macromolecules* **2017,** *50* (4), 1521-1540.

31. Hoffman, J. D.; Miller, R. L.; Marand, H.; Roitman, D. B., Relationship between the lateral surface free energy. sigma. and the chain structure of melt-crystallized polymers. *Macromolecules* **1992,** *25* (8), 2221-2229.
32. Alizadeh, A.; Richardson, L.; Xu, J.; McCartney, S.; Marand, H.; Cheung, Y.; Chum, S., Influence of structural and topological constraints on the crystallization and melting behavior of polymers. 1. Ethylene/1-octene copolymers. *Macromolecules* **1999,** *32* (19), 6221-6235.
33. Stadler, F. J.; Kaschta, J.; Münstedt, H., Dynamic-mechanical behavior of polyethylenes and ethene-/α-olefin-copolymers. Part I. α′-Relaxation. *Polymer* **2005,** *46* (23), 10311-10320.
34. Toda, A.; Taguchi, K.; Nozaki, K.; Konishi, M., Melting behaviors of polyethylene crystals: an application of fast-scan DSC. *Polymer* **2014,** *55* (14), 3186-3194.
35. Toda, A.; Konishi, M., An evaluation of thermal lags of fast-scan microchip DSC with polymer film samples. *Thermochimica Acta* **2014,** *589*, 262-269.
36. Toda, A., Heating rate dependence of melting peak temperature examined by DSC of heat flux type. *Journal of Thermal Analysis and Calorimetry* **2016,** *123* (3), 1795-1808.
37. Marand, H.; Huang, Z., Isothermal lamellar thickening in linear polyethylene: Correlation between the evolution of the degree of crystallinity and the melting temperature. *Macromolecules* **2004,** *37* (17), 6492-6497.
38. Davis, G.; Eby, R.; Colson, J., Thermal expansion of polyethylene unit cell: effect of lamella thickness. *Journal of Applied Physics* **1970,** *41* (11), 4316-4326.
39. Gaur, U.; Wunderlich, B., Heat capacity and other thermodynamic properties of linear macromolecules. II. Polyethylene. *Journal of Physical and Chemical Reference Data* **1981,** *10* (1), 119-152.
40. Abo el Maaty, M.; Bassett, D.; Olley, R.; Jääskeläinen, P., On cellulation in polyethylene spherulites. *Macromolecules* **1998,** *31* (22), 7800-7805.
41. Akpalu, Y.; Kielhorn, L.; Hsiao, B.; Stein, R.; Russell, T.; Van Egmond, J.; Muthukumar, M., Structure development during crystallization of homogeneous copolymers of ethene and 1-

octene: time-resolved synchrotron X-ray and SALS measurements. *Macromolecules* **1999,** *32* (3), 765-770.

42. Lambert, W. S.; Phillips, P. J., Crystallization kinetics of fractions of branched polyethylenes: 2. Effect of molecular weight. *Polymer* **1996,** *37* (16), 3585-3591.
43. Shimizu, K.; Wang, H.; Wang, Z.; Matsuba, G.; Kim, H.; Han, C. C., Crystallization and phase separation kinetics in blends of linear low-density polyethylene copolymers. *Polymer* **2004,** *45* (21), 7061-7069.
44. Wagner, J.; Phillips, P. J., The mechanism of crystallization of linear polyethylene, and its copolymers with octene, over a wide range of supercoolings. *Polymer* **2001,** *42* (21), 8999-9013.
45. Cho, T. Y.; Shin, E. J.; Jeong, W.; Heck, B.; Graf, R.; Strobl, G.; Spiess, H. W.; Yoon, D. Y., Effects of comonomers on lamellar and noncrystalline microstructure of ethylene copolymers. *Macromolecular rapid communications* **2006,** *27* (5), 322-327.
46. Crist, B., Analysis of small-angle X-ray scattering patterns. *Journal of Macromolecular Science, Part B* **2000,** *39* (4), 493-518.
47. Xia, Z.; Sue, H.-J.; Wang, Z.; Avila-Orta, C. A.; Hsiao, B. S., Determination of crystalline lamellar thickness in poly (ethylene terephthalate) using small-angle X-ray scattering and transmission electron microscopy. *Journal of Macromolecular Science, Part B* **2001,** *40* (5), 625-638.
48. Knudsen, K. D.; Hemmingsen, P. V.; Mo, F., Temperature-induced structural changes in some random ethylene/1-hexene copolymers. *Polymer* **2007,** *48* (11), 3148-3161.
49. Fetters, L.; Lohse, D.; Colby, R., Chain dimensions and entanglement spacings. In *Physical properties of polymers handbook*, Springer: 2007; pp 447-454.
50. Pearson, D.; Ver Strate, G.; Von Meerwall, E.; Schilling, F., Viscosity and self-diffusion coefficient of linear polyethylene. *Macromolecules* **1987,** *20* (5), 1133-1141.

Chapter 6. Analysis of the Crystallization Temperature and Chain Length Dependences of the Spherulite Growth Rate of Poly(ethylene oxide)

Hadi Mohammadi, Zhenyu Huang, Samantha Talley and Hervé Marand

6.1. Attribution

Samantha Talley contributed to this work by conducting the wide angle X-ray diffraction experiments. Zhenyu Huang measured the spherulite growth rates. Design of the experiments, conventional DSC experiments, and processing and analysis of the data were all performed by Hadi Mohammadi. The paper was prepared by Hadi Mohammadi and Hervé Marand.

6.2. Abstract

Zero-entropy production melting temperatures for initial lamellae of isothermally crystallized poly(ethylene oxide) fractions were analyzed in the context of the non-linear Hoffman-Weeks method, leading to a limiting equilibrium melting temperature of 81.4 ± 1.0^{o}C, 12.5^{o}C higher than that estimated by Buckley and Kovacs. Analysis of the spherulite growth rate and wide angle X-ray diffraction data revealed that the value of the equilibrium fold surface free energy derived from crystal growth rate data matches that calculated from lamellar thickness and melting data. The regime I/II transition undercooling, equilibrium fold surface free energy, strength of the stem length fluctuations, and substrate length at the regime I/II transition are found to be independent of chain length. The magnitude of the apparent chain friction

coefficient during crystal growth is significantly lower for poly(ethylene oxide) than for linear polyethylene, possibly as a result of a much more active α_c-relaxation for the former polymer.

6.3. Introduction

Poly(ethylene oxide) (PEO) has been one of the most extensively studied semi-crystalline polymers for the last 50 years.[1-6] Crystallization of poly(ethylene oxide) is particularly interesting in the sense that even at very low temperatures crystalline chains undergo a rapid α_c-relaxation.[7-9] For instance, at room temperature the net rate of displacement of PEO chains through helical jumps along the c-axis is about 15 times faster than that for linear polyethylene (LPE) chains in orthorhombic crystals at 100^{o}C.[7-12] As a result of the rapid α_c-relaxation, isothermal crystallization of low to intermediate molecular weight poly(ethylene oxide) fractions (M_n< 20 kg/mol) at ambient pressure gives rise to extended-chain crystals.[13-14] Understanding of the role played by segmental mobility in the crystal phase on the crystallization mechanism, is however still lacking.[15] To start it is of interest to compare the molecular weight dependence of the crystallization rate for LPE under ambient and under high pressure. The exponent of the power law dependence of the spherulite growth rate of orthorhombic crystals on chain length at constant undercooling is -1.7.[15-16] Examination of experimental data for a large number of narrow molar mass LPE fractions allowed us to relate the magnitude of this exponent to the apparent chain friction coefficient during transport to the crystal growth front.[16] This exponent increases to -0.7 for growth rates of hexagonal crystals prepared at constant undercooling via crystallization under high pressure.[15, 17-19] Significantly higher segmental mobility is observed for LPE chains in the hexagonal phase compared to the orthorhombic phase.[8, 17-19] It is anticipated that studies of the isothermal crystallization of poly(ethylene oxide), a polymer with similar α_c-mobility as hexagonal crystals of LPE, may enable us to get some insight on the role of segmental mobility in the crystal phase on the crystallization mechanism.

The first step in analyzing the crystallization behavior of any polymer is to determine its equilibrium melting temperature, T_m^{eq}.[16, 20] Using an analysis similar to that proposed by Flory and Vrij,[21] Buckley and Kovacs[22-23] suggested that the equilibrium melting temperature of an infinite molecular weight PEO sample, $T_m^{eq,\infty}$, is equal to 68.9 ± 0.4°C. Later, Mandelkern and Stack[24] noted that the extrapolative method of Buckley and Kovacs[22-23] has two major problems: 1) the samples used in the analysis were not rigorously monodisperse, thus, the crystals were not molecular crystals with paired chain-ends and 2) the free energy expansion was not performed correctly. Furthermore, we noticed that for PEO fractions with molecular weights between 2 to 10 kg/mol, the melting data of used in the extrapolation was not characteristic of extended-chain crystals but included chain-folded crystals or had crystallinity not exceeding 90-95%.[13-14, 23] In the case of fractions studied by Buckley and Kovacs, the crystallinity of their extended-chain crystals reached a maximum value of 70%.[23] A lower concentration of extended-chain crystals leads to an artificially lower equilibrium melting temperature. These errors strongly affect the relationship obtained for the chain length dependence of the equilibrium melting temperature of PEO.[24] Mandelkern and Stack[24] suggested that the equilibrium melting temperatures of high molecular weight PEO fractions are essential for obtaining a reliable relationship between chain length and equilibrium melting temperature. Using the Hoffman-Weeks method, Afifi-Effat and Hay,[2] Marentette and Brown,[25] Alfonso and Russell,[26] Beech and Booth[27] and Allen[28] have reported values in the range of 75 to 80°C for the equilibrium melting temperature of poly(ethylene oxide) for molecular weights in excess of 10^5 g/mol. However, as we have showed in a number of publications,[29-30] the linear Hoffman-Weeks method underestimates the equilibrium melting temperature of polymers. Therefore, a non-linear Hoffman-Weeks analysis of the melting behavior of high molecular weight poly(ethylene oxide) fractions is necessary.[16, 30]

In this paper we discuss the melting data obtained using a conventional calorimeter for four poly(ethylene oxide) fractions crystallized isothermally at different temperatures over a range of crystallization times. We consider the heating rate dependence of the calorimetric data to minimize annealing and melting-recrystallization-remelting phenomena, and to account for superheating and thermal lag effects.[31-32] We extrapolate the experimental melting data to zero heating rate, zero crystallinity conditions and use these extrapolated melting temperatures in the context of the non-linear Hoffman-Weeks method to determine the equilibrium melting temperature for these PEO fractions.[29-30] We then use these values to determine the parameters of the Huggins equation relating equilibrium melting temperature to chain length.[29, 33] We then analyze spherulite growth rate data for five PEO fractions with number average molecular weights ranging from 21 to 157 kg/mol using the modified Lauritzen-Hoffman (LH) theory.[16] The modified LH theory accounts for the temperature dependence of both the fold $(\sigma_{ec,c})$ and lateral (σ) surface free energies on the spherulite growth rate of PEO.[16, 20, 34-36] We estimate the substrate length for these PEO fractions at the undercooling, $\Delta T_{I\rightarrow II}$, for the regime I/II transition using lattice coherence length measurements carried out by wide angle X-ray diffraction.[37-38] The substrate length obtained by this method is used to determine the apparent chain friction coefficient during crystal growth.[16] The results of such analyses are used to shine some light on the crystallization mechanism of poly(ethylene oxide).

6.4. Experimental

6.4.1. Material

Nine narrow molecular weight poly(ethylene oxide) fractions with weight average molecular weights ranging from 21 to 232 kg/mol were purchased from Scientific Polymer Products and Polymer Laboratories and used as received. The molecular characteristics of

these fractions are given in Table 1. These samples were kept in an evacuated desiccator in the dark prior to usage to minimize degradation.[39-40]

6.3.2. Differential Scanning Calorimetry

The melting behavior of four PEO fractions (PEO 34K, 70K, 100K, and 232K) was studied using sealed Tzero™ pans in a conventional TA Instruments Q2000 differential scanning calorimeter (DSC) under a dry nitrogen flow of 50 mL/min. Thermal calibration during heating was performed with indium, tin, and zinc standards using TA Instruments' calibration wizard. The PEO films used in these experiments were prepared using a Carver laboratory press operated at 100°C under a nitrogen atmosphere. Thermal lag studies for the conventional DSC were carried out following the melting of a small piece of indium (mass less than 0.1 mg) sandwiched between two PEO 70K films.[16] Our results indicate that indium and indium sandwiched between two 50 μm thick PEO films had the same melting temperature in the range of heating rates between 70 and 110°C/min.[16] Similar experiments carried out with significantly thicker (e.g. 1 mm thick PEO films) showed systematic deviations between the indium sandwich and the indium standard. All DSC studies discussed here used 50 μm thick PEO films with average mass of about 1.5 mg.

All calorimetric experiments were initiated by heating the sample to 110°C and holding it at this temperature for 30s to erase prior thermal history. The samples were then cooled down to 0°C with a cooling rate of 20°C/min and held at this temperature for 30s. The samples were subsequently heated (with a heating rate of 50°C/min) to a self-seeding temperature about 5°C higher than the peak melting temperature. At this point, most of the crystalline sample was molten. The samples were then cooled to specific crystallization temperatures at a rate of 20°C/min and crystallized for various times, t_c. The small crystalline fraction remaining from the self-seeding procedure acted as nucleation sites during isothermal crystallization. While this self-seeding technique is highly reproducible, it does not alter the crystallization behavior of

PEO.[1, 14] Crystallization temperatures, T_c, were chosen on the low temperature side to ensure that crystallization did not take place during cooling or during subsequent heating prior to melting. On the high temperature side, crystallization was limited to temperatures where crystal growth occurs much faster than isothermal lamellar thickening. Under such conditions, the melting temperature is approximately constant at the earliest stages of crystallization. Samples were subsequently melted by heating at a rate ranging from 70 to 110°C/min (in increments of 5°C/min) and their peak melting temperature and heat of fusion were recorded. For every crystallization temperature, a baseline heating trace was also recorded for a sufficiently short crystallization time where no crystals had time to develop. This baseline was subtracted from the heating trace of partially crystallized samples to minimize the error (less than 1%) in the measured heat of fusion. The lower the degree of crystallinity, the narrower the breadth of the melting endotherm, the smaller the expected error.[41] The degree of crystallinity of each sample was estimated using the heat of fusion of PEO, 188 J/g.[24] For each crystallization temperature, the initial melting temperature, T_m, of non-thickened lamellae is defined as the melting temperature of samples exhibiting the lowest crystallinity, where T_m does not change with time. The zero-entropy production melting temperature of these non-thickened lamellae was obtained for each crystallization temperature by extrapolation to zero heating rate using Equation 6.1 proposed by Toda et al.[31-32]

$$T_m = T_m(\mathrm{K} = 0) + \omega_1 \mathrm{K}^z + \omega_2 \mathrm{K} \tag{6.1}$$

where K, ω_1, and ω_2 are the heating rate, and constant prefactors, respectively. The terms $\omega_1 \mathrm{K}^z$ and $\omega_2 \mathrm{K}$ account for the effect of melting kinetics and instrumental thermal lag on the melting temperature of the standard, respectively. The thermal lag constant ($\omega_2 \times 10^3 = 6.9 \pm 0.1$ min) was determined from the slope of the indium onset melting temperature *vs.* heating rate plot.[29] Crystals of low thermal stability undergo melting without an activation barrier,

therefore, a z of 0.5 was used to extrapolate the peak melting temperature of initial lamellae to zero heating rate, Equation 6.1.[29, 31]

6.3.3. Spherulite Growth Rate Measurements

Spherulite growth rates of five PEO fractions (PEO 21K, 44K, 75K, 113K, and 157K) were measured by optical microscopy.[42] Thin PEO films (ca. 30 μm) were prepared using a Carver laboratory press operated at 100°C under a nitrogen atmosphere. Small pieces of the films were sandwiched between clean glass cover slips and placed in a Linkam THM 600 heating-cooling stage under a dry nitrogen flow of 50 ml/min. The sample temperature was regulated within ±0.1°C using a Linkam TMS 93 temperature controller. Temperature calibration for the stage and temperature controller was performed in the range of 50 to 110°C using 5 melting standards: benzophenone (T_m = 48.5°C), 1,3-diphenoxy-benzene (T_m = 60°C), 2,6-di-tert-butyl-4-methylphenol (T_m = 70°C imidazole (T_m = 90°C) m-toluic acid (T_m = 111°C) Before each spherulite growth rate measurement, the PEO films were heated to 100°C and kept in the melt state for 3 minutes to erase previous thermal history. The films were subsequently cooled at a rate of 50°C/min to the desired crystallization temperature and the spherulite growth was monitored using an Olympus BX-50 polarized light optical microscope interfaced to a video camera. Using the ImageJ image analysis software, spherulite radii were measured as a function of time for four spherulites at each crystallization temperature. Spherulite growth rates were calculated as the slope of the observed linear increase of the radius with time.[42] As the crystal growth front of poly(ethylene oxide) changes around 51°C,[25, 43] the spherulite growth rate measurements were only analyzed for T_c > 51°C. For all isothermal spherulite growth experiments in the 51 to 62°C temperature range, the relative standard deviation on the average spherulite growth rate was determined to be less than 5%.[42]

6.3.4. Lattice Coherence Length Measurements

Lattice coherence lengths of four PEO fractions (PEO 34K, 70K, 100K and 232K) were determined using wide angle X-ray diffraction. The widths of the (120) reflection of semicrystalline PEO was measured at the regime I to regime II transition temperature using a Rigaku S-Max 3000 SAXS/WAXD instrument at Virginia Tech. This diffraction set-up used a Micromax-007HF high intensity microfocus rotating anode copper source (CuK_α, λ = 0.154 nm, operated at 40 kV and 30 mA) and a gas filled 2-D multiwire, proportional counting detector. The X-ray beam was collimated using three pinholes. Samples were pressed into 1 mm thick films using a Carver Laboratory Press at 100°C under a nitrogen atmosphere. The films were then cut into 1×1×1 mm^3 specimens and sandwiched between two Kapton™ films. Each sandwich was then affixed to the sample platform of a Linkam THMS 600 heating/cooling stage using an o-ring and then placed in the diffractometer. The Linkam stage had a 1 mm diameter hole to allow the passage of the X-rays. The sample temperature was regulated within ±0.1°C using a Linkam T-95-PE temperature controller. Temperature calibration of the heating stage was performed in the range of 50 to 150°C using 6 melting standards: benzophenone (T_m = 48.5°C), 2,6-di-tert-butyl-4-methylphenol (T_m = 70°C), imidazole (T_m = 90°C), m-toluic acid (T_m = 111°C), methylhydroquinone (T_m = 128°C), and l-xylose (T_m = 150°C). Before each WAXD measurement the PEO sample was heated to 100°C at a heating rate of 30°C/min under vacuum and kept at this temperature for 1 minute to erase its previous thermal history. The sample was then cooled at a rate of 30°C/min to room temperature and held there for 1 minute. The sample was heated to the self-seeding temperature at a rate of 30°C/min and finally cooled to $T_{I\to II}$ at a rate of 30°C/min. WAXD patterns of the crystallized samples were recorded in a 0.05 - 0.28 nm^{-1} q range (i.e. 2θ between 7 and 40°) for 30 min under vacuum at the appropriate crystallization temperatures using a Fujifilm™ HR-V image plate (with an aperture of 0.375" diameter and a sample-to-image plate distance of 92.0 mm). The image plate was scanned

using a RAXIA-Di™ image plate reader. Angular calibration was performed using the third-order diffraction ring of a silver behenate standard. Using the SAXSGUI™ software package, the WAXD scattering intensity was corrected for Kapton™ scattering as well as absorption. Similar measurements were performed using a lanthanum hexaboride standard to evaluate the instrumental peak broadening. After subtraction of the amorphous halo, the (120), θ_p = 9.5°, diffraction peak of PEO crystals was fitted with a Gaussian function, Equation 6.2.

$$I(\theta) = a_1 \exp\left(-\frac{(\theta - \theta_p)^2}{2a_2^2}\right) \tag{6.2}$$

where θ_p, $I(\theta)$, a_1 and a_2 are the Bragg angle at maximum intensity, the angular dependent diffraction intensity, the diffraction peak height and the standard deviation of the Gaussian intensity distribution, respectively. The integral breath of the diffraction peak, Λ, was then obtained using:

$$\Lambda = a_2\sqrt{2\pi} \tag{6.3}$$

The integral breadth (Λ_{stnd} = 0.169) for the diffraction of lanthanum hexaboride at θ_p = 10.5° was obtained following the same method. The instrumental broadening contribution to the observed peak broadening of PEO crystals was then accounted for using the integral breadth of the standard, Λ_{stnd}, Equation 6.4.

$$\Lambda_{corr}^2 = \Lambda^2 - \Lambda_{stnd}^2 \tag{6.4}$$

Λ_{corr} is the corrected integral breadth for the diffraction peak. The lattice coherence length associated with the (120) growth front, $D_{(120)}$, was then calculated using the Scherrer equation,[44] Equation 6.5.

$$D_{(120)} = \frac{\lambda}{2\Lambda_{corr}\cos\theta_p} \tag{6.5}$$

Measurements were performed in triplicate for each PEO fraction.

6.4. Results and Discussion

6.4.1. Chain Length Dependence of the Equilibrium Melting Temperature for Poly(ethylene oxide)

Figure 6.1a shows the evolution of the melting endotherm with crystallization time for PEO 34K crystallized isothermally at 52.6^{o}C. These melting endotherms were recorded with a heating rate of 70^{o}C/min. Since all melting studies were carried out at rates in excess of 70^{o}C/min, melting-recrystallization-remelting and annealing were avoided during heating.[23, 29] The degree of crystallinity (Figure 6.1b) and melting temperature (Figure 6.1c) of PEO 34K exhibit a sigmoidal increase with logarithm of crystallization time, which is related to the nucleation and growth of new lamellae and the thickening of old lamellae at earlier and later crystallization times, respectively.[29] The melting temperature of initial lamellae is shown with an arrow in Figure 6.1c for PEO 34K crystallized isothermally at 52.6^{o}C. These lamellae have not had enough time to thicken, therefore, an increase in melting temperature is not observed. The effect of thermal lag on the melting of initial lamellae of PEO was corrected using the thermal lag constant in Equation 6.1 ($\omega_2 \times 10^3$ = 6.9 ± 0.1 min).[29, 31-32] Figure 6.2 shows the melting temperatures of initial lamellae of *vs.* square root of heating rate for PEO samples crystallized isothermally at different crystallization temperatures. As expected, the corrected melting temperature increases linearly with the square root of heating rate.[29, 31-32] The zero-entropy production melting temperature of initial lamellae at each crystallization temperature, $T_m(\mathrm{K}=0)$, was estimated from the intercept of the corresponding plot. In the model proposed by Toda and Konishi,[31] the melting kinetics constant (ω_1) is proportional to $1/z$. As z = 0.5 is constant for the studied PEO fractions, the values of ω_1 are found to be independent of crystallization temperature for each fraction.

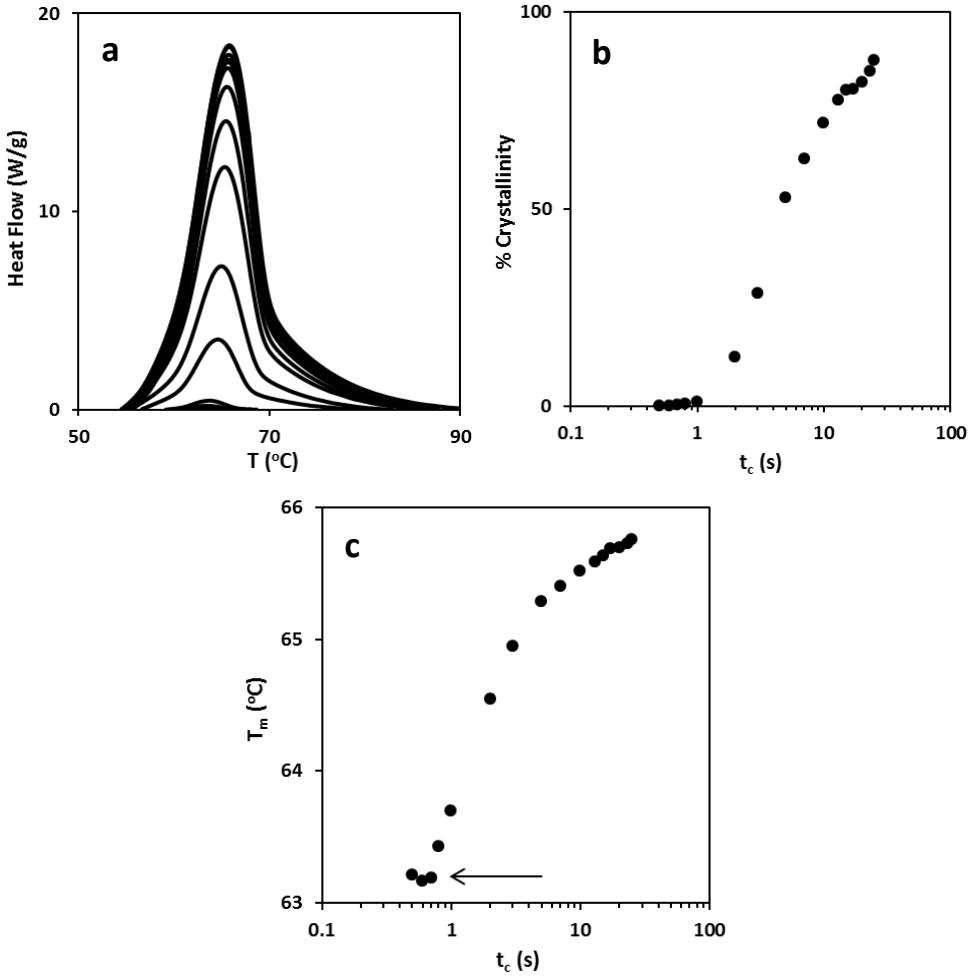

Figure 6.1. (a) Evolution of the melting endotherm for PEO 34K crystallized for different times at 52.6°C. (b) Degree of crystallinity *vs.* crystallization time for PEO 34K crystallized at 52.6°C. (c) Melting temperature *vs.* crystallization time for PEO 34K crystallized at 52.6°C. Melting behavior of this fraction was studied at a heating rate of 70°C/min. The arrow in Figure 6.1c indicates the peak melting temperature of the initial lamellae.

Using the initial melting temperatures for non-thickened lamellae formed at different crystallization temperatures, normalized melting, M, and crystallization, X, temperatures are calculated for different choices of the equilibrium melting temperature.[29-30] Once the correct equilibrium melting temperature is used, M and X exhibit a linear relationship with slope of one, Figure 6.3.[29-30] Equilibrium melting temperatures of 78.8 ± 1.0, 80.8 ± 0.6, 81.0 ± 1.5, and 80.8 ± 1.2°C are determined by this method for PEO 34K, 70K, 100K, and 232K, respectively. The

value of 81.0 ± 1.5 °C estimated for PEO 100K is higher than any equilibrium melting temperature value reported in the literature for PEO fractions.[2, 26-28] The equilibrium melting temperatures of these PEO fractions overlap within the uncertainty limits, however, the data obtained for PEO are consistent with the increase in equilibrium melting temperature with increasing molecular weight, expected on the basis of chain-end effects.[29]

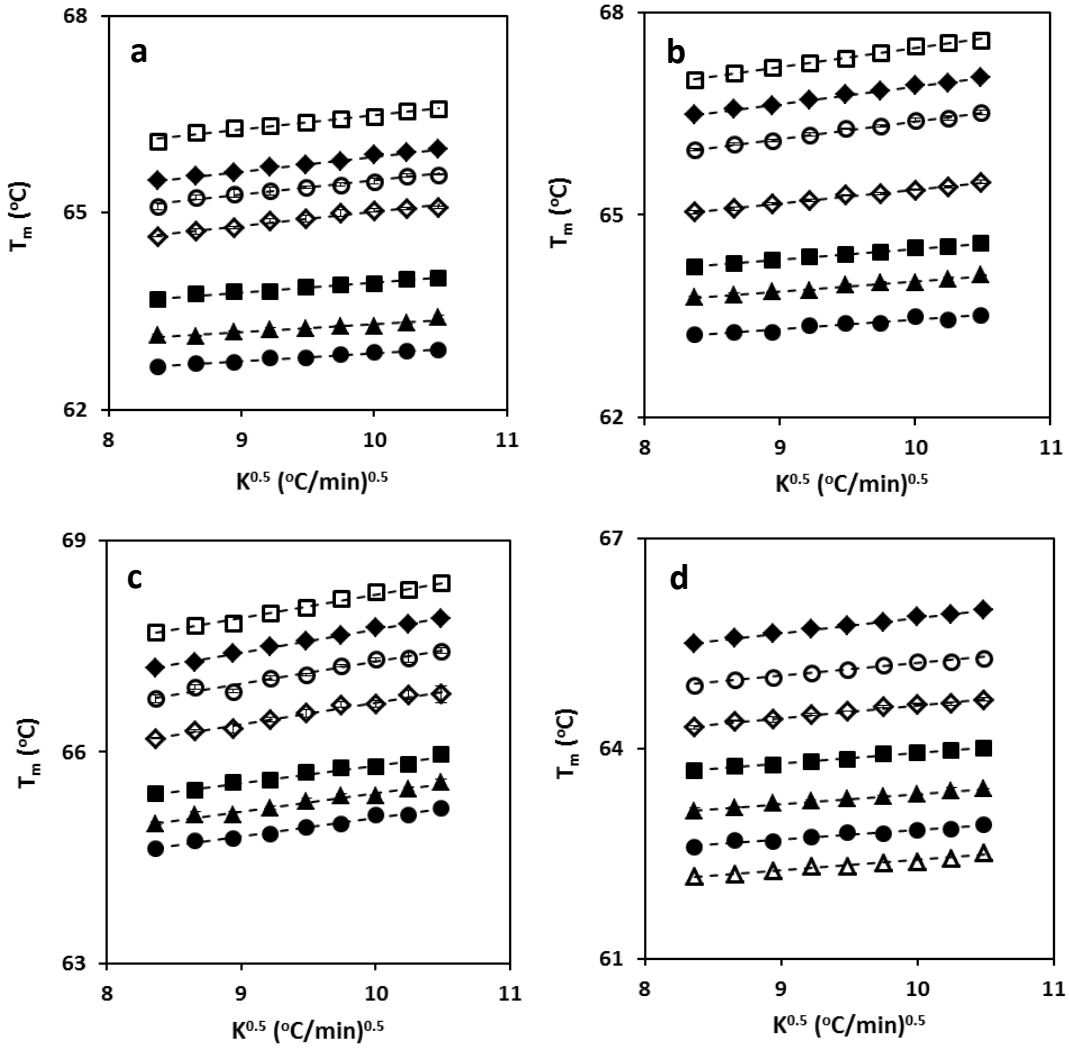

Figure 6.2. Melting temperature *vs.* $K^{0.5}$ for non-thickened lamellae of: (a) PEO 34K crystallized at 51.6 (●), 52.6 (▲), 53.6 (■), 54.6 (◊),55.6 (○), 56.6 (♦) and 57.6°C (□). (b) PEO 70K crystallized at 51.6 (●), 52.6 (▲), 53.6 (■), 54.6 (◊),55.6 (○), 56.6 (♦) and 57.6°C (□). (c) PEO 100K crystallized at 51.6 (●), 52.6 (▲), 53.6 (■), 54.6 (◊),55.6 (○), 56.6 (♦) and 57.6°C (□). (d) PEO 232K crystallized at 50.6 (Δ), 51.6 (●), 52.6 (▲), 53.6 (■), 54.6 (◊),55.6 (○) and 56.6 °C (♦). The dashed lines represent the best fit of the melting temperature data to Equation 6.1.

The equilibrium melting temperatures obtained for PEO fractions by the non-linear Hoffman-Weeks method are about 13°C higher than these predicted by the Buckley-Kovacs equation.[22-23] The values of the non-linear Hoffman-Weeks constant, $\bar{a}$. determined from the intercept of the M *vs.* X plot are also independent of chain length ($\bar{a}$ = 6.9 ± 0.6), see the insert in Figure 6.5.[29, 41]

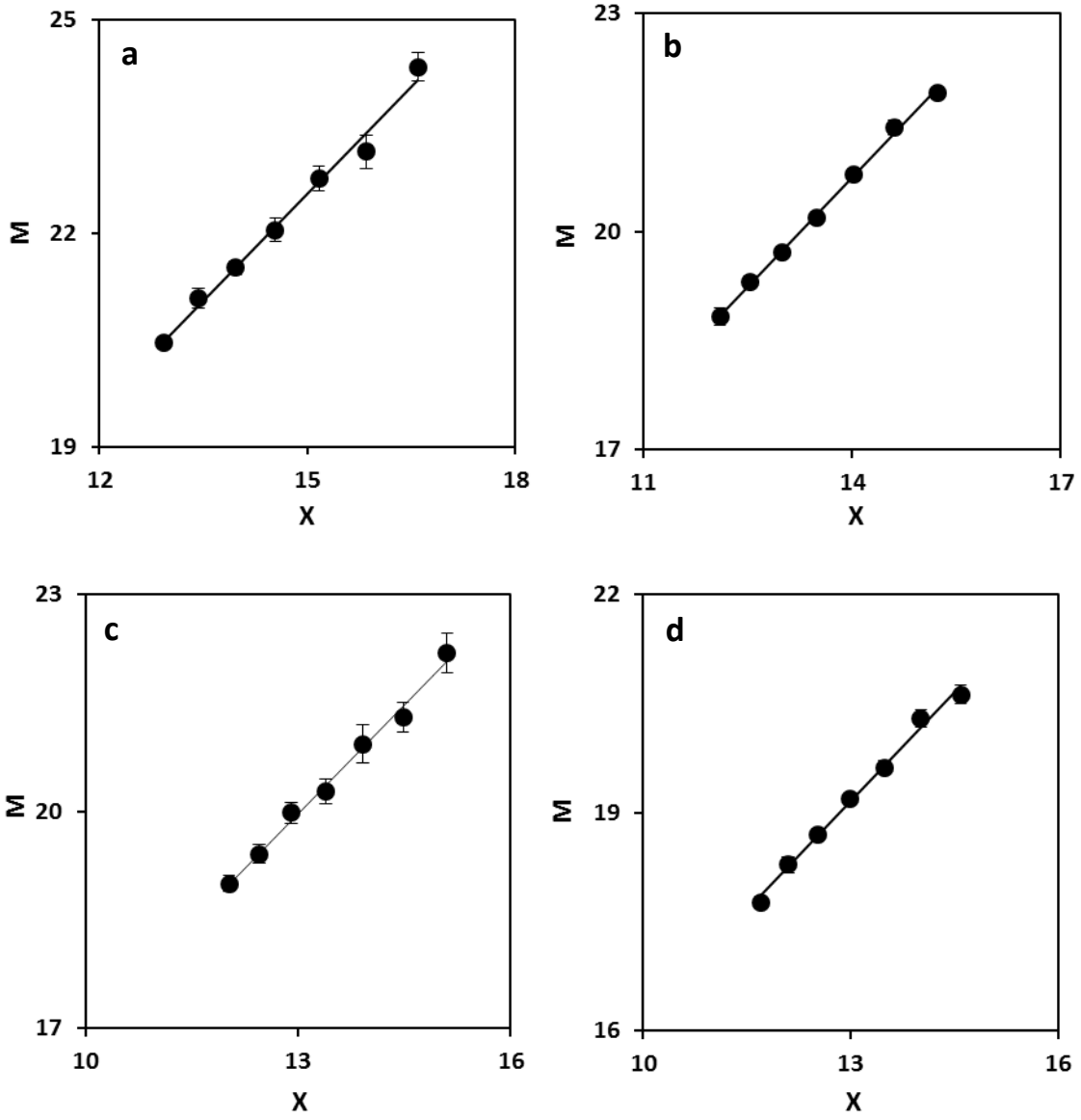

Figure 6.3. M vs. X for (a) PEO 34K, (b) PEO 70K, (c) PEO 100K and (d) PEO 232K. The plots were drawn using the equilibrium melting temperature leading to a slope of unity for each M-X plot. Error bars associated with M values arises from the uncertainty in the observed melting temperature.

Plots of observed melting temperature vs. crystallization temperature are shown in Figure 6.4 for the various fractions. For each PEO fraction, the intercept of the linear regression line with the $T_m = T_c$ line (the linear Hoffman-Weeks extrapolation) leads to an apparent equilibrium melting temperature that is about 10°C lower than the non-linear counterpart.

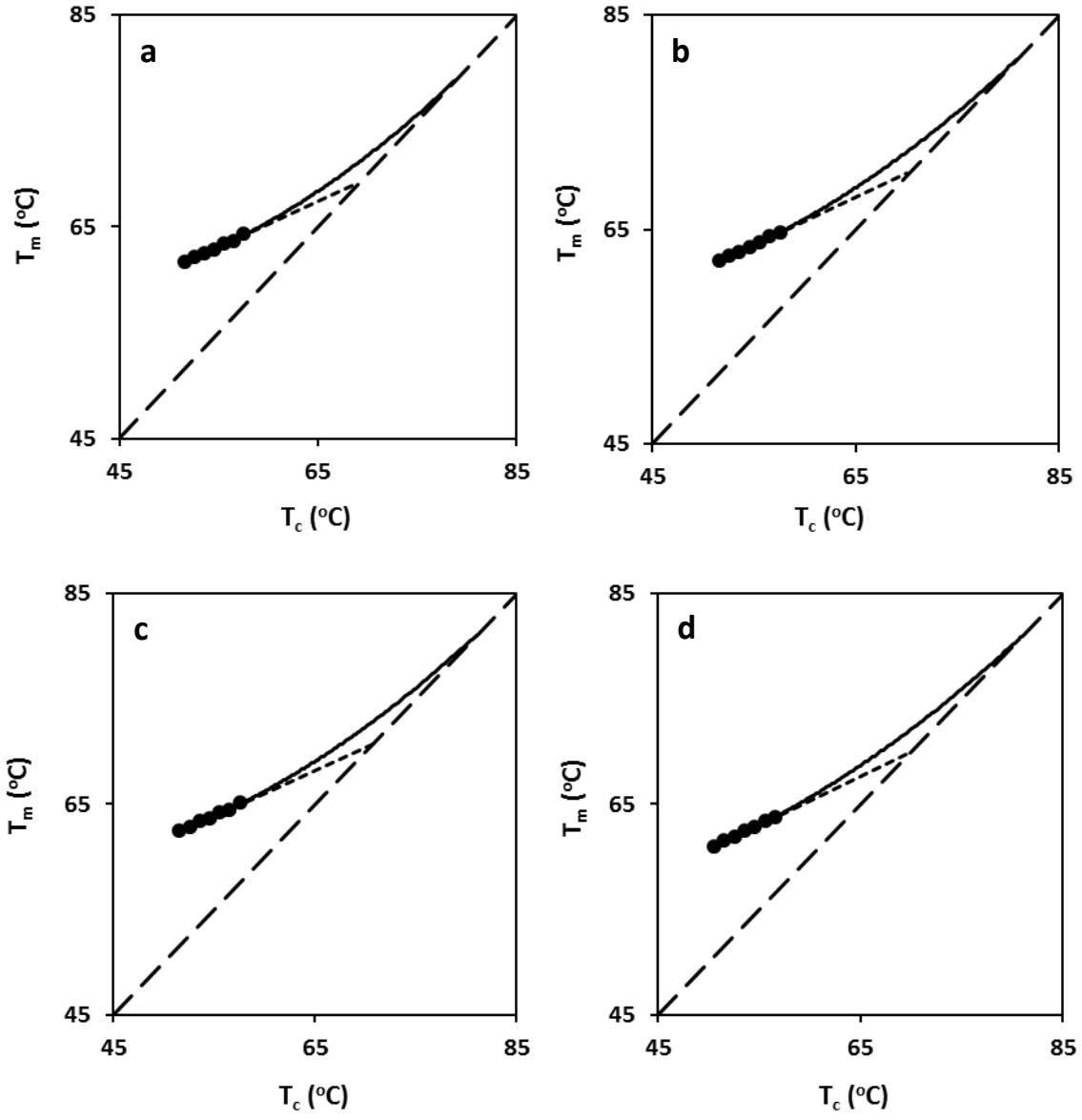

Figure 6.4. T_m *vs.* T_c for (a) PEO 34K, (b) PEO 70K, (c) PEO 100K and (d) PEO 232K. The short-dash line and the solid line are the linear Hoffman-Weeks and the non-linear Hoffman-Weeks extrapolations, respectively. The long-dash line is the $T_m = T_c$ line.

To obtain the chain length dependence of equilibrium melting temperature of PEO, the values estimated in this work as well as those reported by Afifi-Effat and Hay,[2] Buckley and Kovacs,[22-23] Qiu et al.,[45] and Kovacs and Straupe[46] for the melting of low molecular weight (M_n< 2 kg/mol) extended chain crystals were fitted to a Huggins equation, Figure 6.5.[33]

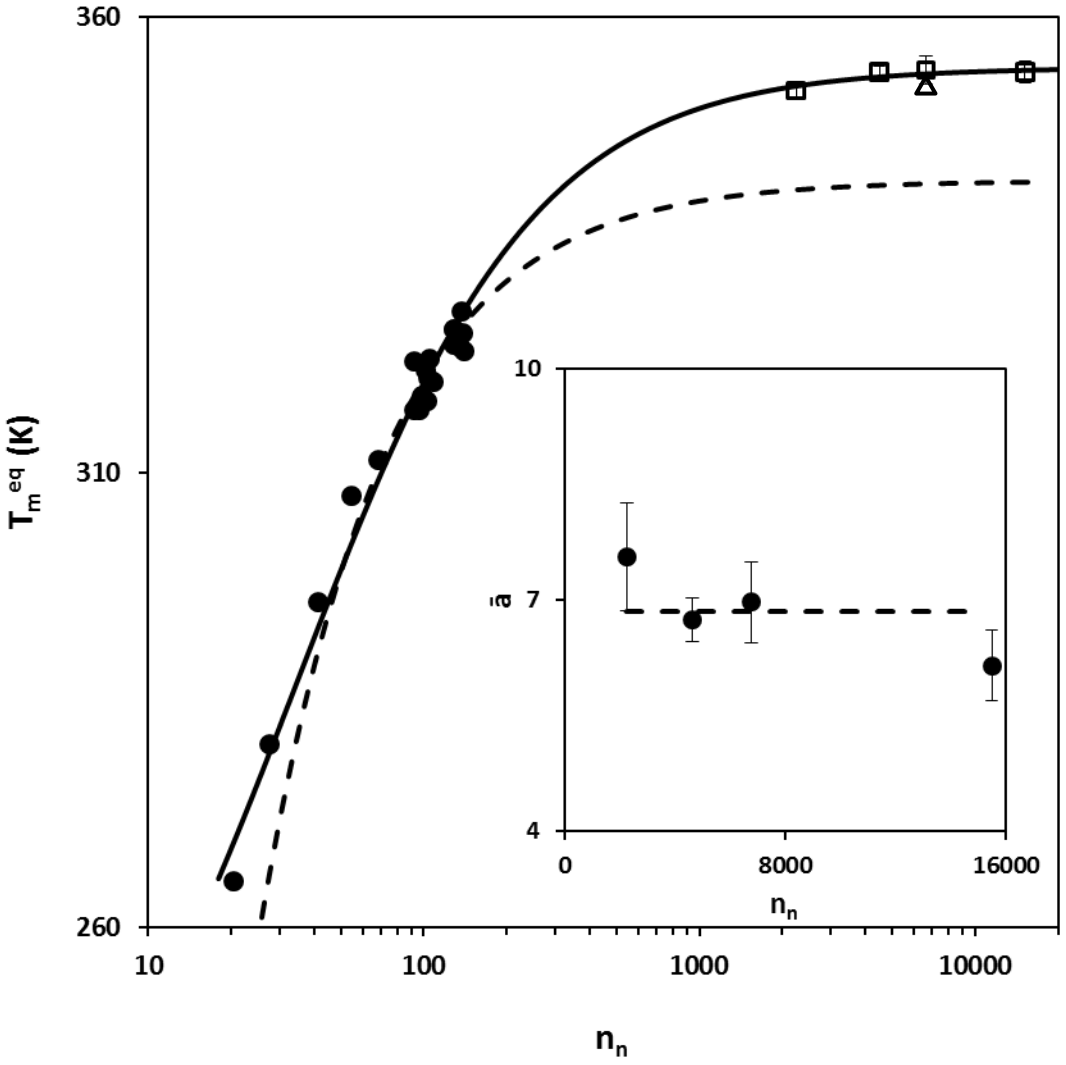

Figure 6.5. Equilibrium melting temperature *vs.* n_n, the number average number of backbone carbon atoms per chain. Data from melting of extended chain crystals reported by: Afifi-Effat and Hay,[2] Buckley and Kovacs,[22-23] Qiu et al.,[45] and Kovacs and Straupe[46] (•), the Gibbs-Thomson Plot[47] (Δ), and the present work using the non-linear Hoffman-Weeks approach (□). The solid line shows the best fit to the experimental results with a Huggins equation while the dash line represents the prediction from the Buckley-Kovacs equation.[22-23] The error bars correspond to one standard deviation.
The inset shows $\bar{a}$ *vs.* n_n.

This plot also includes the equilibrium melting temperature of a PEO fraction with number average molecular weight of 100 kg/mol determined from a Gibbs-Thomson plot.[47] Equation 6.6 shows the parameters associated to the best Huggins fit to the data:

$$T_m^{eq} = 354.5\ K \left(\frac{n_n + 21.0}{n_n + 34.1}\right) \tag{6.6}$$

where n_n is the number average number of bonds per chain. The equilibrium melting temperature of an infinitely long poly(ethylene oxide) chain is 81.4 ± 1.0°C, 12.5°C higher than that estimated by Buckley and Kovacs.[22-23] In contrast with the relationship found for linear polyethylene,[29] both constants in the numerator and the denominator of Equation 6.6 are positive. As the constant in the numerator is related to the melting of chain ends, Buckley and Kovacs attributed this positive value to hydrogen bonding of the hydroxy terminated chains.[22-23]

6.4.2. Analysis of the Spherulite Growth Rates for Poly(ethylene oxide)

The average number of bonds per chain, n, was calculated by Equation 6.7 for each fraction used in the isothermal spherulite growth rate analysis (Table 6.1).

$$n = \sqrt{n_n \times n_w} \tag{6.7}$$

where n_w is the weight average number of bonds per chain. Figure 6.6 shows the isothermal spherulite growth rate *vs.* crystallization temperature data for the PEO fractions studied here.[42] The spherulite growth rate data are analyzed by the modified LH theory (see Appendix D) for T_c > 51°C, as the crystal growth front of PEO lamellae changes from the (210) plane to the (010) plane at crystallization temperatures around 51°C.[25, 43] All thermodynamic, crystallographic and other constants necessary for the analysis of spherulite growth rate data of PEO are given in Table 6.2.

Table 6.1. Molecular characteristics of the poly(ethylene oxide) fractions used in this study.

Sample	M_w (g/mol)	M_w/M_n	n
PEO 21K	21000	1.08	1380
PEO 34K	33600	1.02	2300
PEO 44K	43500	1.1	2830
PEO 70K	70000	1.06	4910
PEO 75K	74900	1.03	5030
PEO 100K	101200	1.04	7250
PEO 113K	113200	1.13	8200
PEO 157K	157000	1.09	10240
PEO 232K	231600	1.04	16090

Table 6.2. Constants used for the analysis of spherulite growth rate data of poly(ethylene oxide).

a_o	4.62×10^{-8} cm [25, 48]	Q_d^*	17 kJ/mol [6, 49]
b_o	4.62×10^{-8} cm [25, 48]	R	8.3145 J/mol
ℓ_b	1.46×10^{-8} cm [48]	k	1.3806×10^{-23} J/K
ℓ_u	0.93×10^{-8} cm [48, 50]	C_∞	5.7 at 80°C [51]
ΔH	231 J/cm^3 [24]	ζ	-0.3×10^{-3} °C^{-1} [52]

The crystal growth regimes of poly(ethylene oxide) were determined by plotting $\ln G + \frac{Q_d^*}{RT_c} - \ln\psi(T_c) - \Sigma(T_c)[1-\chi(T_c)]$ and $\ln G + \frac{Q_d^*}{RT_c} - \ln\varphi(T_c) - \frac{\Sigma(T_c)}{2}[1-\chi(T_c)]$ *vs.* $\exp(\zeta\Delta T)\left[\frac{1}{\Delta T} + \frac{\bar{a}}{T_m^{eq}}\right][1-\chi(T_c)]$, Equations 6.8 and 6.9 (Equations D.3 and D.4 in the Appendix).

$$\ln G_I + \frac{Q_d^*}{RT_c} - \ln\psi(T_c) - \Sigma(T_c)[1-\chi(T_c)] = \ln G_{oI} - K_{gI}^o\exp(\zeta\Delta T)\left[\frac{1}{\Delta T} + \frac{\bar{a}}{T_m^{eq}}\right][1-\chi(T_c)] \qquad (6.8)$$

$$\ln G_{II} + \frac{Q_d^*}{RT_c} - \ln\varphi(T_c) - \frac{\Sigma(T_c)}{2}[1-\chi(T_c)] = \ln G_{oII} - K_{gII}^o\exp(\zeta\Delta T)\left[\frac{1}{\Delta T} + \frac{\bar{a}}{T_m^{eq}}\right][1-\chi(T_c)] \qquad (6.9)$$

The regime I/II transition temperature is determined from the point where the slope of these plots alters significantly. The values of $T_{I\rightarrow II}$ found by the analysis of the spherulite growth rate data are very close to these estimated by Allen et al.[5] from calorimetric data.

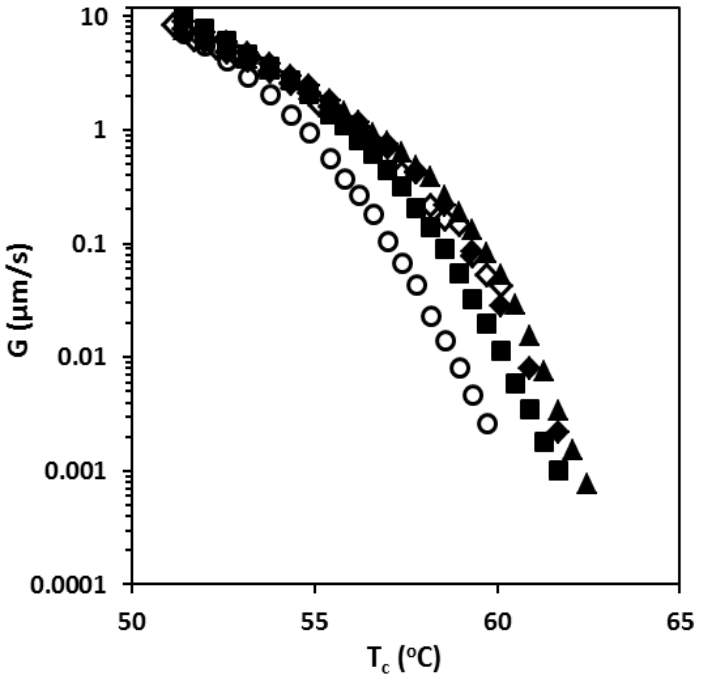

Figure 6.6. Spherulite growth rate *vs.* crystallization temperature for PEO fractions: PEO 21K (○), PEO 44K (■), PEO 75K (♦), PEO 113K (◊) and PEO 157K (▲).

Figure 6.7 illustrates the chain length dependence of the undercooling at the I/II regime transition, $\Delta T_{I\rightarrow II}$. As for linear polyethylene,[29] the undercooling at the I/II regime transition of poly(ethylene oxide) shows no dependence on chain length ($\Delta T_{I\rightarrow II}^{avg}$ = 23.0 ± 0.4°C). After finding the undercooling limits associated with regimes I and II, we can evaluate the chain length dependence of spherulite growth rate for each regime. Figure 6.8a shows a plot of G *vs.* n at ΔT = 23.6°C in regime II. The dependence of the spherulite growth rate on chain length exhibits a power law behavior with an exponent of -0.54 ± 0.05. Figure 6.8b illustrates the changes in - s the power law exponent in $G \propto n^{-s}$ with undercooling. Within experimental uncertainty the chain length dependence of G is almost the same in both regimes I and II. The

average power law exponent found here (-0.38 ± 0.06) is much smaller than that reported for LPE.[29]

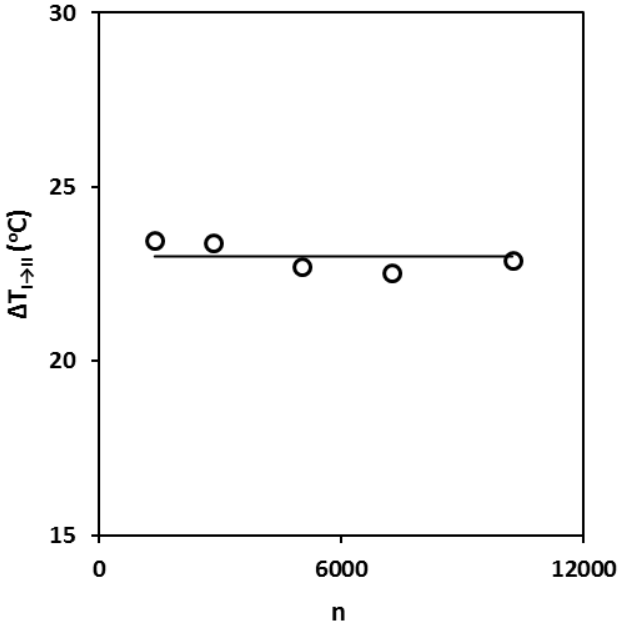

Figure 6.7. $\Delta T_{I\to II}$ *vs.* n. The solid line represents the average $\Delta T_{I\to II}$ = 23.0 ± 0.4°C.

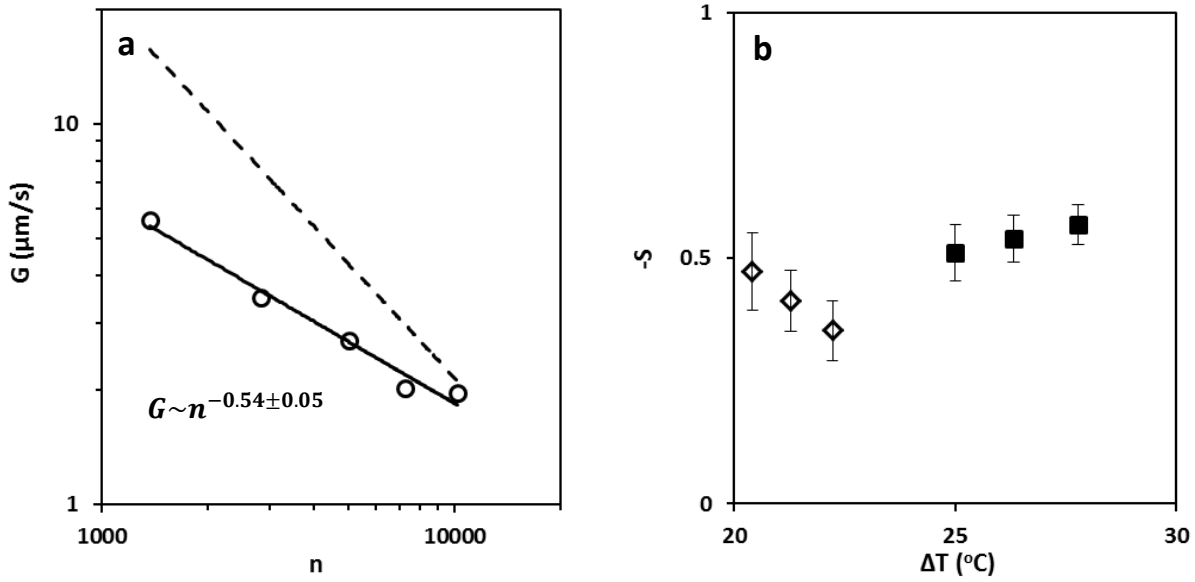

Figure 6.8. (a) G *vs.* n at ΔT = 23.6°C, in regime II. The solid line represents the best fit to the data. The dashed line is a power law behavior with exponent of -1. (b) Power law exponent for the dependence of G on n in regime I (◊) and regime II (■). Error bars correspond to one standard deviation.

The values of K_g^o and σ_{ec}^o for each fraction in regimes I and II are determined using Equations D.3 to D.10, Figure 6.9. The ratio K_{gI}^o/K_{gII}^o is equal to 2.06 ± 0.15, in agreement with theoretical predictions.[16, 20, 34]

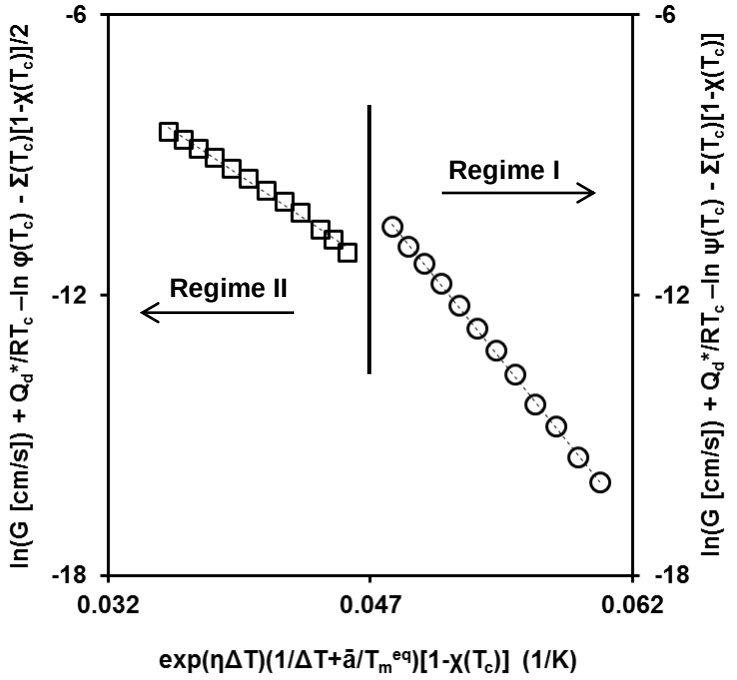

Figure 6.9. $\ln G + \frac{Q_d^*}{RT_c} - \ln \psi(T_c) - \Sigma(T_c)[1-\chi(T_c)]$ and $\ln G + \frac{Q_d^*}{RT_c} - \ln \varphi(T_c) - \frac{\Sigma(T_c)}{2}[1-\chi(T_c)]$ *vs.* $\exp(\zeta \Delta T)\left[\frac{1}{\Delta T} + \frac{\bar{a}}{T_m^{eq}}\right][1-\chi(T_c)]$ for PEO 44K. The dashed lines represent the best fit to the data in regime I (○) and regime II (□). The solid line shows the transition between regimes I and II.

Figure 6.10a shows the changes of the equilibrium fold surface free energy with chain length. Values of σ_{ec}^o in regimes I and II are randomly scattered about their average $\sigma_{ec,I}^o$ = 55.0 ± 3.0 erg/cm^2 and $\sigma_{ec,II}^o$ = 53.4 ± 2.4 erg/cm^2. The average value of σ_{ec}^o in regimes I and II for the PEO fractions with M_n values ranging from 34 to 232 kg/mol is 54.2 ± 2.7 erg/cm^2 is independent of chain length. A Gibbs-Thomson analysis of Schönherr and Frank's data[47] for a PEO fraction with number average molecular weight of 100 kg/mol yields σ_{em} = 49.8 ± 1.4 erg/cm^2. Within the limits of experimental error, all values reported here for σ_{ec}^o and σ_{em} for melt

crystallized PEO fractions are almost identical. In the range of chain lengths considered here, we also find that the strength of stem length fluctuations, y = 0.016 $^{o}C^{-1}$, is independent of chain length. The power law dependence of G_o on chain length ($G_o \sim n^{-t}$) for PEO fractions in regimes I and II is also shown in Figure 6.10b. The power law exponents in regime I and II are -0.35 ± 0.05 and -0.55 ± 0.04, respectively.

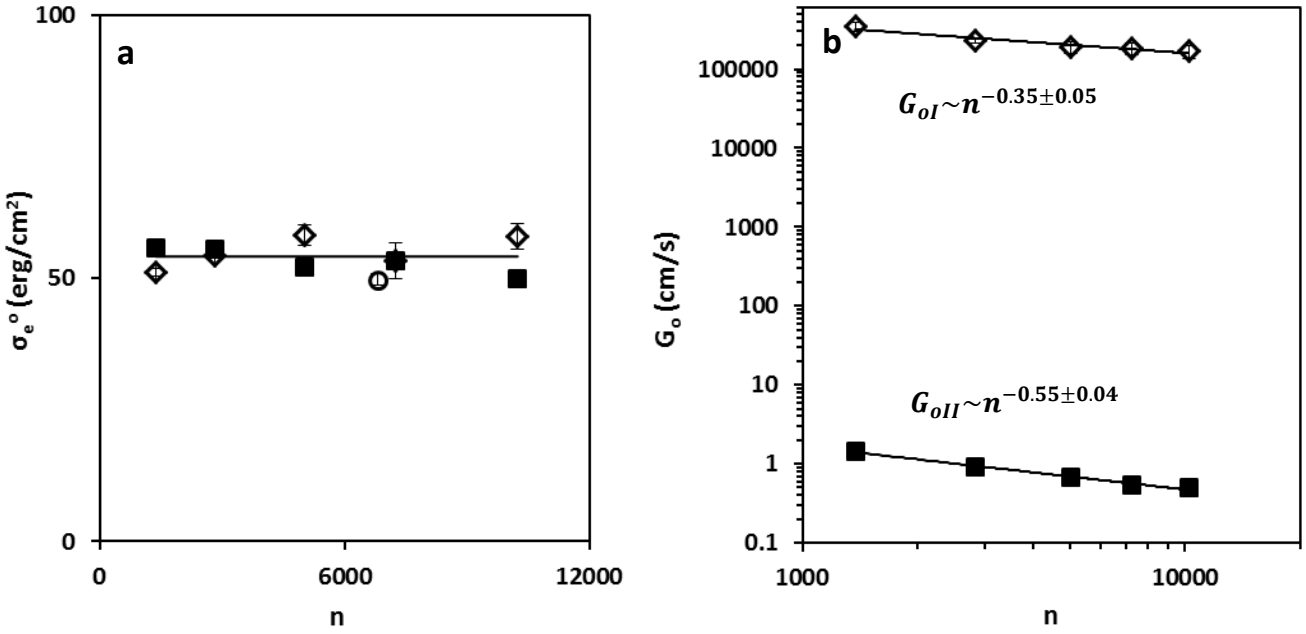

Figure 6.10. (a) σ_{ec}^{o} *vs.* n from spherulite growth of PEO fractions in regime I (◊) and in regime II (■) and from a Gibbs-Thomson analysis (○).[47] The solid line shows the average value σ_{ec}^{o} = 54.2 ± 2.7 erg/cm^2. Error bars correspond to one standard deviation. (b) G_o *vs.* n for regime I (◊) and regime II (■). The solid lines represent the best fit to the data.

Figure 6.11a shows the WAXD pattern for the PEO 34K fraction crystallized isothermally at 55.8^{o}C (regime I/II transition temperature) in the range of 2θ of 16 to 20^{o}. In this range of diffraction angles, PEO exhibits diffraction peaks for the (120), (111) and (013) crystal planes.[53-54] After deconvolution of these peaks, the (120) substrate length was estimated from the integral breadth of the (120) diffraction peak. In the given range of molecular weights, the (120) substrate length at the regime I/II transition temperature, $L_{(120)}$, was independent of chain

length ($L_{(120)}$= 350 ± 20 Å), Figure 6.11b. A similar behavior was observed for linear polyethylene.[16] The width of the critical nucleus, defined by $L_s = \nu_s a_o$, is the minimum size necessary for a nucleus to reach the zone of thermodynamic stability (Appendix D).[16, 20, 34] L_s and $L_{(120)}$ are plotted as a function of chain length in Figure 6.11b. The width of the critical nucleus is smaller than the measured (120) substrate length, satisfying an important criterion for any realistic model of crystal growth.

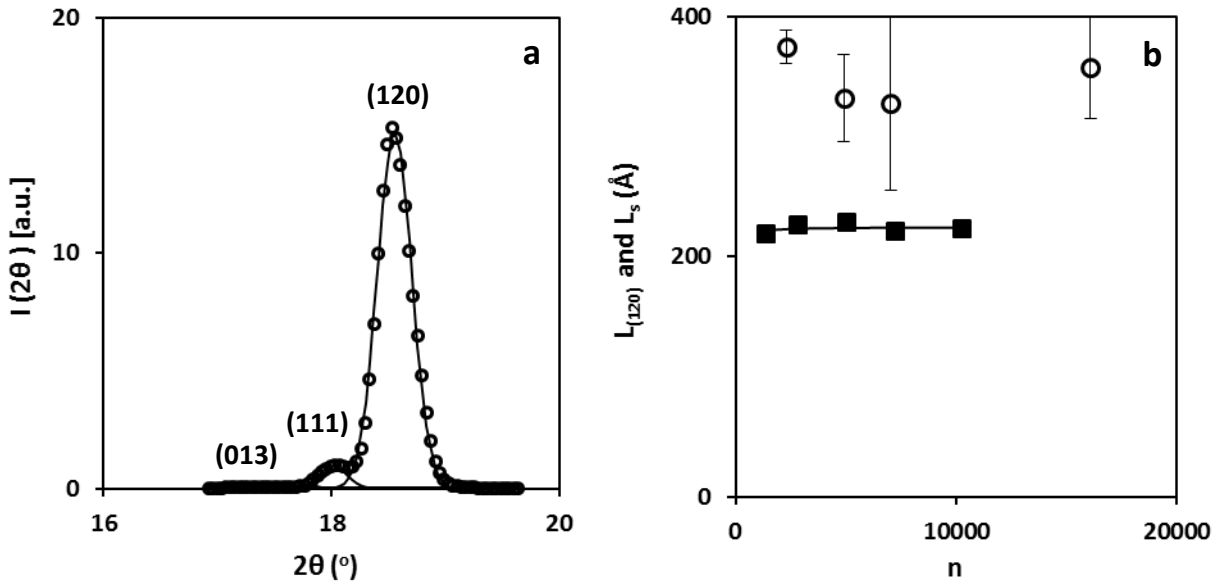

Figure 6.11. (a) Diffracted intensity *vs.* 2θ for PEO 34K crystallized isothermally at 55.8°C. The solid lines show the deconvoluted diffraction peaks. (b) $L_{(120)}$ (○) and L_s (■) *vs.* n at the regime I/II transition temperature. The solid line is the best fit to the L_s *vs.* n data. Error bars correspond to the standard deviation on triplicate measurements.

Given the quantities of $L_{(120)}$, σ_{ec}^{o}, G_{oI}, and G_{oII} at the regime I to II transition temperature, we determine C_o, the configurational path degeneracy, and ξ_c^o, the apparent chain friction coefficient during crystallization normalized to a reference temperature of T_o = 100°C (Appendix D). The values of configurational path degeneracy obtained by this method are about an order of magnitude higher than these determined for linear polyethylene at its regime I/II transition

temperature.[16] Different power law dependences of G_{oI} and G_{oII} on chain length leads to a chain-length dependent configurational path degeneracy ($C_o \sim n^{0.39\pm0.08}$), Figure 6.12. As the chain length increases, the number of possible paths for crystallization increase. ξ_c^o, the apparent friction coefficient during crystallization normalized to a reference temperature of T_o = 100°C is plotted as a function of chain length in Figure 6.13.

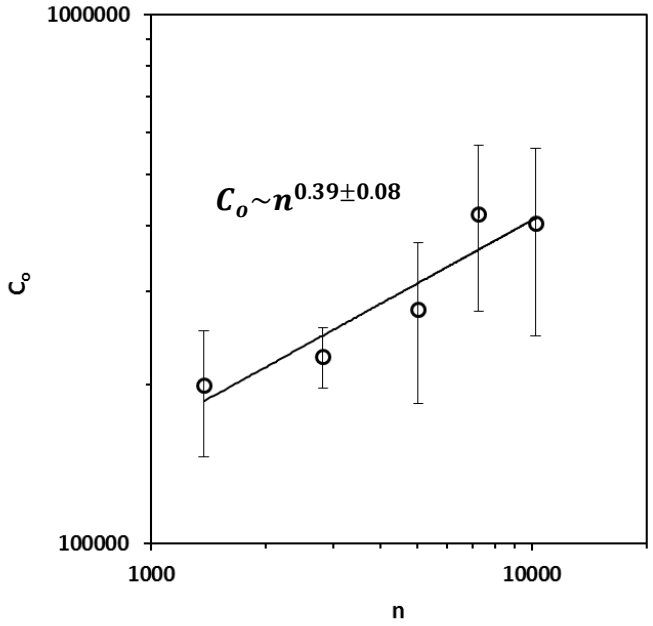

Figure 6.12. *C_o vs. n* at the regime I/II transition. The solid line represents the best fit to the data.

ξ^o, the friction coefficient associated with chain reptation in a pure melt accounting for constraint release and contour length fluctuations at the reference temperature of T_o = 100°C is also depicted in Figure 6.13.[16] Values of ξ^o were calculated using experimental values for the center of mass diffusion coefficient of poly(ethylene oxide) reported in the literature at 100°C.[6, 49, 55] The values of ξ^o calculated here are in agreement with the values obtained by Niedzwiedz et al.[56] from rheology and neutron spin-echo experiments. The center of mass diffusion coefficient of PEO exhibits a power law dependence on chain length, where the power exponent is -2.34 ± 0.07.[6, 49, 55] This leads to a relationship of $\xi^o \sim n^{1.34}$, similar to the power law

relationship observed for linear polyethylene.[16] Unlike LPE, however, the values of ξ_c^o are much smaller (about 20 to 60 times) than ξ^o. The apparent friction coefficient during crystallization also exhibits a power law dependence on chain length, $\xi_c^o \sim n^{0.74\pm0.06}$, where the power law exponent is much lower than for LPE (0.7 *vs.* 1.7).[16]

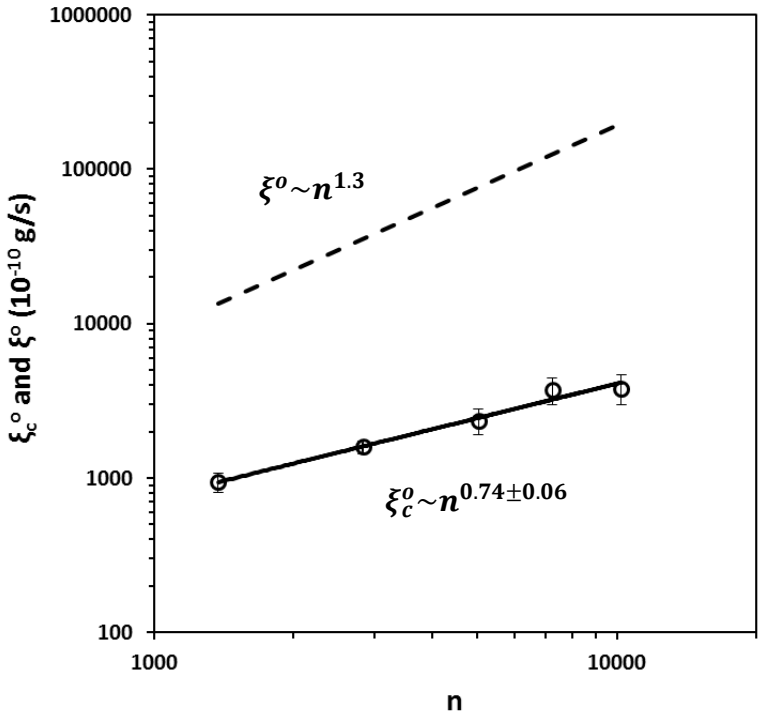

Figure 6.13. Apparent chain friction coefficient for PEO during crystallization (○) and curvilinear chain friction coefficient in the melt (- - -) at the reference temperature of 100°C. The solid line is the best fit to the apparent chain friction coefficient of PEO during crystallization.

To understand the nature of PEO's apparent friction coefficient during crystallization, we compare the spherulite growth rates of two pairs of LPE and PEO fractions with similar average number of bonds per chain, Figure 6.14. At low undercooling (regime I), the spherulite growth rate of LPE is significantly larger than that of PEO, while the difference between the spherulite growth rates decreases with increasing undercooling. Table 6.3 shows the values of different parameters defined in the LH theory controlling the spherulite growth rate (Equation D.3) of LPE and PEO at ΔT = 10°C in regime I.

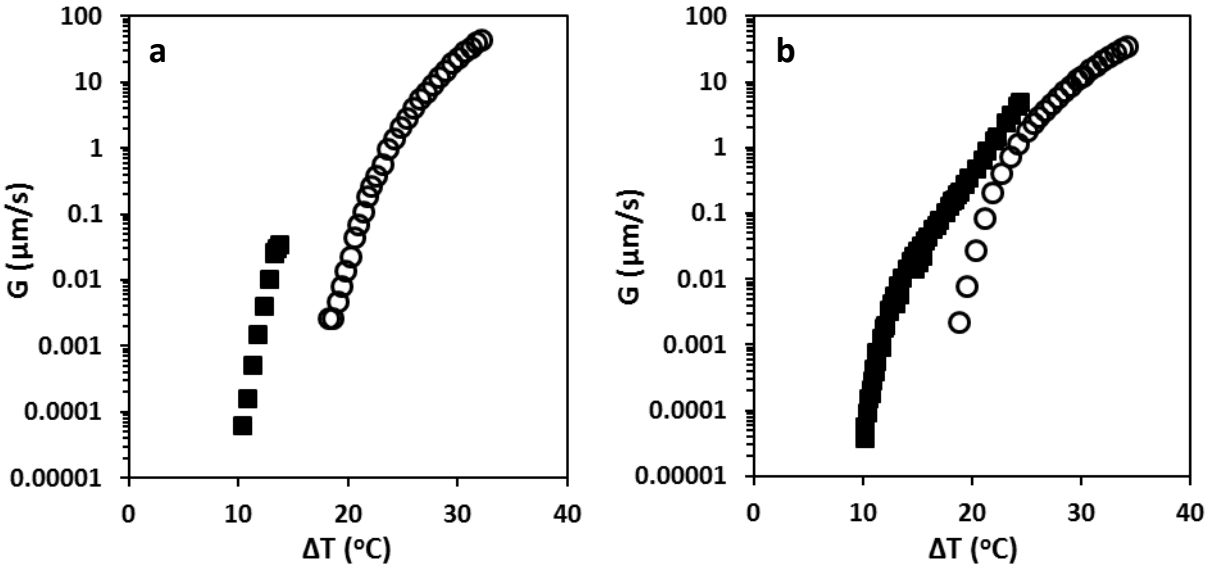

Figure 6.14. Spherulite growth rate *vs.* undercooling for LPE (■) and PEO (○) fractions with average number of bonds per chain of: (a) 1380 and (b) 5030.[38, 57]

Table 6.3. Parameters defined in the LH theory controlling spherulite growth rate of LPE and PEO at ΔT = 10°C (regime I).[29]

n = 1380 at ΔT = 10°C						
Sample	$\psi(T_c)$ ($K^3s^2g^{-1}$)	$\Sigma(T_c)$	$\chi(T_c)$	$\left[\frac{1}{\Delta T}+\frac{\bar{a}}{T_m^{eq}}\right]$ (K^{-1})	G_{oI} (10^6 cm/s)	K_{gI}^o (K)
LPE	21.1	1.87	0.15	0.14	0.013	200
PEO	21.6	1.90	0.11	0.12	3.43	460
n = 5030 at ΔT = 10°C						
Sample	$\psi(T_c)$ ($K^3s^2g^{-1}$)	$\Sigma(T_c)$	$\chi(T_c)$	$\left[\frac{1}{\Delta T}+\frac{\bar{a}}{T_m^{eq}}\right]$ (K^{-1})	G_{oI} (10^6 cm/s)	K_{gI}^o (K)
LPE	21.1	1.87	0.15	0.14	0.022	200
PEO	21.6	1.90	0.11	0.12	1.90	460

In the range of molecular weights studied, values of $\psi(T_c)$, $\Sigma(T_c)$, $\chi(T_c)$, and $\left[\frac{1}{\Delta T}+\frac{\bar{a}}{T_m^{eq}}\right]$ are independent of chain length and are almost identical for LPE and PEO. The larger spherulite growth rates for LPE than for PEO are therefore related to the higher secondary nucleation constant of PEO ($K_g^o(PEO)/K_g^o(PE)$ ~ 2.3), which leads to a lower rate of secondary nucleation.

On the other hand, the larger G_o values for poly(ethylene oxide) lead to smaller differences between the spherulite growth rates at higher undercooling where the effects of secondary nucleation on the ratio of the spherulite growth rates decreases. Our calculations related PEO's large G_o value to low apparent friction coefficients. However, any coupling between lamellar thickening and crystal growth is ignored in the LH theory. Polymers with high α_c-relaxation rates adjust for lamellar thickening during crystal growth, which lead to additional forces on the chains during crystallization. As a result, by not considering the contribution of these forces on transfer of the segments through the melt-crystal interface, we underestimate the value of the apparent friction coefficient during crystallization. Such underestimation may also influence the chain length dependence of ξ_c^o.

6.5. Conclusions

The melting behavior of four poly(ethylene oxide) fractions with weight-average molecular weights of 34, 70, 100, and 232 kg/mol is studied as a function of crystallization time and temperature by conventional calorimetry. The initial melting temperatures of non-thickened lamellae formed under isothermal conditions over a range of crystallization temperatures are used in the context of the non-linear Hoffman-Weeks method to determine the equilibrium melting temperature. T_m^{eq} values of 78.8 ± 1.0, 80.8 ± 0.6, 81.0 ± 1.5, and 80.8 ± 1.2^{o}C for PEO 34K, 70K, 100K, and 232K, respectively. Fitting the dependence of equilibrium melting temperature on chain length to a Huggins equation leads to a limiting equilibrium melting temperature of 81.4 ± 1.0^{o}C for an infinitely long poly(ethylene oxide) chain. Spherulite growth rate data of five narrow molecular weight poly(ethylene oxide) fractions with weight average molecular weights of 21, 44, 75, 113, and 157 kg/mol are analyzed at low to moderate undercoolings using the modified LH theory. The regime I to II transition occurs at an undercooling $\Delta T_{I\rightarrow II}$ = 23.0 ± 0.4^{o}C independent of chain length. In both regimes, G is

proportional to $n^{-0.4}$. The value of σ_{ec}^{o} is equal to 54.2 ± 2.7 erg/cm^2 and independent of chain length. The ratio of K_{gI}^{o}/K_{gII}^{o} is equal to 2.06 ± 0.15, matching the LH model's prediction. G_{oI} and G_{oII} exhibit different dependencies on chain length (i.e. $G_{oI} \propto n^{-0.35\pm0.05}$ and $G_{oII} \propto n^{-0.55\pm0.04}$). Combination of the non-linear Hoffman-Weeks and spherulite growth rate analyses leads to a value y of 0.016 $^{o}C^{-1}$ at $\Delta T_{I\rightarrow II}$, independent of chain length. The substrate length for PEO 34K, 70K, 100K, and 232K fractions were measured at their $\Delta T_{I\rightarrow II}$ using WAXD. The length of the (120) growth fronts were independent of molecular weight. The apparent friction coefficient and configurational path degeneracy of a crystallizing poly(ethylene oxide) chain were proportional to $n^{0.74\pm0.06}$ and $n^{0.39\pm0.08}$, respectively. The magnitude of the apparent chain friction coefficient during crystal growth is significantly lower for PEO than for LPE, possibly the result of a much more active α_c-relaxation for the former polymer. Observation of significantly larger spherulitic growth rates for LPE than for PEO at low undercooling is explained by the higher secondary nucleation constant for PEO than for LPE ($K_g^o(PEO)/K_g^o(PE)$ ~ 2.3). The difference in spherulitic growth rates between PEO and LPE at high undercooling is smaller due to the lower apparent friction coefficient of PEO.

6.6. Acknowledgments

This research was partially funded by the National Science Foundation (DMR-0706210). This work was also supported by a grant from the Petroleum Research Funds administered by the American Chemical Society. Furthermore, the authors would like to thank TA Instruments for the temporary loan of a Q2000 differential scanning calorimeter.

6.7. Appendix D: Modification of the LH Theory

The modified LH theory was initially developed for the analysis of the lamellar thickness and spherulite growth rate data of linear polyethylene.[29] In the modified LH theory, the fold surface free energy during crystallization at low to intermediate undercooling is assumed to be a linear function of undercooling, Equation D.1.[35]

$$\sigma_{ec} = \sigma_{ec}^{o}(1 + y\Delta T) \tag{D.1}$$

Here, σ_{ec}^{o} and y are the equilibrium fold surface free energy during crystallization and the strength of stem length fluctuations, respectively.[35] The lateral surface free energy is also regarded as a function of crystallization temperature, Equation A.2.[36]

$$\sigma = \frac{T_c \exp(\zeta \Delta T)}{T_m^{eq}} \sigma^{o} \tag{D.2}$$

where σ^{o} is the lateral surface free energy at the equilibrium melting temperature, $\sigma^{o} = \left(\frac{\Delta H a_o}{2}\right)\left(\frac{\ell_b}{\ell_u}\right)\frac{1}{C_{\infty,T_m^{eq}}}$.[16] Here, ΔH, a_o, ℓ_u, ℓ_b, and $C_{\infty,T_m^{eq}}$ are the volumetric heat of fusion, the crystallized stem width, the average bond length, the average bond length projected along the c-axis, and the limiting characteristic ratio at the equilibrium melting temperature, respectively. ζ, is a constant providing access to the undercooling dependence of the chain dimensions (Equation D.2). Using the modified LH theory, we can relate the spherulite growth rate, G, of isothermally crystallized PEO at regime I (Equation D.3) and regime II (Equation D.4) to the crystallization temperature and the equilibrium fold surface free energy during crystal growth, σ_{ec}^{o}.[16]

$$\ln G_I + \frac{Q_d^*}{RT_c} - \ln \psi(T_c) - \Sigma(T_c)[1 - \chi(T_c)] = \ln G_{oI} - K_{gI}^{o} \exp(\zeta \Delta T)\left[\frac{1}{\Delta T} + \frac{\bar{a}}{T_m^{eq}}\right][1 - \chi(T_c)] \tag{D.3}$$

$$\ln G_{II} + \frac{Q_d^*}{RT_c} - \ln \varphi(T_c) - \frac{\Sigma(T_c)}{2}[1 - \chi(T_c)] = \ln G_{oII} - K_{gII}^o \exp(\zeta \Delta T)\left[\frac{1}{\Delta T} + \frac{\bar{a}}{T_m^{eq}}\right][1 - \chi(T_c)] \quad \text{(D.4)}$$

where

$$\psi(T_c) = \left[\frac{T_c \Delta T \exp(-\zeta \Delta T)}{2\sigma^o T_c \exp(\zeta \Delta T) + a_o \Delta H \Delta T}\right]\left[\frac{1}{\Delta T} + \frac{\bar{a}}{T_m^{eq}}\right]^{-2} \quad \text{(D.5)}$$

$$\varphi(T_c) = \psi(T_c)\sqrt{\frac{4\sigma^o T_c \exp(\zeta \Delta T) + a_o \Delta H \Delta T}{T_c}} \quad \text{(D.6)}$$

$$\Sigma(T_c) = \left[\frac{a_o \Delta H \Delta T + 4\sigma^o T_c \exp(\zeta \Delta T)}{a_o \Delta H \Delta T + 2\sigma^o T_c \exp(\zeta \Delta T)}\right] \quad \text{(D.7)}$$

$$\chi(T_c) = \frac{a_o \Delta H \Delta T}{2\sigma^o T_c \exp(\zeta \Delta T)} \quad \text{(D.8)}$$

$$K_{gI}^o = \frac{4 b_o \sigma^o \sigma_{ec}^o}{k \Delta H} \quad \text{(D.9)}$$

$$K_{gII}^o = \frac{2 b_o \sigma^o \sigma_{ec}^o}{k \Delta H} \quad \text{(D.10)}$$

Q_d^*, R, a_o, b_o, k and ΔH are the activation energy for center-of-mass diffusion, the universal gas constant, the width and thickness of a crystallized stem, Boltzmann's constant and the volumetric enthalpy of fusion of the copolymer, respectively. G_{oI} and G_{oII} are the spherulite growth rate constants in regime I and II, respectively. $\bar{a}$ is the constant in the non-linear Hoffman-Weeks equation, which is related to y by:[16, 29-30]

$$y = \frac{\bar{a}}{T_m^{eq}} - \frac{k \Delta H \cos\theta \exp(-\zeta \Delta T)}{4 b_o \sigma^o \sigma_{ec}^o}\left[\frac{a_o \Delta H \Delta T + 4\sigma^o T_c \exp(\zeta \Delta T)}{a_o \Delta H \Delta T + 2\sigma^o T_c \exp(\zeta \Delta T)}\right] \quad \text{(D.11)}$$

The configurational path degeneracy, C_o, and the apparent friction coefficient for the crystallizing chain at the regimes I/II transition temperature, ξ_c, can be calculated from Equations D.12 and D.13.[16]

$$C_o = \frac{2\ell_u b_o}{k{n_L}^2 T_m^{eq}}\left(\frac{G_{oI}}{G_{oII}}\right)^2 \tag{D.12}$$

$$\xi_c = \frac{k a_o b_o \Delta H^3}{4 n_L \sigma^o {\sigma_{ec}^o}^2 T_m^{eq2}}\left(\frac{G_{oI}}{{G_{oII}}^2}\right)\exp\left(\frac{Q_d^*}{RT_c}\right) \tag{D.13}$$

Here, n_L is the number of stems per substrate length. For each PEO fraction, ξ_c is normalized to a reference temperature of T_o = 100°C by:[6, 49, 58]

$$\xi_c = \xi_c^o \exp\left(\frac{Q_d^*}{RT_c}\right)\exp\left(-\frac{Q_d^*}{RT_o}\right) \tag{D.14}$$

where ξ_c^o is the apparent chain friction coefficient at the reference temperature. The minimum number of stems necessary for a secondary surface embryo to become a stable nucleus, ν_s, is also written as:[16]

$$\nu_s = \frac{4\sigma\sigma_{ec}T_m^{eq2}}{a_o\delta\Delta H^2\Delta T^2} - \frac{2T_m^{eq}}{\Delta H\Delta T}\left[\frac{\sigma_{ec}}{\delta} - \frac{\sigma}{a_o}\right] \tag{D.15}$$

where[16]

$$\delta = \frac{kT_m^{eq}\exp(-\zeta\Delta T)}{2b_o\sigma^o}\left[\frac{a_o\Delta H\Delta T + 4\sigma^o T_c\exp(\zeta\Delta T)}{a_o\Delta H\Delta T + 2\sigma^o T_c\exp(\zeta\Delta T)}\right] \tag{D.16}$$

6.8. References

1. Kovacs, A.; Gonthier, A., Crystallization and fusion of self-seeded polymers. *Kolloid-Zeitschrift und Zeitschrift für Polymere* **1972,** *250* (5), 530-552.
2. Afifi-Effat, A.; Hay, J., Enthalpy and entropy of fusion and the equilibrium melting point of polyethylene oxide. *Journal of the Chemical Society, Faraday Transactions 2: Molecular and Chemical Physics* **1972,** *68*, 656-661.
3. Zardalidis, G.; Mars, J.; Allgaier, J.; Mezger, M.; Richter, D.; Floudas, G., Influence of chain topology on polymer crystallization: poly (ethylene oxide)(PEO) rings vs. linear chains. *Soft matter* **2016,** *12* (39), 8124-8134.
4. Cheng, S. Z.; Chen, J.; Janimak, J. J., Crystal growth of intermediate-molecular-mass poly (ethylene oxide) fractions from the melt. *Polymer* **1990,** *31* (6), 1018-1024.
5. Allen, R. C.; Mandelkern, L., On regimes I and II during polymer crystallization. *Polymer Bulletin* **1987,** *17* (5), 473-480.
6. Cheng, S. Z.; Barley, J. S.; Von Meerwall, E. D., Self-diffusion of poly (ethylene oxide) fractions and its influence on the crystalline texture. *Journal of Polymer Science Part B: Polymer Physics* **1991,** *29* (5), 515-525.
7. Hu, W. G.; Schmidt-Rohr, K., Polymer ultradrawability: the crucial role of α-relaxation chain mobility in the crystallites. *Acta Polymerica* **1999,** *50* (8), 271-285.
8. Schmidt-Rohr, K.; Schmidt-Rohr, K.; Spiess, H. W., *Multidimensional solid-state NMR and polymers*. Academic Press: 1994.
9. Kim, B. S.; Porter, R. S., Uniaxial draw of poly (ethylene oxide) by solid-state extrusion. *Macromolecules* **1985,** *18* (6), 1214-1217.
10. Johansson, A.; Tegenfeldt, J., NMR study of crystalline and amorphous poly (ethylene oxide). *Macromolecules* **1992,** *25* (18), 4712-4715.

11. Mansfield, M.; Boyd, R. H., Molecular motions, the α relaxation, and chain transport in polyethylene crystals. *Journal of Polymer Science Part B: Polymer Physics* **1978,** *16* (7), 1227-1252.
12. Hu, W.-G.; Boeffel, C.; Schmidt-Rohr, K., Chain flips in polyethylene crystallites and fibers characterized by dipolar 13C NMR. *Macromolecules* **1999,** *32* (5), 1611-1619.
13. Cooke, J.; Viras, K.; Yu, G.-E.; Sun, T.; Yonemitsu, T.; Ryan, A. J.; Price, C.; Booth, C., Large cyclic poly (oxyethylene) s: chain folding in the crystalline state studied by Raman spectroscopy, X-ray scattering, and differential scanning calorimetry. *Macromolecules* **1998,** *31* (9), 3030-3039.
14. Cheng, S. Z.; Chen, J.; Barley, J. S.; Zhang, A.; Habenschuss, A.; Zschack, P. R., Isothermal thickening and thinning processes in low molecular-weight poly (ethylene oxide) fractions crystallized from the melt. 3. Molecular weight dependence. *Macromolecules* **1992,** *25* (5), 1453-1460.
15. Hikosaka, M.; Watanabe, K.; Okada, K.; Yamazaki, S., Topological mechanism of polymer nucleation and growth–the role of chain sliding diffusion and entanglement. In *Interphases and Mesophases in Polymer Crystallization III*, Springer: 2005; pp 137-186.
16. Mohammadi, H. On Melting and Crystallization of Linear Polyethylene, Poly(ethylene oxide) and Metallocene Linear Low Density Polyethylene. Virginia Polytechnic Institute and State University, 2018.
17. Hikosaka, M.; Amano, K.; Rastogi, S.; Keller, A., Lamellar thickening growth of an extended chain single crystal of polyethylene. 1. Pointers to a new crystallization mechanism of polymers. *Macromolecules* **1997,** *30* (7), 2067-2074.
18. Hikosaka, M.; Amano, K.; Rastogi, S.; Keller, A., Lamellar thickening growth of an extended chain single crystal of polyethylene (II): ΔT dependence of lamellar thickening growth rate and comparison with lamellar thickening. *Journal of materials science* **2000,** *35* (20), 5157-5168.

19. Wunderlich, B.; Davidson, T., Extended-chain crystals. I. General crystallization conditions and review of pressure crystallization of polyethylene. *Journal of Polymer Science Part B: Polymer Physics* **1969,** *7* (12), 2043-2050.
20. Hoffman, J. D.; Miller, R. L., Kinetic of crystallization from the melt and chain folding in polyethylene fractions revisited: theory and experiment. *Polymer* **1997,** *38* (13), 3151-3212.
21. Flory, P.; Vrij, A., Melting points of linear-chain homologs. The normal paraffin hydrocarbons. *Journal of the American Chemical Society* **1963,** *85* (22), 3548-3553.
22. Buckley, C.; Kovacs, A., Melting behaviour of low molecular weight poly (ethylene-oxide) fractions. In *Polymere Aspekte*, Springer: 1975; pp 44-52.
23. Buckley, C.; Kovacs, A., Melting behaviour of low molecular weight poly (ethylene-oxide) fractions. *Colloid and Polymer Science* **1976,** *254* (8), 695-715.
24. Mandelkern, L.; Stack, G. M., Equilibrium melting temperature of long-chain molecules. *Macromolecules* **1984,** *17* (4), 871-878.
25. Marentette, J.; Brown, G., The (010)–(120) crystal growth face transformation in poly (ethylene oxide) spherulites. *Polymer* **1998,** *39* (6-7), 1405-1414.
26. Alfonso, G.; Russell, T., Kinetics of crystallization in semicrystalline/amorphous polymer mixtures. *Macromolecules* **1986,** *19* (4), 1143-1152.
27. Beech, D.; Booth, C., Thermodynamic melting point of poly (ethylene oxide). *Journal of Polymer Science Part C: Polymer Letters* **1970,** *8* (10), 731-734.
28. Allen, R. C. Crystalline morphology and thermodynamic properties of poly (ethylene oxide) fractions. Florida State University, 1980.
29. Mohammadi, H.; Vincent, M.; Marand, H., Investigating the equilibrium melting temperature of linear polyethylene using the non-linear Hoffman-Weeks approach. *Polymer* **2018**.
30. Marand, H.; Xu, J.; Srinivas, S., Determination of the equilibrium melting temperature of polymer crystals: linear and nonlinear Hoffman− Weeks extrapolations. *Macromolecules* **1998,** *31* (23), 8219-8229.

31. Toda, A.; Konishi, M., An evaluation of thermal lags of fast-scan microchip DSC with polymer film samples. *Thermochimica Acta* **2014,** *589*, 262-269.
32. Toda, A.; Taguchi, K.; Nozaki, K.; Konishi, M., Melting behaviors of polyethylene crystals: an application of fast-scan DSC. *Polymer* **2014,** *55* (14), 3186-3194.
33. Huggins, M. L., Certain Properties of Long-chain Compounds as Functions of Chain Length. *Journal of Physical Chemistry* **1939,** *43* (8), 1083-1098.
34. Hoffman, J. D.; Davis, G. T.; Lauritzen, J. I., The rate of crystallization of linear polymers with chain folding. In *Treatise on solid state chemistry*, Springer: 1976; pp 497-614.
35. Lauritzen, J.; Passaglia, E., Kinetics of crystallization in multicomponent systems: II. Chain-folded polymer crystals. *J Res Natl Bur Stand. A* **1967,** *71*, 261-75.
36. Hoffman, J. D.; Miller, R. L.; Marand, H.; Roitman, D. B., Relationship between the lateral surface free energy. sigma. and the chain structure of melt-crystallized polymers. *Macromolecules* **1992,** *25* (8), 2221-2229.
37. Frank, F., Nucleation-controlled growth on a one-dimensional growth of finite length. *Journal of Crystal Growth* **1974,** *22* (3), 233-236.
38. Armistead, J.; Hoffman, J. D., Direct evidence of regimes I, II, and III in linear polyethylene fractions as revealed by spherulite growth rates. *Macromolecules* **2002,** *35* (10), 3895-3913.
39. Sheth, M.; Kumar, R. A.; Davé, V.; Gross, R. A.; McCarthy, S. P., Biodegradable polymer blends of poly (lactic acid) and poly (ethylene glycol). *Journal of applied polymer science* **1997,** *66* (8), 1495-1505.
40. Nijenhuis, A.; Colstee, E.; Grijpma, D.; Pennings, A., High molecular weight poly (L-lactide) and poly (ethylene oxide) blends: thermal characterization and physical properties. *Polymer* **1996,** *37* (26), 5849-5857.
41. Marand, H.; Huang, Z., Isothermal lamellar thickening in linear polyethylene: Correlation between the evolution of the degree of crystallinity and the melting temperature. *Macromolecules* **2004,** *37* (17), 6492-6497.

42. Huang, Z. Crystallization and Melting Behavior of Linear Polyethylene and Ethylene/Styrene Copolymers and Chain Length Dependence of Spherulitic Growth Rate for Poly (Ethylene Oxide) Fractions. Virginia Tech, 2004.
43. Point, J.-J.; Damman, P.; Janimak, J., Is the break in the curve giving the thermal dependence of crystal growth rate a signature of regime II→ III transition? *Polymer* **1993,** *34* (18), 3771-3773.
44. Scherrer, P., Determination of the size and internal structure of colloidal particles using X-rays. *Nachr. Ges. Wiss. Göttingen* **1918,** *2*, 98-100.
45. Qiu, W.; Pyda, M.; Nowak-Pyda, E.; Habenschuss, A.; Wunderlich, B., Reversibility between glass and melting transitions of poly (oxyethylene). *Macromolecules* **2005,** *38* (20), 8454-8467.
46. Kovacs, A.; Straupe, C.; Gonthier, A. In *Isothermal growth, thickening, and melting of polyethylene oxide) single crystals in the bulk. II*, Journal of Polymer Science: Polymer Symposia, Wiley Online Library: 1977; pp 31-54.
47. Schönherr, H.; Frank, C. W., Ultrathin films of poly (ethylene oxides) on oxidized silicon. 2. In situ study of crystallization and melting by hot stage AFM. *Macromolecules* **2003,** *36* (4), 1199-1208.
48. Takahashi, Y.; Tadokoro, H., Structural studies of polyethers,(-(CH2) mO-) n. X. Crystal structure of poly (ethylene oxide). *Macromolecules* **1973,** *6* (5), 672-675.
49. Appel, M.; Fleischer, G., Investigation of the chain length dependence of self-diffusion of poly (dimethylsiloxane) and poly (ethylene oxide) in the melt with pulsed field gradient NMR. *Macromolecules* **1993,** *26* (20), 5520-5525.
50. Fritzsching, K. J.; Mao, K.; Schmidt-Rohr, K., Avoidance of density anomalies as a structural principle for semicrystalline polymers: the importance of chain ends and chain tilt. *Macromolecules* **2017,** *50* (4), 1521-1540.

51. Smith, G. D.; Yoon, D. Y.; Jaffe, R. L.; Colby, R. H.; Krishnamoorti, R.; Fetters, L. J., Conformations and structures of poly (oxyethylene) melts from molecular dynamics simulations and small-angle neutron scattering experiments. *Macromolecules* **1996,** *29* (10), 3462-3469.
52. Fetters, L.; Lohse, D.; Colby, R., Chain dimensions and entanglement spacings. In *Physical properties of polymers handbook*, Springer: 2007; pp 447-454.
53. Ślusarczyk, C., Crystallization and melting behavior of poly (ethylene oxide) and its blend with styrene-based ionomer using time-resolved SAXS/WAXS experiments. *Radiation Physics and Chemistry* **2011,** *80* (10), 1078-1083.
54. Huang, C. I.; Chen, J. R., Crystallization and chain conformation of semicrystalline and amorphous polymer blends studied by wide-angle and small-angle scattering. *Journal of Polymer Science Part B: Polymer Physics* **2001,** *39* (21), 2705-2715.
55. Fischer, E.; Kimmich, R.; Beginn, U.; Möller, M.; Fatkullin, N., Segment diffusion in polymers confined in nanopores: A fringe-field NMR diffusometry study. *Physical Review E* **1999,** *59* (4), 4079.
56. Niedzwiedz, K.; Wischnewski, A.; Pyckhout-Hintzen, W.; Allgaier, J.; Richter, D.; Faraone, A., Chain dynamics and viscoelastic properties of poly (ethylene oxide). *Macromolecules* **2008,** *41* (13), 4866-4872.
57. Hoffman, J.; Frolen, L.; Ross, G.; Lauritzen, J., Growth-rate of spherulites and axialites from melt in polyethylene fractions-regime-1 and regime-2 crystallization. *Journal of Research of the National Bureau of Standards Section a-Physics and Chemistry* **1975,** *79* (6), 671-699.
58. Pearson, D.; Ver Strate, G.; Von Meerwall, E.; Schilling, F., Viscosity and self-diffusion coefficient of linear polyethylene. *Macromolecules* **1987,** *20* (5), 1133-1141.

Chapter 7. General Conclusions and Future Work

7.1. General Conclusions

Investigations of the melting and crystallization behaviors of series of narrow molecular weight distribution linear polyethylene and poly(ethylene oxide) fractions using ultra-fast and conventional differential scanning calorimetry, wide angle X-ray diffraction, and optical microscopy were discussed in Chapters 3, 4, and 6. Most significantly, we have shown that the non-linear Hoffman-Weeks treatment leads to equilibrium melting temperatures that are within the experimental uncertainty identical with these measured directly for extended chain crystals or derived from a Gibbs-Thomson analysis. Our results indicate that the chain length dependence of the equilibrium melting temperature of these polymers follows a Huggins type equation with limiting equilibrium melting temperatures of 141.4 ± 0.8^{o}C and 81.4 ± 1.0^{o}C for linear polyethylene and poly(ethylene oxide), respectively, significantly different from that predicted by the Flory-Vrij[1] and Buckley-Kovacs[2] equations. Using equilibrium melting temperatures obtained from the non-linear Hoffman-Weeks analysis, we have shown for the first time that the value of the equilibrium fold surface free energy derived from crystal growth rate data using the modified Lauritzen-Hoffman theory matches that calculated from lamellar thickness and melting data through the Gibbs-Thomson equation for both linear polyethylene and poly(ethylene oxide). We reported that the regime I/II transition undercooling, equilibrium fold surface free energy, and strength of the stem length fluctuations and substrate length at the regime I/II transition of linear polyethylene and poly(ethylene oxide) are independent of chain length. The apparent chain friction coefficient during crystal growth exhibits different power law exponents than that found for reptation in the melt. The magnitude of the apparent chain friction coefficient during crystal growth is significantly lower for PEO than for LPE, possibly the result of

a much more active α_c-relaxation for the former polymer (note that any coupling between lamellar thickening and crystal growth is ignored in the LH theory). Observation of significantly larger spherulitic growth rates for LPE than for PEO at low undercooling is explained by the markedly higher secondary nucleation constant for PEO than for LPE ($K_g^o(PEO)/K_g^o(PE)$ ~ 2.3). The fact that the difference in spherulitic growth rates between PEO and LPE at high undercooling is smaller than expected on the basis of their K_g^o ratio is explained by the lower apparent friction coefficient of PEO.

In Chapter 5, the role of short-chain branching in the crystal growth kinetics of ethylene/1-hexene copolymers is discussed. It is observed that the fold surface free energies during crystallization and during melting are both function of the undercooling. The ratio of the former to the latter decreases with increasing undercooling, suggesting that the extent of the relaxation of stem-length fluctuations during heating and melting also decreases with increasing undercooling. We proposed that this behavior may be related to the concentration of short-chain branches at the surface of the lamellae, where higher concentration leads to lower relaxation.

7.2. Future Work

7.2.1. On the Crystallization Mechanism of Linear Flexible Polymers

One of the most important aspects of our spherulite growth rate analysis was concerned with accounting for the effect of stem length fluctuations in Lauritzen-Hoffman secondary nucleation theory. Using this approach, we were able to answer one of the main discrepancies observed between the Lauritzen-Hoffman kinetic theory and the Gibbs-Thomson thermodynamic analysis: why are the fold surface free energies during melting and crystallization different? However, we were not able to draw definite conclusions on the chain length dependence of the strength of stem length fluctuations. Performing the non-linear

Hoffman-Weeks analysis at more crystallization temperatures and for a larger number of narrow molecular weight distribution fractions would lead to better statistics and possibly allow us to determine whether or not the strength of stem-length fluctuation is chain length dependent.

Our results also indicated that the segmental mobility within the crystalline phase may play an important role in the crystal growth mechanism (coupling of lamellar thickening and chain-folded lamellar growth). Such observation needs to be confirmed through measurement of apparent friction coefficients for other semi-crystalline polymers with high α_c-relaxation rates. Polytetrafluoroethylene and *t*-polybutadiene are two polymers meeting that criterion.[3] After determining the equilibrium melting temperature of these polymers via the non-linear Hoffman-Weeks method, the spherulite growth rate and wide angle X-ray diffraction data can be analyzed, allowing us to look for similar trends in the chain length dependence of their apparent friction coefficient as for poly(ethylene oxide) and the hexagonal phase of linear polyethylene.

Analysis of the spherulite growth rate of m-LLDPE copolymers with less than 2 mol% short branches can also be useful in this regard. While these copolymers experience lamellar thickening during crystallization,[4] the rate of their α_c-relaxation can be adjusted by varying concentration of the short-chain branches.

7.2.1. On the Crystallization and Melting of Semi-Crystalline m-LLDPE

It is imperative to confirm the effect of short-chain branching on the morphology of semi-crystalline m-LLDPE copolymers with other experimental techniques. The morphological aspects suggested here can be examined by studying single crystals of m-LLDPE at various undercoolings via longitudinal acoustic mode Raman scattering, small angle X-ray scattering and atomic force microscopy. These single crystals can be obtained by crystallization from the melt or solution.[5-6] One would also like to study the effect of the overall concentration of the short-chain branches on both the fold surface energies during crystallization and during melting for copolymer lamellae at various undercoolings.

7.3. References

1. Flory, P.; Vrij, A., Melting points of linear-chain homologs. The normal paraffin hydrocarbons. *Journal of the American Chemical Society* **1963,** *85* (22), 3548-3553.
2. Kovacs, A.; Gonthier, A.; Straupe, C. In *Isothermal growth, thickening, and melting of poly (ethylene oxide) single crystals in the bulk*, Journal of Polymer Science: Polymer Symposia, Wiley Online Library: 1975; pp 283-325.
3. Hu, W. G.; Schmidt-Rohr, K., Polymer ultradrawability: the crucial role of α-relaxation chain mobility in the crystallites. *Acta Polymerica* **1999,** *50* (8), 271-285.
4. Cho, T.; Heck, B.; Strobl, G., Equations describing lamellar structure parameters and melting points of polyethylene-co-(butene/octene) s. *Colloid and Polymer Science* **2004,** *282* (8), 825-832.
5. Toda, A.; Keller, A., Growth of polyethylene single crystals from the melt: morphology. *Colloid and Polymer Science* **1993,** *271* (4), 328-342.
6. Liu, J.; Xie, F.; Du, B.; Zhang, F.; Fu, Q.; He, T., Lateral habits of single crystals of metallocene-catalyzed low molecular weight short chain branched polyethylene from the melt. *Polymer* **2000,** *41* (24), 8573-8577.